Development and Characterization of Fly ash Based Ceramic Membranes for the Separation of Oil-in-Water Emulsions

Kanchapogu Suresh

भारतीय प्रौद्योगिकी संस्थान गुवाहाटी
Indian Institute of Technology Guwahati

Development and Characterization of Fly ash Based Ceramic Membranes for the Separation of Oil-in-Water Emulsions

Thesis

Submitted in partial fulfillment of the
requirements for the degree of

DOCTOR OF PHILOSOPHY

by

Kanchapogu Suresh

Roll No.: 126107004

Department of Chemical Engineering

Indian Institute of Technology, Guwahati

Guwahati-781039

October, 2016

भारतीय प्रौद्योगिकी संस्थान गुवाहाटी
Indian Institute of Technology Guwahati

Dedication

To My Family

भारतीय प्रौद्योगिकी संस्थान गुवाहाटी
Indian Institute of Technology Guwahati

Department of Chemical Engineering
Indian Institute of Technology Guwahati
Guwahati - 781039 (INDIA)

CERTIFICATE

It is certified that the work contained in the thesis entitled "**Development and Characterization of Fly ash based Ceramic Membranes for the Separation of Oil-in-Water Emulsions"** by **Kanchapogu Suresh** has been carried out under my supervision and that this work has not been submitted elsewhere for a degree.

Date:

(**Dr. G. Pugazhenthi**)
Professor
Department of Chemical Engineering
Indian Institute of Technology Guwahati
Guwahati-781039, India.

.

भारतीय प्रौद्योगिकी संस्थान गुवाहाटी
Indian Institute of Technology Guwahati

Acknowledgement

I would like to make my deepest appreciation and gratitude to **Prof. G. Pugazhenthi** for his invaluable guidance, constructive criticism and encouragement during my thesis work. I must say I am blessed to have he as my supervisor. My most heartfelt thanks to **Prof. Ramgopal V. S. Uppaluri** for his kind help, suggestions and constant encouragement in writing manuscripts as well as editing the thesis files of my research work within stipulated short period of time.

My sincere acknowledgement goes to **Prof. V.S. Moholkar** and **Prof. B. P. Manda**l, former and present Heads of Chemical Engineering Department. I thank them for their encouragement, guidance, and support from the initial to the final stages of my PhD work. I am also indebted to the members of Doctoral Committee **Prof. B. P. Mandal**, **Dr. Nanda Kishore**, of the Department of Chemical Engineering and **Prof. K. Pakshirajan** of the Department of Biosciences and Bioengineering, for their precious suggestions about critical issues related to my work.

I am also thankful to **Dr. Senthil Kumar** of Department of Biosciences and Bioengineering, who have made me learn working with Design-Expert® Software Version 9, and for his continuous motivation and support during analysis of experimental results using Response Surface Methodology (RSM).

Acknowledgement is made to all my well-wishers both faculty and students of Indian Institute of Technology Guwahati for their support, encouragement and critique. I also acknowledge the financial support provided by IIT Guwahati.

Contact angle instrument used in this work was financially supported by a grant for Center of Excellence for Sustainable Polymers at IIT Guwahati from Department of Chemicals & Petrochemicals, Ministry of Chemicals and Fertilizers, Government of India. XRD, used in this work, was financially supported by a FIST grant (SR/FST/ETII-028/2010) from the Department of Science and Technology (DST), Government of India.

I am also deeply grateful to the scientific officers **Dr. K. K. Senapati** and **Mr. K. K. Singh**, Scientific Officers, at the Central Instruments Facility of IIT Guwahati for allowing me to carry out SEM analysis on my own. I am also grateful to the **Mr. B. Choudhury** of Central Workshop, IIT Guwahati for helping me in the fabrication of my experimental setup which was very much essential in my research work.

I would like to extend my sincere thanks to all my beloved friends Mr. Mood Mohan, Mr. Tekula Srinu, Mr. Rajasekhar Ravula, Dr. Kamal Kumar Bhatluri, Mr. Bandi Chandra Sekhar, Mr. V Shyam Kumar Yadav, Mr. Rahul Patwa, for helping me in experimental work and for their involvement in the discussions about research problems and Mr. Tharun Dolla, Mr. Ramesh Pallekonda, Mr. Kankipati Kiran Kumar, Mr. Naveen, Mr. Rahul, for their help in proof reading of my thesis. I am also thankful to my Lab mates i.e., Dr. Ashim Kumar Basumathary, Mr. Manish Kumar, Mr. Kelothu Suresh, Mr. Vinoth Kumar, Mr. Mohan and lobby mates i.e., Mr. Binay Deogam, Mr. Kishant Kumar, Mr. Prudhvi Raj, Mr. Bisweswar Das, Mr. Abhik Bhattacharjee, Mr. Rupak Kishore with whom I have come in contact during my stay at IIT Guwahati. The friendship and unforgettable attachments shared with them has made my life pleasant. I am also thankful to summer internship students namely Mr. Manpadu Ramesh, Ms. Priyanka Kumari, Ms. Monikangkana Talukdar, for their wonderful support during the experimental investigations. I extend my indebted gratitude towards the church, with whom I cherished my good times, for their support and encouragement in all tough times and most of all their prayers for me and my project.

A special thanks to my family. Words cannot express how grateful I am to my mother, father, sisters and brothers for all of the sacrifices that they've made on my behalf. Their prayer for me was what sustained me this far. Finally I thank my God, my good Father, for letting me through all the difficulties. I have experienced your guidance day by day. You are the one who let me finish my degree. I will trust you in future as well. Thank you, Lord.

October, 2016

IIT Guwahati

(Kanchapogu Suresh)

Abstract

Liquid Considering the available prior art in the field of inexpensive ceramic and titania membranes and their applicability for oil-in-water emulsions treatment, this work addresses experimental and theoretical investigations in four major themes namely:

- ❖ Fly ash based inexpensive ceramic membrane fabrication and characterization
- ❖ Dead end and Cross flow microfiltration (MF) of oil-in-water emulsions using inexpensive ceramic membranes
- ❖ Fabrication of titania-fly ash composite membranes for oil-in-water emulsion treatment
- ❖ Response surface methodology for the parametric optimization of inexpensive ceramic membrane based dead end and cross-flow MF of oil-in-water emulsions.

From a novelty perspective, the Ph.D thesis can be summarized as follows:

a) Dead end oil-in-water MF studies with low cost ceramic membranes possessing lower average pore size (1.32–2.97 µm).

b) Dead end MF studies with fly ash based inexpensive ceramic membranes (1.30–1.44 µm) using synthetic oil-in-water emulsions (50–200 mg/L feed concentration).

c) Cross flow MF investigations with lower pore size inexpensive membranes and lower feed concentration (50–200 mg/L) and subsequent parametric optimality investigations using RSM.

d) Performance enhancement of ceramic membranes by titania coating via hydrothermal method and their comparative assessment in MF of oil-in-water emulsions with conventional low cost ceramic membranes.

The first phase of the Ph.D. thesis involved the fabrication of inexpensive mixed clays based membranes (SP1–SP4) using uni-axial dry compaction method in which the SP4 membrane provided 99.2% oil rejection and 4.1×10^{-8} m^3/m^2 s flux at 69 kPa and 200 mg/L feed concentration. Further, new compositions have been identified that refer to maximum constitution of fly ash in the M1-M3 membranes fabricated with uni-axial dry compaction method. Membrane characterization was conducted using thermo gravimetric analysis (TGA) field emission scanning electron microscopy (FESEM), X-ray diffraction (XRD) analysis, N_2 permeation studies. The M1-M3 membranes have been evaluated to possess 1.30 – 1.44 µm average pore size and 30 – 43% average porosity.

Among M1-M3 membranes, M2 membrane provided optimal flux and rejection of 2×10^{-4} m^3/m^2 s and 98.47%, respectively for 345 kPa pressure differential and 200 mg/L initial oil concentration. The RSM based optimization of dead end MF process with M2 membrane inferred that the optimal flux and rejection values are 2.6×10^{-4} and 96.94%, respectively for 345 kPa applied pressure and 176.07 mg/L feed concentration.

Cross-flow MF studies carried out with titania-fly ash composite membrane provided better performance in comparison with the M2 membrane. During cross flow MF conducted at 207 kPa applied pressure, 0.1769 m/s cross flow velocity and 200 mg/L feed concentration, the titania fly ash membrane provided an optimal flux and rejection of 42.85×10^{-4} m^3/m^2 s and 98.82% respectively, which are marginally better than those provided by the M2 membrane (40.9×10^{-4} m^3/m^2 s and 98.37%, respectively). The RSM based analysis inferred similar insights on parametric optimality.

For comparative purposes, clay, titania-clay and γ-Al_2O_3-clay composite membranes were prepared with clay, $TiCl_4$ and $AlCl_3$ as source material and hydrothermal method for asymmetric membrane fabrication. During dead end MF of oil-in-water emulsions (50-250 mg/L feed concentration), the titania-clay membrane provided optimal flux and rejection of

8.481×10^{-5} m^3/m^2 s and 98.96%, respectively at 69 kPa and 200 mg/L of oil concentration. On the other hand, corresponding optimal flux and rejection of γ-Al_2O_3-clay composite membrane (0.97 µm pore size) are 6.119×10^{-5} m^3/m^2 s and 98.46%, respectively.

Further, during cross flow MF with 200 mg/L feed concentration, among titania-clay and clay membranes, titania-clay membrane provided optimal combinations of membrane flux (186.60×10^{-6} m^3/m^2 s) and rejection (99.56%) at 207 kPa applied pressure and 0.1769 m/s cross flow velocity. Corresponding flux and rejection values for clay membrane have been determined to be 87.08×10^{-6} m^3/m^2 s and 93.24%, respectively.

Among all membranes, titania-fly ash composite membranes provided best performance for oil-in-water emulsion treatment. For 100 mg/L feed concentration, 207 kPa applied pressure and 0.1769 m/s cross flow velocity, the titania-fly ash composite membrane provided an optimal flux of 51.6372×10^{-4} m^3/m^2 s, which was higher than that obtained with M2 membrane (49.97×10^{-4} m^3/m^2.s). For higher feed concentration of 200 mg/L, applied pressure of 207 kPa and cross flow velocity of 0.1769 m/s, the titania-fly ash composite membrane provided flux and rejection of 42.85×10^{-4} m^3/m^2.s and 98.82%, respectively, which were higher than those provided by TiO_2-clay composite membrane (1.86×10^{-4} m^3/m^2 s and 99.56% rejection). Hence, titania-fly ash composite membrane fabricated with M2 membrane as support is inferred to be the best for oil-in-water emulsion treatment. From the perspective of available prior-art, this inference is significant, given the fact that there has not been any literature that refers to the optimality of titania-fly ash composite membranes for oil-in-water emulsion treatment.

Conceptual retail cost analysis (inclusive chemical, electrical, labor, etc.,) of the fabricated low cost ceramic membrane (M1-M3) indicated that their cost is about 462-465 $\$/m^2$, respectively. Thus, it has been inferred from cost analysis that the membranes are 3-5 times inexpensive than other ceramic membranes.

In summary, the Ph.D thesis highlights the relevance and promising opportunities for fly ash based low cost ceramic membranes towards oil-in-water emulsion filtration. In addition, the thesis provides useful insights into the fabrication engineering aspects of low cost TiO_2 composite membranes. The commercial application of fly ash and fly ash composite membranes needs to be further investigated using industrial oil-in-water emulsions in the near future to translate the utility of waste material such as fly ash as a value added product in separation process technologies.

Contents

List of tables

भारतीय प्रौद्योगिकी संस्थान गुवाहाटी
Indian Institute of Technology Guwahati

List of figures

Nomenclature

Symbols

ε - Porosity of the membrane

W_D - Weight of dry membrane (g)

W_W - Weight of the membrane with pores filled with water (pores are filled with water under vacuum) (g)

W_A- Weight of the membrane saturated with water measured in water (A refers to Archimedes) (g)

σ - Flexural strength (Pa)

F - Load at the fracture point (N)

L - Span length (m)

b - Width of the sample (m)

t - Thickness of the sample (m)

J_w - Pure water flux (m^3/m^2 s)

V - Volume of water permeated (m^3)

A - Membrane area (m^2)

ΔT - Sampling time (s)

r_m - Pore radius of the membrane (μm)

L_h - Hydraulic permeability of the membrane (m^3/m^2sPa)

μ - Viscosity of water (Pa s)

ΔP – Applied pressure (kPa)

l_p - Pore length (m)

P - Average pressure acting on the membrane (Pa)

v - Molecular mean velocity of the gas (m/s)

η - Viscosity of gas (Pa s)

q - Tortuosity

K - Effective permeability factor

P_2 - Membrane pressure at permeate side (Pa)

S - Permeable area of the membrane (m^2)

r_g – Average pore size of the membrane (μm)

Y - Predicted response

V - Volume of permeate (m^3)

A - Membrane area (m^2)

J - Permeate flux (m^3/m^2 s)

L_h - the permeability of the membrane (m^3/m^2 s kPa)

R - Rejection of oil (%)

C_f - Oil concentration in feed (mg/L)

C_p - Oil concentration in permeate (mg/L)

d_i - Diameter of the i^{th} pore (μm)

n_i - Number of pores on the membrane

D_{avg} - Average value of membrane pore diameter (μm)

ΔX_i - Step change content of uncoded variable i

X_o - Real value of an independent variable (X_i) at the centre point

Z_i - Dimensionless coded value of an independent variable

Y - Predicted response (permeate flux and rejection)

β_{ij} - the interaction coefficients,

β_{ii} - the quadratic effect,

β_i - the linear effect

β_0 -the intercept

ε_{ijk} -the random error,

X_i, X_j - the uncoded independent variables.

Abbreviations

SEM – Scanning Electron Microscope

FESEM – Field Emission Scanning Electron Microscope

FTIR – Fourier Transform Infrared Spectrophotometer

XRD – X-Ray Diffraction

TGA – Thermogravimetric analysis

DTG – Differential Thermogravimetric analysis

PSD – Particle Size Distribution

RSM – Response Surface Methodology

MF – Microfiltration

UF – Ultrafiltration

NF – Nanofiltration

RO – Reverse Osmosis

COD – Chemical Oxygen Demand

TOC – Total Organic Carbon

CFV – Cross Flow Velocity

TMP – Transmembrane Pressure

CCD – Central Composite Design

भारतीय प्रौद्योगिकी संस्थान गुवाहाटी
Indian Institute of Technology Guwahati

CHAPTER-1

Introduction and Literature Review

भारतीय प्रौद्योगिकी संस्थान गुवाहाटी
Indian Institute of Technology Guwahati

CHAPTER 1 Introduction and Literature Review

After presenting a brief overview of fly ash materials and ceramic membranes in sections 1.1 and 1.2, respectively, this chapter addresses the available prior art in the fields of ceramic support fabrication, composite membrane fabrication, and ceramic membrane based oil-in-water emulsion separation studies and applications pertaining to response surface methodology for membrane separation processes in section 1.3. Thereby, possible scope for further research, objectives of the thesis and its organization are being presented in sections 1.4, 1.5 and 1.6, respectively.

1.1 Fly ash material

1.1.1 History

Electrical power generating produce millions of tons of fly ash and related by-products by burning coal. With increasing electricity demand and with abundance of coal in nature, fly ash generation is increasing enormously. According to Ahmaruzzaman (2010), only 16% of fly ash is utilized by existing techniques. Out of this, the cement industry utilizes about 30% of fly ash and the remaining portion is disposed to landfill and ash ponds. Due to the existence of transition metal oxides, fly ash is known to provide adverse environmental effect. Among various viable alternatives for fly ash utilization, the fabrication of efficient ceramic membranes is an important alternative, owing to the utilization of fly ash to further address potential adverse environmental effects caused by discharged wastewater such as oil-in-water emulsions.

Listed as sixth largest in terms of electrical power generation, India produces significant amount of fly ash. While majority of fly ash is being used for cement manufacture, roadways

and brick manufacture, large quantities of fly ash is stored in ponds. Currently, only 50% of the fly ash is used in the annual production capacity of 160 million tones in India.

Fly ash is abrasive, refractory and also alkaline. It consists of macronutrients (P, K, Ca, Mg) and micronutrients (Zn, Fe, Cu, Mn, B and Mo) and can be adopted for plant growth. Lime binding capacity of the fly ash enables it for cement manufacturing, concrete building materials and other relevant products. Chemical constitution of fly ash corresponds to significant proportion of silica (60-65%) followed with alumina (25-30%), magnetite and Fe_2O_3 (6-15%). Due to this, Iyer and Scott (2011) have opined that it can be used for the synthesis of zeolite, alum and precipitated silica. With appropriate physiochemical properties (bulk density, particle size, porosity, water holding capacity and active surface area), fly ash has been suggested to be adsorbent (Blissett and Rowson, 2012). Further, agricultural and engineering materials can be also developed from fly ash.

1.1.2 Physical Properties

Table 1.1 presents the physical properties of fly ash. Typically, fly ash contains spherical solid or hollow amorphous powder particles. Further, fly ash also contains angular shaped particles of carbonaceous materials. The particle size distribution is about 1-150μm (Ilic et al., 2003). Specific gravity and specific surface area vary from 2.1 – 3.0 and 170 – 1000 m^2/kg, respectively. Depending upon unburned carbon content, the colour of fly ash varies from tan to black.

Table 1.1: Physical properties of fly ash

Properties	Range
Specific Gravity	2.1-3.0
Specific surface area (m^2/kg)	170-1000
Color	Grey-black
Particle size (μm)	1-150

1.1.3 Chemical Properties

Depending upon the type of coal burnt and handling/storage procedures, fly ash chemical properties vary significantly. Fundamentally, fly ash classification is based on the type of coal (anthracite, bituminous, sub-bituminous and lignite) used during combustion (Ahmaruzzaman, 2010; Iyer and Scott, 2011; Blissett and Rowson, 2012). While bituminous coal based fly ash consists of silica, alumina, iron oxide, calcium and carbon, the fly ash obtained from sub-bituminous coal consists of higher constitution of magnesium and calcium oxide and lower amounts of silica, iron oxide and carbon.

Table 1.2: Classification of fly ash by ASTM standards

Class	$SiO_2+Al_2O_3+Fe_2O_3$ (%)	SO_3 (%)	Ca (%)	Moisture (%)	Loss of Ignition (%)
C	50-70	<5	30-40	<3	<6
F	>70		1-12		<12

The American Society for Testing Materials (ASTM) classification (C618) of fly ash refers to class F and C categories (Table 1.2). This is based on the constitution of alumina, silica, iron oxide and lime in fly ash. With low lime, class F fly ash possesses 70% overall weight percentage of alumina, silica, and iron oxide. However, for class C fly ash, the overall weight

percentage of alumina, silica, and iron oxides is about 50 – 70% along with abundance of lime content. Generally, class C fly ash is obtained by low rank coals i.e. lignite and sub-bituminous coal with cementations properties. On the other hand, class F fly ash is obtained from the combustion of higher rank pozzolanic coals. The main differences between these ashes are in calcium, alumina, silica and iron content. While calcium content in class F varies from 1 – 12%, it varies from 30 – 40 % in class C. Another variation in the composition corresponds to alkali (sodium and potassium) and sulfate content. This is higher for class C fly ash but not class F fly ash. European standards based fly ash constitution is being presented in Table 1.3.

Table 1.3: Classification of fly ash based on European standards EN 450-1

Class	$SiO_2+Al_2O_3+Fe_2O_3$ (%)	SO_3 (%)	Reactive Silica (%)	LOI (%)
A	>70	<3	>25	<5
B	-	-	-	2-7
C	-	-	-	4-9

The general classification of coal fly ash typically ignores the mineralogy aspects of the coal. Vassilev and Vassileva (2007) indicated that the coal fly ash classification does not systematic scientific basis, despite being addressed from industrial coal utilization perspective. Thereby, European coal fly ash classification system has been developed in which the bulk oxides have been grouped together to classify fly ash (shown in Table 1.4). Fly ash has been analyzed to have significant variations in available phases such as kaolinite, mullite, illite and siderate that includes calcite, pyrite and hematite. Low calcium ash has

quartz and mullite as major constituents. On the other hand, fly ash with high calcium content consists quartz, Tricalcium Aluminate (C3A), Calcium Silicate (CS) and Tetracalcium Alumino Silicate (C4AS) (Bruce and Mathew, 2004). Fly ash has significant amount of glass, which is typically explored to develop road construction materials by facilitating reaction with lime (Pozzolanic reaction). Fly ash with its promising features of adhesivity, glass content, crystalline content and strength is eventually used in cement production and concrete admix.

Table 1.4: Classification of coal fly ash on chemical composition

Class	**SiO_2 + Al_2O_3 + K_2O + TiO_2 + P_2O_5 (%)**	**CaO + MgO + SO_3 + Na_2O + MnO (%)**	**Fe_2O_3**
Sialic	>77	<11.5	<11.5
Calsialic	<89	>11.5	<11.5
Ferrisialic	<89	<11.5	>11.5
Ferricalcsialic	<77	>11.5	>11.5

1.1.4 Applications

Eminent features of fly ash are spherical texture, pozzolanic properties, low alkali content, and moisture insensitivity, low cost, ease of handling, good shear strength, consistent quality and low carbon content. The drinking force behind application oriented research on fly ash is upon the development of products with technical and commercial value. A plethora of potential applications have been already identified with fly ash as economically viable source. These include:

- Synthesis of zeolites by hydrothermal method (Querol et al., 1995).

- Raw material for concrete addition and road construction and (Mathur, 2000).
- Raw material for blended cements in concrete blocks; filling of voids, mine shafts and sub-surface mine works; restoration and re-cultivation in open cast mining (Hansen, 1991; Nanni et al., 1996; Delagrave et al., 1997).
- Material to offer compaction and lower head of hydration in dam construction materials. Further, fly ash blended concrete increased durability of structure two to three times, as against ordinary Portland cement and hence could be used in irrigation projects (Gao et al., 2007).
- Raw material for the pavement base course foundation material production; drying agent for wet soils and structural fill (Gonzalez, 2009).
- Raw material for brick production (Lin, 2006).
- Low cost adsorbent for organic compounds (Phenol, Ortho-chloro phenol, 2,4 Dichloro phenol, Cresol), flue gas (SiO_2, NO_x) and metals (Zn^{+2}, Cd^{+2}, Pb^{+2}, Cu^{+2}, Ni^{+2}, Cr^{+3}, Cr^{+6}, Hg^{+2}, As^{+3}, As^{+5}) removal from industrial effluents (Akgerman and Zardkoohi, 1996; Daifullah and Gad, 1998; Davini, 2002; Banerjee et al., 2003; Apak et al., 1998; Kelleher et al., 2002; Banerjee et al., 2004; Pattanayak et al., 2000).
- Fabrication of low cost ceramic supports (Jedidi et al., 2009; Dong et al., 2010; Fang et al., 2011).

In the above applications, the application of fly ash for separation and treatment of waste water streams is an important area of research that is presently investigated to a significant extent (Jedidi et al., 2009; Dong et al., 2010; Fang et al., 2011). The major objective of this thesis is to address the membrane application potential of fly ash and therefore, the next section summarizes a brief overview of membrane processes.

1.2 Overview of Membrane Processes

Membranes are functional semi-permeable active or passive barriers that permit the preferential retention/permeation of one or several components (molecules, particles or polymers) in gaseous and/or liquid mixtures (Hsieh, 1996). In due course of separation, the primary species that are rejected and retained are termed as retentate solutes and the species that pass through the membranes are termed as permeate solutes. In general, the driving force to accomplish desired separation is brought forward by the application of pressure or concentration or potential difference across the membrane.

Membranes have been found to be advantages and promising separation technology when compared to other separation technologies such as adsorption, distillation, extraction and crystallization. In this regard, lower capital cost, higher separation factors, compact design and the elimination of secondary separation units are regarded to be some of the primary advantages of the membrane technology.

The performance of the membrane depends upon various factors such as porosity, pore diameter distributions, particle size distributions amongst the solutes that are processed in addition to the solubility/diffusivity of the permeating molecules. Therefore, membrane technology needs to be studied thoroughly in order to ensure its versatility for industrial applications.

1.2.1 Materials based classification

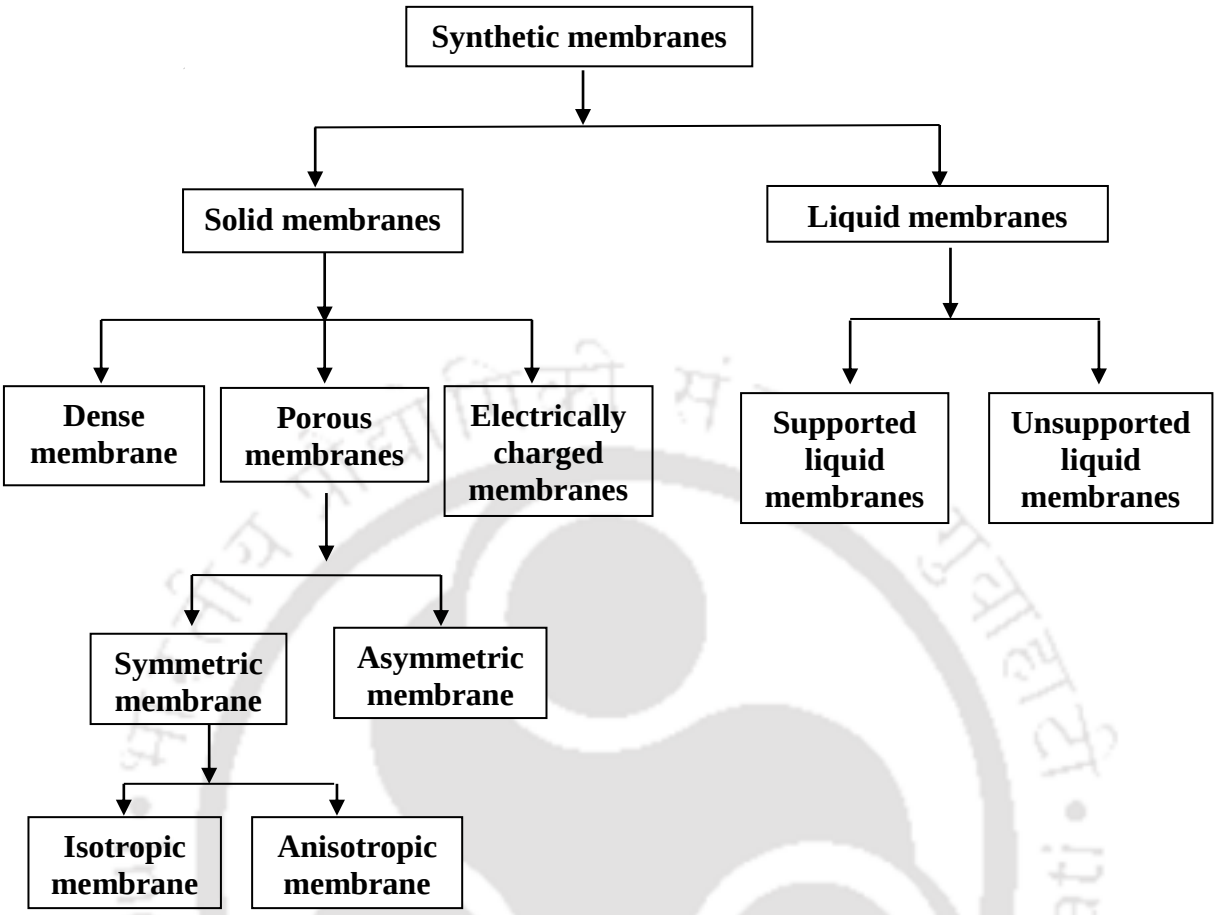

Figure 1.1: Classification of synthetic membranes

In general, membranes can be classified into two major types, namely biological and synthetic membrane (Cheryan, 1998; Mulder, 1991 and Nunes and Peinemann, 2001). While biological membranes refer to those that are present in living cells and aid in cellular functional separations, synthetic membranes are those that are prepared using various materials such as solids and liquids. A conventional example for biological membrane is nephrons present in human kidney which facilitate separation of waste compounds (urea and excess sugars) from the blood in living beings.

The classifications of membranes are presented in Fig.1.1. Generally, solid and liquid membranes constitute synthetic membranes. Solid membranes are further classified into

dense, porous and electrically charged membranes. Porous membranes possess highly void structures with random distribution of inter-connected pores in a mechanically rigid morphology. The separation occurs in these membranes due to the size difference of the particles and membrane pores. However, dense membranes consist of dominating non-porous structures and hence separation occurs due to diffusion and activation phenomena. Electrically charged membranes being porous or dense membranes carry fixed positive or negative charge that aid in the separation of solutions with ions. A further structural classification of various membranes indicates symmetric and asymmetric membranes. Symmetric membranes consist of a single layer with homogenous porous structures. On the other hand, asymmetric membranes possess heterogeneous membrane structure that is accomplished using two or more porous structures or layers. Typically, asymmetric membranes possess thin narrow porous layer on a thick macroporous (wider pore) layer (support). In an asymmetric membrane, while the thin film provides higher separation and permeation characteristics of the membrane, the support provides higher mechanical strength to the membrane with minimum resistance to permeation. Therefore asymmetric membranes are always regarded to be advantageous than symmetric membranes. A pore size distribution based classification indicates symmetric membranes to be either isotropic or anisotropic. While uniform membrane pore sizes throughout the membrane structure are present in isotropic membranes, varied pore sizes throughout the membrane structure are present in anisotropic membranes. Solid phase symmetric and asymmetric membranes are primarily used for pressure driven membrane separation processes.

Based on the different types of materials with which these membranes are fabricated, the membranes are classified as polymeric and ceramic symmetric membranes and polymer-polymer, polymer-ceramic, ceramic-ceramic asymmetric membranes. While symmetric membranes are typically fabricated using single functional materials, asymmetric

multilayered membranes are typically fabricated by depositing a thin film of polymeric, inorganic or any other suitable materials over a porous support.

1.2.2 Separation process based classification

Depending upon the nature of the driving force and transport mechanism of feed materials through the membrane, membrane separation processes can be classified. While some of these processes are well established in the industry, a few of them are still in experimental stages and large scale industrial applications are yet to be realized. Based on the membrane transport mechanism, various membrane separation processes can be classified as follows (Mulder, 1991):

1. **Processes with pressure as driving force** – Microfiltration (MF), ultrafiltration (UF), nanofiltration (NF) and reverse osmosis (RO)
2. **Concentration driven processes** – Gas separation, pervaporation (PV), dialysis, membrane extraction, supported liquid membrane (SLEM) and emulsion liquid membrane (ELM).
3. **Temperature driven processes** – Membrane distillation and thermo-osmosis
4. **Electrically driven processes** – Electrodialysis, electrofiltration and electrochemical ion exchange.

Membrane flow pattern can be classified into either dead end or cross flow. It is based on the relative feed stream direction in conjunction with the membrane orientation. The different flow patterns are depicted in Fig.1.2. In dead end flow pattern, both feed and permeate flow are perpendicular to membrane surface and it is a batch processes. In cross flow pattern, both permeate and feed flow parallel to the surface of the membrane. Cross flow can be operated in co current or counter current mode using a sweep stream. In counter current flow the upstream and downstream moves parallel to the membrane surface in opposite direction. But in co-current flow, the two streams flow in same direction.

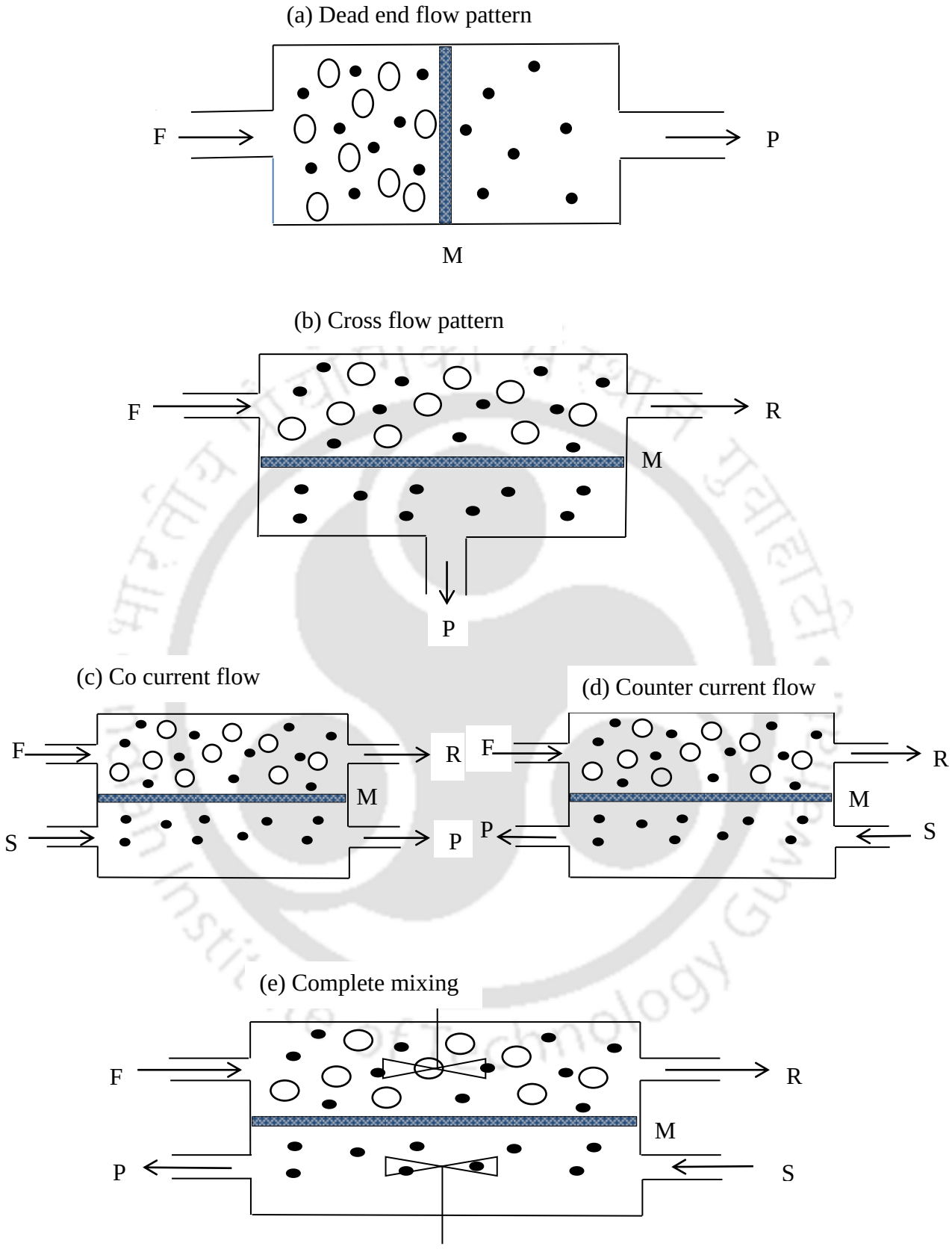

Figure 1.2: Different modes of operation in membrane processes (F-Feed, P-Permeate, R-Retentate, S-Stream and M-Membrane)

1.2.3 Industrial applications of membrane technology

Numerous industrial applications of synthetic solid symmetric and asymmetric membranes exist for MF and UF membranes.

a) Potable water production from alternate sources to remove various particles as well as bacteria

b) Biotechnological applications such as protein recovery, milk concentration and separation of fat from milk.

c) Treatment of industrial waste streams such as oily wastewater, pulp and paper wastewater, leather wastewater etc., for suspended solids removal in the wastewater streams.

d) Production of clarified fruit juices which possess long term storage characteristics and thereby enable the reduction of transportation costs of food products.

The industrial applications of other membrane separation processes such as NF, RO, pervaporation, dialysis, electro dialysis and gas separation are presented as follows:

1. NF and RO: Desalination of sea water to generate drinking water, treatment of various industrial wastewaters, removal of nitrates, fluorides, heavy metals, etc.

2. Pervaporation: separation of organic and azeotropic mixtures (such as ethanol-water) those are difficult to separate using conventional methods such as distillation.

3. Dialysis and electro dialysis: Removal of different harmful components from human blood during kidney failure.

4. Gas permeation: To produce oxygen enriched air, nitrogen enriched air and hydrogen recovery using porous as well as dense membranes. In addition, dense membranes are used to accomplish carrier facilitated separations.

1.2.4 Polymeric membranes

Polymeric materials and ceramics are the most widely used functional membrane materials to prepare symmetric membranes for industrial scale applications. The asymmetric membranes are usually prepared from symmetric polymeric or ceramic membrane materials or both. In an asymmetric membrane, usually the support layer provides desired mechanical strength and the thin skin layer constituting either polymeric or ceramic caters towards the desired separation characteristics.

Polymeric membranes are thin films of 10-100 μm thickness. Different types of polymers such as polysulphone (PSU), cellulose acetate (CA), polyamide (PA), polyethersulphone (PES), Polyvinylidene fluoride (PVDF), polyacrylonitrile (PAN), polytetrafloroethylene (PTFE), polyetherimide (PEI), polypropylene (PP) are widely used to fabricate the polymeric membranes.

Advantages	***Disadvantages***
1. Wider ranges of pore sizes varying from MF to RO are available.	1. Low solvent resistance
2. Comparatively low cost than ceramic membrane	2. Lower applicable range of pH and hence low chemical stability
3. Easy to fabricate	3. Low temperature ranges
4. Ease to scale up	4. Lower life span (12-18 months)

1.2.5 Ceramic membranes

Ceramic membranes are synthetic membranes prepared with inorganic materials such alumina, zirconia, silica, titania, kaolin etc., Ceramic membranes possess superior chemical, thermal and mechanical stability. Usually, ceramic membranes have about 2 – 5 mm thickness for the porous support. Asymmetric ceramic membranes constitute thin film (10-100 μm) of ceramic coating over a thick porous symmetric support.

Advantages	***Disadvantages***
1. Very high corrosion resistance. 2. Applicability to wider pH ranges (0.5-14). 3. Applicability of wider temperature ranges (350-500^{o}C). As a result they are used in industrial scale separations without any feed pre-conditioning steps. 4. Less fouling tendency. 5. Inertness to common chemicals and solvents. 6. Higher mechanical strength.	1. Most ceramic membranes are available in pore diameters within the MF and UF range (0.010 – 10 μm). 2. Comparatively higher cost. 3. They are brittle in nature

1.2.6 Ceramic membrane fabrication methods

Symmetric membranes are fabricated using uni-axial and paste methods (Baker, 2004; Judd and Jafferson, 2003). Both these methods involve the preparation of an inorganic mixture using suitable pore forming organic and inorganic materials along with binder materials. The uni-axial method involves casting an inorganic mixture in a suitable disk or

tubular shape and kept under very high pressure (30-50 MPa). Subsequently, the disk or tubular type mould is sintered to prepare the membrane.

The paste method involves the preparation of a paste using the inorganic mixture using suitable solvent which is eventually casted into suitable shape and sintered at high temperature. The composition of the raw materials, sintering temperature and process including the schedule of heating, sintering and cooling significantly influence the properties and morphology of the ceramic membranes.

Asymmetric ceramic membranes are prepared by allowing the deposition of a thin film of inorganic materials over the porous symmetric ceramic membranes (support). Slip coating followed with casting, sol-gel and dip coating methods are usually deployed for the fabrication of asymmetric ceramic membranes whose properties are dependent upon both support as well as thin skin layer morphology.

Using a suspension of finer particles in cellulosic polymer or polyvinylalcohol (to serve as binder and viscosity enhancement), the slip-coating process involves the coating of the support surface with the said suspension followed with drying and sintering at high temperature to achieve a fine micro porous surface layer.

The literature presents membrane fabrication by targeting specific combinations of raw materials and sintering temperature. Expensive materials, used for many years to manufacture membranes, are now-a-days replaced by low cost clays. Over the past several years, several literatures indicate upon the utility of ceramic membranes for microfiltration of oil-in-water emulsion studies are investigated and understood. In subsequent sections, a detailed review on development of TiO_2 composite membrane along with experimental and application in oil-in-water emulsion treatment is discussed.

1.3 State-of-the-art

In this section, the available prior-art in the field of ceramic composite membrane fabrication and application is being addressed. The available prior-art has been presented for three themes, namely ceramic supports, composite membranes and their applications and application of response surface methodology for microfiltration research. The following sub-sections elaborate upon the available literature data for each case.

1.3.1 Preparation of ceramic membrane supports

Several literatures report upon ceramic membrane fabrication using various raw materials. These are α- alumina, stainless steel (Rs. 150000/m^2) (Judd and Jafferson, 2003; Yoshino et al., 2005; Defriend et al., 2003; Benito et al., 2005), γ-alumina, zirconia, titania and silica etc., (Judd and Jafferson, 2003; Wang et al., 2006; Tsuru, 2001; Falamaki et al., 2004). The cost of these membranes is significantly high due to the higher costs of the raw materials. Hence, from economic perspective, these membranes are not viable for environmental process engineering applications. As an alternative for their economic infeasibility, current research addresses other low cost ceramic membrane precursor utility to reduce the cost.

On the other hand, it is also evident in the literature that fly ash is abundantly available waste material that is often generated from power plants by burning coal. There are good number of litertaures that address the preparation of inexpensive ceramic membranes using cheaper raw materials such as fly ash, raw clay, Moroccan clay, apatite powder, dolomite, kaolin, Tunisian clay, sepiolite clay and Algerian clay (Saffaj et al., 2005; Saffaj et al., 2006; Khemakhem et al., 2006; Weir et al., 2001; Khider et al., 2004; Bouzerara et al., 2006).

In addition, preparation methods for ceramic membrane involve additional fabrication complexities that also contribute to the overall cost. While many fabrication methods exist, Xia and Liu (2001) have opined that uni-axial dry compaction method is a simple, highly cost effective method for laboratory and pilot plant scale ceramic membrane fabrication. In the

next few paragraphs, a brief account of the available prior-art is being presented in the area of ceramic membrane support preparation.

Using dry compaction method, Wang et al. (2008) prepared inorganic membrane using sol-coated alumina powder (mean particle size = 27.5 μm). The membrane sintered at 1350 ºC possessed 39% open porosity, 45 MPa mechanical strength and 7.71 μm average pore size. The authors examined the role of sintering temperature on membrane morphological properties and have concluded that the sol-coating and sintering conditions strongly influence membrane microstructure.

Using high purity α-alumina powder, Shqau et al. (2006) prepared macroporous ceramic membrane support by adopting colloidal processing method and various sintering temperatures. The best membrane has been evaluated to possess 28 nm average pore size and 20 % porosity after sintering was carried out at 1000 ºC.

Using Moroccan clay, Saffaj et al. (2006) prepared ceramic membrane support by extrusion method and sintered at various temperatures. The pore diameter and mechanical strength of the membranes enhanced with increasing sintering temperature. However, the membrane porosity reduced with increased sintering temperature. The optimal membrane corresponds to that prepared at 1225 ºC at which the membrane possessed an average pore size of 10.25 μm and mechanical strength of 10 MPa.

Masmoudi et al. (2007) reported the development of low cost membrane support from natural apatite powder. Extrusion method was adopted by the authors along with alternate sintering temperatures. The obtained result revealed that the pore diameter and mechanical strength increased with increasing sintering temperature and membrane porosity reduced with increasing sintering temperature. With good chemical resistance in basic media (5% weight loss) and poor chemical resistance in acidic media (25% weight loss), the ceramic membrane possessed 6 μm mean pore size and 47% porosity after sintering at 1160 °C.

Bouzerara et al. (2006) reported the preparation of ceramic membrane support from kaolin and kaolin-dolama mixtures. Four different processing routes were investigated with two different configurations (tubular and flat). The tubular support was prepared by extrusion whereas the flat support prepared with dry and roll pressing. Membrane properties such as average pore size, mechanical strength and porosity were investigated with respect to variations in sintering temperature. Their research confirmed that mechanical strength, pore size, porosity and pore size distribution got significantly varied with variations in sintering temperature and processing route. Using extrusion method and sintering temperature of 1250 ^{o}C for 1 h, membranes with 43% porosity, uniform pore size distribution, 28 µm average pore size were obtained. On the other hand, when roll pressing was adopted for same sintering temperature, membranes with higher porosity (51%) were fabricated.

Using Tunisian natural illite clay, Khemakhem et al. (2006) prepared UF membrane by adopting slip casting method for UF layer deposition on the MF support prepared using aqueous colloidal suspension and sintering temperature of 800 ^{o}C. With 185 KDa molecular weight cut off, the membrane water permeability was evaluated as 88 L/h m^2 bar.

Using low cost industrial grade cordierite powder, Dong et al. (2007) targeted the effect of sintering temperature on membrane properties. It has been evaluated that while mechanical strength increased, the porosity decreased with increasing sintering temperature. The optimal condition for membrane fabrication was at 1380 ^{o}C sintering temperature, at which, 8.66 µm pore size and 36.2% porosity were obtained for the membrane with poor corrosion resistance.

Nandi et al. (2008) studied the influence of sintering temperature on porosity, average pore size, mechanical stability and chemical resistance of low cost ceramic membranes. Low cost materials such as kaolin, quartz, calcium carbonate, sodium carbonate, boric acid and sodium metasilicate were used by the authors to infer upon a new formulation and paste method. With increasing sintering temperature, while membrane pore size, mechanical strength and

chemical stability increased, the membrane porosity decreased. At an optimal sintering temperature of 900 ^{o}C, average pore diameter, porosity and mechanical strength were evaluated to be 0.70 µm, 40 % and 6 MPa, respectively.

Monash and Pugazhenthi (2011a) used low cost clays such as kaolin, quartz, ball clay, feldspar, calcium carbonate and pyrophyllite. The membrane support was prepared by uni-axial dry compaction method and sintered at different temperature. Their research affirmed that while porosity reduced, pore diameter, chemical stability and mechanical strength increased with increasing sintering temperature. With good chemical resistance in both acidic and basic media, the membrane sintered at 950 ^{o}C possessed porosity, flexural strength and average pore size of 44%, 28 MPa and 1.01 µm, respectively.

Jedidi et al. (2009) prepared inexpensive microfiltration tubular ceramic membrane using coal fly ash at 800 ^{o}C sintering temperature for 2 h sintering time. The membrane possessed 4.5 µm average pore size and 51% porosity. The authors adopted slip coating method with a suspension of fly ash powder, water and PVA to expound mesoporous layer on the support. Thereby, the active layer with 0.25 µm pore size and 20 µm thickness offered 475 L/m^2 h bar membrane permeability. The membrane was tested for the treatment of dying effluent streams generated after washing operations in textile industry. COD and color removal efficiency of the membrane were evaluated to be 75% and 90%, respectively.

Dong et al. (2011) developed the ceramic support using dry compaction method and industrial waste fly ash and natural bauxite as raw materials. The average particle size of the flyash, bauxite and mixture were evaluated as 1.76, 1.13 and 1.52 µm, respectively. It has been evaluated that the open pore size and porosity of the ceramic membrane reduced with increasing sintering temperature.

Thomas et al. (2011) prepared fly ash based membrane for microfiltration of mining waters. Initially, fly ash was grinded to get particle size less than 63µm for fabricating porous module

using mould casting method and sintered at 1000 ^{o}C. The final skin layer was fabricated using similar constituents such as fly ash, PVA and NaOH and the membrane was sintered at 1000 ^{o}C for 5 hr. With good combinations of mechanical strength and thermal stability, the average membrane pore size and porosity were evaluated as 0.026-0.063 μm and 49%, respectively. Using mining water, membrane flux and permeability were evaluated.

Fang et al. (2011) prepared tubular shaped ceramic membrane by slip casting method by using refined fly ash with three different sizes (15.41, 5.01 and 1.41 μm). Initially, macro porous fly ash based support was fabricated by extrusion method using fly ash with larger particle size, methylcellulose, and water. For the membrane fabrication, the sintering temperature was 1190 ^{o}C for 2 h. The intermediate layer and tope layer were deposited on support by adopting slip casting method and two different sintering temperatures. The average pore size of the support, intermediate layer and top layer were evaluated as 2.13, 1.94 and 0.77 μm, respectively. The performance of the support and multiple coated membranes indicates good water flux and permeability. At a pressure of 0.1 MPa and room temperature, the water flux of the support, intermediate layer and top layer were evaluated to be 2.26, 1.86 and 1.56×10^{4} L/m^{2} h bar, respectively.

The fuel cell performance of low cost ceramic membranes were investigated by Fukui et al. (2009). The authors utilized fly ash generated from waste incineration and chicken bone powder as raw materials to achieve calcium phosphate hydrogel membrane. To achieve the said membrane, the authors used amorphous calcium phosphate hydro gel along with said raw materials. After melting the mixture in air at 1200 ^{o}C for 30 min, the mixture was poured on an iron plate. Subsequently, the membrane electrode assembly was fabricated to achieve 50.0 μm thick crystallized calcium phosphate hydrogel layer on a carbon electrode with Pt

catalyst layer and thin gas diffusion layer. It was evaluated that the mechanical strength of the calcium hydrogel layer increased after drying the anode for 24 h at room temperature.

Using refined fly ash as raw material and by adopting slip casting method, Fang et al. (2013) prepared asymmetric MF ceramic membranes. After fabricating macro porous fly ash based support, the authors prepared aqueous fly ash solution with 3 wt% to achieve skin layer on the inner surface of the membrane support. Subsequently, the membrane was sintered at 1000 ^{o}C. For multiple coatings, the authors used a freshly prepared fly ash suspension with a concentration of 2.0 wt. % and used similar drying and sintering conditions that were adopted for the support. The membrane with 0.77 µm pore size provided higher water flux of 1.56×10^{-4} L/m^2 h. At 0.1 MPa transmembrane pressure, the prepared membrane was used for MF of particle suspension and oil-in-water emulsions. The membrane provided higher membrane fluxes of 2270 L/m^2 h and 159 L/m^2 h for particle suspension and emulsion separation studies respectively. Corresponding separation efficiencies were 99.9 % and 95.5 %, respectively.

Adopting uni-axial dry compaction method, Dong et al. (2010) prepared porous mullite membranes by using fly ash, calcined bauxite and titania (sintering additive). The authors examined the role of titanium dioxide on the sintering behavior and main properties of porous mullite. With increasing titania content (0 – 6%), it was observed that the sintering ability and mechanical strength of the membranes increased and the average pore size of the membrane decreased from 7.28 to 6.28 µm. For all cases, the pore size distribution referred to bimodal distribution in pore sizes.

Using coal based fly ash, Jedidi et al. (2011) reported the preparation of extrusion based ceramic membrane support fabrication at a sintering temperature of 1125 °C. The membrane average pore size and porosity were evaluated as 4.5 µm and 51%, respectively. Along with these, mechanical strength and corrosion resistance were also studied. Further, slip casting

method was adopted at 800 ^{o}C sintering temperature to achieve a skin layer with 0.25 µm pore size. The composite membrane provided a water flux of 475 L/h m^2 bar. Also, the obtained membrane properties such as membrane flux and separation efficiency were compared with those of alumina based membrane.

Using fly ash and titania as raw materials, Jo et al. (1997) prepared fly ash and titania membranes by adopting dip coating procedure and stainless steel mesh substrates. The coating was achieved by preparing an optimal composition of a suspension with fly ash or titania, distilled water, PVA, Glycerol (plasticizer) and dispex (dispersant). For fly ash and titania membranes, the average pore size was 2.5 and 0.2 µm, respectively. The apparent air permeability for the membranes were evaluated as 7.0×10^{-14} m^2 and 2.1×10^{-15} m^2 at 450 ^{o}C.

Using coal based fly ash and extrusion method, Jedidi et al. (2009) prepared porous tubular supports. The fly ash powder was prepared by burning charcoal at 800 ^{o}C. The plastic ceramic paste was prepared with the resultant powder (84%), organic additives (4% amijel, 4% methocel), porosity agent (4% starch) and water. After sintering at 1125 ^{o}C, the membranes were evaluated to have a pore diameter of 4.5 µm and porosity of 51%.

Dong et al. (2006) reported the membrane preparation using fly ash and magnesium carbonate. Initially, the green bars were prepared by uni-axial cold pressing. Subsequently, tubular supports were prepared using extrusion method at a sintering temperature of 1380 ^{o}C. Eventually, using a mixture of fly ash powder and magnesium carbonate and by adopting modified dip coating method, skin layers were achieved at various sintering temperature. The membrane support possessed an average pore size of 18.0 µm, porosity of 41.1% and mechanical strength of 28.7 MPa. For membranes prepared at various sintering temperature, the average pore size of composite membrane and nitrogen permeance were evaluated to be 3.6-6.4 µm and 7.52-9.82 $\times10^{4}$ m^3/m^2 h MPa, respectively.

1.3.2 Preparation of composite membranes

Composed of inorganic oxides, ceramic membranes have excellent combinations of chemical resistance, mechanical strength, thermal stability, higher selectivity and applicability for high temperature and corrosive process environment. It is well known that the membrane performance is dependent upon various properties such as pore size distribution and average porosity of the membrane, particle size distribution of the solutes and solubility/diffusivity of the permeating molecules.

Usually, ceramic membranes are prepared by simple preparation methods such as uniaxial compaction, paste method. In these methods, a symmetric support is generally prepared by shaping powder in a die and subsequent consolidation of green body using sintering process. A schematic of ceramic support fabrication is presented in Fig. 1.3. Both uniaxial compaction and paste methods involve the preparation of an inorganic mixture using suitable pore forming organic and inorganic materials and binder materials. The uniaxial compaction method involves casting an inorganic mixture in a suitable disk or tubular by applying higher pressure in the casting process (30-50 MPa). Subsequently, the disk or tubular type mould is sintered to prepare the membrane. The paste method involves the preparation of a paste using inorganic mixture with suitable solvent, which is eventually casted into suitable shape and sintered at high temperature. Thereby, the ceramic membrane properties are strongly influenced with the raw materials composition, sintering temperature and process including the schedule of heating, sintering and cooling. On the other hand, asymmetric ceramic membranes are prepared by facilitating the deposition of thin film of inorganic materials on porous symmetric ceramic membranes (support). Usually, slip casting followed with casting, sol-gel and dip coating methods are adopted for asymmetric membrane fabrication. The skin layer morphology is strongly influenced with the particle size of deposited materials and morphology of the support.

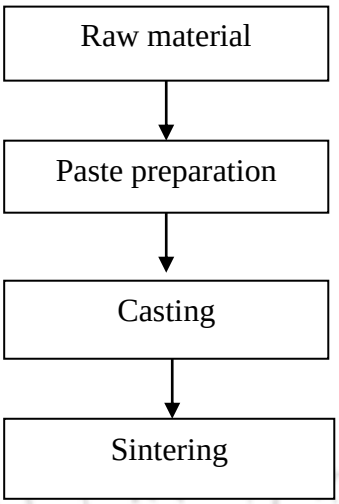

Figure 1.3: Flow chart displaying the steps involved in ceramic membrane preparation by paste method

Using hydrothermal crystallization approach, analcime zeolite composite membranes were prepared by Potdar et al. (2002) on clay supports. Eventually, gas phase nitration was conducted by using nitrous oxide gases (NOx) and the nitrated zeolite was aminated with hydrazine hydrate. Subsequently, unmodified, nitrated and animated zeolite membranes were investigated for surfactant separation using ultrafiltration process. The authors inferred that surface modification allowed 300% enhancement in surfactant retention along with an enhancement in the membrane flux.

Kazemimoghadam et al. (2004) prepared the Zeolite NaA and hydroxy sodalite membranes. The membranes were prepared by coating of these materials on the porous mullite support made by extrusion method and the supports were sintered at 1250 ^{o}C for 5 h. It was analyzed that while separation factor for hydroxyl sodalite based membrane is higher than that obtained for NaA membrane, it offers lower flux. Therefore, for lower concentration of unsymmetrical dimethylhydrazine (UDMH), zeolite NaA membrane has been opined by authors in comparison with hydroxyl sodalite membrane and vice-versa.

Erdem et al. (2006) adopted a two-step approach for ceramic composite membrane fabrication in which the first step refers to slip casting followed with dip-coating to fabricate thin selective layers subsequently in the second step. With an average porosity of 40%, the membrane has been evaluated to have excellent lactose separation characteristics in which the solute is characterized with high protein content (80%) and relatively low lactose retention (7%). The membrane flux was evaluated to be 40 L/m^2 h.

Adopting porous clay supports, Workneh et al. (2008) allowed the deposition of sodalite octahydrate zeolite particles to partially block the mouth of the porous structure. Also, casting method was adopted by the authors using low cost inorganic precursors to obtain the support with average pore size of 0.2 microns and 51% porosity. During the separation studies conducted for SDS (Sodium dodecyl sulfate), the maximum rejection of 46% was obtained for a feed concentration of 10 g/L at a membrane flux of 1.2×10^{-5} (m/s).

Cross-linked poly methyl methacrylate-ethylene glycol dimethacrylate (PMMA-EGDM) UF membrane was fabricated by Neelakandan et al. (2003) in which low cost inorganic precursors were used to prepare the ceramic support. Following the preparation of the support, the polymer composite membrane was prepared by coating the polymeric material followed with cross-linking at 60 ^oC. During separation studies conducted for Cr (VI), the modified PMMA membrane provided higher membrane flux in comparison with the unmodified membrane.

Shukla et al. (2007) reported the modification of zeolite-clay composite ultrafiltration membranes and applied to the chromic acid separation from its solution. Initially, the membrane support coated with kaolin by dip coating method and sintered at 900^oC for 8h. Further, insitu crystallization allowed zeolite to fill up the membrane pores and reaction with NOx was facilitated to achieve chemically modified zeolite membrane. The modified

membrane with 10-30 nm surface pore size provided a rejection of 74% for the chromate ions in aqueous solution.

Adopting two-stage modification technique, Pugazhenthi et al. (2005) prepared non-interpenetrating charged carbon UF membrane. In the fabrication procedure, the authors reported that the first step consists of nitration of carbon membrane using NOx at 250 ^{o}C and subsequent amination with hydrazine hydrate at 60 ^{o}C to induce charge on the membrane. The pore radii of unmodified, nitrated and animated carbon membranes were 2.0, 2.8 and 3.3 nm, respectively. During Cr (VI) separation from aqueous solution, for the said sequence of membranes, the rejection was evaluated as 96%, 84% and 88%, respectively.

Alem et al. (2009) prepared disk-shaped ceramic membrane using α-Al_2O_3 by adopting uni-axial pressing method. With an applied pressure of 31 MPa, the membrane was sintered at 1350 ^{o}C to achieve 15 mm diameter, 2 mm thickness and 38% porosity.

Chowdhury et al. (2003) prepared disk shaped support with α-Al_2O_3 as raw material using the colloidal filtration method. Their process involved sintering of the support at 1100 ^{o}C. The composite membrane with ~1 µm support thickness and ~30 nm thickness surface silica layer has 0.08-0.12 µm pore size and MCM-48 structure.

Patterson et al. (2006) prepared tubular shaped support with α-Al_2O_3 as raw material using centrifugally casted method and sintered the support at 1200 ^{o}C. The membrane was subsequently subjected to dip-coating with an average pore size of 0.16 µm.

Basumatary et al. (2016) synthesized zeolite composite membranes with a pore size of 0.142-0.173 µm. The zeolite membranes refer to MCM-41, MCM-48 and Faujasite (FAU) zeolite based membranes that were fabricated on ceramic support using hydrothermal method. Subsequently, the membranes were applied to cross flow microfiltration of Cr (VI) from aqueous solution. Membranes provided 82% (FAU), 75% (MCM-41) and 77% (MCM-48) of

Cr (VI) removal efficiency using the feed concentration of 1000 mg/L and cross flow rate of 1.11×10^{-7} m^3/s, at 345 kPa of applied pressure.

In another work, Basumatary et al. (2016) investigated the potential of MCM-48 ceramic composite membranes by separation of $FeCl_3$ from aqueous solution. The membrane was characterized to have porosity and an average pore size of 22% and 0.142 µm, respectively. With $FeCl_3$ salt solution concentration of 250 mg/L, pH of 2, and 276 kPa applied pressure, the maximum observed rejection was found to be 86%

Kumar et al. (2015) prepared zirconia-ceramic composite membrane through in-sity hydrothermal method using zirconium oxychloride as a sintering material. The hydrothermal crystallization process was carried out at 90 °C for 60 h and finally calcined at 400 °C for 6 h. The zirconia membrane possessed 42% porosity, 0.66 µm average pore size and 1.44×10^{-6} m^3/m^2 s kPa water permeability. The membrane attained 61% of methyl orange rejection from aqueous solution and permeate flux of 2.28×10^{-5} m^3/m^2 s at 68 kPa.

A summary of literature data with respect to classification based on support preparation is presented in Table 1.5.

Table 1.5: Literature data summary for ceramic supports

Author	Raw Material	Method of preparation	Sintering Temperature (°C)	Pore size (μm)	Porosity (%)
Wang et al. (2008)	α-Al_2O_3	Dry compaction	1350	7.71	39
Shqau et al. (2006)	α-Al_2O_3	Colloidal processing	1000	0.028	20
Saffaj et al. (2006)	Moroccan clay	Extrusion	1225	10.25	-
Masmoudi et al. (2007)	Natural apatite powder	Extrusion	1160	6	47
Bouzerara et al. (2006)	Kaolin and dolama	Extrusion	1250	28	43
Dong et al. (2007)	Cordierite	Extrusion	1380	8.66	36.2
Nandi et al. (2008)	Clays	Paste	900	0.7	40

1.3.3 Literature review for titania coating on ceramic membrane support

Titania composite membrane with nano-structural morphology has been fabricated by Alem et al. (2009a) using sol-gel method. The authors opined that membrane thickness, calcination time and calcination temperature strongly influence its photo-catalytic characteristics. The optimal membrane with a thickness of 1 μm was prepared with titania sol (made with tetra-isopropyl orthotitanate containing organic additives, hydroxylpropyl methycellulose (HPMC) and polyvinylalcohol). The membrane was calcined for 1 h at 450 °C at a heating rate of

10°C/h. The sintered alumina support at 1350 °C for 1 h possessed 38% porosity and permeability of 52.61 cm^3 /min bar cm^2. The composite membrane possessed 4.7 nm average surface pore size and 30.09 cm^3 /min bar cm^2 water permeability.

Wang et al. (2007) have prepared tubular shaped 100% pure titania membrane and studied the effect of sintering on open pore structure and chemical stability. Rutile support with 2.1 µm average pore size, 43.09% porosity, 1641 m^3/m^2 h bar water permeability was prepared by the authors. Titania sol was prepared using hydrolyzed $TiSO_4$ in acidic conditions in tri-ethanol amine and polyvinyl alcohol media at room temperature. Subsequently, anatase powder with 0.37 µm average particle size was used to dip coat the rutile membrane and eventually sintered at 500-700 °C for 2h. The prepared composite membrane possessed an average pore size of 100 nm and active membrane layer thickness of 15-20 microns. The composite membranes exhibited higher membrane flux and insitu photocatalytic behavior during degradation of methylene blue dye in synthetic aqueous media.

Patterson et al. (2006) carried out direct dip-coating of anatase to achieve defect free titania composite membrane using α-Al_2O_3 tubular support. The ceramic support with average pore size of 1600 nm was centrifugally casted to achieve a titania top layer thickness of 1.5 – 1.6 microns. The sintering was carried out at 450 °C for 30 min. The authors reported that the water permeability for support and membrane was 40.8 and 9.72 L/m^2 h bar, respectively. The average pore size of titania top layer was 300 – 500 microns with which a retention of 4% ethanol and 53.7% isopropanol was obtained with an average separation factor of 2.64.

Chou et al. (1999) have made ceramic supports using mixtures of alumina and kaolin by adopting dry pressing method. They have used anatase titania particles of two average sizes (0.5, 0.03 µm) to coat two layers on the ceramic support and sintered the membranes at 900 and 750 °C. As a result, the authors evaluated that the membrane average pore size is about 0.8 and 0.12 microns and the gas permeability was 250×10^{-7} mol/m^2 s Pa. It was also

observed that the variations in porosity and average pore size are a function of membrane layer thickness.

Adopting sol-gel method, Alem et al. (2009b) have prepared mesoporous photocatalytic titania multilayer membrane on α-Al_2O_3 support. Polymeric titania sol was prepared with tetra-isopropyl orthotitanate as a titania precursor along with other chemicals such as nitric acid, isopropanol in aqueous media. The membrane was calcined at 450 ^oC for 1 h. The prepared membrane with an average pore size of 11.7 nm and minimum particle size of 5.8 nm and lowest pore size of 4 nm was evaluated to have 83 m^2/g surface area and lower crystallinite size (10.3 nm). For methyl orange degradation, the titania multi-layer membrane was evaluated to allow 41.9% degradation after 9 h of UV irradiation.

Saffaj et al. (2004) studied the performance of TiO_2-$ZnAl_2O_4$ multilayer UF membranes prepared with cordierite support. Using cordierite particles in the range of 0-125 μm, the support was fabricated with a heating rate of 5 ^oC/min and with a sintering temperature of 1275 ^oC for 1 h. The prepared cordierite tubular support possessed an average porosity and pore size of 40% and 7 μm, respectively. Subsequently, the intermediate layers on microporous support were prepared with slip casting of powdered zirconia suspension. The sintered zirconia composite membrane at 1100 ^oC for 2 h possessed an average pore size and thickness of 0.23 μm and 23 μm, respectively.

The top layer in the UF membrane was prepared by sol-gel method using titania sol (titanium isopropoxide, nitric acid solution, and water mixture) and zirconia sol ($ZnAl_2O_4$ boehmite solution, zinc nitrate solution, deionized water and hydroxyethyl cellulose mixture). TiO_2–$ZnAl_2O_4$ sol coated cordierite tubular support was sintered at 400 ^oC for 2 h. The composite UF membrane has been characterized with 6.3 L/h m^2 bar water permeability, 1.2 μm average thickness and 4 nm average pore size. The membrane performance was further tested for the separation of methylene blue and Cr(III), Pb(II) and Cd(II) containing aqueous solutions. It

was also affirmed that the interaction with NaCl and Na_2SO_4 containing solutions altered solute rejection rates.

A summary of literature data available for the preparation of titania membranes with alternative titania precursors is presented in Table 1.6.

Table 1.6: Literature data for TiO_2 based composite membranes

Author	Membrane material	Method	Pore size (μm)	Porosity (%)	Sintering Temperature (°C)	Calcination Temperature (°C)
Chou et al. (1999)	Alumina, Kaolin, Titania	Sol-gel process	0.12, 1.5	40	900	750
Wang et al. (2007)	Titanium sulfate (Anatase), PAA	Sol-coated process	0.10	-	1200	500-700
Patterson et al. (2006)	Titanium(IV) butoxide, α-Al_2O_3	Dip coating	0.3-0.5	-	-	450
Saffaj et al. (2004)	Titanium-isopropoxide, HNO_3, $ZnAl_2O_4$, cordierite	Sol-gel process & slip casting	0.004	40	-	400
Alem et al. (2009)	Tetra isopropyl-Orthotitanate, HPMC, H_2O, PVA, α-Al_2O_3	Sol-gel process	0.0047	38	1350	450

1.3.4 Ceramic membrane based microfiltration of oil-in-water emulsions

Various industries, including metallurgical, petroleum, and food processing produce highly concentrated (500-1000 mg/L) oil-in-water emulsions (Ezzati et al., 2005; Mohammadi et al., 2004; Abadi et al., 2011), which are harmful threat to aquatic and human life. The destructive impact of oil-in-water emulsions on ecosystems and environment necessitates the separation of oil from oily wastewater from ecological safety perspective (Yang et al., 1998). Thereby, maximum discharge values have been set to restrict oil/grease concentration in

industrial effluents by pollution control board and several government agencies. Therefore, several researchers have been exploring new technologies and to upgrade existing technologies to produce treated oily wastewater with oil concentration below the standard discharge limit i.e. 5-10 mg/L (Cumming et al., 2000; Hua et al., 2007; Abadi et al., 2011; Cui et al., 2008). In the last two decades, several methods such as electrocoagulation process (Bensadok et al., 2008), coagulation (Zouboulis et al., 2000), dissolved air floatation (Al-Shamrani et al., 2002), gravity separation (Krebs et al., 2012), de-emulsifications process (Salam et al., 2013), skimming (John, 2010) and flocculation (Kang et al., 2012) have been suggested and studied for the separation of oil from oily wastewater. Among these, many methods are not efficient to achieve the norms/standards set by the pollution control agencies. Further, they also produce a secondary waste stream/product in large quantities (Ahmadun et al., 2009). In the past few years, owing to their promising features such as higher chemical, mechanical and thermal stability, longer shelf life, excellent defouling characteristics, good combinations of separation efficiency and membrane flux and susceptibility and ease for process clean up, there is a renewed interest in ceramic membranes for industrial applications. (Abadi et al., 2011; Zhong et al., 2003; Monash and Pugazhenthi, 2011). Thereby, ceramic membrane technology has been proven for the treatment of industrial effluents, including pharmaceutical, beverages, refinery, dairy, food and electronic industry (Singh, 2015).

Cui et al. (2008) prepared NaA/Al_2O_3 zeolite ceramic composite membranes with average pore sizes of 1.2 µm, 0.4 µm and 0.2 µm. Thereby, membranes with pore sizes of 1.2 and 0.4 µm were utilized for oil-in-water emulsion treatment at a feed concentration of 100 mg/L. The authors reported that the permeate contained oil concentration lower than 1 mg/L and the wider pore size membrane provided 99% oil rejection and 95 L/m^2 h at 50 kPa trans-membrane pressure.

Nandi et al. (2010) reported mixed clay based membranes for oil-in-water emulsion treatment. For a feed concentration of 250 mg/L, the authors reported 98.8% oil rejection and 5.36×10^{-6} m^3/m^2 s flux after 60 min of dead end MF at 68.95 kPa trans-membrane pressure.

Using commercial ceramic membrane, Lobo et al. (2006) studied the effect of pH and cross flow velocity on the ultrafiltration of oil-in-water emulsion. They observed that the COD retention varied from 92-96% and decreased significantly at lower pH of the solution. The authors also observed higher concentration polarization at lower cross flow velocity.

Rezvanpour et al. (2009) used two commercial membranes (cellulose and polysulphone) to study the effect of different parameters (type of membrane, transmembrane pressure, feed concentration, cross-flow velocity and pH) on the ultrafiltration of kerosene-water emulsion. Their results affirmed upon higher permeate flux for membrane with high pore size and stronger hydrophiliicity and constant permeate flux at 3 bar. Further, the authors reported that the membrane flux reduced with feed oil concentration and did not enhance significantly with variation in cross-flow velocity, pressure and pH.

Yang et al. (1998) have prepared ZrO_2/α-Al_2O_3 composite ceramic membranes with pore size of 10 nm, 0.2 μm, 1.0 μm and 0.2 μm for oil-in-water emulsion treatment. The experiments were conducted at 0.1-0.15 MPa transmembrane pressure and 3-5 m/s surface velocity. The membranes provided an oil rejection and membrane flux of 99.8, 99.9, 94.3, 99.8% and 18, 22, 27, 93 L/m^2 h bar, respectively.

Hua et al. (2007) reported the performance of α-Al_2O_3 ceramic membranes with an average pore size of 50 nm for oil-in-water emulsion treatment. The authors investigated the effect of various operating parameters including trans-membrane pressure (TMP), cross flow velocity (CFV), feed oil and salt concentration and pH on total orgonic carbon (TOC) removal and membrane flux. The authors obtained 92.4% TOC removal efficiency for all experimental

conditions and higher membrane flux at combinations of higher TMP, higher CFV and lower feed oil concentration. Further, membrane flux increased significantly for pH variation from 3.8 – 5.8.

Cumming et al. (2000) used polyvinyl-pyrrolidone (PVP) coated commercial membranes with various pore sizes (2, 5, 8 and 10 μm) for microfiltration of oil-in-water emulsion. They studied the influence of pore size on filtration flux and oil rejection for 1000 mg/l feed oil concentration. The 2 μm filter exhibited a membrane flux of 215 L/m^2 h at trans-membrane pressure (TMP) of 450 Pa which reduced to 107 L/m^2 h at a TMP of 2860 Pa. The larger pore size (5, 8 and 10 μm) filters exhibited flux values of 202, 227 and 381 L/m^2 h, respectively at 450 Pa, which are comparable to that obtained for 2 μm filter. The authors also predicted oil rejection for all membranes using relevant modeling procedures. It has been reported that the predicted rejection was significantly close to that measured for 2 μm filter (99-96% at 470 – 2800 Pa TMP). Also, the deviation between predicted and measured rejection has been evaluated to be increasing with an increase in the pore size of membrane.

Using sol-gel method, Benito et al. (2005) deposited intermediate α-Al_2O_3 and top γ-Al_2O_3 layer on alumina supports. The composite membrane has been characterized to possess a top layer with 4 nm average pore size and 72% porosity. The authors investigated the effect of sol concentration and calcinations temperature on the membrane structure to achieve optimal pore size and porosity.

Mueller et al. (1997) used α-alumina ceramic membranes (0.2, 0.8 μm pore size) and surface modified polyacrylonitrile membrane (0.1 μm) for the cross flow microfiltration of oil-in-water. The membranes were evaluated to have significant fouling and flux decline during MF operation. The membranes provided different initial fluxes which culminated to be similar final fluxes (30-40 kg/m^2 h) after 2 h of MF with 250 ppm feed oil concentration at 10 psig trans-membrane pressure (TMP).

Zhong et al. (2003) studied oil-in-water emulsion treatment using flocculation and subsequent MF based treatment of flocculated effluents using 0.2 μm ZrO_2 membrane. Their investigations affirmed that flocculation reduced membrane fouling and enhanced membrane flux and permeate quality. The authors also evaluated the effect of TMP, CFV on flux and permeate quality. Based on their investigations, the authors reported that the optimal TMP and CFV values are 0.11 MPa and 2.56 m/s, respectively.

The treatment of oil-field produced waters was conducted by Ebrahimi et al. (2009) using various membranes. The authors carried out cross-flow MF pre-treatment with optional UF and NF processes to evaluate upon average flux and TOC removal efficiency. The MF process involved the utilization of 0.1 and 0.2 μm membranes. The 0.1μm membrane exhibited membrane flux variation from 1150 – 200 L/m^2 h for a time period of 1 – 5 h with 58-59% oil and 33.39% TOC removal at 1 bar TMP. The 0.2 μm membrane provided flux decline from 300 to 55 L/m^2 h and 82% of oil, 27% of TOC removal at 1 bar TMP. Utilizing a 0.05μm membrane, the UF process achieved 99% of oil, 39% of TOC removal at 1 bar TMP for 120 min time period. Similarly, the NF process was reported to provide 84% oil removal at 1 bar and 60 min time period.

With alumina as support, Wang et al. (2000) used alumina and zirconia as top layers for two different membranes for the treatment of waste rolling emulsion. The membranes with an average pore size of 0.1 – 0.2 μm were evaluated to provide good combinations of oil rejection (99.9% and 99.8% for zirconia and alumina composite membrane, respectively) and membrane flux (100 L/m^2 h and 43 L/m^2 h for zirconia and alumina composite membrane, respectively).

Hyun et al. (1997) used commercial α-alumina tubes (35% porosity and 0.8 μm average pore size) and prepared alumina and zirconia composite membranes by coating slurries (α-alumina slurry with particle size of 0.6 μm; zirconia slurry with particle size of 0.4 μm; 2-propanol as

dispersion medium and ethyl cellulose as binder) on support surface via reverse dip-drawing technique. The membranes were calcined at 1200 and 950 °C, respectively. The effective average pore size of alumina and zirconia membranes were 0.16 µm and 0.07 µm, respectively. Oil (Kerosene) separation ability of membranes were tested in the crossflow microfiltration system at transmembrane pressure of 0.98-2.94 bar, cross flow velocity of 0.27-0.55 m/s and oil-in-water emulsion concentration of 600-11000 ppm. At lower feed concentration of 600 ppm, TMP 2.94 bar, CFV at 0.27 m/s condition, alumina membrane exhibited flux of 280 (L/m^2 h) and 95.7% rejection of oil, while zirconia membrane provided 40 (L/m^2 h) flux and 96.7% oil rejection.

Li et al. (2006) fabricated surface modified Al_2O_3 membrane for the treatment of oil-in-water emulsions (15.5 mg/L) in cross flow operation. The authors achieved 98.04% rejection and 149.81 L/m^2 h bar membrane flux at 7.8 m/s cross flow velocity.

Zhou et al. (2010) used a commercial tubular alumina membrane (average porosity of 40% and average pore size of 0.2 µm) and fabricated zirconia-alumina composite membrane by dip coating method for the treatment of engine oil emulsions (20 engine oil (1 g/L), Tween 80 (0.5 g/L), span 80 (0.5 g/l) with an average droplet size of 1.79 µm. The authors obtained a maximum permeate flux of 506 L/m^2 h and rejection of 97.8% for zirconia-alumina at cross flow velocity of 5 m/s and TMP of 0.16 MPa.

Abbasi et al (2010) used kaolin, clay and alumina powder to fabricate mullite and mullite-alumina based ceramic membrane for the cross flow microfiltration of oil-in-water emulsions with a feed concentration of 250 mg/L. Cylindrical shaped mullite membrane was prepared with extrusion method and calcined at 1250 °C (1350 °C for mullite-alumina). The prepared mullite membrane possessed an average pores size of 0.289 µm, porosity of 32% (56% for mullite-alumina) and provided a membrane water flux of 18 L/m^2 h (582 L/m^2 h for mullite-alumina) at 1 bar and 1 m/s CFV. The authors reported a maximum membrane flux of

72.7 L/m^2 h (244 L/m^2 h for mullite-alumina) and rejection of 93.8% (81.3% for mullite-alumina) for the mullite membrane.

Abadi et al (2011) used a tubular commercial ceramic α-alumina membrane for the microfiltration of oil-in-water emulsions in cross flow operation. The prepared membrane with an average pore size of 0.2 μm and 33% porosity provided a maximum membrane flux of 290 L/m^2 h at 1.25 bar TMP, 2.25 m/s and 32.5 °C.

Masoudnia et al. (2013) used 0.45 μm pore sized polivinylidene fluoride (PVDF) membrane for the treatment of 3000 ppm synthetic oil-in-water emulsion. For a cross-flow Reynolds number of 2500 and 1 bar TMP, the membrane provided 80% oil removal and membrane flux of 1151.2 kg/m^2 h.

Vasanth et al. (2013) prepared kaolin membrane for the microfiltration of oil-in-water emulsions using cross flow operation. The prepared membrane has an average pore size of 1.06 μm and porosity of 26%. The authors reported a maximum membrane flux of 1990 L/m^2 h and rejection of 87% at 207 kPa.

Zhu et al. (2016) applied TiO_2-Mullite composite membrane for the treatment of 200 mg/L oil-in-water emulsion. The authors obtained maximum membrane flux (150 L/m^2 h bar) and rejection (97%) at 0.025 bar and 0.15 m/s cross flow velocity.

Hu et al. (2015) modified commercial Al_2O_3 MF membrane (average pore size 200 nm) with graphene oxide (GO) by adopting vacuum based transfer method. The membranes were subjected to cross flow microfiltration of oil-in-water emulsion (Machine oil concentration of 1 g/L; average droplet size of 1.8 μm) at 1 bar TMP and cross flow rate of 5 m^3/h. The modified membranes provided a flux of 667 L/m^2 h bar, (522 L/m^2 h bar unmodified) and 98.7% of rejection (98.1% unmodified), respectively.

A summary of literature reviews on separation of oil-in-water emulsion with various membranes is listed in Table 1.7.

Table 1.7: Literature reported data for (a) dead-end and (b) cross flow MF of oil-in-water emulsions.

(a) Dead end flow

Author	Pore Size (μm)	ΔP (kPa)	C_0 (mg/L)	Membrane flux (m^3/m^2 s)	Rejection (%)
Monash and Pugazhenthi, (2011)	1.30	276.4	125	2.21×10^{-6}	85
Nandi et al. (2009)	0.98	345.4	200	2.31×10^{-7}	96
Vasanth et al. (2011)	0.55	41.37	50	3.28×10^{-7}	97.3
Vasanth et al. (2013)	1.06	69	200	2.34×10^{-6}	96

(b) Cross flow

Author	Type of membrane	Pore size (μm)	C_0 (mg/L)	CFV (m/s)	ΔP (kPa)	Membrane flux (m^3/m^2 s)	Rejection (%)
Li et al. (2006)	Al_2O_3-PVDF	-	15.5	7.8	100	4.16×10^{-5}	98.04
Hua et al. (2007)	α-Al_2O_3	0.05	500	1.68	100	1.78×10^{-5}	98.1
Zhou et al. (2010)	ZrO_2-Al_2O_3	0.2	1000	5	0.16	-	98.7
Abadi et al. (2011)	α-Alumina (Commercial)	0.2	92	2.25	127.1	69.4×10^{-6}	95
Abbasi et al. (2010)	Mullite-alumina	0.57	500	1.5	305.1	27.7×10^{-6}	93.8
Vasanth et al. (2013)	Low cost clays	1.06	100	13.9 $\times10^{-7}$ m^3/s	207	55.4×10^{-6}	87

1.3.5 Response Surface Methodology (RSM)

The removal of oil droplets from oil-in-water emulsions depends on the feed characterization parameters, membrane properties and operating parameters. In general, initial feed concentration, applied pressure and cross flow rate are prominent microfiltration process parameters that critically influence the process efficacy (Masoudnia et al., 2013). Based on rigorous experimentation and modeling approaches, optimization methodologies can be adopted to identify optimal process variables in the MF of oil-in-water emulsions. Optimization of MF process parameters is extremely important to visualize the potential of the membrane process in terms of cost minimization for desired flux and rejection combinations (Montgomery, 2001).

While classical optimization processes are well known for process optimality, they require efficient model development that demands significant man power requirements for model fitness and experimental investigations. On the other hand, multivariate statistical methods are highly effective and preferable for the study of interactions among factors and thereby allow the identification of optimal process parameter values for which treatment cost and operational time would be minimal (Montgomery, 2001). The statistical experimental design implicates the approximating the coefficients involved in the mathematical model, checking the adequacy of the model and predicting the response. Many researchers used central composite design (CCD) method to estimate response surface (Montgomery, 2001; Abadikhah, 2015).

Recently, few researchers (Salahi et al., 2013; Abadokhah et al., 2014; Jokic et al., 2010; Rastegar et al., 2011) used RSM to analyze the variation of performance involved during wastewater treatment. This is due to the reason that RSM facilitates effective search in the design space, which is not possible in conventional experimentation that involves discretized variation in a parameter of interest for constant values of all other parameters. Thus, RSM

with its ability to provide maximum or minimum reference points further extends the limitations of experimental investigations in the design space (Jokic et al., 2010). Thereby, the methodology allows the identification of influential or significant terms that contribute towards process efficiency with small number of simulation experiments.

Jokic et al. (2010) used a commercial ceramic membrane for cross flow microfiltration of yeast suspensions. Further, RSM via Box-Behnken design was employed for the optimization of process parameters (TMP: 0.2-1.0 bar; feed flow rate: 80-180 L/h; concentration: 2-10 g/L) and considered responses as permeate flux, reduction of specific energy consumption (ER). Finally, authors reported the optimal conditions for MF process at 1 bar TMP, 2 g/L concentration and feed flow rate 122.70 L/h at which the optimal values for membrane flux (189.53 L/m^2 h) and ER (44.36%) were obtained with 0.964 desirability.

Yi et al. (2011) studied the optimization of process conditions using RSM methodology for anionic polyacrylamide (APAM)-oil-in-water emulsion treatment using polyvinylidene fluoride (PVDF) membrane modified by TiO_2/Al_2O_3 materials. The authors obtained an optimal permeate relative flux ratio (J/J_0) of 21.51% at optimal process conditions of C_{APAM} (20 mg/L), C_{oil} (20 mg/L), pH (2) and TMP (0.05 MPa).

Salahi et al. (2013) have used polyacrylonitrile membrane during cross flow MF of oily wastewater. The MF process was optimized using RSM tool with which the optimal process conditions have been identified as 45 ºC feed temperature, 4 bar TMP, 1.3 m/s CFV, 10 pH and 11.2 g/L salt concentration. At these conditions, optimal permeate flux was obtained as 180.1 L/m^2.h for a corresponding measurement based flux value of 172.75 L/m^2 h.

Sadeghian et al. (2015) studied the application of RSM to optimize operating conditions during ultrafiltration of oil-in-water emulsion. The optimum conditions were obtained as 1 bar and 3 m/s for TMP and velocity, respectively at which the optimal process variable values

were 79%, 77% and 50 L/m^2 h for turbidity removal, COD removal and permeate flux, respectively.

Arzani et al. (2016) have employed CCD based RSM to examine the effects of three operating parameters namely NaOH solution temperature (30-90°C), NaOH solution concentration (5-45 wt%) and removal time (2-10 h) on free silica removal of mullite microfiltration membranes. The authors reported that the optimal process conditions correspond to 75°C of NaOH solution temperature, 35 wt% of NaOH solution concentration and 8 h as removal time at which the optimal porosity has been evaluated to be 49.4%. Corresponding experimental value for the variable is 48.3%.

Table 1.8 presents RSM based optimization for various MF processes.

Table 1.8: Response surface methodology based optimization for various MF processes

Author	Membrane	Feed	RSM tool	Process parameters	Optimal Responses	
					Experimental	Predicted
Jokic et al. (2010)	TAMI (Commercial)	Yeast suspensions	Box-Behnken	TMP: 0.2 – 1.0 bar CFV: 80 - 180 h C_0 = 2 -10 g/L	TMP: 1 bar, CFV = 130 L/h, C_o = 2 g/L, Flux = 189.2 L/m^2.h and ER = 34.55%	TMP: 1 bar, CFV = 130 L/h, C_o = 2 g/L, Flux = 189.5 L/m^2.h and ER = 44.36%
Yi et al. (2011)	TiO_2/Al_2O_3 PVDF	APAM-oil-emulsion	Central composite rotatable design (CCRD)	$C_{APAM\ oil}$: 0-200 mg/L C_{oil}: 0-200 mg/L, TMP: 0.05-0.15 MPa C_{TDS}: 0-8000 mg/L pH: 1-13.	$C_{APAM\ oil}$: 20 mg/L C_{oil}: 20 mg/L TMP: 0.05 MPa pH: 2 Relative flux (21.51%)	$C_{APAM\ oil}$: 20 mg/L C_{oil}: 20 mg/L TMP: 0.05 MPa pH: 2 Relative flux (19.34%)
Salahi et al. (2013)	Polyacrylonitrile	Oily wastewater	Box-Behnken	TMP: 0.5-4.5 bar CFV: 0-1.5 m/s) C_0: 0-200 g/L pH: 4-10 Temperature: 25-50 °C.	TMP: 4 bar CFV: 1.3 m/s) C_0: 11.2 g/L pH: 10 Temperature: 45 °C Flux (172.75 L/m^2 h)	TMP: 4 bar CFV: 1.3 m/s) C_0: 11.2 g/L pH: 10 Temperature: 45 °C Flux (180.1 L/m^2 h)
Sadeghian et al. (2015)	Polyvinylidene fluoride membrane	Oil-in-water emulsion	CCD	TMP: 0.7-2.8 bar CFV: 1.0-4.2 m/s.	TMP: 1 bar CFV: 3.16 m/s Flux (50 L/m^2 h); turbidity (79%); COD (77%)	TMP: 1 bar CFV: 3.16 m/s Flux (50.66 L/m^2 h); turbidity (78.83%); COD (76.63%)
Arzani et al. (2016)	Mullite	Free silica removal	CCD	T_{NaOH}: 45-90 °C Removal time: 4-10 h C_{NaOH} : 15-45 wt%.	T_{NaOH}: 75 °C Removal time: 8 h C_{NaOH} : 35 wt% Porosity (48.3%)	T_{NaOH}: 75 °C Removal time: 8 h C_{NaOH} : 35 wt% Porosity (49.4%)

1.4 Possible scope for further research

Despite having few limitations, membrane based separation processes have been proven to be effective for the separation of oil from oily wastewater (Alzahrani et al. 2014; Padaki et al., 2015). For instance, reverse osmosis requires high-applied pressure in treatment and RO membranes have low permeability induced high fouling problem (Jamaly et al., 2014). Also, due to lower pore size, ultrafiltration (Wijmans et al., 1984; Berg and Smolders, 1990; Garcia et al., 2012) and nanofiltration (Bruggen et al., 2008; Mohammad et al., 2015; Masoudnia et al., 2013) produce lower permeate flux. Therefore, microfiltration is promising due to its higher water permeability and lower pressure requirements (Abadi et al., 2011; Yang et al., 1998; Cui et al., 2008; Masoudnia et al., 2013).

Broadly, further research in the field of MF range ceramic membranes can be addressed in three areas. Firstly, preparation and characterization of inexpensive ceramic membranes with optimized compositions is to be addressed. Secondly, application of prepared membranes is to be targeted. Thirdly, theoretical insights to experimental data can be carried out to visualize deeper aspects of parametric optimality. The following sub-sections detail upon these issues:

1.4.1 Preparation, characterization and application of ceramic membranes from mixed clays

Till date, among various materials, α-alumina (Lin and Burggraaf, 1991), γ-alumina (Defriend et al., 2003), zirconia (Yang et al., 1998), TiO_2 (Wang et al., 2006) and silica (Yoshino et al., 2005) based ceramic membranes have been extensively studied. These membranes are expensive due to the higher cost of raw materials and higher sintering temperature (1300 ^oC). Therefore, the process cost is significantly high for these membranes and hence ceramic membranes are likely not to be applied in industrial process schemes.

Alternative approaches to reduce the high cost of ceramic membranes refer to the utilization of cheaper inorganic precursors (raw clay (Saffaj et al. 2005), Moroccan clay (Saffaj et al., 2004), powdered apatite (Masmoudi et al., 2007), dolomite (Zhou et al., 2010), kaolin (Bouzerara et al. 2006), Tunisian clay (Khemakhem et al., 2006), sepiolite clay (Weir et al., 2001) and Algerian clay (Khider et al., 2004)) with which the sintering temperature can be significantly lowered to 900 – 1100 ^{o}C. Further, Xia and Liu (2001) indicated that uni-axial dry compaction method is an inexpensive method and can be used to prepare membranes on a laboratory scale (Xia and Liu, 2001). While reported compositions of inorganic materials in the literature for inexpensive ceramic membrane preparation refer to the utilization of materials such as quartz, $CaCO_3$, kaolin and feldspar, ceramic membranes have not been reported till date with both conventional materials (quartz, calcium carbonate, etc.) with waste materials such as fly ash. Therefore, the preparation, characterization and application of ceramic membranes that consist of the said materials is to be targeted first to judge upon the utility of fly ash for membrane preparation. Based on the membrane performance, further improvement in inorganic material composition can be targeted.

1.4.2 Preparation, characterization, optimization and application of low cost fly ash based ceramic membranes

In the previous sub-section, research efforts have been dovetailed towards the verification of fly ash as an important constituent in inexpensive ceramic membrane fabrication. However, a key feature of the mixed clay membranes is that the membranes consist of significantly higher quantities of materials other than fly ash. In this regard, it is important that fly ash constitutes the highest composition in the ceramic membranes and only in such a scenario, the membrane cost would be significantly lower due to the enhanced utilization of waste material for value added product development. Therefore, the thesis need to eventually target

the preparation and characterization of inexpensive fly ash based ceramic membranes, which need to have significantly different composition than those reported for mixed clays in the literature (Abadi et al., 2011; Yang et al., 1998; Cui et al., 2008). The fly ash based ceramic membrane cost is expected to be significantly low due to three reasons, namely significant utilization of fly ash waste material whose value is insignificant, lower sintering temperature (1100 ^{o}C) and simpler fabrication method such as uni-axial dry compaction method. Thereby, the thesis primarily targets the resolution of environmental issues associated to fly ash by producing a value added product such as ceramic membrane with applications such as treatment of oily wastewater streams.

1.4.3 Preparation, characterization and application of TiO_2–Fly ash composite membrane

Generally, ceramic clay and polymeric membranes are characterized to be hydrophobic. Due to this feature, these membranes require higher transmembrane pressure (in the order of several bars) to separate water from other constituents (Chakrabarty et al., 2008). Hence, quicker flux decline, greater fouling and lower flux are apparent. To counter such effect, surface modification techniques are adopted to enhance the hydrophilicity of the membranes (Li et al., 2009; Ahmad et al., 2011; Yi et al., 2011; Sadeghian et al., 2015). The hydrophilic surface modification refers to the deposition of hydrophilic nanoparticles of various materials such as γ-Al_2O_3 (DeFriend et al., 2003), ZrO_2 (Zhou et al., 2010) and TiO_2 (Chang et al., 2014) in the ceramic membrane porous structure. These nanoparticles enable an enhancement in the hydroxyl groups existent on the membrane surface and hence greater hydrophilicity and reduction in transmembrane flux decline (Tsuru et al., 2008; Pan et al., 2012). Among several mentioned materials, titania and alumina are inexpensive materials for the alteration of morphological and separation characteristics of ceramic membranes. Among

these two, titania is inexpensive compared to alumina and therefore the first choice in this section is to fabricate titania composite membrane.

Generally, hydrothermal method was extensively used to deposit TiO_2 and Al_2O_3 particles on the ceramic clay supports (Chou et al., 1999; Wang et al., 2007) but not on fly ash membrane supports. In this method, usually, alkoxide precursors of alumina are used which are expensive and significantly toxic (Patterson et al., 2006). However, for the same method, the utilization of $TiCl_4$ instead of titanium butoxide, titanium-isopropoxide is promising due to its lower cost and relatively non-toxic nature (Zhang et al., 2001).

In the available prior-art, titania composite membranes have been prepared utilizing mixed clay (Chou et al., 1999), α-Al_2O_3 (Chowdhury et al., 2003; Li et al., 2006) and Cordierite (Saffaj et al., 2004) as supports. However, TiO_2-fly-ash composite membrane has not been reported in the literature till date (Dong et al., 2010; Fang et al., 2011; Jedidi et al., 2011). Therefore, there is scope to fabricate a new low cost and non-toxic TiO_2 composite membrane. Needless to convey, the ceramic membranes shall also have better separation efficiencies towards the separation of oil-in-water emulsions. Hence, the next area of research that needs to be addressed in this work is with respect to the preparation, characterization and application of low cost TiO_2-fly ash composite membranes.

Also, the application of TiO_2-fly ash composite membrane needs to target the cross-flow microfiltration of oil-in-water emulsions as these studies would ensure the actual performance of the membranes for synthetic emulsions. This may not be the case for dead-end microfiltration studies.

1.4.4 Response Surface Methodology for the MF performance of membranes

Till date, RSM based parametric analysis and optimization have been studied for various processes including nanofiltration (Salahi et al., 2013; Abadikhah et al., 2014), microfiltration (Jokic et al., 2010, Rastegar et al., 2011), biosorption (Ghaedi and Kokhdan, 2015),

adsorption (Savasari et al., 2015; Santos and Boaventira, 2008), electrocoagulation (Tir and Moulai-Mostefa, 2008; Chavalparit and Ongwandee, 2009; Gengec et al., 2012; Un et al., 2014; Olmez et al., 2009), electrochemical (Thirugnanasambandham et al., 2015; Kushwaha et al., 2010; Yue et al., 2015; Mohajeri et al., 2010; Korbahti and Tanyolac, 2008), coagulation-flocculation (Wang et al., 2014; Wang et al., 2011; Wang et al., 2007; Ghafari et al., 2009; Tringh and Kang, 2011; Jadhav and Mahajan, 2014), ion exchange (Bashir et al., 2010) and wet peroxide oxidation (Shi et al., 2014). In the field of microfiltration, very few studies were conducted and only one study carried out RSM analysis for oil-in-water emulsion treatment using ceramic membranes. Hence, it can be concluded from the prior-art that while RSM is a useful technique for the optimal analysis of flux and rejection characteristics with variation in process parameters. The RSM based oily wastewater treatment using ceramic membrane based microfiltration process has not been reported till date and is the primary objective of this work.

Thus, there is enough scope to conduct research and examine the optimality of dead-end and cross flow MF process parameters for oil-in-water emulsion treatment using several membrane data obtained in this work. Based on further analysis of experimental data, the research has been confined to fly ash and titania-fly ash composite membranes.

1.4.5 Preparation, characterization and application of TiO_2–clay, γ-Al_2O_3– clay and clay membranes

After a thorough examination of available prior-art, it is also apparent that the additional research in the preparation, characterization and application of titania, γ-alumina-clay composite membranes is also beneficial for a comparative outlook with respect to titania-fly ash membranes. Also, while literature refers to experimental investigations for higher oil feed concentration, studies are scarce with feed concentration as low as 250 mg/L. Therefore, there is enough possible scope for the preparation, characterization and application of clay

and titania/γ-alumina clay composite membranes so as to infer upon the performance efficiency of fly ash membranes from both experimental and theoretical point of view. The titania and γ-alumina layer on the clay membranes are to be targeted using hydrothermal method. Further, the membranes have been investigated for their separation characteristics during dead-end MF operation.

1.4.6 Cross flow microfiltration studies for TiO_2–clay and clay membranes

Till date, several investigations targeted the microfiltration of titania-clay (Chou et al., 1999; Saffaj et al., 2004) and clay membranes (Potdar et al., 2002; Benito et al., 2005; Nandi et al., 2010; Fang et al., 2013). However, it is well known that the clay membrane performance is a strong function of its composition. Therefore, the clay membranes prepared in this work have to be judged so as to understand upon their real performance. This is also due to the fact that membranes prepared with uni-axial dry compaction method may not have exactly similar morphology than those prepared with other methods such as extrusion, slip casting, etc. Therefore, while data is available in the literature for the said membranes, cross flow microfiltration has to be conducted for these membranes to infer upon the optimality of fly ash based composite membranes for oil-in-water emulsion treatment.

1.5 Objective of the Thesis

Based on the state of the art presented in sections 1.2.1 to 1.2.4, the PhD thesis targets the fulfillment of the following major objectives:

1. Preparation, characterization and application of
    a) ceramic membranes from mixed clays
    b) low cost fly ash based ceramic membranes
    c) TiO_2-Fly ash composite membrane
    d) TiO_2–clay and γ-Al_2O_3–clay and clay membranes

2. Cross flow microfiltration of oil-in-water emulsions using TiO_2–clay and clay membranes
3. RSM based optimization of process parameters of dead-end and cross-flow MF of oil-in-water emulsions using fly-ash and titania-fly ash membranes.

1.6 Organization of the Thesis

The PhD thesis is organized in eight chapters. A brief account of the chapters in the thesis is presented in the following paragraphs:

Chapter 1 addresses the available prior-art in the chosen area of research and possible scope for further research followed with objective and organization of the thesis.

Chapter 2 addresses the experimental and modeling methodology adopted in the Ph.D. thesis. Precisely it refers to (a) preparation of inexpensive mixed clay, fly ash, titania-fly ash, titania-clay, γ-alumina-clay and clay ceramic membranes (b) characterization of membranes using XRD, TGA, BET, PSD, FTIR, FESEM, mechanical and chemical stability, porosity, nitrogen and water permeation tests and average membrane pore size determination procedures (c) preparation of synthetic crude oil-in-water emulsions (d) dead-end and cross-flow MF of oil-in-water emulsions and (e) RSM based parametric optimization of dead-end and cross-flow MF performance of various ceramic membranes.

Chapter 3 describes the results obtained for inexpensive mixed clay membranes. These include characterization and dead-end MF performance of oil-in-water emulsions. This refers to the evaluation of flux and rejection characteristics during MF studies.

Chapter 4 elaborates upon the results obtained for fly ash based membranes. These pertain to surface and membrane characterization and dead-end MF performance (flux and rejection characteristics) for oil-in-water emulsion treatment. Subsequently, the chapter applies RSM methodology for the identification of optimal process conditions during dead-end MF studies.

Chapter 5 summarizes the results obtained for the TiO_2-fly ash inexpensive ceramic membranes. These include the results obtained from characterization and cross-flow studies for flux and rejection characteristics. Thereby, RSM based optimization was conducted for the cross-flow MF data to evaluate upon the optimality of process parameters such as feed concentration, cross-flow velocity and operating pressure.

Chapter 6 addresses the results obtained for TiO_2-clay, γ-Al_2O_3 –clay and clay membranes. These include characterization results and the dead-end MF performance of the membranes for oil-in-water emulsions. Based on the obtained data, best membrane has been identified.

For the best membrane identified in Chapter 6, **Chapter 7** presents the cross-flow MF based comparative assessment of clay composite and clay membranes. For the obtained data, fouling analysis was conducted using pore blocking models.

Chapter 8 summarizes the conclusions obtained from the research output in this work. Eventually, based on the insights of the obtained data and research methodologies, the chapter also outlines possible directions for future work.

CHAPTER-2

Materials and Methods

भारतीय प्रौद्योगिकी संस्थान गुवाहाटी
Indian Institute of Technology Guwahati

CHAPTER 2 Materials and Methods

Section 2.1 addresses the preparation and characterization of ceramic membranes (SP1-SP4) from mixed clays. This section also presents dead end microfiltration experiments for the removal of oil. Section 2.2 addresses the preparation, characterization, optimization and application of low cost fly ash based ceramic membranes (M1-M3), which were manufactured with variant pore sizes by altering the compositions of the low cost ceramic precursors. Section 2.3 summarizes the preparation and characterization of TiO_2-Fly ash composite membrane and explains RSM modeling approaches for cross flow MF of oil-in-water emulsions. Section 2.4 addresses the preparation, characterization and application of TiO_2-clay, γ-Al_2O_3-clay and clay membranes. Along with membrane fouling analysis, Section 2.5 presents the cross flow MF studies of TiO_2-clay and clay membranes for the separation of oil from synthetic oil-in-water emulsions.

2.1 Preparation, characterization and application of ceramic membranes from mixed clays

2.1.1 Starting materials

The composition of raw materials used for the fabrication of ceramic membranes was listed in the Table.2.1. Quartz was collected from Kanpur, India. Calcium carbonate, TiO_2 were procured form Merck (I) Ltd. Fly ash was collected from Guwahati, India. All the raw materials were used as received without any further purification. Millipore water obtained from Millipore system (ELIX-3) was used throughout this work.

2.1.2 Fabrication

The fabrication procedure of membrane was schematically represented in Fig. 2.1 (a and b).

Table 2.1: Composition of raw materials used for fabrication of ceramic membranes

Raw materials	Quartz (g)	$CaCO_3$ (g)	Fly ash (g)	TiO_2 (g)	$W_{TiO_2} / W_{Fly\ ash}$
Membrane, SP1	30	20	50	0	0
Membrane, SP2	30	20	40	10	0.25
Membrane, SP3	30	20	30	20	0.67
Membrane, SP4	30	20	20 ↓	30 ↑	1.50 ↓

The raw materials listed in Table 2.1 were mixed in a ball mill at 40 rpm for 20 min. The resulting powder was then sieved using 30 mesh standard screens and requisite amount was pressed in a hydraulic pressing machine at a pressure of 50 MPa with the help of stainless steel mould. The obtained circular disk-shaped membranes were first dried at 100 ^oC and then at 200 ^oC for 24 h in a hot air oven (make: Reico, India; model: ROV/DG). The above controlled drying process ensures a maximum removal of moisture and also reduces any thermal stress during moisture removal. Subsequently, the membranes were sintered at 1100 ^oC for 6 h in a muffle furnace (make: Lab Tech, Korea; model: LEF-115P-2) with a controlled heating rate. After sintering, the rigid and porous ceramic membranes were polished on both sides using silicon carbide abrasive paper (No.C-220) to obtain ceramic membranes with uniform surface. Then these membranes were washed with Millipore water in an ultrasonic bath [make: Elma, India; model: T460] for 15 min to remove the loose particles adhered on the surface of membranes.

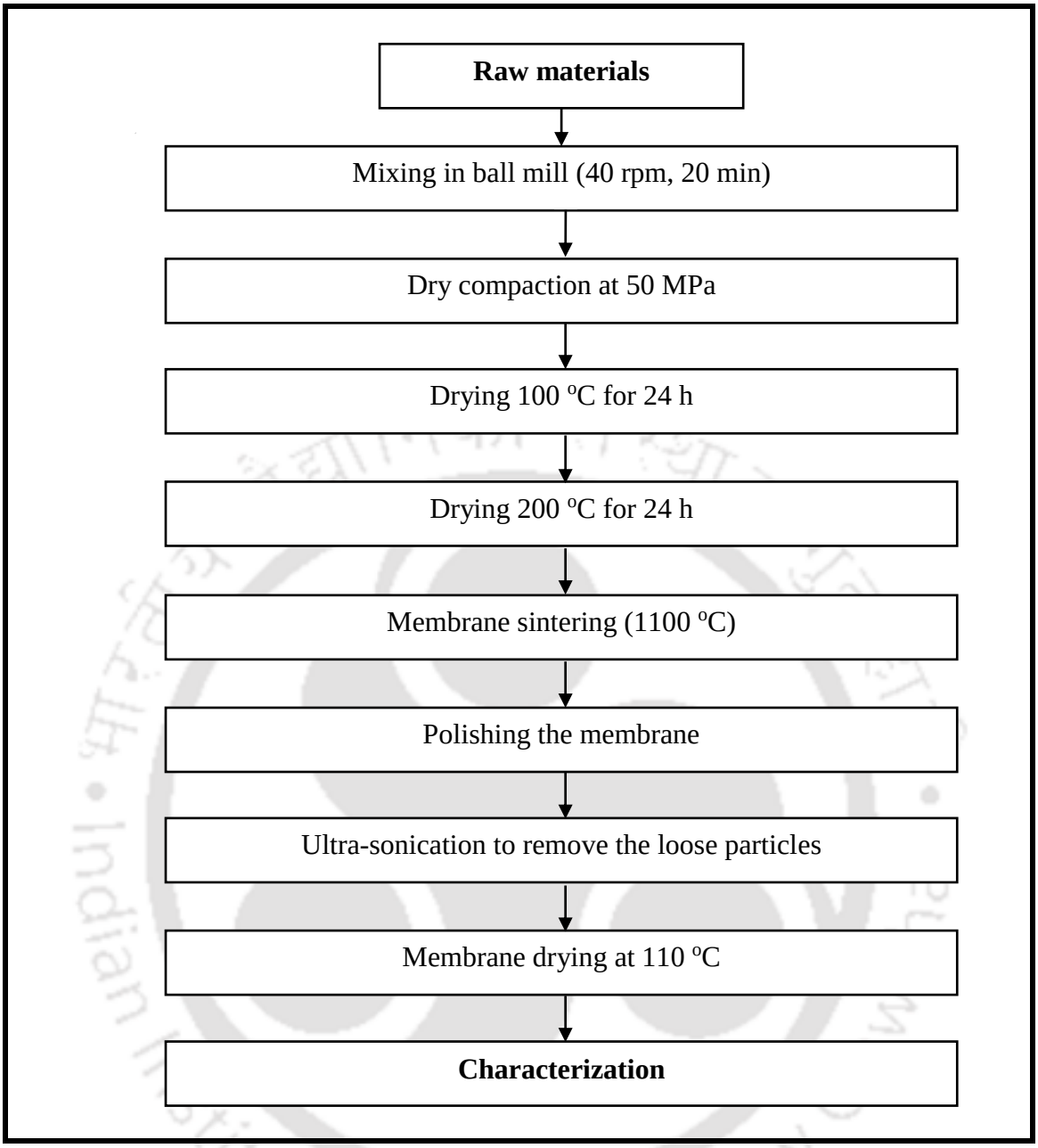

Figure 2.1 (a): Schematic for the preparation of low cost ceramic membrane supports (SP1-SP4)

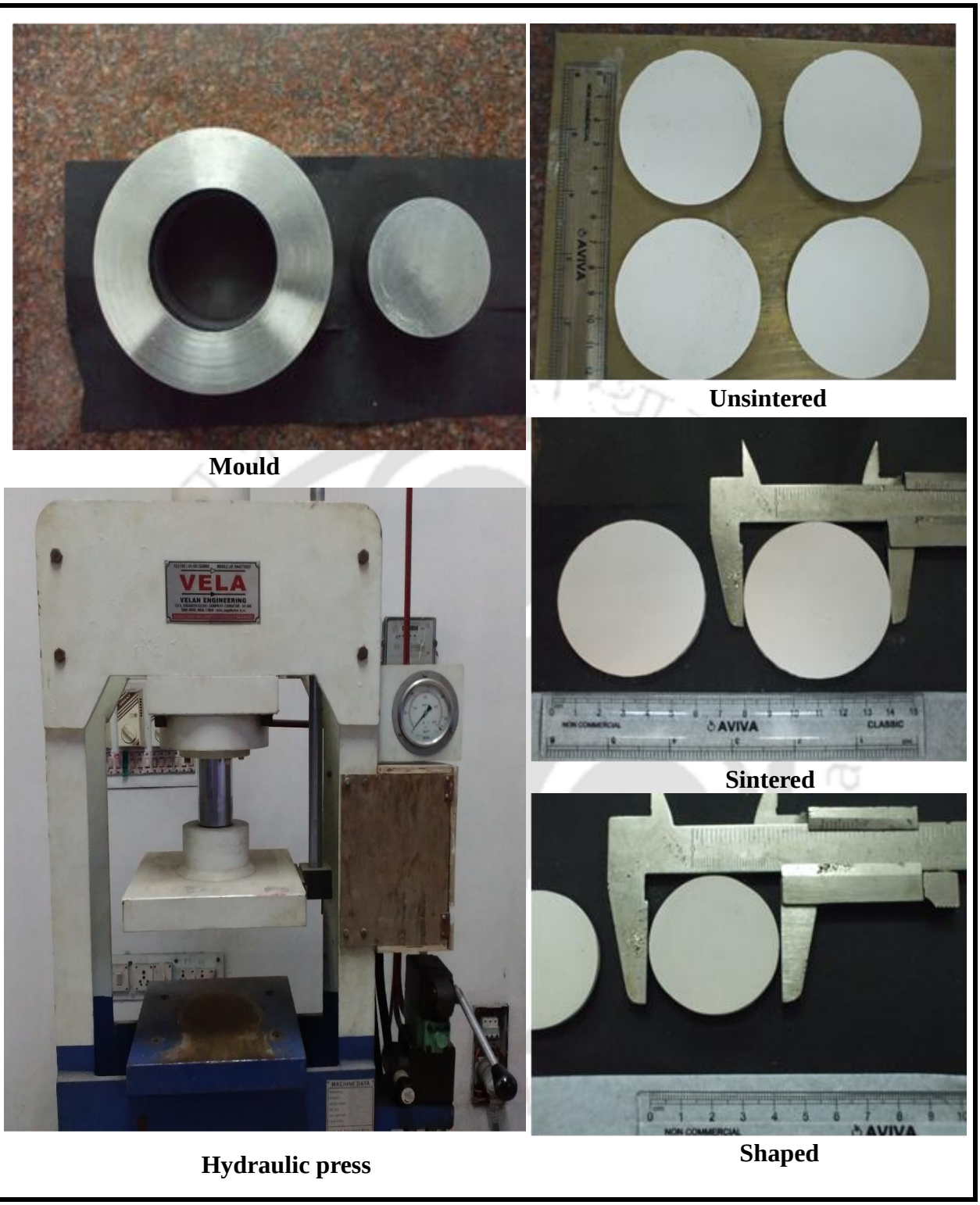

Figure 2.1 (b): Photograph of hydraulic machine, unsintered membrane, sintered membrane and polished membrane

2.1.3 Characterization

The characterization of raw materials and membrane were done by particle size distribution (PSD), X-ray diffraction analysis (XRD), morphological study using field emission scanning electron microscope (FESEM), average porosity, mechanical and chemical stability determination, and evaluation of average pore size and permeability of the ceramic membrane.

2.1.3.1 Particle size distribution (PSD)

The particle size distribution (PSD) of the raw materials was performed by particle sizing machine, Malvern Mastersizer 2000 (APA 5005® hydro MU, Malvern Instruments, Worcestershire, U.K.) in wet dispersion mode.

2.1.3.2 X-ray diffraction analysis (XRD)

XRD analysis of the individual raw materials and ceramic membranes was conducted to evaluate the extent of phase transformations during sintering by Bruker AXS instrument (Karlsruhe, Germany) using CuKα (1.5406 Å) radiation operating at 40 kV and 40 mA. The patterns were acquired for 2θ ranging between 1^o and 80^o with a scan speed of 0.5^o/s.

2.1.3.3 Field emission scanning electron microscope (FESEM)

The images of membrane surface were taken to analyze the morphology of the membranes by field emission scanning electron microscope (FESEM, ∑IGMA, Carl Zeiss). The membrane samples were coated with gold to a thickness of approximately 150 Å. After that, FESEM images of top surface of the membrane at different magnifications were obtained to calculate the porosity and pore size of the membrane.

2.1.3.4 Porosity

Porosity of the membrane was determined using Archimedes' principle. Firstly, the membrane was dried in a hot air oven at 110 ^{o}C for 6 h to remove complete moisture present in the membrane and its dry weight (W_D) was determined. Then, it was immersed in water for 24 h. After that, the membrane was removed and water on the outer surface was removed using tissue paper and the wet weight of the membrane (W_W) was measured. Then the membrane was immersed in water to measure the weight of the membrane when it was saturated with water (W_A). The porosity (ε) of the membrane was determined using the following relation **(Monash and Pugazhenthi 2011; Laux et al., 2005)**:

$$\varepsilon = \frac{W_W - W_D}{W_W - W_A} \qquad (2.1)$$

Surface porosity of the membranes was also estimated using images obtained from FESEM. For this, ImageJ software (Open source software provided by National Institute of Health (NIH), web link: http://rsbweb.nih.gov/ij/download.html) was adopted after thresholding (threshold the pores) the 8-bit image using "Analyze particles" feature of this software. Since the pores are interconnected during thresholding, the porosity of the membranes was measured manually by choosing three rectangular sections (area) of four images of similar magnification at different location.

2.1.3.5 Mechanical strength

The flexural strength of the membranes was tested with a three point bending method on 55×5×5 mm rectangular bars using Universal Testing Machine (DUTT-101, M/s Deepak Polyplast, and Mumbai, India). The flexural strength was evaluated by the following expression.

$$\sigma = \frac{3FL}{2bt^2} \qquad (2.2)$$

Where, σ is the flexural strength (Pa), *F* is the load at the fracture point (N), *L* is the span length (m), *b* is the width of the sample (m), and *t* is the thickness of the sample (m).

2.1.3.6 Chemical stability

Chemical stability of the membrane was determined by subjecting the membrane individually into acid (pH 1) and alkali solution (pH 14). The pH of the solution was adjusted using HCl and NaOH. The stability was measured in terms of mass loss before and after corrosion. For this, the membrane was placed in acid and alkali solution for one week at atmospheric condition. Then the membrane was taken out from the solution, washed with Millipore water and dried at 110 ^{o}C for 6 h. The mass loss of the membrane characterizes the chemical stability.

2.1.4 Dead end Microfiltration

2.1.4.1 Experimental set up

The water flux and hydraulic permeability of the membrane was determined using homemade dead-end filtration setup made up of stainless steel. The setup (as shown in Fig. 2.2) used for this experiment consists of two parts, a cylindrical top part and a base plate with a provision

to keep a membrane. The membrane was placed on a perforated casing and placed in the bottom compartment. The upper compartment of the batch cell was pressurized using N_2 gas by setting a desired pressure through regulator attached with the nitrogen cylinder.

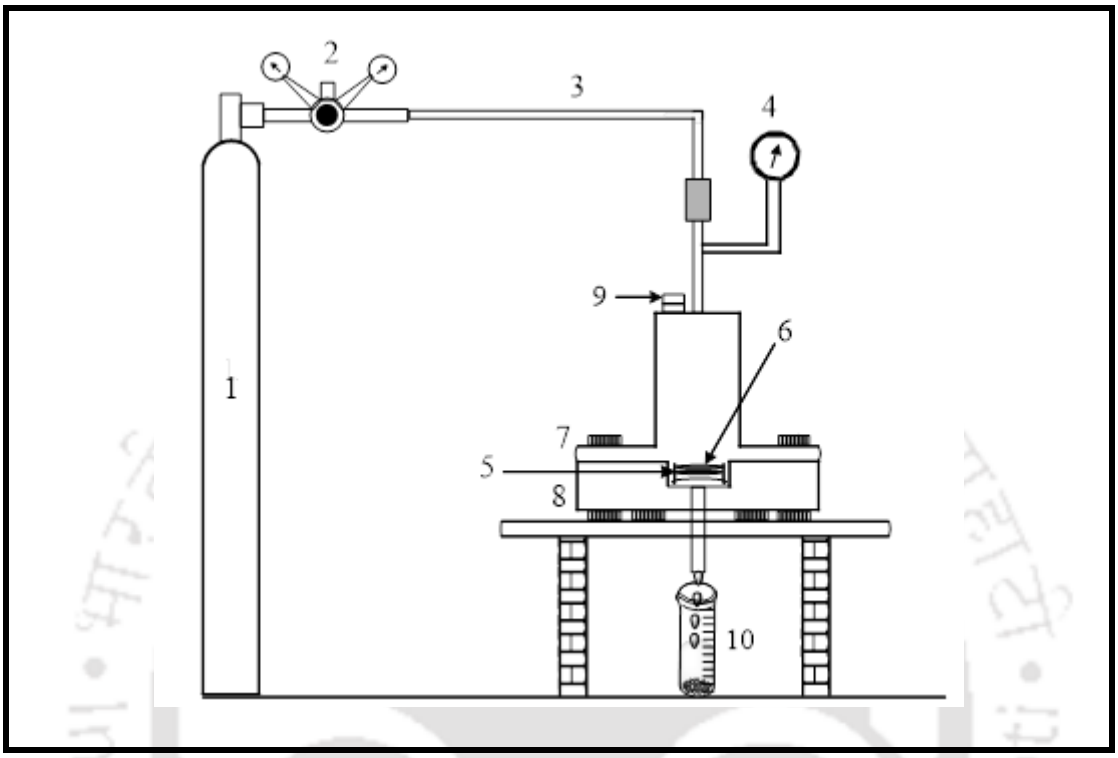

Figure 2.2: Schematic of dead-end microfiltration setup (1-N_2 gas cylinder, 2-pressure regulator, 3-connecting tube, 4-pressure gauge, 5-membrane, 6-rubber gasket, 7-top compartment, 8-bottom base plate, 9-feed inlet and 10-permeate measuring cylinder).

2.1.4.2 Hydraulic permeability and average pore size of membranes

The hydraulic permeability and average pore size of the membranes were determined by measuring their water flux using in-house made dead-end filtration setup (Fig 2.2). Prior to the experiment, the pure water was passed through the membrane several times at higher pressure to remove any loose particles present in the pores. After that, the water flux was measured at different applied pressures (69-345 kPa). All the experiments were carried out by filling 150 ml of Millipore water in the dead-end filtration setup. After discarding the first 50

ml of water at a fixed pressure, the time required to collect next 50 ml was noted down to calculate the water flux at that particular applied pressure using the following equation:

$$J_w \text{ (Pure water flux, } m^3/m^2 s) = \frac{V \text{ (Volume of water permeated, } m^3)}{A \text{ (Membrane area, } m^2) \times \Delta t \text{ (Time, } s)} \quad (2.3)$$

The average pore size of the membrane in terms of radius is estimated by assuming presence of cylindrical pores using the following equation deduced from Hagen-Poiseuille equation.

$$r_m = \left[\frac{8\mu l_p L_h}{\varepsilon}\right]^{0.5} \quad (2.4)$$

Where, r_m is the pore radius of the membrane, L_h is the hydraulic permeability of the membrane, μ is the viscosity of water, l is the pore length and ε is the porosity of the membrane

In addition, the pore size distribution and average pore diameter of the membranes are estimated from FESEM micrographs using ImageJ software**.** For each membrane, six images with various magnifications are selected for analysis to minimize the error of image analysis. The average pore size, D_{avg} of the membrane was calculated using the following equation:

$$D_{avg} = \frac{\sum_{i=1}^{n} n_i d_i}{\sum_{i=1}^{n} n_i} \quad (2.5)$$

Where, D_{avg} is the average pore diameter (μm), n is the number of pores and d_i is the diameter of the i^{th} pore (μm).

2.1.4.3 Dead end MF of oil-in-water emulsions

The oil-in-water emulsion (200 mg/L) was prepared by mixing crude oil (collected from Guwahati Refinery, IOCL, India) with Millipore water in sonicator for 15 h at room temperature (25 ^{o}C). No surfactant was added because natural surfactant present in the crude oil stabilizes the oil-in-water emulsion sufficiently for performing the experiments.

The droplet size of the emulsion (200 mg/L) was determined using particle size analyzer (Malvern Mastersizer 2000, Model APA 5005). The prepared oil-in-water emulsion (concentration of 200 mg/L) was utilized for microfiltration experiments. The experiments were performed in the same dead-end filtration setup as shown in Fig 2.2 with varying applied pressures. In all experiments, the feed volume of 150 mL was filled into the filtration setup. The first 10 mL of permeate was discarded and time taken for collection of second 10 mL of permeate was noted down to calculate permeate flux. All the experiments were conducted at room temperature (25 ^{o}C) and the percentage removal (R) of oil and permeate flux was evaluated according to the following expression

The membrane flux (J) was evaluated using the expression:

$$J\ (Membrane\ flux,\ m^3/m^2 s) = \frac{V\ (Volume\ of\ the\ permeate,\ m^3)}{A\ (Membrane\ area,\ m^2) \times \Delta t\ (Sampling\ time,\ s)} \quad (2.6)$$

The membrane rejection was estimated using the following expression:

$$R\ (Rejection,\ \%) = 1 - \frac{C_p (Oil\ concentration\ in\ permeate,\ mg/L)}{C_f (Oil\ concentration\ in\ feed,\ mg/L)} \times 100 \quad (2.7)$$

The concentration of oil in permeate was evaluated using a UV-vis spectrophotometer (Spectrascan, UV 2300) at a wave length of 239 nm, where the maximum absorbance was observed.

2.1.4.4 Membrane cleaning

In order to regenerate a fouled membrane, the membrane was initially rinsed with water for 1 h. Subsequently, the membrane was cleaned using surf excel solution for 1 h. Finally, at higher applied pressure, water was passed through the membrane to facilitate the removal of oil droplets that adhere or adsorb to the surface of the membrane. After completing the cleaning process, the water flux was once again measured so as to confirm upon the complete restoration of water permeability

2.2 Preparation, characterization, optimization and application of low cost fly ash based ceramic membranes

2.2.1 Membrane fabrication

The inorganic precursors used for ceramic membrane (M1-M3) fabrication are presented in Table 2.2. The procedure for membrane fabrication is presented in section 2.1.2. Firstly, the required materials and 4 mL of polyvinyl alcohol (PVA) solution (2 wt. %) were thoroughly mixed in a ball mill for 1200 s at 40 rpm. The rest of the procedure was same as mentioned in section 2.1.2 and pressed at a load of 150 Kg/cm^2. The procedure discussed in section 2.1.2 was followed for drying, sintering and cleaning of membranes.

Table 2.2: Materials used to make ceramic membranes

Raw materials	Membrane, M1 (Wt. %)	Membrane, M2 (Wt. %)	Membrane, M3 (Wt. %)
Fly ash	80	80	70
Quartz	20	10	20
Calcium Carbonate	-	10	10

2.2.2 Characterization

The XRD analysis, evaluation of membrane flexural strength, and chemical stability measurement procedures were elaborated in section 2.1.3. Scanning electron microscopy (SEM) was conducted to examine the surface morphology using SEM instrument (Make: LEO, Model: 1430VP®, Oxford). ImageJ analysis software based SEM image analysis and the average membrane pore size determination was discussed in sub-section 2.1.4.2.

In order to examine the thermal transformation during sintering, thermo-gravimetric analysis (TGA) was conducted for the mixture of inorganic precursors using TGA instrument (Make NetzscR, Model: STA449F3A00). TGA was conducted using argon as a carrier gas and 10 ^{o}C/min heating rate from ambient temperature to the sintering temperature. Nano-particle size analyzer (NPSA) (Make: Beckmann Coulter, Model: Delsa nano C) was used to determine the particle size distribution of powder mixtures.

In order to evaluate the pore size of the membranes, the permeation of N_2 gas through these membranes was carried out using an in-house made permeation set up as shown in Fig. 2.3. The setup consists of a tubular shaped hollow top dome ended with circular shape (stainless steel) and at bottom, circular shaped flat plate has a facility to place membrane inside the flat plate and it was airtight by means of rubber gaskets. Then the setup was pressurized at various applied pressures by using N_2 gas and the outlet gas flow rate was calculated by using digital gas flow meter (Make: Agilent Technologies, Model: ADM 1000 Universal Gas Flowmeter), which was connected to the outlet of the bottom flat plate. Each test was carried out at 25°C and before every test; the whole setup was checked for air leakage by dipping the setup in the detergent solution contained bucket. After finding out no leakage in the set up, then N_2 gas permeation tests were carried out. From the nitrogen permeation experiments, the measured data corresponds to flow rate (Q) versus applied pressure (ΔP) that was generated for the membranes. The nitrogen gas effective permeability factor (K) of the membranes was

derived from these gas permeation data and average pore radius (r_g) was calculated as follows:

$$K = 2.133\frac{r_g \nu}{l_p q^2} + 1.6\frac{r_g^2}{l_p \eta q^2} P \qquad (2.8)$$

Where, P is the average pressure acting on the membrane, ν denotes the molecular mean velocity of the gas (m/s), η describes the viscosity of gas (Pa s), q denotes the tortuosity, lp represents pore length (m) and K denotes the effective permeability factor.

The effective permeability factor is calculated using the following expression:

$$K = \frac{P_2 Q}{S \Delta P} \qquad (2.9)$$

Where, ΔP denotes the applied pressure, Q represents the volumetric flow rate (m^3/s), P_2 is the membrane pressure at permeate side and S denotes the permeable area of the membrane.

The average pore size of the membrane can be obtained from the following expression:

$$r_g = 1.333\frac{B}{C}\nu\eta \qquad (2.10)$$

Where B and C are the intercept and slope, respectively, obtained from the expression (2.8).

In addition, pure water flux tests were conducted to measure the hydraulic permeability using indigenously designed dead end microfiltration experimental setup (Fig. 2.2).

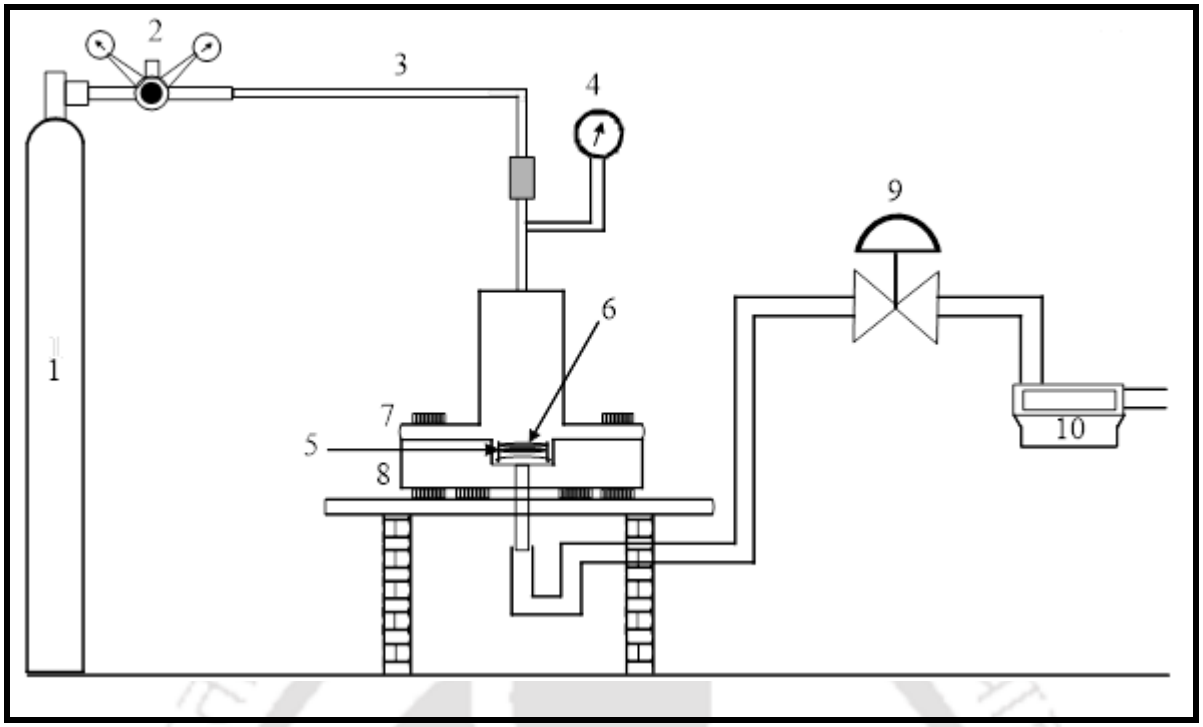

Figure 2.3: Schematic of N_2 gas permeation test setup

(1-N_2 gas cylinder, 2-pressure regulator, 3-connecting tube, 4-pressure gauge, 5-membrane, 6-rubber gasket, 7-top compartment, 8-bottom base plate, 9-flow control valve and 10-digital flow meter)

2.2.3 Dead end flow microfiltration experiment

Section (2.1.4.1-2.1.4.3) elaborated upon the experimental setup (Fig. 2.2) and procedures followed to evaluate pure water permeability and oil permeation studies. With synthetic oil-in-water emulsions (50- 200 mg/L solution concentration), microfiltration tests were conducted in the applied pressure range of 69-345 kPa. The membrane flux (J) and rejection (R) was determined using the equations 2.6 and 2.7, respectively.

The procedure followed for the membrane regeneration was explained in sub-section 2.1.4.4.

2.2.4 RSM based simulation studies

An efficient experimental design involves detailed experimental plan with which experiments can be conducted systematically with optimal effort. The optimum experimental design

allows the maximization of the information while performing the experiment. The design of experiments starts with concept of choosing the process model. For better performance of process optimization, CCD methodology from the RSM is effectively used and is therefore employed in the present work. At the center point location, the total number of possible combinations of experiments are obtained by the design of experiments targeted with the number of independent variables that strongly influence the process performance in terms of flux and rejection. Three levels are considered (+1,0,-1) for a particular variable while performing the CCD analysis using variables of experiments such as feed concentration (X_1) and applied pressure (X_2) to obtain response effects. Out of the three levels, '0' level is considered as the center point or the middle level. The factorial design influences the amount of the values in high and low levels. In this case, both the high and low level of the point are chosen as 1.414, which is obtained from the relation $2^{(k/4)}$ (where k = number of factors = 2). Five levels are considered ranging from -1.414, -1, 0, +1, +1.414, for every process variable in this study. The formulae $2^k + 2k + n_0$, is used for the determination of the number of possible experiments. In this formula, the first term signifies the factorial points, second term indicates the axial points and the third indicates the central run.

In the present study, CCD method is used by considering two factors. In substituting the two factors in the above formula, 4 factorial nodes, 4 axial nodes and 5 replicates at the center point are obtained. Hence, in the present study, in total, 13 experiments were carried out using these parameter variables. A second order regression polynomial model was developed for the reconstruction of the response using the independent variables and their corresponding interactions. The process performance is denoted using the equation:

$$Y = \beta_0 + \sum_{i=1}^{n} \beta_i X_i + \sum_{i=1}^{n} \beta_{ii} X_i^2 + \sum_{i=1, i \le j}^{n} \sum_{j=1, i \le j}^{n} \beta_i X_i X_j + \varepsilon_{ij} \quad (2.11)$$

where Y describes recovered response, β_0 denotes offset parameter, β_i is linear performance variation, β_{ii} is the squared effect, β_{ij} indicates effect of interaction, ε_{ij} is the random error and X_i and X_j are the independent uncoded variables.

In the present work, a polynomial of second order is derived using independent uncoded parameters mentioned below:

$$Y = \beta_0 + \beta_1 X_1 + \beta_2 X_2 + \beta_{12} X_1 X_2 + \beta_{11} X_1^2 + \beta_{22} X_2^2 \quad (2.12)$$

Design expert software (Version 7.0) was used to carry out RSM studies that feature experimental design matrix, ANOVA studies, response surfaces, normal plots of residuals and contour points.

2.3 Preparation, characterization and application of TiO_2-Fly ash composite membranes

2.3.1 Synthesis of TiO_2-Fly ash composite membrane

TiO_2-Fly ash composite membrane was prepared with low cost fly ash ceramic membrane (M2) using in-situ hydrothermal crystallization. To do so, firstly, at room temperature, a slow drop wise addition of $TiCl_4$ was allowed in water at constant stirring condition to achieve 5 vol.% solution. Thereby, the solution pH is enhanced to 9.0 by contacting aqueous ammonia in dropwise fashion. Eventually, the synthesized solution was poured on the already kept fly ash ceramic membrane (M2) in an autoclave reactor [Teflon coated stainless steel] of 250 mL capacity. The crystallization was carried out in a hot air oven facilitated with appropriate temperature controller with reactor subjected to hydrothermal treatment at 160 °C for 12 h. After crystallization process, the reactor was cooled to room temperature. The membrane coated with TiO_2 and residual powder were recovered from the autoclave and washed

abundantly with water to eliminate loosely adhering crystals. Subsequently, the washed membrane and powder sample were then dried for 12 h at 110 °C. Finally, calcination [400 °C, 1 °C/min] was conducted for 3 h for both coated membrane and powder samples to subject them to characerization studies.

2.3.2 Characterization

The structural morphology and porosity of the membranes were evaluated by following the procedure detailed in sub-section 2.1.3.3 and sub-section 2.1.3.4, respectively. In addition, the average pore size of the membrane was also evaluated with N_2 gas permeation tests conducted in an indigenous permeation set-up. Details of the procedure have been presented in section 2.2.2. Contact angle (CA) measurements for fly ash membrane (M2) and TiO_2-Fly ash composite membrane were conducted with Drop shape analyzer [Model: DSA25, Make: Kruss] using sessile drop method and water droplets (4 µL) at 0.16 mL/min falling rate and 16 frame rate. For each membrane, the average value of the CA was measured by conducting experiments at five distinct locations on the membrane surfaces.

2.3.3 Cross flow microfiltration

2.3.3.1 Experimental set up

The experimental setup refers to a peristaltic pump supplemented with inlet and outlet connections (see Fig. 2.4). The inlet connection of the pump is connected to the feed tank and the outlet connection to the membrane module that hosts the circular membrane disc. A pressure gauge kept at the membrane module allows the measurement of retentate/feed pressure on the membrane. The membrane module retentate outlet is connected to an adjustable valve and a flow meter to alter and measure the flow rate, respectively. Subsequently, the outlet of the flow meter is connected back to the feed tank. Thereby, a

glass beaker is kept on a weighing balance to collect the permeate solution from the membrane module base plate. Thereby, weight measurement of permeate samples at specific time intervals is noted to evaluate the membrane flux. Further, adjustable valves facilitate the pressure adjustment in the system.

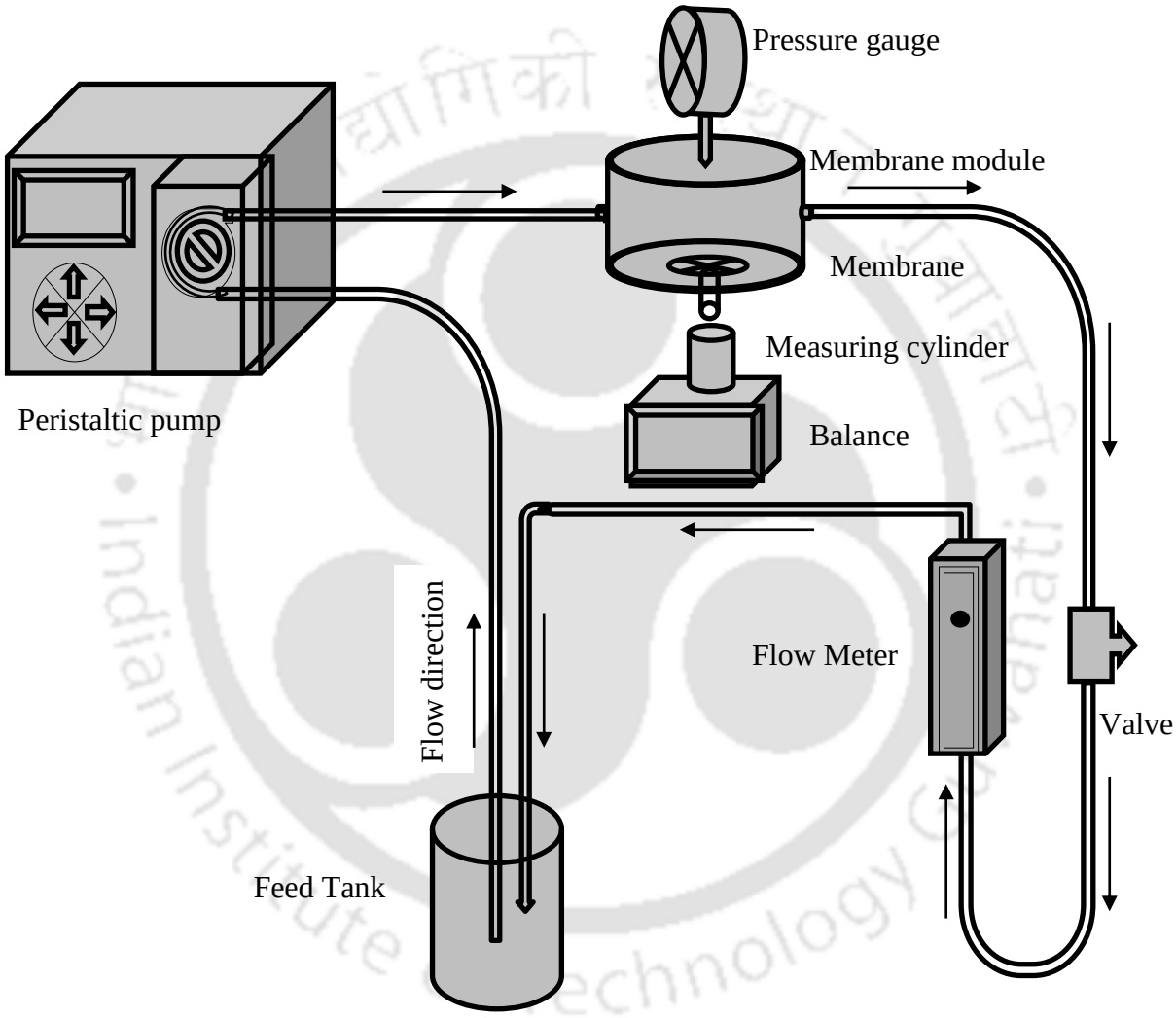

Figure 2.4: Cross flow microfiltration set up

2.3.3.2 Microfiltration Tests

Synthetic oil-in-water emulsions (100-200 mg/L) were prepared by dissolving 0.1-0.2 g of crude oil in 1 L of water with help of sonication bath for 15 h. The separation experiments were carried out in cross flow microfiltration mode with the experimental setup depicted in Fig. 2.4. Prior to the experimental investigation with synthetic oil-in-water emulsions, water was circulated in the membrane process system at pressure higher than the maximum pressure of operation to remove loose particles on the porous flow path and to allow compaction. Eventually, water flux measurements were conducted in the pressure range of 69 – 207 kPa. The membrane performance was evaluated for various combinations of applied pressure, feed concentration and cross flow velocity, which were varied from 69-207 kPa, 100-200 mg/L and 0.0885-0.1736 m/s, respectively. For all experiments, 5 L of feed solution was used. During the MF process, time duration to collect the desired permeate volume was noted at different cumulative time periods. Thereby, the membrane rejection and membrane flux was determined using the equation 2.6 and 2.7, respectively. The procedure followed for the membrane regeneration was explained in sub-section 2.1.4.4

2.3.4 RSM modeling studies

The CCD design framework constituted a three level-three factor approach with six axial points ($\alpha = \pm 1.68$), eight orthogonal factorial points and six replicates at central points. This affirmed upon the need to conduct 20 experimental runs (Aleboyeh et al., 2008). Thereby, RSM technique was adopted to analyse the obtained cross flow MF data for oil-in-water emulsion separation. In the RSM, the selection of independent variables and their levels for the responses as permeate flux and rejection were 69-207 kPa applied pressure (X_1), 100 – 200 mg/L feed concentration (X_2), and 0.0885 – 0.1769 m/s cross flow velocity (X_3). The design matrix of independent variables, predicted and experimentally obtained responses

(permeate flux and rejections) of TiO_2-Fly ash membrane and M2 membrane subjected to ANOVA analysis. Design expert software® trial version 7 (Stat-Ease, inc., Minneapolis, MN, USA) was employed for graphical analysis and regression of model analysis for the obtained results. The relation between coded (Z_i) and real values (X_i) during statistical analysis is according to the expression (Khataee and Dehghan, 2011):

$$Z_i = \frac{X_i - X_o}{\Delta X_i} \quad i = 1, 2 \text{ and } 3 \qquad (2.14)$$

Where, X_i is independent variable real value, ΔX_i is the step change content of uncoded variable *i*, X_o is independent variable real value at the centre point and Z_i is the dimensionless independent variable coded value. For each independent variable, variations involved three levels such as centre point, factorial points (+ and -) and axial points (+ and -). Subsequently, the system response was assumed to be describable using a second–order polynomial model of independent variables (Khataee and Dehghan, 2011).

$$Y = \beta_0 + \sum_{i=1}^{n} \beta_i X_i + \sum_{i=1}^{n} \beta_{ii} X_i^2 + \sum_{i=1, i\le j}^{n} \sum_{j=1, i\le j}^{n} \beta_{ij} X_i X_j + \varepsilon_{ijk} \qquad (2.15)$$

Where, β_{ij} , β_{ii} , β_i and β_0, are interaction coefficients, quadratic, linear and the intercept, respectively, ε_{ijk} is the random error, X_i, X_j are uncoded independent variables and *Y* is the predicted response (permeate flux and rejection). In the above expression, the variables numbers represented by *i, j, k,* and *n* need to be integers. For the case where $i < j$, β_{ij} refers to the interaction effect of X_i and X_j variables. The statistical significance of the model is analysed based on the model F-value (Fisher's satirical test (F-test)) and probability value ($P < 0.05$), which are obtained by the analysis of a variance (ANOVA) test (Liu and Chiou,

2005). The model adequacy is evaluated by fitting the predicted response vs experimental response with which the regression coefficient value (R^2) could be obtained for further analysis on the fitness.

2.4 Preparation, characterization and application of TiO_2-clay, γ-Al_2O_3-clay composite and clay membranes

2.4.1 Materials

The clay powders (feldspar, kaolin, pyrophyllite, ball clay and quartz,) were collected from Kanpur, India. Calcium carbonate, polyvinyl alcohol (PVA), aluminium chloride (99.5% pure, $AlCl_3.6H_2O$) and aqueous ammonia solution (25 wt. %) were supplied by Merck (I) Ltd., Mumbai, India. Titanium tetrachloride ($TiCl_4$, 99.5% pure) was purchased from Loba Chemie, Mumbai, India. Crude oil used in this work was procured from IOCL Refinery, Guwahati, India. The Millipore system (ELIX-3) was used for Millipore water collection.

2.4.2 Preparation of membranes

The manufacturing procedure followed for clay membrane was same as in section 2.2. Here, the required composition of clay powders was mixed with PVA solution, and support was sintered for 6 h at temperature of 950 °C .

For the preparation of TiO_2 membrane, the procedure was explained in section 2.3.1, While section 2.3.1 refers to TiO_2-Fly ash composite membrane from M2 membrane, this section refers to fabraication of TiO_2-clay membrane on clay membrane. Rest of the procedure used is same as section 2.3.1.

Similarly, γ-Al_2O_3 membrane was prepared by hydrothermal method using $AlCl_3$ as a starting material. 4 wt. % $AlCl_3$ solution was prepared and aqueous ammonia solution was added dropwise into the $AlCl_3$ solution with continuous stirring until the pH of the solution reached 8.0. Then the solution was transferred to a Teflon coated SS autoclave reactor and the dried clay membrane was also placed in the reactor. The hydrothermal reaction was performed at 150 °C for 8 h. The membrane and as-synthesized powder were calcined at 600 °C for 3 h.

2.4.3 Characterization

Thermal degradation behavior of as synthesized powders was analyzed in Netzsch thermo gravimetric analyzer (Make: Netzsch, Model: STA449F3A00) in argon atmosphere with the temperature increment of 10 °C/min. The X-ray diffraction (XRD) analysis was acquired at 2θ values of 10-80° using a scanning rate of 0.05 °C/s in an equipment (Make: Bruker, Model: D8 ADVANCE) with Cu Kα (λ=0.154506 nm) radiation operating at 40 kV and 40 mA. The crystallite size was calculated from X-ray diffraction patterns using Debye-Scherrer equation, $D = K\lambda/(\beta\cos\theta)$, where λ is the wavelength of the X-ray radiation (λ = 0.154506 nm), K is a constant (0.9), β is the peak full width at half maximum height, and θ is the diffraction angle. The particle size distribution (PSD) of the TiO_2 and γ-Al_2O_3 sols were measured using Delsa nano C (Beckman Coulter). FTIR spectra of the prepared TiO_2 and γ-Al_2O_3 powders were analyzed using Shimadzu Fourier Transform Infrared Spectrosopy (FTIR) (Model: IRAffinity-1) to identify the functional groups present in the prepared powders. Nitrogen adsorption/desorption isotherms for calcined TiO_2 and γ-Al_2O_3 powder samples were determined at -196 °C using the BET method in the instrument, Quantachrome surface area and pore size analyzer (Make: Quantachrome, Model: Autosorb-IQ MP). Before

N_2 adsorption/desorption analysis, both the samples (TiO_2 powder and γ-Al_2O_3 powder) were completely degassed under the temperature of 200 °C with 3 h duration.

The structural morphology, porosity and contact angle of the clay membrane and composite membranes were evaluated according to the procedure detailed in section 2.1.3.3, Sub-section 2.1.3.4 and section 2.3.2, respectively. In addition, average pore size was evaluated by N_2 gas permeation study.

2.4.4 Dead end Microfiltration of oil-in-water emulsions

The stable oil-in-water emulsions having the concentrations of 50-250 mg/L were produced by following the procedure described in section 2.1.4.3. Then the droplet size distributions of prepared four different concentrations of oil-in-water emulsions (50-250 mg/L) were measured with the instrument, particle size analyzer (Make: Malvern, UK; Model: Master Sizer 2000).

The prepared membranesTiO_2-clay, γ-Al_2O_3-clay and clay membrane were applied to remove oil from the oil-in-water emulsions using dead-end flow setup (see Fig. 2.2). Each experiment was conducted using 150 mL quantity of feed oil solution in the experimental setup. For every applied pressure, the first 10 mL of the collected permeate was rejected and the time taken for the collection of second 10 mL of permeate was used to measure the permeate flux. The equations 2.6 and 2.7 were used to estimate the permeate flux and oil rejection values of the membrane. The membranes were regenerated by following steps mentioned in section 2.1.4.4.

2.5 Cross Flow MF studies for TiO_2–clay and clay membranes

In order to achieve better performance of membranes in separation of oil-in-water emulsions, this section targeted the cross flow MF process with the TiO_2-clay and clay membranes.

2.5.1 Cross flow MF Tests

The microfiltration procedures, analytical methods used and experimental set up for cross flow microfiltration have been presented in section 2.3.3. The pure water flux of clay and TiO_2-clay membrane was determined at three different applied pressures (69-207 kPa) by keeping a constant cross flow velocity of 0.0885 m/s. The performance of the membranes was tested with oil-in-water emulsion of 200 mg/L and the applied pressure between 69 and 207 kPa at three cross flow velocities (0.0885-0.1769 m/s). The expressions (2.6) and (2.7) were employed to measure the permeate flux (J) and oil rejection (R).

After finishing of every experimental run, the TiO_2–clay membrane and clay membrane were cleaned and regenerated according to the procedure mention in sub-section 2.1.4.4.

2.5.2 Membrane fouling analysis

The fouling of the membrane in cross flow microfiltration process was studied with the help of intermediate pore blocking, cake filtration, complete pore blocking and standard pore blocking models.

(i) Complete pore blocking

Complete pore blocking happens when the solute particles sizes are greater than the membrane pore sizes. Consequently, pore blocking takes place over surface of the membrane and not within the membrane pores.

$\ln(J^{-1}) = \ln(J_0^{-1}) + k_b t$	(2.15)

(ii) Standard pore blocking

Standard pore blocking assumes that the molecules penetrate into the pores of the membrane and deposit over the pore walls because of the abnormality in the pore passages. Generally,

standard pore blocking arises when the sizes of the solute particles are smaller than that of membrane pore size and thereby, pore blocking happens inside the membrane pores. In this manner, the membrane pore volume reduces proportionally to the filtered permeate volume.

$$J^{-0.5} = J_0^{-0.5} + k_s t \quad (2.16)$$

(iii) Intermediate pore blocking

Intermediate blocking arises when both the solute particles and the membrane pores are similar in the size. For such a scenario, it is expected that the solute molecules do not essentially block the membrane pore and few particles may settle over others. Hence, the non-blocked membrane surface area reduced with time and a few molecules are relied upon to deter the membrane pore passage without hindering the pore completely.

$$J^{-1} = J_0^{-1} + k_i t \quad (2.17)$$

(iv) Cake filtration

Cake filtration relates to a situation where particles bigger than the normal pore size aggregate on the membrane surface and thus facilitate the development of a "cake". The cake develops with time and offers an extra porous barrier (and subsequently hydraulic resistance) to the permeating liquid.

$$J^{-2} = J_0^{-2} + k_c t \quad (2.18)$$

The plot of J^{-2} vs. t, J^{-1} vs. t, $J^{-0.5}$ vs. t, and $\ln(J^{-1})$ vs. t shall be a straight-line with slope of k_c, k_i, k_s and k_b with y-intercept of J^{-2}, J^{-1}, $J^{-0.5}$ and $\ln(J^{-1})$ for cake filtration model, intermediate pore blocking, standard pore blocking and complete pore blocking, respectively. The fitness of any one of the above models is based on the maximum value of coefficient of correlation (R^2) of the microfiltration permeation data.

CHAPTER-3

Preparation, Characterization and Application of Ceramic Membranes from Mixed Clays

भारतीय प्रौद्योगिकी संस्थान गुवाहाटी
Indian Institute of Technology Guwahati

CHAPTER 3 Preparation, characterization and application of ceramic membranes from mixed clays

After a brief overview, sections 3.2.1-3.2.7 address the characterization of rawmaterials and membranes (SP1-SP4), section 3.2.8 elaborates upon the dead end MF performance of SP4 membrane. Following this, section 3.2.9 summarizes the retail cost analysis followed with the summary of the research findings in section 3.3.

3.1 Overview

In this chapter, results obtained from surface, physical, flux characterization of SP1-SP4 membranes are presented first. Eventually, dead end MF performance of the SP4 membrane is summarized. Finally, the evaluated conceptual retail cost of the membrane is presented.

3.2 Results and Discussion

3.2.1 Particle size distribution (PSD)

The particle size distribution (PSD) of the raw materials was done to get an idea of the particle size and its uniformity of the particles. The size of the raw materials determines the porosity and pore size of the sintered membrane. Pore growth mainly depends on the initial particle size of the raw materials and compaction pressure (Tsuru, 2001). Finer particles require a relatively low temperature for sintering and conversely it results in a large transport resistance because of too small effective pore size. On the other hand, coarser particles need higher sintering temperature resulting in macroporous membranes with reduced mechanical strength (Wang et al., 2007). The particle size distribution of the individual raw materials and powder mixture used for the fabrication of four fly ash based membranes (SP1-SP4) is shown in Fig. 3.1 (a, b). It can be seen from Table 3.1 and Fig. 3.1 (b) that the size of particles are in the ranges of 0.96-138.0 μm, 1.26-316.23 μm, 1.26-138.0 μm and 1.26-91.2 μm for the

membrane SP1, SP2, SP3 and SP4, respectively. Moreover, a volume median diameter ($d_{0.5}$) of the raw material mixtures is found to be 7.3, 5.9, 5.0 and 4.8 µm for the membrane SP1, SP2, SP3 and SP4, respectively. These sized raw material mixtures would be reasonably useful for the preparation of porous fly ash based membrane with maximum porosity (Wang et al., 2007; Monash and Pugazhenthi, 2011b; Vasanth et al., 2011a). For the powder mixtures used for the fabrication of membranes (SP4-SP1), the span values are found to be in the range of 2.18-6.07. This specifies that width of the particle size distribution offers good mixing and uniform distribution between the particles.

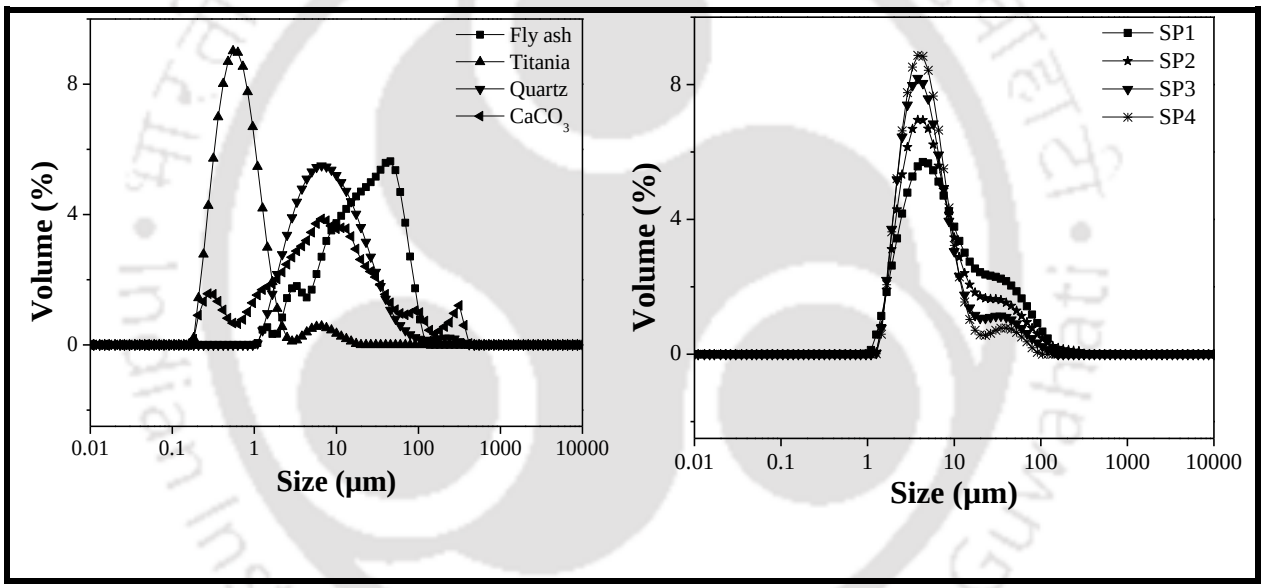

Figure 3.1: Particle size distribution of (a) individual raw materials and (b) powder mixtures used to fabricate membranes (SP1-SP4)

Table 3.1: Particle size distribution of the clay mixtures used to fabricate membrane (SP1-SP4)

Membrane	SP1	SP2	SP3	SP4
Average particle size (μm)	26.514	28.263	17.694	12.497
Span value	6.075	5.983	4.152	2.181
Volume weighted mean (μm)	16.963	14.88	10.265	7.947
Particle size range	0.955-138.038	1.259-316.228	1.259-138.038	1.259-91.201
d0.1 (μm)	2.536	2.499	2.398	2.423
d0.5 (μm)	7.282	5.888	5.017	4.847
d0.9 (μm)	46.775	37.724	23.232	12.993

3.2.2 XRD analysis

Fig 3.2 displays the XRD profiles of individual raw materials before and after calcination at 1100 ^{o}C. It is clearly seen that the chemically pure TiO_2 contains two type of crystalline phases such as anatase (major phase) and rutile (minor phase). Similar phases were also identified by Dong et al., (2010) for pure TiO_2. In the fly ash, the observed crystalline phases are quartz (SiO_2) and corundum (Al_2O_3), which are consistent with the results reported by Jedidi et al. (2011). It is also noticed that in the fly ash, the intensity of quartz peak decreases due to conversion of quartz to corundum at the sintering temperature.

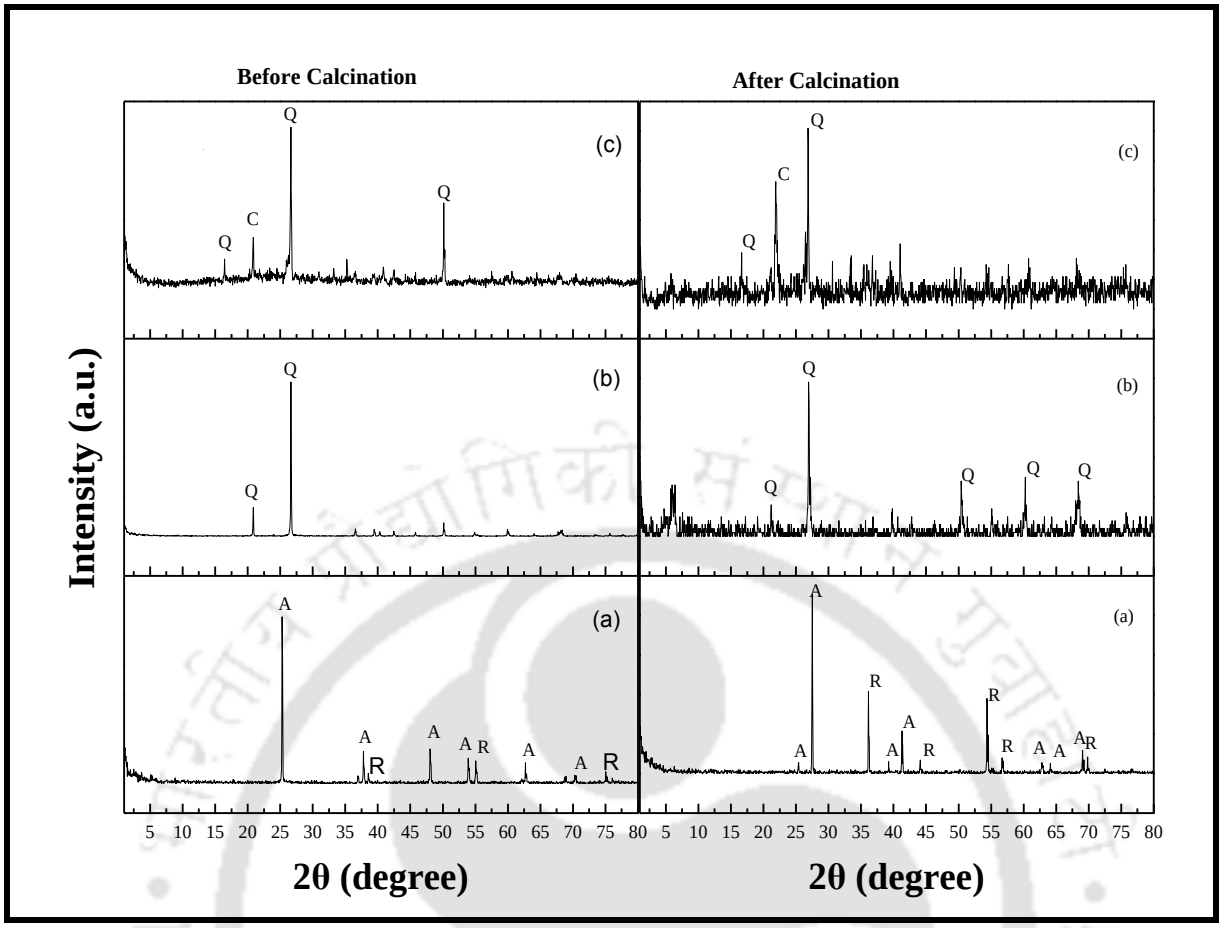

Figure 3.2: XRD of raw materials (a) Titanium dioxide (b) Quartz and (c) Fly ash (Q-Quartz, A-Anatase, R-Rutile, C- Corundum)

It is clearly seen from Fig. 3.2(b) that in comparison with before calcination, the peaks corresponding to the quartz are not changed in the XRD pattern of quartz after calcination. This signifies that the quartz is not affected by the sintering temperature. According to the literatures (Monash and Pugazhenthi 2011b; Vasanth et al., 2011a), no phase change is observed in the quartz during sintering. In addition, TGA analysis of quartz confirms that there is no significant weight loss during sintering (Vasanth et al., 2013; Monash and Pugazhenthi 2011b; Vasanth et al., 2011a). In view of the above, it can be concluded that quartz is thermally stable at the studied sintering temperature.

The XRD reflections of the membranes (SP1-SP4) before and after sintering are presented in Fig 3.3. In most cases, sintering produces series of reactions or phase transformations that

lead to the formation of new phases. As a result, the disappearance and shift in the peak positions are observed in the XRD analysis.

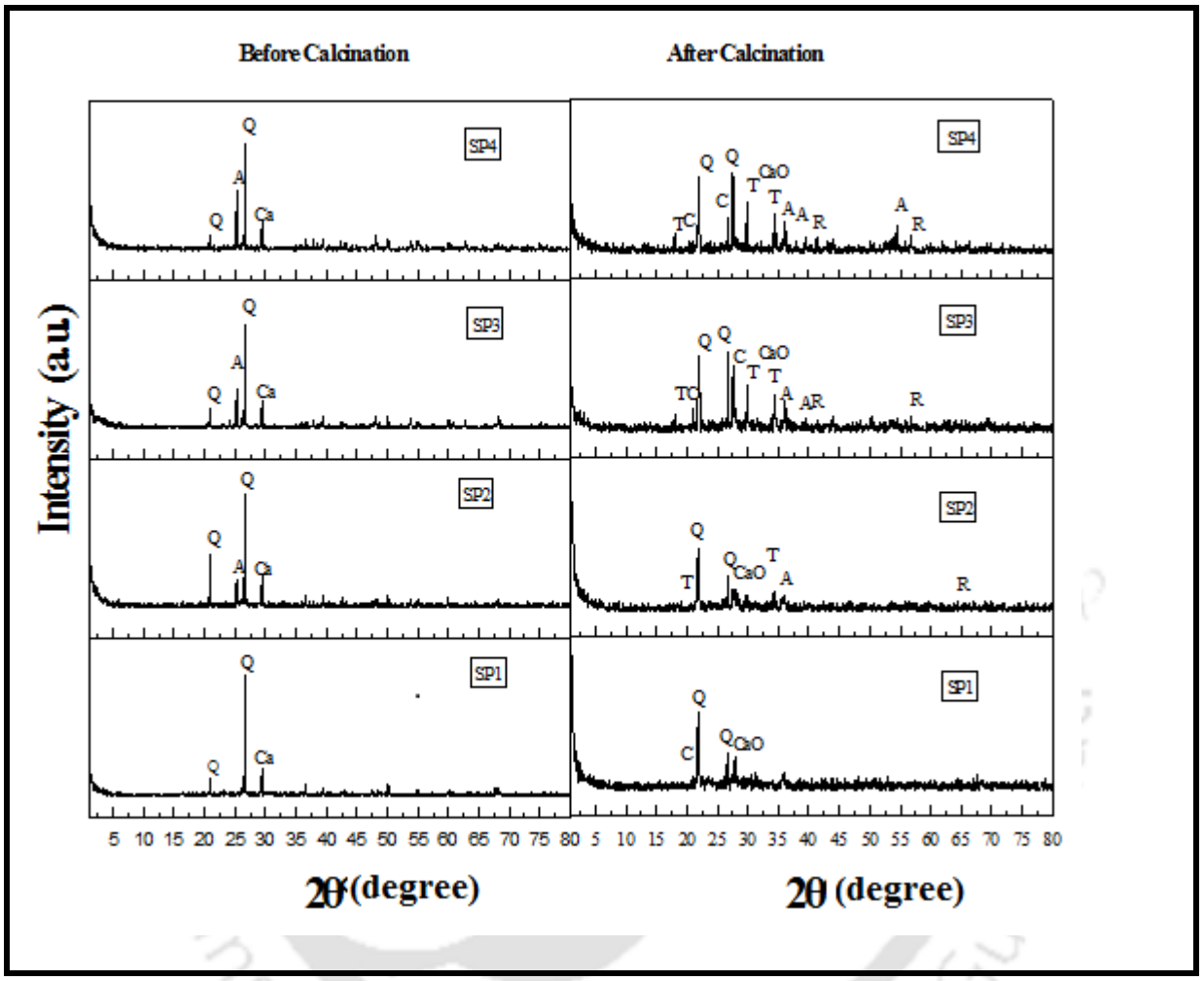

Figure 3.3: XRD analysis of powder mixtures used to fabricate of membranes (SP1-SP4) (Q-Quartz, Ca-Calcium carbonate, A-Anatase, C-Corundum and Cristobalite, T-Aluminum Titanate, R-Rutile, CaO- Calcium Oxide)

Although many phase transformations occur during sintering of the membrane, the formation of new phase for the prepared membrane is aluminum titanate ($Al_2O_3.TiO_2$) by reaction of rutile with corundum. During sintering, quartz reacts with rutile and converts to cristobalite and corundum (Jedidi et al., 2009). The background noise in the XRD pattern of the sintered

membrane suggests that there may be an existence of amorphous silica (Monash and Pugazhenthi 2011b; Gualtieri et al., 1995; Cultrone et al., 2001).

3.2.3 FESEM analysis

Surface morphology of the sintered membranes was studied using FESEM as depicted in Fig 3.4. These images demonstrate the membrane surface with rough morphological structure. The superficial observation of the FESEM images indicates that the membranes do not have any pinholes and cracks.

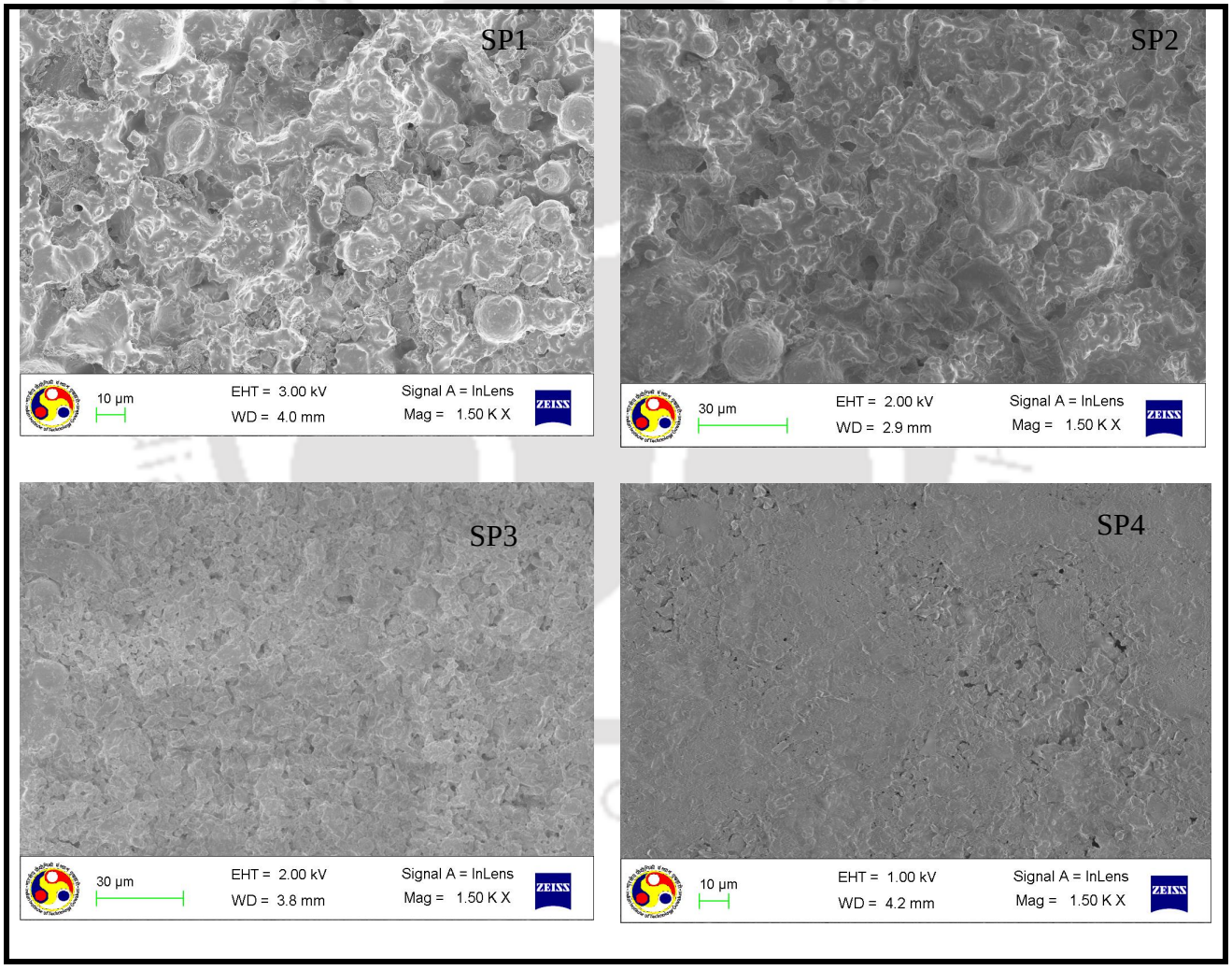

Figure 3.4: FESEM images of the membranes (SP1, SP2, SP3 and SP4)

The average pore size of the membranes estimated from FESEM images is found to be 3, 2.95, 2.79 and 2.28 µm for the membrane SP1, SP2, SP3 and SP4, respectively. The pore size distribution of membranes is presented in Fig 3.5. It is observed that the pore diameter of the membrane decreases with an increase in the TiO_2 content, which is due to binding ability of TiO_2 during sintering. Some of the pores may even disappear during sintering. It is well documented in the literature that the membrane pore size is significantly influenced by TiO_2 content and sintering temperature (Dong et al., 2010).

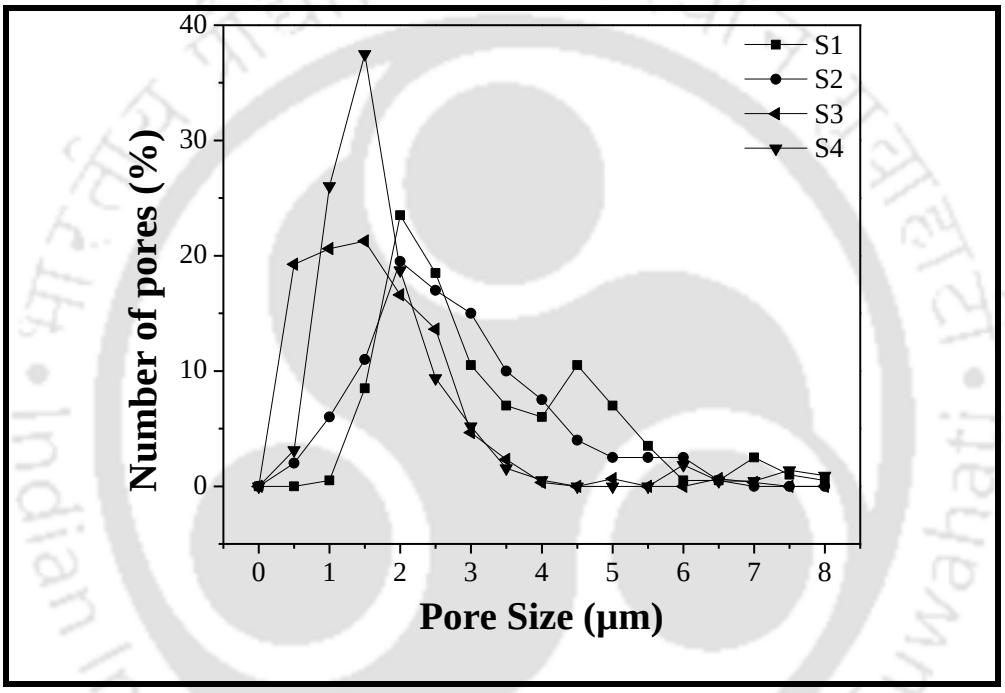

Figure 3.5: Pore size distribution analysis of the membranes (SP1-SP4) from FESEM images

3.2.4 Porosity

The porosity of the membranes determined by Archimedes principle and FESEM analysis is illustrated in Fig 3.6. The results clearly indicate that substantial changes are observed in the porosity of the membranes when the TiO_2 content increases in the precursor formulations. In general, the porosity of the membrane mainly depends on the amount of porosifier ($CaCO_3$) and an additive (TiO_2) present in the sample. However in this study, quantity of porosifier

($CaCO_3$) is kept constant for all membrane compositions and hence, the variation of porosity is due to the increased TiO_2 content. It is seen from the Table 2.1 (Chapter 2) that the domination of TiO_2 (W_{TiO2}/ $W_{fly\ ash}$) increases from 0 to 1.50. Consequently, the porosity of the membranes increases with an increase in the TiO_2 content and maximum porosity of 48 % is obtained for SP4 membrane. It is noticed that the surface porosity of the membranes determined by FESEM analysis is higher due to difficulty in controlling the threshold of the pores of the membranes.

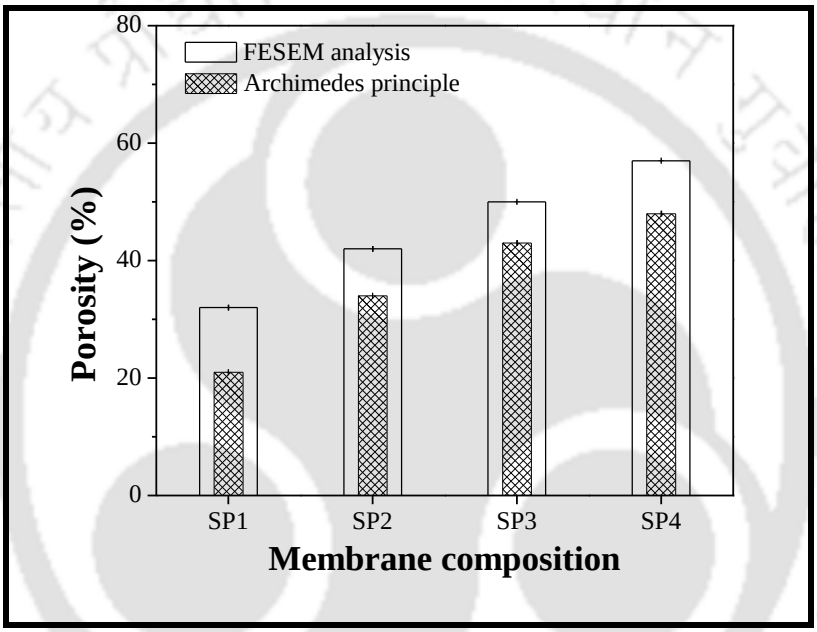

Figure 3.6: Porosity of membranes from FESEM analysis and Archimedes principle

3.2.5 Chemical stability

The chemical stability of the membranes was evaluated in terms of mass loss after keeping the membrane in contact with acid and alkali solutions individually. As the TiO_2 content increases, the weight loss of the membranes due to corrosion of acid decreases from 6 to 2% as depicted in Fig 3.7. The weight loss of the membrane due to alkali is found to be around 1% for all the membranes. The results reveal that the membranes exhibit better corrosion resistance in both acidic and basic medium. The obtained results are comparable with

cordierite (Dong et al., 2006) and alumino-silicate microfiltration membranes (Almandoza et al., 2004).

3.2.6 Mechanical strength

Fig 3.8 demonstrates that with increasing TiO_2 content in the precursor formulations, the flexural strength of the membranes increases from 6.02 to 13.82 MPa. Similar observation was also reported by Dong et al., (2010). In general, calcium carbonate ($CaCO_3$) is used as porosifier as well as sintering aid. Besides, the flexural strength of the membrane primarily depends on the amount of sintering aid present in the precursor sample (Bouzerara et al., 2006; Boudaira et al., 2009; Falamaki et al., 2004). However, in this study, the amount of $CaCO_3$ is kept constant for all the membrane formulations. Hence the enhanced flexural strength of the membrane is due to the increased densification with higher amount of TiO_2 at the sintering temperature (1100 ^oC) (Dong et al., 2010).

3.2.7 Hydraulic permeability and average pore size of membranes

All the prepared membranes were characterized for their hydraulic permeability. Pure water flux was measured by applying different pressures ranging between 28 to 69 kPa as depicted in Fig 3.9. It is observed that the flux of the membranes depends on the applied pressure and also increases with an increase in the applied pressure. The hydraulic permeability of the membranes is estimated to be 1.58×10^{-8}, 1.14×10^{-8}, 0.87×10^{-8} and 0.63×10^{-8} (m^3/m^2sPa) for the membrane SP1, SP2, SP3 and SP4, respectively.

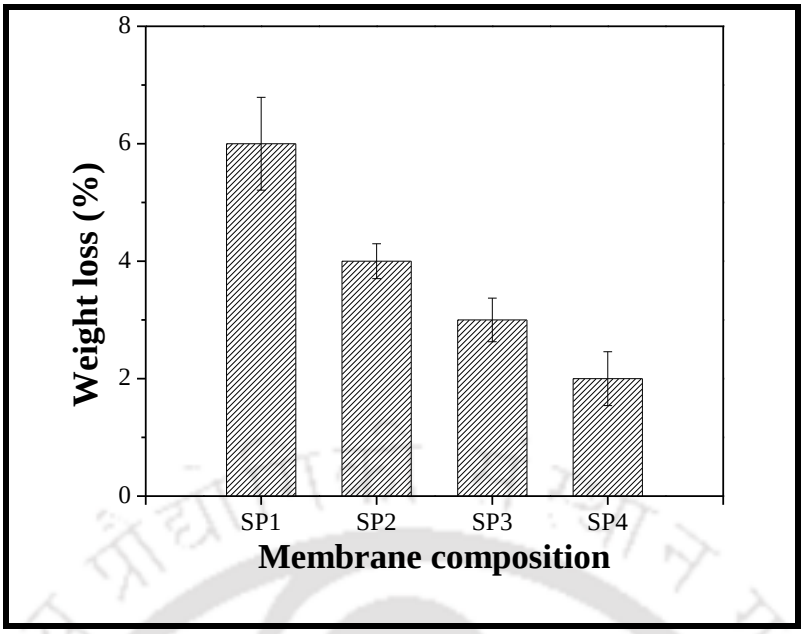

Figure 3.7: Chemical stability of the membranes (SP1-SP4) in acid

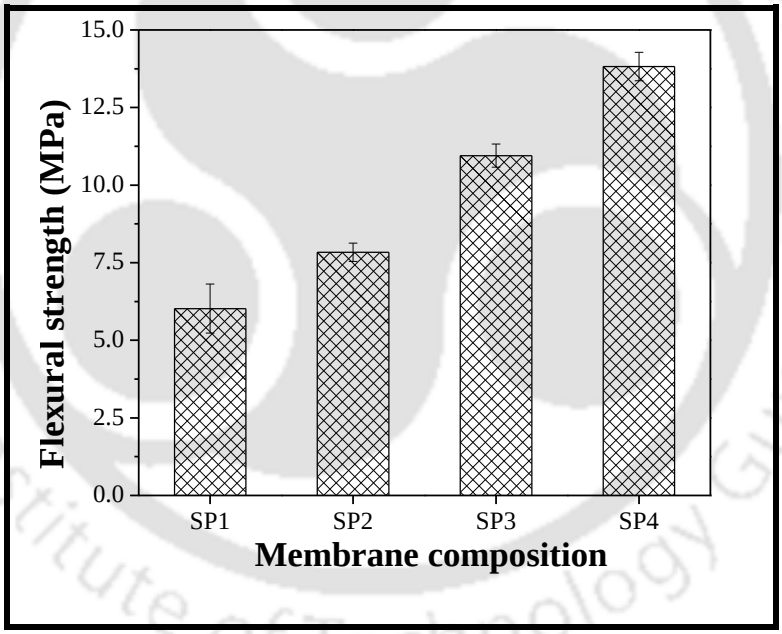

Figure 3.8: Flexural strength of the membranes (SP1-SP4)

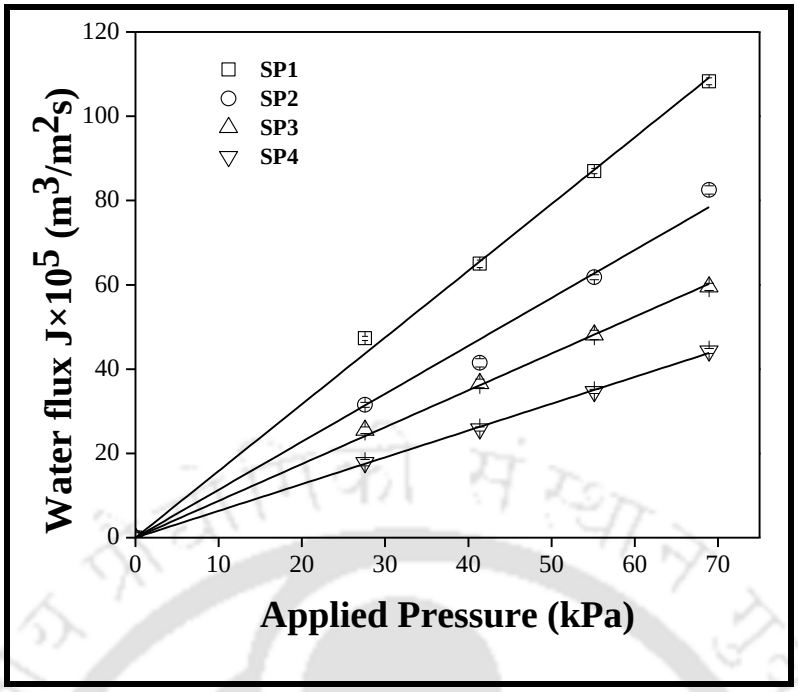

Figure 3.9: Variation of pure water flux of the membranes at different applied pressure

The average pore diameter of the membranes calculated from hydraulic permeability data is found to be 2.97, 1.77, 1.57, 1.32 μm for the membrane SP1, SP2, SP3 and SP4, respectively. The reduction in the pore size and pure water flux of the membranes with increasing TiO_2 content in the precursors is due to better densification of the membranes. The pore size of the ceramic membranes measured by FESEM analysis is slightly higher than those calculated from pure water permeability data. FESEM tends to overestimate the pore size as it can only assess the pore diameter at the surface of the membrane and some of the pores may be dead end pores (not through pores). The pore size obtained from water permeability data corresponds to a minimal size of the pore constriction through in which water passes and is smaller than the surface pore size. Thus the pore size obtained from water permeability is more accurate than FESEM analysis.

3.2.8 Separation of oil-in-water emulsion

Among the prepared membranes, the lowest pore size membrane (SP4) was tested for the separation of oil-in-water emulsion. Fig 3.10 illustrates the variation of the permeate flux and percentage removal of oil with various applied pressures (69-345 kPa) for the initial oil concentration of 200 mg/L.

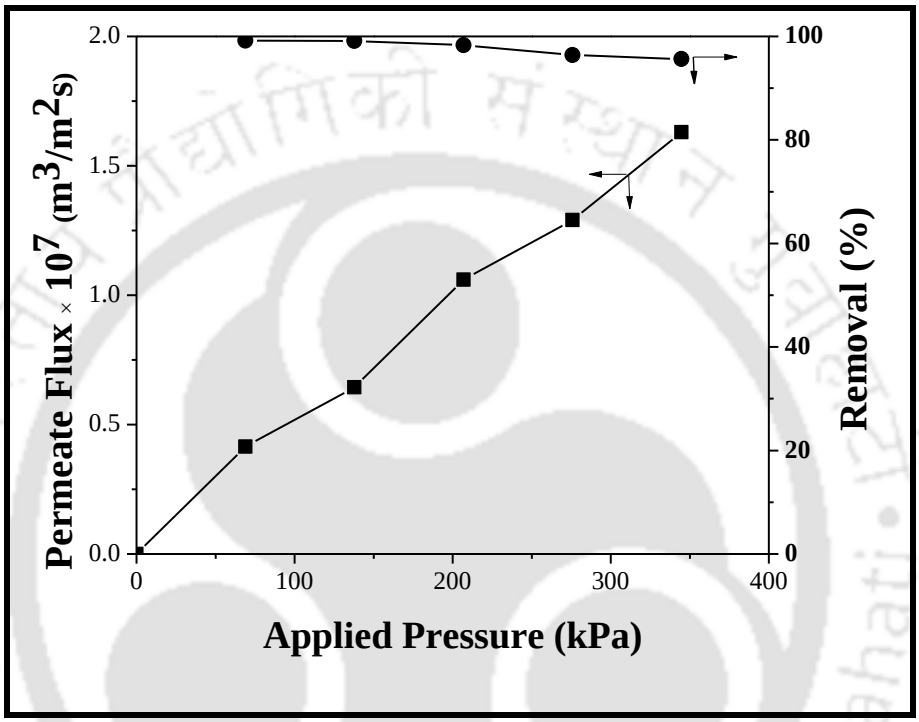

Figure 3.10: Variation of permeate flux and percentage removal of oil at different applied pressures for SP4 membrane

As expected, the removal of oil decreases slightly with an increase in the applied pressure. This is due to the fact that the higher pressure enhances the wetting and coalescence of oil droplets and this would enforce the oil droplets to pass through the membrane along with the permeate. The observed results are consistent with the results reported in the literature (Abadi et al., 2011; Arnot et al., 2000). The maximum rejection of 99.2% is observed at a lower applied pressure of 69 kPa. As the applied pressure increases from 69 to 345 kPa, the permeate flux also increases due to enhancement of the driving force across the membrane. A large difference between permeate flux and pure water flux under same condition is observed

Table 3.2: Comparison of oil removal percentage of fabricated membrane with other membranes

Membrane/support Material	Mean Pore size	Type of oil	Applied pressure (kPa)	Feed Concentration (mg/L)	Permeate flux×10^6 (m^3/m^2 s)	Removal (%)	Reference
α- Al_2O_3/ α-Al_2O_3	1.0 µm	Vegetable oil	100	5000	7.5	94.3	Yang et al., (1998)
α- Al_2O_3/α- Al_2O_3	0.2 µm	Vegetable oil	100	5000	6.11	99.9	Yang et al., (1998)
ZrO_2/ α- Al_2O_3	0.2 µm	Vegetable oil	100	5000	25.83	99.8	Yang et al., (1998)
NaA zeolite/ α- Al_2O_3	1.2 µm	Lubricant oil	50	100	5.0	98.8	Cui et al., (2008)
α- Al_2O_3	2.1 µm	Lubricant oil	50	100	2.083	55.0	Cui et al., (2008)
NaA zeolite/ α- Al_2O_3	0.4 µm	Lubricant oil	50	100	0.694	99.4	Cui et al., (2008)
Al_2O_3	0.16 µm	Lubricant oil	50	600 to 11000	7.083	98.0	Cui et al., (2008)
α- Al_2O_3	0.1 µm	Refinery oil	100	150	88.61	61.4	Ebrahimi et al.,(2010)
TiO_2/TiO_2	1000 Da	Refinery oil	100	565	17.78	99.5	Ebrahimi et al.,(2010)
Membrane, SP4	1.32 µm	Crude oil	69	200	0.04	99.2	Present study

for the studied membrane (SP4) on account of pore blocking and concentration polarization (see Figs 3.9 and 3.10).

For industrial application point of view, the membranes should possess higher removal efficiency with good permeate flux. Hence it can be concluded that the prepared membrane, SP4, displays better rejection (99.2-95.6%) of oil with permeate flux. In comparison with other membranes (see Table 3.2), the performance of the prepared membrane in terms of rejection and permeate flux, is comparable or even better than those reported in the literature. It can be concluded from Table 3.2 that the membrane (SP4) prepared from fly ash is useful for treating oily wastewater in the form of oil-in-water emulsion.

3.2.9 Cost estimation

Based on the retail cost of the raw materials, the average cost of the ceramic membranes is estimated as Rs. 3, 5, 6.5, and 8.5 per one circular shaped membrane for SP1, SP2, SP3 and SP4, respectively that corresponds to 15-40 ($/m^2) as listed in Table 3.3. The cost of the prepared membranes is comparable and even lower than the membranes reported in the literature (Emani et al., 2013; Vasanth et al., 2011b; Nandi et al., 2011; Jana et al., 2010; Mittal et al., 2011). It is worth to mention that the cost of the ceramic membranes prepared by Emani et al., (2013), Vasanth et al., (2011b), Nandi et al., (2011) and Mittal et al., (2011) is 78, 67, 130 and 34 ($/m^2), respectively. Moreover, cost of the inorganic membranes is projected to be around 500-1000 ($/m^2) (Koros et al., 2000; Nunes and Peinemann 2001; Ceramiques techniques & industrielles, 2007). The cost of the commercial membrane made of α-Al_2O_3 is reported to be 989-1220 ($/m^2) (Krauczyk and Jonsson 2014).

Table 3.3: Cost estimation of membranes (SP1-SP4)

Raw materials	Unit price (Rs./ kg)	Amount of raw materials used for the fabrication of one membrane (kg)	Cost estimated for the Fabrication of one membrane (Rs.)			
			SP1	SP2	SP3	SP4
Quartz	10.00	7.50×10^{-3}	0.075	0.075	0.075	0.075
Calcium carbonate	520	5.00×10^{-3}	2.6	2.6	2.6	2.6
Fly ash	28.0	12.5×10^{-3}	0.35	0.28	0.21	0.14
Titania	720	2.5×10^{-3}	-	1.8	3.6	5.4
Raw materials cost for one membrane fabrication			3.02	4.76	6.48	8.22
Cost of one ceramic membrane of 5 mm thickness and 63 mm diameter (rounded value)			3	5	6.5	8.5
Estimated raw materials cost per unit area of the fabricated membrane			963/m^2 (15 \$/m^2)	1605/m^2 (25 \$/m^2)	2086/m^2 (33 \$/m^2)	2567/m^2 (40 \$/m^2)

Cost is always considered as a massive apprehension in the membrane process, which is mainly from energy consumption and membrane replacement. The use of conventional membranes in wastewater treatment requires high energy input in order to keep constant efficiency due to lower membrane permeability. Generally membranes made of clay based raw materials possess higher permeability than conventional membranes; as a result, lower cost on energy. Currently, natural clays and fly ash are most preferred membrane materials when compared with other materials because of their low cost. Typically, the membrane separation process using alumina and zirconia based membranes is more expensive than those

using clay based membranes because of the costly raw materials. On the contrary, fly ash is rather cost effective compared to conventional membranes. In addition, enhanced antifouling ability of the clay based membranes extends the back flushing interval and membrane life span that also increases the price gap between the clay membranes and commercial membranes.

3.3 Summary

The porosity of the membranes is found to be 21, 34, 43 and 48% for the membrane SP1, SP2, SP3 and SP4, respectively. The prepared membranes with various composition offer good mechanical strength (6.02-13.82 MPa). The weight loss of the membranes (SP1-SP4) in acid and alkali solution is found to be 6-2%, 1%, respectively indicating that these membranes are more stable in both acidic and basic medium. The average pore size of the membranes calculated from water permeability data is found to be 2.97, 1.77, 1.57 and 1.32 μm for the membrane SP1, SP2, SP3 and SP4, respectively. The performance of the fabricated membrane (SP4) is demonstrated by separation of oil from oil-in-water emulsion. The maximum removal of oil is observed to be 99.2% with permeate flux of 4.1×10^{-8} (m^3/m^2s) at an applied pressure of 69 kPa for the initial oil concentration of 200 mg/L. Based on the cost of raw materials, cost of the membranes is estimated to be around 15-40 ($\$/m^2$).

CHAPTER-4

Preparation, Characterization, Optimization and Application of Low Cost Fly ash Based Ceramic Membranes

भारतीय प्रौद्योगिकी संस्थान गुवाहाटी
Indian Institute of Technology Guwahati

CHAPTER 4 Preparation, characterization, optimization and application of low cost fly ash based ceramic membranes

After brief overview on fabrication of membranes (M1-M3) in section 4.1, sections 4.2.1-4.2.8 present the results obtained during characterization and dead end MF of oil-in-water emulsions for the low cost fly ash based ceramic membranes (M1-M3). Section 4.2.9 summarizes the flux and rejection profiles and followed its subsequent analysis using RSM model in section 4.2.11. Section 4.2.10 presents the overall cost estimation for the membranes during microfiltration studies. Finally, section 4.3 presents a summary of the dead end MF and RSM data.

4.1 Overview

This chapter addresses further maximum quantity of fly ash usage in raw materials composition to fabricate fly ash based ceramic membranes of variant morphological properties. Fly ash/$CaCO_3$/Quartz addition/removal has been carried out to target the necessary variations. Three new compositions were identified for the fabrication of membranes with maximum utilization of fly ash. The membranes (M1-M3) were prepared with identified new compositions of fly ash by following uniaxial compaction method. The main objective of this chapter is to evaluate various membrane properties such as average pore size, porosity, chemical and mechanical stability and pure water permeability. The prepared membranes (M1-M3) were subjected to dead-end flow microfiltration of oil-in-water emulsions. In addition to that, the effect of feed concentration and applied pressure on rejection of oil and permeate flux was investigated. Finally, the parametric optimization study was carried out by response surface methodology.

4.2 Results and Discussion

4.2.1 Particle size distribution

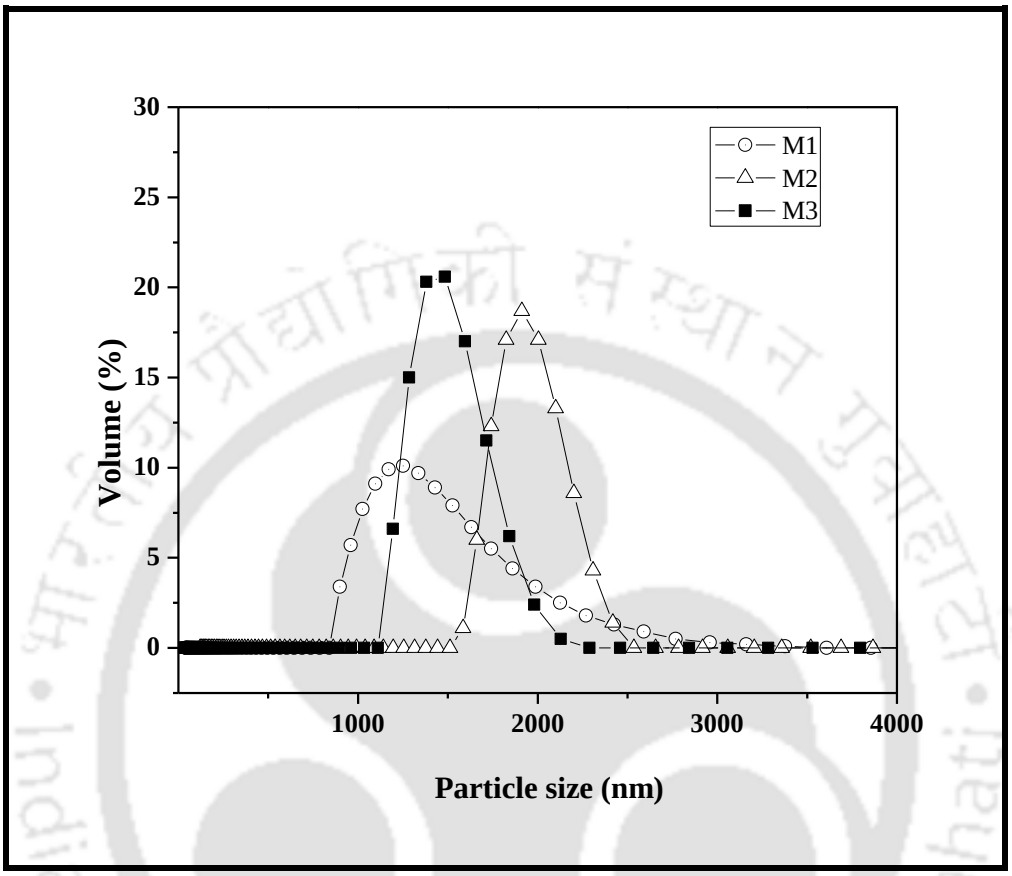

Figure 4.1: Particles size distribution of the membrane powder mixture (M1-M3)

Three powder mixtures (M1, M2 and M3) were analyzed for their particle size distributions. It is well known that the size distributions of the inorganic precursor mixture strongly influence the membrane morphological properties including pore size and porosity. Therefore, particle size distribution analysis of three composition mixtures was performed and the results are shown in Fig. 4.1. It is apparent from Fig. 4.1 that in comparison with M2 and M3, M1 sample has smaller particle size. The possible reason could be that some particles of M1 sample have smaller particle size (fly ash) than that of quartz and absence of $CaCO_3$.

4.2.2 Thermo gravimetric analysis

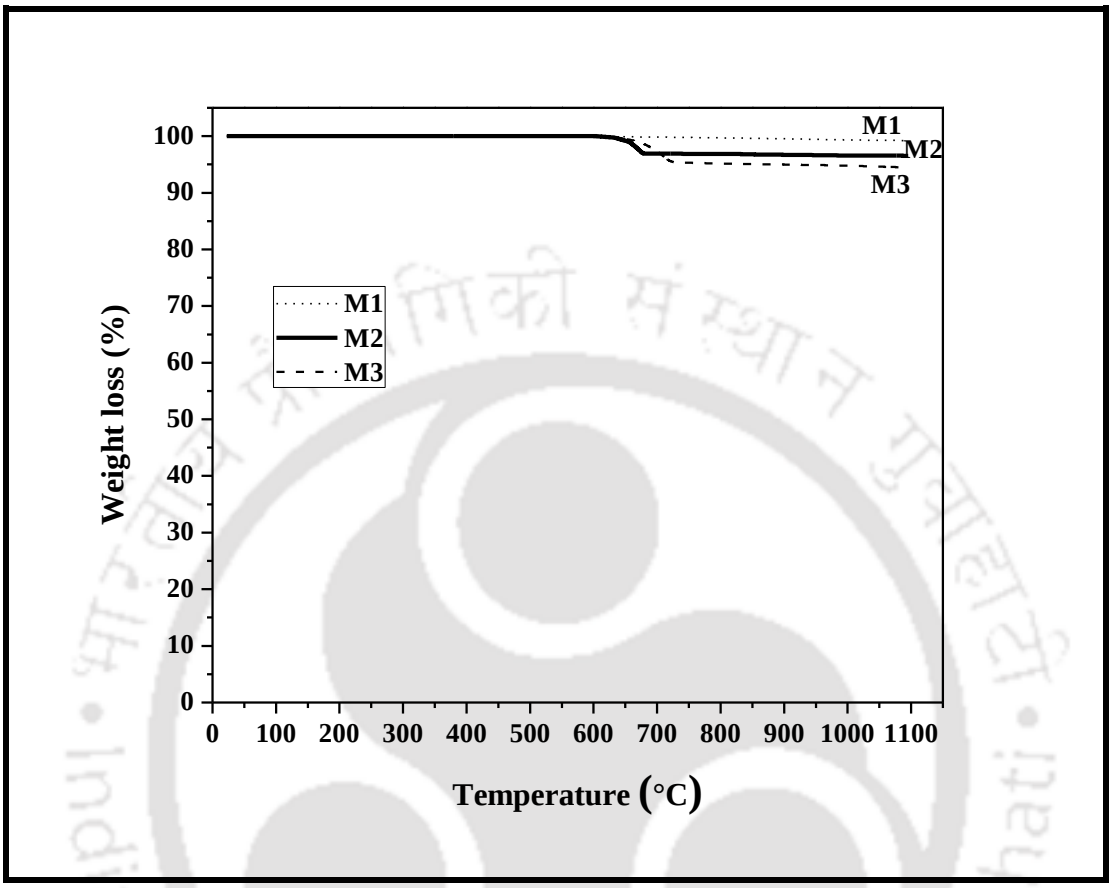

Figure 4.2: TGA graph of the membrane powder mixture (M1-M3)

TGA curves of the raw materials mixtures are shown in Fig. 4.2. As indicated in the figure, maximum weight loss occurs due to the decomposition of $CaCO_3$ and generation of CO_2. The membrane porosity is primarily dependent on the released CO_2 gas moved path. Moreover, for both membranes M2 and M3, almost same (4%) net weight loss is obtained for the powder mixture. This result infers that the weight loss of the membrane mainly depends upon the quantity of calcium carbonate of samples. Above 800 ^oC, it is also observed that all samples affirm insignificant weight loss and thereby confirm upon the validity of preposition that the minimum sintering temperature needs to be higher than 800 ^oC. For M2 and M3, the

slower mass decrease in the powder mixture (<800 °C) is possibly due to $CaCO_3$ thermal decomposition. The TGA curve for M1 membrane mixture indicates upon an insignificant weight loss due to fly ash and absence of $CaCO_3$ (Monash and Pugazhenthi, 2011).

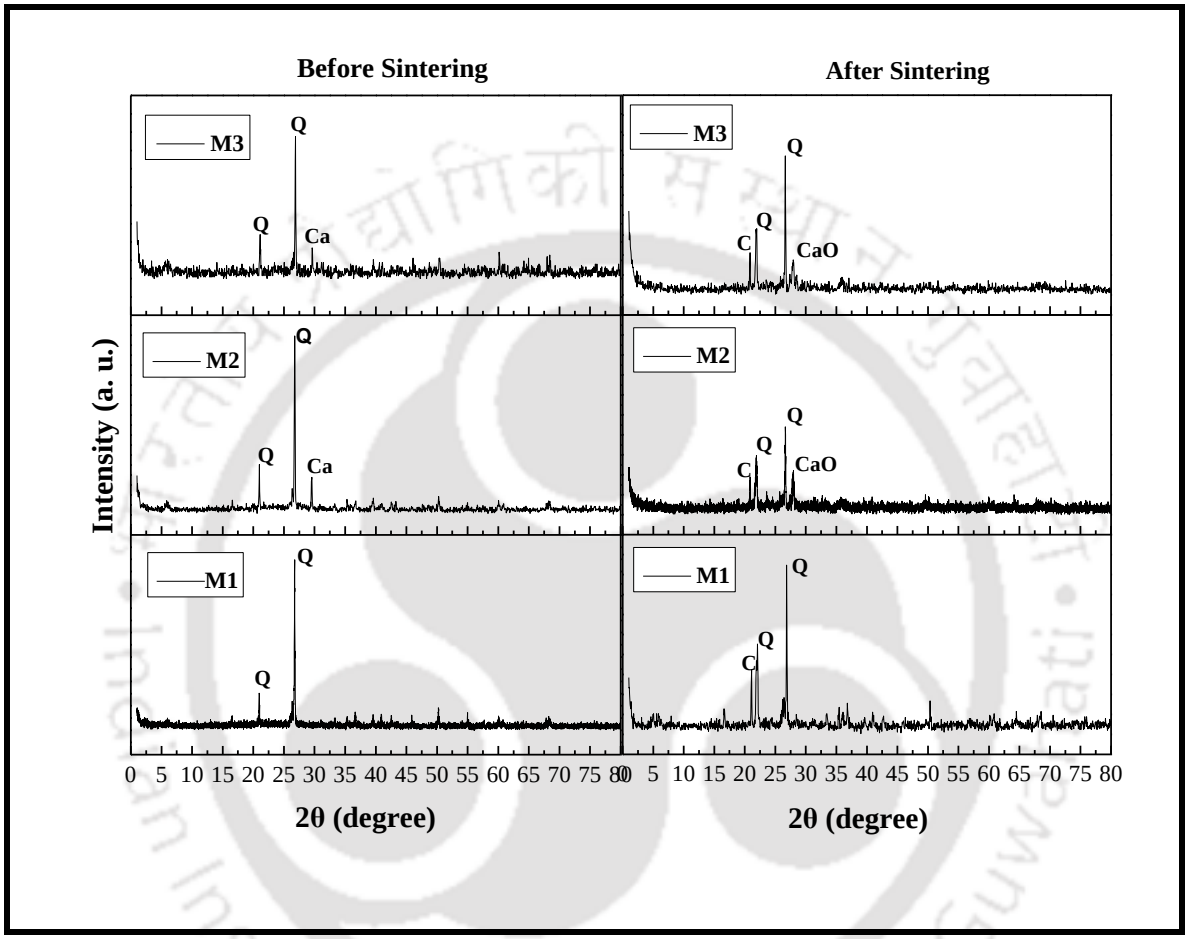

Figure 4.3: XRD analysis of raw material powder mixture (M1-M3) (Q-Quartz, Ca-Calcium carbonate, CaO-Calcium oxide, C-Cristobalite and Corundum)

4.2.3 XRD

The XRD analysis facilitates the identification of various phases that exist before and after sintering and thereby visualize various phase transformations and newer phase formations during membrane sintering. Fig. 4.3 presents the XRD patterns of the unsintered

and sintered membrane (M1-M3) samples. For the fly ash, it has been reported that quartz (SiO_2) and corundum (Al_2O_3) crystalline phases exist (Suresh and Pugazhenthi, 2016). For both unsintered and sintered samples of fly ash, it has been observed that there are changes in the peaks corresponding to the quartz and this confirms that during sintering, quartz is converted to cristobalite and corundum. Similar observations are reported in the literature (Jedidi et al, 2009).

4.2.4 Porosity

The average porosity was evaluated to be 30, 39 and 43% for M1, M2 and M3 membranes, respectively. Thus, for M1 membrane, lower porosity exists and significant differences in the porosities of the membranes is due to the porosifier concentration (calcium carbonate) in the precursor mixture. Even though the amount of calcium carbonate available in the M2 and M3 membrane composition is same, the variation of porosity is due to the variant quantities of fly ash. Thus, the membrane porosity increases with increasing concentrations of $CaCO_3$ and fly ash and highest porosity of 43% was obtained for M3 membrane.

4.2.5 Chemical stability

For membranes, the acid corrosion based weight loss is 28 (M1), 26 (M2) and 24 (M3) %, respectively. Significant weight loss during acidic corrosion tests is due to the presence of CaO in the membrane morphology. For all membranes, only 1% weight loss was evaluated during base corrosion tests. Thereby, the membranes can be concluded to be highly relevant for processing basic but not acidic media.

4.2.6 Flexural strength

The membrane flexural strength is evaluated as 1.68 (M1), 6.99 (M2) and 9.25 (M3) MPa. It is observed that the flexural strength increases with the addition of $CaCO_3$ content for M2, and M3 membranes in comparison with M1. Hence, the significant increase in the flexural strength is due to strong interaction between the quartz and $CaCO_3$ and large interfacial area between them. These observations confirm that $CaCO_3$ serves as both porosifier and sintering aid in the membrane morphology and sintering process. The membrane densification is strongly influenced by the inorganic precursor composition. Therefore, membrane densification increased with enhancement of sintering aid and thereby increased flexural strength. These observations and reasoning statements are in agreement for the membrane densification trends presented for literature reported variation in $CaCO_3$ compositions for clay membranes (Monash and Pugazhenthi, 2011; Suresh and Pugazhenthi, 2016).

4.2.7 SEM analysis

It is well known that the membrane morphologies are crucial factors to influence the membrane performance. Therefore, SEM based investigations of the membrane surface morphologies was conducted. Fig. 4.4 presents the surface image of M1, M2 and M3 at same magnification. These images confirm that no surface defects such as pinholes and cracks exist on the surface. Fig. 4.4 shows that the smooth surface membrane has number of smaller pores and some of them have been identified as bigger pores from image. Hence, the membrane (M1) with this kind of morphology may probably provide good performance. In comparison with M1, the membrane M2 has smoother surface with more number of smaller pores. Moreover, membranes M1 and M2 have the same content of fly ash and different amount of $CaCO_3$. Although membranes M2 and M3 possess same quantity of $CaCO_3$, the membrane

M3 demonstrates the smooth surface with larger pores due to the increased amount of quartz in comparison with the M2. Based on the analysis, it has been observed that the membrane pore size varied from 0.001 – 2.75 µm and affirms diverse porous structure. The SEM image analysis based pore size is evaluated as 2.0 (M1), 1.75 (M2) and 1.79 (M3) µm, respectively. Corresponding membrane pore density has been estimated as 4.12×10^{14}, 6.49×10^{14}, 7.42×10^{14} (number of pores/m^2), respectively. Thus, it is apparent that the membrane pore density is strongly influenced with the precursor composition variation (Table 2.2). The N_2 gas permeation data based effective permeability factor variation with average pressure is presented in Fig. 4.5(a) for various cases. Among all cases, for M2 membrane, lowest combinations of effective permeability factor and pore size have been obtained. The N_2 permeation based average membrane pore size values are 1.36 (M1), 1.30 (M2) and 1.44 (M3) µm, respectively. Corresponding SEM analysis based mean pore size values are 2.0, 1.75 and 1.79 µm, respectively. Significant variation in the SEM analysis based mean pore size and that determined with N_2 permeation study is due to the reason that gas permeation based data refers to open channel pores, which is not the case for SEM based analysis in which even dead pores are as well counted for pore size evaluation.

4.2.8 Water flux and Hydraulic permeability

In agreement with the Darcy's law, Fig. 4.5(b) affirms that membrane water flux linearly increases with increasing applied pressure and refers to a straight line passing through the origin. Using the water flux plot, membrane hydraulic permeability (L_h) is determined (Srijaroonrat et al, 1999).

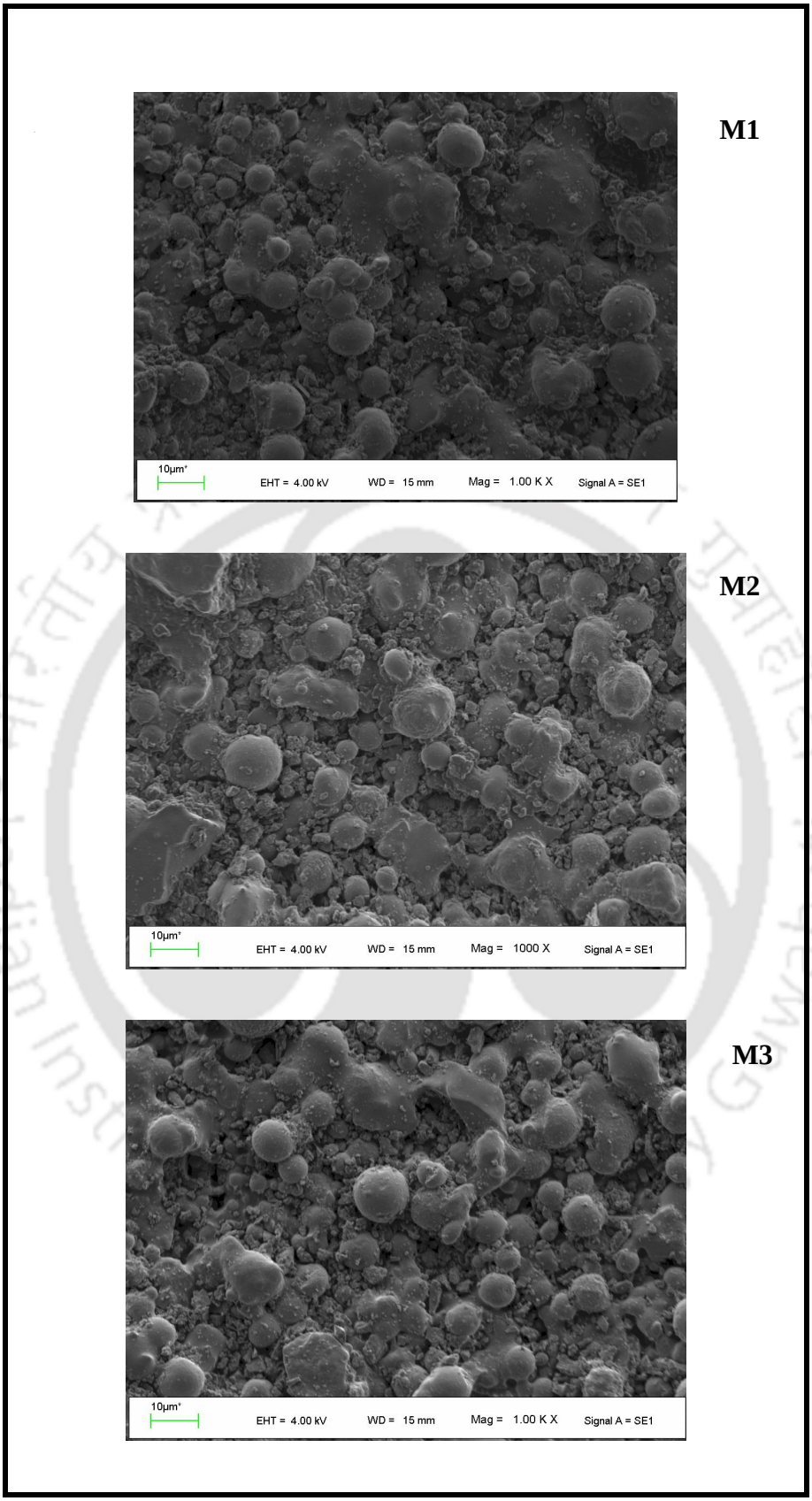

Figure 4.4: SEM images of membrane (M1-M3)

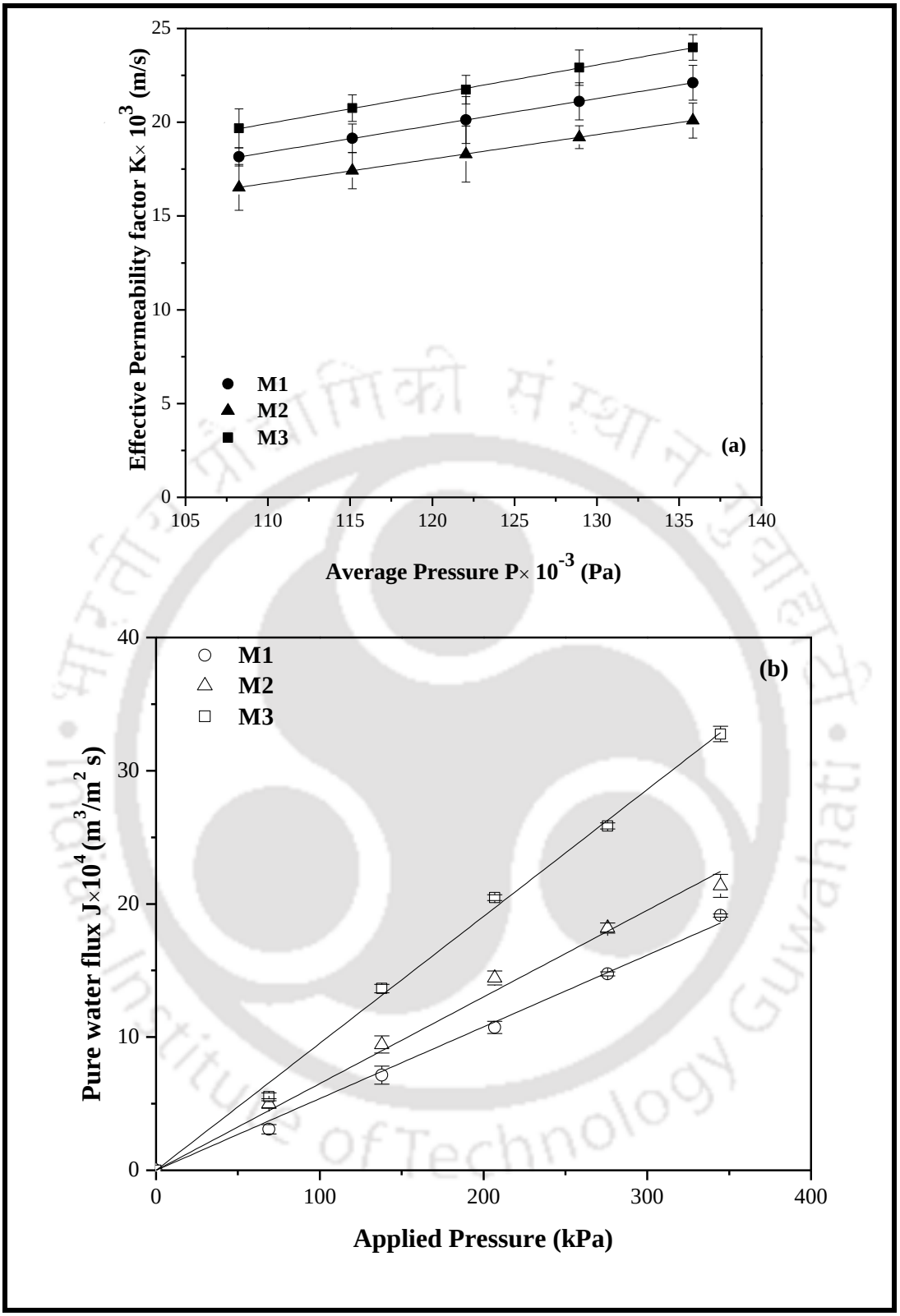

Figure 4.5: Variation of (a) N_2 gas permeate flux (b) pure water flux with applied pressure for membrane M1-M3

In the Figure, the solid line refers to the regression of the data with a condition that the line needs to pass through the origin i.e., water flux value is zero for applied pressure value of zero. The membrane hydraulic permeability values are subsequently evaluated as 5.384×10^{-6} (M1), 6.508×10^{-6} (M2) and 9.53×10^{-6} (M3) (m^3/m^2s kPa).

All characterization parameters evaluated for M1-M3 membranes are presented in Table 4.1. Table 4.2 presents a comparative assessment of obtained results with those presented in the literature for other ceramic membranes. From both Tables (4.1 and 4.2), it can be inferred that the fly ash based ceramic membranes prepared at lower sintering temperature have superior morphological characteristics in terms of pore size and porosity.

4.2.9 Dead end MF of oil-in-water emulsions

For prepared emulsions, droplet size of synthetic oil-in-water emulsions varied from 0.5-100 µm. The average droplet size has been evaluated as 1.761, 2.989, 6.037 and 6.928 µm for 50, 100, 150 and 200 mg/L synthetic oil-in-water emulsion solution, respectively [12, 49]. The pH of oil-in-water emulsions of various concentrations is found to be 5.51, 5.63, 5.78 and 6.05 for 50, 100, 150 and 200 mg/L, respectively.

Fig. 4.6 presents the permeate flux and membrane rejection variation with pressure. Compared to water flux, the membrane flux is significantly low for the MF of emulsion. The figure is in accordance with the theoretical insight that refers to enhancement in membrane flux with increasing driving force. Further, membrane flux has been observed to reduce with increasing feed concentration. This is due to the reason that higher feed concentration refers to greater size distributions of the emulsion droplets, which enhances pore blocking rate. From Fig. 4.6, it is also apparent that membrane M3 flux is higher than that obtained for M1 and M2 membranes. Lowest flux is obtained for M2 membrane and this is due to its lower pore size. For the operating and process conditions of 50 mg/L feed concentration and

345 kPa applied pressure, maximum permeate flux values of 6.55×10^{-4} (M1), 4.42×10^{-4} (M2) and 8.19×10^{-4} (M3) m^3/m^2 s have been evaluated.

Fig. 4.6 also affirms that rejection reduces with increasing pressure. This is due to the enhanced oil droplet wetting and coalescence at higher pressure to allow greater transport of oil droplets through the porous membrane structure. On the other hand, membrane rejection enhanced with increasing feed concentration. This increase of rejection value is an enhancement in both oil droplet size and density with oil concentration. In summary, the prepared membranes are effective to remove oil from oily wastewater. According to the results shown in Fig. 4.6, the treatment of oil-in-water emulsions by microfiltration facilitates a significant reduction in the permeate oil concentration. At 69 kPa applied pressure and 200 mg/L feed concentration, the maximum rejection of oil by M1, M2 and M3 is found to be 99.94%, 99.99% and 96.12%, respectively. The research findings precisely indicate the better performance of the fly ash membranes for oil rejection.

Table 4.3 summarizes a comparative summary of evaluated oil rejection data and literature data. From the Table 4.3, it can be understood that the membranes prepared from low cost materials performed well in treating the oil-in-water emulsions. In addition, despite providing lower flux, membrane M2 performance in terms of rejection is better than that of M1 and M3. At 69 kPa pressure and 200 mg/L feed concentration, M2 membrane provided a flux and rejection of 0.337×10^{-4} (m^3/m^2 s) and 99.99%, respectively. Corresponding values for M1 and M3 membranes are 0.415×10^{-4} m^3/m^2s, 99.94% and 0.413×10^{-4} m^3/m^2s, 96.12%, respectively. Since industrial applications require higher rejection and good flux, membrane M2 is inferred to be the best for industrial applications.

Table 4.1: Characterization results of fabricated membranes

Properties	Membrane M1	Membrane M2	Membrane M3
Pore size (SEM)	2 µm	1.75 µm	1.79 µm
Pore size (from N_2 gas permeate flux)	1.36 µm	1.30 µm	1.44 µm
Porosity (%)	30	39	43
Hydraulic permeance (m^3/m^2s kPa)	5.384×10^{-6}	6.508×10^{-6}	9.53×10^{-6}
Mechanical Strength	1.68 MPa	6.99 MPa	9.25 MPa
Cost of one membrane ($/$m^2$)	462	465	465

Table 4.2: Comparative study of fabricated membranes

Membrane materials	Sintering Temperature (°C)	Average pore size (µm)	Porosity (%)	Mechanical strength (MPa)	Author
Membrane M1	1100	1.41	30	1.68	Present work
Membrane M2	1100	1.36	39	6.99	Present work
Membrane M3	1100	1.53	43	9.25	Present work
Apatite	1150	5	48	14	Masmoudi et al., (2007)
Cordierite	1380	8.66	36	31	Dong et al., (2007)
Kaolin+Dolama	1200	3.77	41	6	Bouzerara et al., (2006)
Kaolin+Dolama	1250	11.09	41	15	Bouzerara et al., (2006)
Morocan clay	1175	10.75	43	3	Saffaj et al., (2006)

Table 4.3: Comparison of oil rejection of fabricated membrane with other membranes

Membrane/support Material	Mean Pore size	Type of oil	Applied pressure (kPa)	Feed (ppm)	Oil droplet size (µm)	Permeate flux×10^6 (m^3/m^2 s)	Rejection (%)	Author
α- Al_2O_3	0.2 µm	Refinery oil	125	26	20	69.44	84.61	Abadi et al., (2011)
γ- Al_2O_3/α- Al_2O_3	10 nm	Vegetable oil	100	5000	-	5.0	99.8	Yang et al., (1998)
α- Al_2O_3/ α-Al_2O_3	1.0 µm	Vegetable oil	100	5000	-	7.50	94.3	Yang et al., (1998)
α- Al_2O_3	500 nm	Kerosene	300	1000	11	175	----	Srijaroonrat et al., (1999)
NaA zeolite/ α- Al_2O_3	1.2 µm	Lubricant oil	100	100	1.5	16.67	98.8	Cui et al., (2008)
NaA zeolite/ α- Al_2O_3	0.4 µm	Lubricant oil	100	100	1.5	1.39	99.4	Cui et al., (2008)
α- Al_2O_3	2.1 µm	Lubricant oil	100	100	1.5	4.17	55.0	Cui et al., (2008)
Clay	0.98 µm	Crude oil	345	200	1.211	79.78	98.6	Monash and Pugazhenthi, (2011)
Polyvinylidene Fluoride (PVDF)	0.45 µm	Gas-oil	300	3000	0.901	134	80	Masoudnia et al., (2013)
α- Al_2O_3	0.1 µm	Refinery oil	100	150	-	88.6	61.4	Ebrahimi et al., (2010)
TiO_2/TiO_2	1000Da	Refinery oil	100	565	-	17.8	99.5	Ebrahimi et al., (2010)
Fly ash	0.77 µm	Crude oil	100	75	2.8	44.17	95.30	Fang et al., (2013)
Coal	1 µm	Crude oil	100	120	5	17.86	97.80	Song et al., (2006)
Membrane M1	1.41 µm	Crude oil	69	200	6.928	41.5	99.94	Present study
Membrane M2	1.36 µm	Crude oil	69	200	6.928	33.7	99.99	Present study
Membrane M3	1.53 µm	Crude oil	69	200	6.928	41.3	96.12	Present study

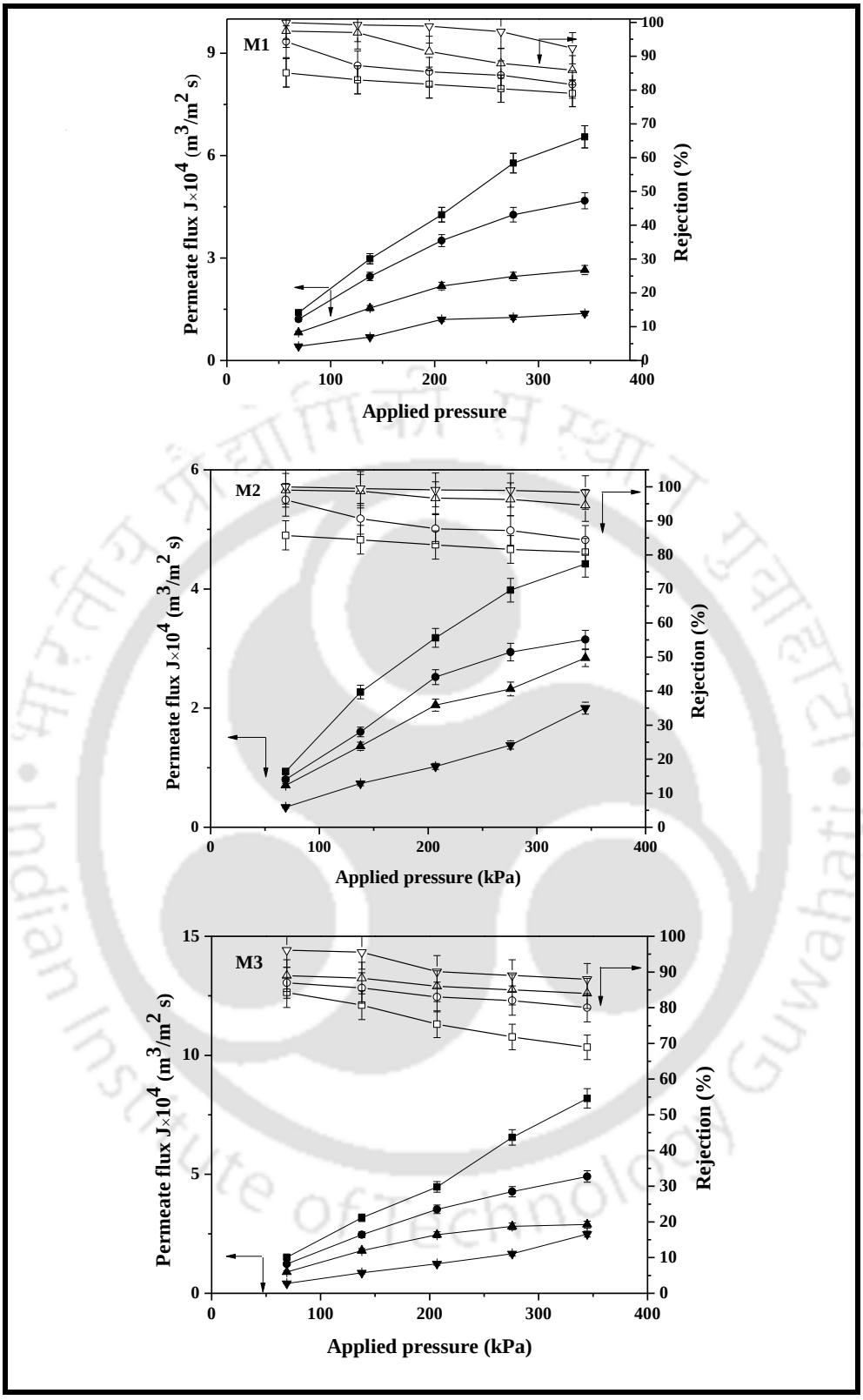

Figure 4.6: Effect of applied pressure and feed concentration on permeate flux and rejection (M1-M3) ■□-50 mg/L; ●○-100 mg/L; ▲Δ - 150 mg/L; ▼▽ -200 mg/L (Filled symbol: Flux, Unfilled symbol: Rejection)

4.2.10 Cost estimation

The in-house made ceramic membranes from fly ash need to be analyzed towards cost effectiveness. Therefore, retail cost estimation has been done for the fabricated membranes (M1-M3). The cost analysis involved the consideration of various parameters associated to the cost of raw materials, manpower, electricity and equipment for the retail cost estimation. The parameters considered for the cost estimation of membranes are presented in Table 4.4. Appendix I summarizes the details with respect to the cost estimation for the membrane fabrication and oil-in-water emulsions treatment. The fabricated ceramic membrane costs are evaluated as 462 (M1), 465 (M2) and 465 (M3) $/m^2. In the literature, ceramic membrane cost is reported to be about 500 – 1000 $/m^2 (Cheryan, 1998; Koros and Mahajan, 2000). The cost of α-Al_2O_3 symmetric ceramic membrane is 500 $/m^2 and the cost of membrane made from stainless steel is about 3000 $/m^2 (Mott Metallurgical Corp., 2007). For polymeric membranes and symmetric α-alumina membranes, the costs vary from 50 – 200 $/m^2 (Cheryan, 1998) and 2000-4000 $/m^2 (Tennison, 2000), respectively. It is further important to note that the membrane cost estimated and reported in this work is conceptual and could vary significantly after detailed cost estimation. However, it is inferred that the fabricated membranes are inexpensive than those prepared with alumina and zirconia from the perspective of raw materials cost and lower sintering temperatures.

Further, cost analysis for oil-in-water emulsion separation with the fabricated membranes for large-scale operation was conducted using obtained experimental results. Total membrane system cost that includes equipment (Dead end flow permeation setup), piping and instrumentation costs ($ 225) and N_2 gas ($ 295.41)) is evaluated as $ 520.41 for 10 years period. Hence, assuming straight-line depreciation, the total fixed cost per year is 52 $/year. The prepared membranes (M1-M3) could be operated for 69 kPa and 200 mg/L applied pressure and feed concentration, respectively at which their flux values are 4.15×10^{-5}

(M1), 3.37×10^{-5} (M2) and 4.13×10^{-5} m^3/m^2 s (M3). Corresponding rejection values are 99.94, 99.99 and 96.12%. With an assumption of 8 h operation per day, total processed oil-in-water emulsion feed in an year are 310752, 252345.6 and 309254.4 L with M1, M2 and M3, respectively. For the treatment, the N_2 gas cost is evaluated as $ 10/year for the dead end MF unit operation. With straight-line depreciation for a time period of 7 years, the ceramic membrane cost is 66 (M1), 67 (M2) and 67 (M3) $/year. A further reduction in membrane shelf life could be considered by taking membrane shelf life as 3 years.

Table 4.4 presents a summary of costs involved with membrane cleaning, maintenance (3% of membrane system cost) and labor cost (2% membrane system cost). The cost estimation presented in Table 4.4 indicated significant variation due to variations in equipment costs and flux production (or feed treated). In summary, the fly ash based ceramic membranes are effective and efficient for oil-in-water separation applications in comparison with highly expensive ceramic membranes.

Table 4.4: Cost estimation for fabrication of membranes and oil-in-water emulsion treatment

Source	M1	M2	M3
Raw materials cost ($/m^2)	4.1913	7.3876	7.1375
Labor cost ($/m^2)	197.4017	197.4017	197.4017
Electricity cost ($/m^2)	156.7317	156.7317	156.7317
Equipment cost ($/m^2)	56.1900	56.1900	56.1900
Miscellaneous cost ($/m^2)	46.5931	46.5931	46.5931
The overall fabrication cost of one membrane ($/m^2)	461.1078 **(462 $/m^2)**	464.3041 **(465 $/m^2)**	464.054 **(465 $/m^2)**

Oil-in-water emulsions treatment cost	M1	M2	M3
Permeate flux through unit (m^2) area of membrane at applied pressure of 69 kPa and feed concentration of 200 mg/L	4.15×10^{-5} (m^3/m^2 s)	3.37×10^{-5} (m^3/m^2 s)	4.13×10^{-5} (m^3/m^2 s)
Amount of oil-in-water emulsions processed per year	310752 (L/Year)	252345.6 (L/Year)	309254.4 (L/Year)
Total direct (fixed) cost [Empty N_2 cylinder cost + dead end flow filtration set up cost)	52 ($/Year)	52 ($/Year)	52 ($/Year)
Operating cost (N_2 gas consumable cost per year for treatment of oil-in-water emulsion by each membrane)	10 ($/Year)	10 ($/Year)	10 ($/Year)
Membrane cost	462 ($/$m^2$)	465 ($/$m^2$)	465 ($/$m^2$)
Depreciation cost	66 ($/Year)	67 ($/Year)	67 ($/Year)
Membrane cleaning and maintenance cost (@ 3% of total cost of the membrane system)	1.56 ($/Year)	1.56 ($/Year)	1.56 ($/Year)
Labor cost (@ 2% of total cost of the membrane system)	1.04 ($/Year)	1.04 ($/Year)	1.04 ($/Year)
The overall cost for the treatment of oil-in-water emulsions ($/Year)	524.60 **(525 $/Year)**	524.60 **(525 $/Year)**	524.60 **(525 $/Year)**

4.2.11 Process model

The experimental investigations confirm that the removal of oil from oily wastewater using ceramic microfiltration process is strongly influenced with operating parameters such as applied pressure and feed concentration. Therefore, process model using regression based approaches would indicate strong significance of these parameters and suitable expressions need to consider these variables. A central composite design approach is followed to correlate operating parameters (feed concentration and applied pressure) with measured or evaluated variables (flux and rejection). The response parameters and design matrix obtained from experimental investigations with M2 membrane are presented in Table 4.5. To evaluate upon the effect of combined parameters, experiments are performed at various chosen parameters in their statistical combinations of values to obtain combined matrix of experimental design. The influential quadratic terms in the model are estimated using the central runs by repeating the experiments for five times.

Eq. (2.11) expresses membrane flux or rejection (Y) in terms of applied pressure (X_1) and feed concentration (X_2). The coefficient values of Eq. (2.12) are determined using the RSM based regression technique using experimental data with help of Design-Expert 7.0.0 software. For M2 membrane, the regression based expressions for membrane flux and rejection are presented in Eq. (4.1) and Eq. (4.2) respectively i.e.

$\text{Flux} = -1.789\times10^{-04} + 1.657\times10^{-06} X_1 + 3.083\times10^{-06} X_2 - 2.482\times10^{-09} X_1X_2 - 1.306\times10^{-09} X_1^2 - 1.195\times10^{-08} X_2^2$	(4.1)
$\text{Rejection} = 84.229 - 0.086X_1 + 0.209X_2 + 3.728\times10^{-4} X_1X_2 + 2.189\times10^{-5} X_1^2 - 6.462\times10^{-4} X_2^2$	(4.2)

The positive and negative values in the above expression represent the synergetic and antagonistic effect respectively. In addition, each term in the expression is not equally

important. Further, the model quality is to be evaluated in terms of the fitness evaluated using coefficient of correlation and hence its determination is very important from the perspective of statistical analysis.

The RSM model results for M1 and M3 membranes are similar to those obtained for M2 and further explanations are not provided. The obtained results for these are presented in Tables 4.6 and 4.7, respectively.

Table 4.5: RSM design and its actual and predicted values for M2 membrane

Run order	Applied pressure (kPa) X1	Concentration (mg/L) X2	Permeate Flux $J\times10^4$ (m^3/m^2 s)		Rejection (%)	
			Actual	Predicted	Actual	Predicted
1	69	100	0.80	1.01	96.21	95.49
2	345	100	3.10	3.40	84.40	84.80
3	207	150	2.20	2.25	96.38	95.98
4	207	150	2.30	2.25	95.47	95.98
5	207	150	2.20	2.25	96.16	95.98
6	207	150	2.40	2.25	95.69	95.98
7	207	79.29	2.60	2.37	85.97	86.20
8	207	220.71	0.91	0.93	99.54	99.29
9	207	150	2.10	2.25	96.18	95.98
10	69	200	0.34	0.34	99.99	99.61
11	402.16	150	3.40	3.20	93.69	92.89
12	345	200	2.00	2.05	98.47	99.21
13	11.84	150	0.39	0.30	99.95	100

Table 4.6: RSM design and its actual and predicted values for M1 membrane

Run order	Applied pressure (kPa)	Concentration (mg/L)	Permeate Flux J×10^4 (m^3/m^2 s)		Rejection (%)	
			Actual	Predicted	Actual	Predicted
1	207	150	2.31	2.23	90.26	90.76
2	207	150	2.25	2.23	90.15	90.76
3	69	200	0.42	0.45	99.95	100.75
4	345	200	1.38	1.45	92.37	92.15
5	207	150	2.19	2.23	91.45	90.76
6	207	150	2.22	2.23	90.36	90.76
7	207	220.71	0.65	0.61	99.04	98.52
8	69	100	1.21	1.29	94.3	93.98
9	11.84	150	0.36	0.31	99.98	99.53
10	345	100	4.68	4.80	81.64	80.3
11	207	79.29	3.67	3.56	84.29	85.35
12	402.16	150	3.61	3.51	82.79	83.78
13	207	150	2.17	2.23	91.56	90.76

Table 4.7: RSM design and its actual and predicted values for M3 membrane

Run order	Applied pressure (kPa)	Concentration (mg/L)	Permeate Flux J×10^4 (m^3/m^2 s)		Rejection (%)	
			Actual	Predicted	Actual	Predicted
1	207	79.29	3.90	3.71	81.21	82.09
2	207	150	2.32	2.49	86.55	85.25
3	69	100	1.23	1.51	87.00	86.03
4	207	150	2.49	2.49	85.02	85.25
5	402.16	150	3.84	4.01	80.54	80.86
6	207	220.71	0.95	1.09	94.54	94.81
7	345	200	2.49	2.26	88.00	87.82
8	207	150	2.46	2.49	86.01	85.25
9	207	150	2.68	2.49	84.00	85.25
10	345	100	4.91	4.91	80.00	79.39
11	69	200	0.41	0.46	96.12	95.58
12	207	150	2.52	2.49	84.69	85.25
13	11.84	150	0.54	0.32	90.22	91.05

4.2.11.1 ANOVA analysis and quadratic model fitness

To ensure upon the model fitness, tests were carried out to evaluate upon the significance of mathematical regression model, model coefficients and lack of fitness. During analysis of variance (ANOVA), the value of F or p (usually denoted as Prob.>F) conveys upon the significance of the coefficients. Coefficients with larger F and small Prob.>F value are regarded to be significant. Table 4.8 summarizes results obtained from ANOVA analysis for M2 membrane using second-order response model. For membrane M2, it can be seen that the model F and Prob.>F values are 58.19 (high) and <0.05 (low), thereby affirming upon the significance of the model. Similarly, the coefficients corresponding to various independent variable terms also need to have a low Prob.>F value to indicate upon their significance. This work aims to evaluate upon the significance of applied pressure (X_1), feed concentration (X_2), the quadratic effect of applied pressure (X_1^2) and feed concentration (X_2^2). The ranking order in terms of significance is $X_1>X_1^2>X_2>X_2^2$ with insignificance of other model terms. Lower lack-of-fit F-value (4.95) conveyed that there has been insignificant lack of fitness for the model. Further, the noise contribution towards the lack of fit F-value is evaluated to be 7.82% by chance, which is also satisfactory. Also, "Pred R-squared" value (0.8606) is in agreement with the "Adj R-squared" value (0.9597). For "Adeq Precision" that refers to a signal to noise ratio value of 22.965 by the ANOVA analysis, the model fitness is assured due to obtaining a value significantly greater than 4. Thereby, model navigation is suitably confirmed in the design space.

After insignificant interaction terms are eliminated in Eq. (4.1), the model can be expressed as in Eq. (4.3). In Eq. (4.3), the identification of any other insignificant model terms requires a further model reduction strategy so as to achieve model improvement.

$\text{Flux} = -1.789\times10^{-04} + 1.657\times10^{-06} X_1 + 3.083\times10^{-06} X_2 - 1.306\times10^{-09} X_1^2 - 1.195\times10^{-08} X_2^2$	(4.3)

Obtained results from sequential model fitness studies are shown in Table 4.8 and affirm that quadratic model is suitable to represent permeate flux.

The second-order response model parameters for the ANOVA of M1 and M3 membrane flux is presented in Table 4.9 and 4.10, respectively. As indicated in Table 4.9, F and Prob.>F have been evaluated to be 446.36 and very low value (<0.05). Thereby, these values affirm upon the significance of the model in terms of X_1, X_2, X_1X_2 and X_1^2 terms. A "Lack of Fit F-value" of 5.84 affirms insignificant lack of fitness in comparison with the error. Further, "Pred-R-squared" value (0.9810) and "Adj R-squared" value (0.9946) are in good agreement. The higher value of "Adeq Precision" (68.534) confirms that the model navigation in the design space can be carried out. For M3 membrane, 90.7 F-value conveys its significance with X_1, X_2 and X_1 X_2 as significant model terms. Acceptable values of "Lack of Fit F-value" (5.23) and close agreement between "Pred R-squared" (0.9090) and "Adj R-squared" (0.9739) are also conveyed in Table 4.10 for the M3 membrane.

Table 4.8: ANOVA for the permeate flux response surface quadratic model of M2 membrane

Source	Sum of Squares	DF	Mean Square	*F*–value	*p*–value (Prob > *F*)
Model	1.15×10^{-7}	5	2.31×10^{-8}	58.19	< 0.0001
X_1-Applied Pressure (kPa)	8.43×10^{-8}	1	8.43×10^{-8}	212.52	< 0.0001
X_2-Concentration (mg/L)	2.06×10^{-8}	1	2.06×10^{-8}	52.00	0.0002
X_1X_2	1.17×10^{-9}	1	1.17×10^{-9}	2.96	0.1291
X_1^2	4.3×10^{-9}	1	4.3×10^{-9}	10.85	0.0132
X_2^2	6.21×10^{-9}	1	6.21×10^{-9}	15.65	0.0055
Residual	2.78×10^{-9}	7	3.97×10^{-10}		
Lack of Fit	2.19×10^{-9}	3	7.29×10^{-10}	4.95	0.0782
Pure Error	5.89×10^{-10}	4	1.47×10^{-10}		
Cor Total	1.18×10^{-7}	12			
Std. Dev.	1.99×10^{-5}		R^2	0.98	
Mean	0.0002		Adj R^2	0.96	
C.V. %	10.43		Pred R^2	0.86	
PRESS	1.65×10^{-8}		Adeq Precision	22.96	

Table 4.9: ANOVA for the permeate flux response surface quadratic model of M1 Membrane

Source	Sum of Squares	Degree of Freedom	Mean Square	*F*–value	*p*–value (Prob > *F*)
Model	2.07×10^{-7}	5	4.14×10^{-8}	446.36	< 0.0001
X_1-Applied Pressure (kPa)	1.02×10^{-7}	1	1.02×10^{-7}	1098.81	< 0.0001
X_2-Concentration (mg/L)	8.75×10^{-8}	1	8.75×10^{-8}	942.88	< 0.0001
X_1X_2	1.57×10^{-8}	1	1.57×10^{-8}	169.07	< 0.0001
X_1^2	1.77×10^{-9}	1	1.77×10^{-9}	19.03	0.0033
X_2^2	3.59E-10	1	3.59×10^{-10}	3.87	0.0900
Residual	6.49×10^{-10}	7	9.28×10^{-11}		
Lack of Fit	5.29×10^{-10}	3	1.76×10^{-10}	5.84	0.0607
Pure Error	1.21×10^{-10}	4	3.02×10^{-11}		
Cor Total	2.08×10^{-7}	12			
Std. Dev.	9.63×10^{-6}		R^2	1.00	
Mean	0.00021		Adj R^2	0.99	
C.V. %	4.62		Pred R^2	0.98	
PRESS	3.95×10^{-9}		Adeq Precision	68.53	

Table 4.10: ANOVA for the permeate flux response surface quadratic model of M3 membrane

Source	Sum of Squares	Degree of Freedom	Mean Square	*F*–value	*p*–value (Prob > *F*)
Model	2.13×10^{-7}	5	4.25×10^{-8}	90.70	< 0.0001
X_1-Applied Pressure (kPa)	1.36×10^{-7}	1	1.36×10^{-7}	289.57	< 0.0001
X_2-Concentration (mg/L)	6.86×10^{-8}	1	6.86×10^{-8}	146.18	< 0.0001
X_1X_2	6.42×10^{-9}	1	6.42×10^{-9}	13.70	0.0076
X_1^2	1.87×10^{-9}	1	1.87×10^{-9}	3.98	0.0863
X_2^2	1.46×10^{-10}	1	1.46×10^{-10}	0.31	0.5943
Residual	3.28×10^{-9}	7	4.69×10^{-10}		
Lack of Fit	2.62×10^{-9}	3	8.72×10^{-10}	5.22	0.0720
Pure Error	6.67×10^{-10}	4	1.67×10^{-10}		
Cor Total	2.16×10^{-7}	12			
Std. Dev.	2.17×10^{-5}		R^2	0.98	
Mean	0.00024		Adj R^2	0.97	
C.V. %	9.16		Pred R^2	0.91	
PRESS	1.96×10^{-8}		Adeq Precision	31.20	

4.2.11.2 ANOVA for rejection

For M2 membrane, model F-value of 118.70 affirms model significance (Table 4.11). A chance of 0.01% for the "Model F-value" confirms that noise is low. "Prob.>F" values less than 0.05 for model terms X_1, X_2, X_1X_2, X_2^2 indicate their significance. Model terms with p values greater than 0.1 indicate insignificant terms and model reduction could further

improve the model fitness. Other ANOVA values affirm that the obtained values are satisfactory (6.32 Lack of fit value; 5.35% chance for Lack of Fit F-value; 0.9284 Pred-R-squared value; 0.98 Adj R squared value; 34.111 signal to noise ratio).

After insignificant interaction terms are eliminated in the regression expression presented in Eq. (4.2), the model is simplified in the following form by refining the model:

$\text{Rejection} = 84.229 - 0.086X_1 + 0.209X_2 + 3.728\times10^{-4}X_1X_2 - 6.462\times10^{-4}X_2^2$	(4.4)

Sequential model fitting results are shown in Table 4.11 and confirms that the quadratic model is the most suitable model to represent rejection. Further, ANOVA analysis was also conducted to evaluate upon the applied pressure and feed concentration effect on oil rejection data. Results obtained for the conducted analysis are presented in Table 4.8 and 4.11 for pressure and feed concentration effect, respectively. P values in both the tables affirm that all terms are significant with 99% confidence. The R^2 values from statistical analysis are satisfactory (0.981 and 0.99 for membrane flux and oil rejection, respectively). Regression coefficients obtained from the analysis are also presented in Table 4.8 and Table 4.11. Regressed model parameters in Eq (4.1-4.2) convey upon the effect of operational parameters and their possible interactions on dependent variables. From Table 4.8 and Eq. (4.1), a positive effect of pressure and feed concentration on membrane flux can be seen. Similar insights can be deduced from Table 4.11 and Eq. (4.2).

The results obtained for the second-order response model using ANOVA analysis for rejection data of membranes M1 and M3 are presented in Table 4.12 and Table 4.13, respectively. For M1 membrane rejection data, high F value (85.52) conveys model significance. 0.01% chance for model-F value affirms that there is little noise. Also, X_1, X_2

and X_1X_2 have been identified as significant model terms. 3.63 value for "Lack of Fit" parameter affirms insignificant lack of fitness in comparison with the pure error. A good agreement of "Pred R squared value" (0.9095) and "Adj R-squared value" (0.9274) is apparent. 29.968 noise to signal ratio confirms adequacy of signal. Similar results have been obtained for the M3 membrane (53.08 model F-value; X_1, X_2 and X_2^2 significant terms; 1.04 Lack of fit F-value; Pred R squared value of 0.8972; Adj R squared value of 0.9559; Adeq. Precision of 23.056). Thereby, model navigation is also affirmed by the ANOVA in the design space.

Table 4.11: ANOVA for the rejection response surface quadratic model of M2 membrane

Source	Sum of Squares	DF	Mean Square	*F*–value	*p*–value (Prob > *F*)
Model	280.43	5	56.09	118.70	< 0.0001
X_1-Applied Pressure (kPa)	61.51	1	61.51	130.18	< 0.0001
X_2-Concentration (mg/L)	171.50	1	171.50	362.97	< 0.0001
X_1X_2	26.47	1	26.47	56.02	0.0001
X_1^2	1.21	1	1.21	2.56	0.1536
X_2^2	18.16	1	18.16	38.42	0.0004
Residual	3.31	7	0.47		
Lack of Fit	2.73	3	0.91	6.32	0.0535
Pure Error	0.58	4	0.14		
Cor Total	283.74	12			
Std. Dev.	0.69		R^2	0.99	
Mean	95.24		Adj R^2	0.98	
C.V. %	0.72		Pred R^2	0.93	
PRESS	20.32		Adeq Precision	34.11	

Table 4.12: ANOVA for the oil rejection response surface quadratic model of M1 Membrane

Source	Sum of Squares	DF	Mean Square	*F*–value	*p*–value (Prob > *F*)
Model	431.29	5	86.26	85.52	< 0.0001
X_1-Applied Pressure (kPa)	248.09	1	248.09	245.96	< 0.0001
X_2-Concentration (mg/L)	173.35	1	173.35	171.86	< 0.0001
X_1X_2	6.45	1	6.45	6.40	0.0393
X_1^2	1.41	1	1.41	1.39	0.2764
X_2^2	2.42	1	2.42	2.40	0.1655
Residual	7.06	7	1.01		
Lack of Fit	5.16	3	1.72	3.63	0.1227
Pure Error	1.90	4	0.47		
Cor Total	438.35	12			
Std. Dev.	1.00		R^2	0.98	
Mean	91.40		Adj R^2	0.97	
C.V. %	1.10		Pred R^2	0.91	
PRESS	39.68		Adeq Precision	29.97	

Table 4.13: ANOVA for the rejection response surface quadratic model of M3 membrane

Source	Sum of Squares	Degree of Freedom	Mean Square	*F*–value	*p*–value (Prob > *F*)
Model	2.13×10^{-7}	5	4.25×10^{-8}	90.70	< 0.0001
X_1-Applied Pressure (kPa)	1.36×10^{-7}	1	1.36×10^{-7}	289.57	< 0.0001
X_2-Concentration (mg/L)	6.86×10^{-8}	1	6.86×10^{-8}	146.18	< 0.0001
X_1X_2	6.42×10^{-9}	1	6.42×10^{-9}	13.70	0.0076
X_1^2	1.87×10^{-9}	1	1.87×10^{-9}	3.98	0.0863
X_2^2	1.46×10^{-10}	1	1.46×10^{-10}	0.31	0.5943
Residual	3.28×10^{-9}	7	4.69×10^{-10}		
Lack of Fit	2.62×10^{-9}	3	8.72×10^{-10}	5.22	0.0720
Pure Error	6.67×10^{-10}	4	1.67×10^{-10}		
Cor Total	2.16×10^{-7}	12			
Std. Dev.	2.17×10^{-5}		R^2	0.98	
Mean	0.00024		Adj R^2	0.97	
C.V. %	9.16		Pred R^2	0.91	
PRESS	1.96×10^{-8}		Adeq Precision	31.20	

4.2.11.3 Response surface and contour plots

The graphical surfaces of response and contour plots are obtained using the RSM methodology from the developed regression equation. These response function plots of the surface and contour plots are useful in understanding the effects of combined factors. In addition, the obtained parameters are useful to analyze upon three-dimensional interactions.

The effect of the studied range of variables with interactions is analyzed by keeping the other parameters constant. This results in two response and corresponding contour plots for membrane M2 (Fig. 4.7 and 4.8 respectively). Fig. 4.7 demonstrates the three dimensional response surface relationships between dependent variables and independent variables (applied pressure (X_1) and feed concentration (X_2)) for M2 membrane. The contour plots depict that the expected dependence of membrane flux with pressure and feed concentration. However, membrane flux increases with increasing feed concentration and marginally declines with increasing pressure. The contour plots for oil rejections is depicted in Fig. 4.8 that illustrates the combined effect of X_1 (pressure) and X_2 (feed concentration) on rejection.

The contour plot shapes convey upon the level and nature of the interactions that can be viewed by the elliptic nature of the plots of contours. However, the non-useful or low case interactions are also evident with the circular shape of few contours. These plots depict that the cumulative interaction parameters of operating variables selected in this investigation are much more important. Similar findings are also observed for the M1 and M3 membranes. Fig. 4.9-4.12 depicts the corresponding plots for these membranes.

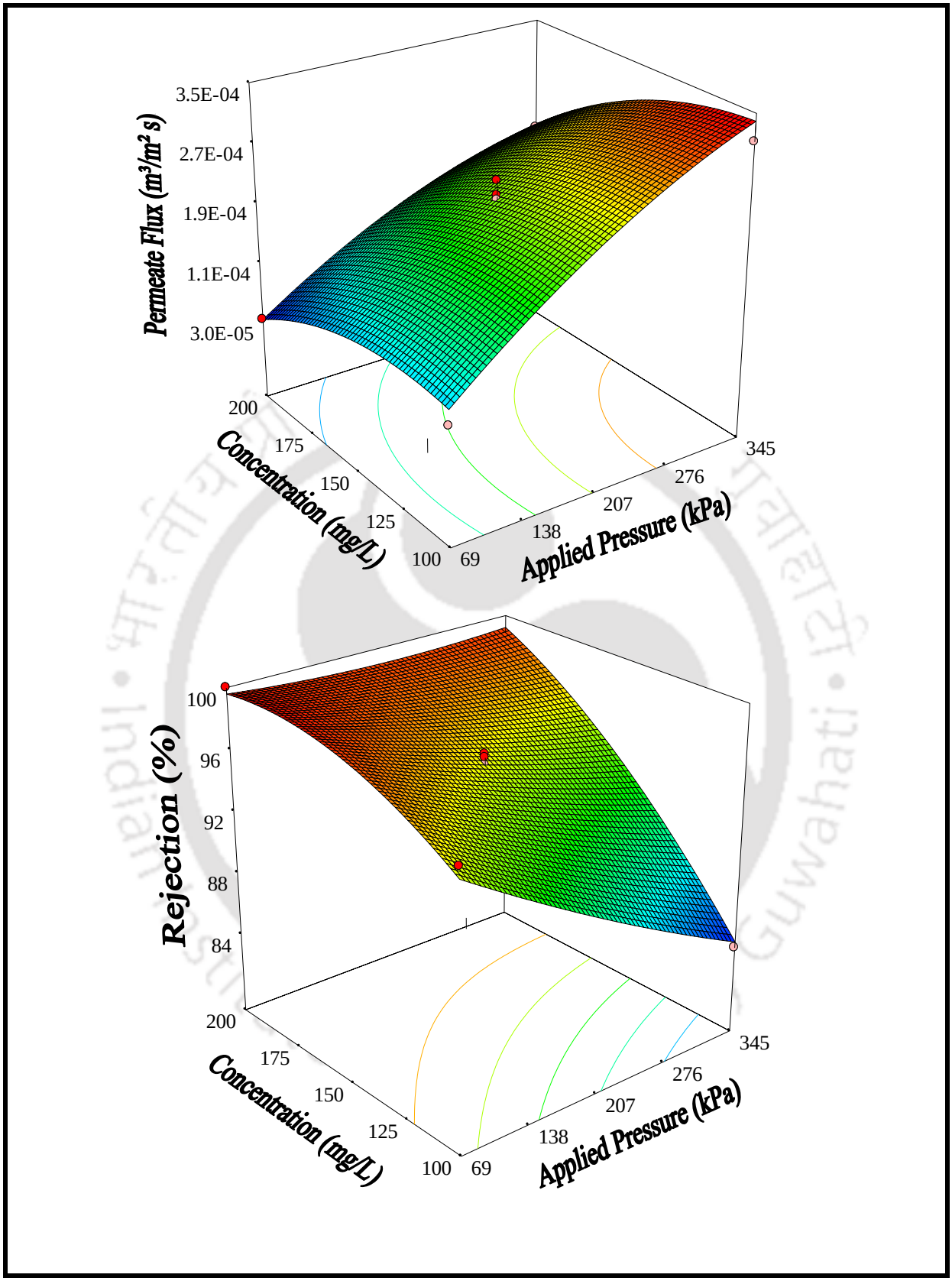

Figure 4.7: Response surface plots for permeate flux and oil rejection of M2 membrane

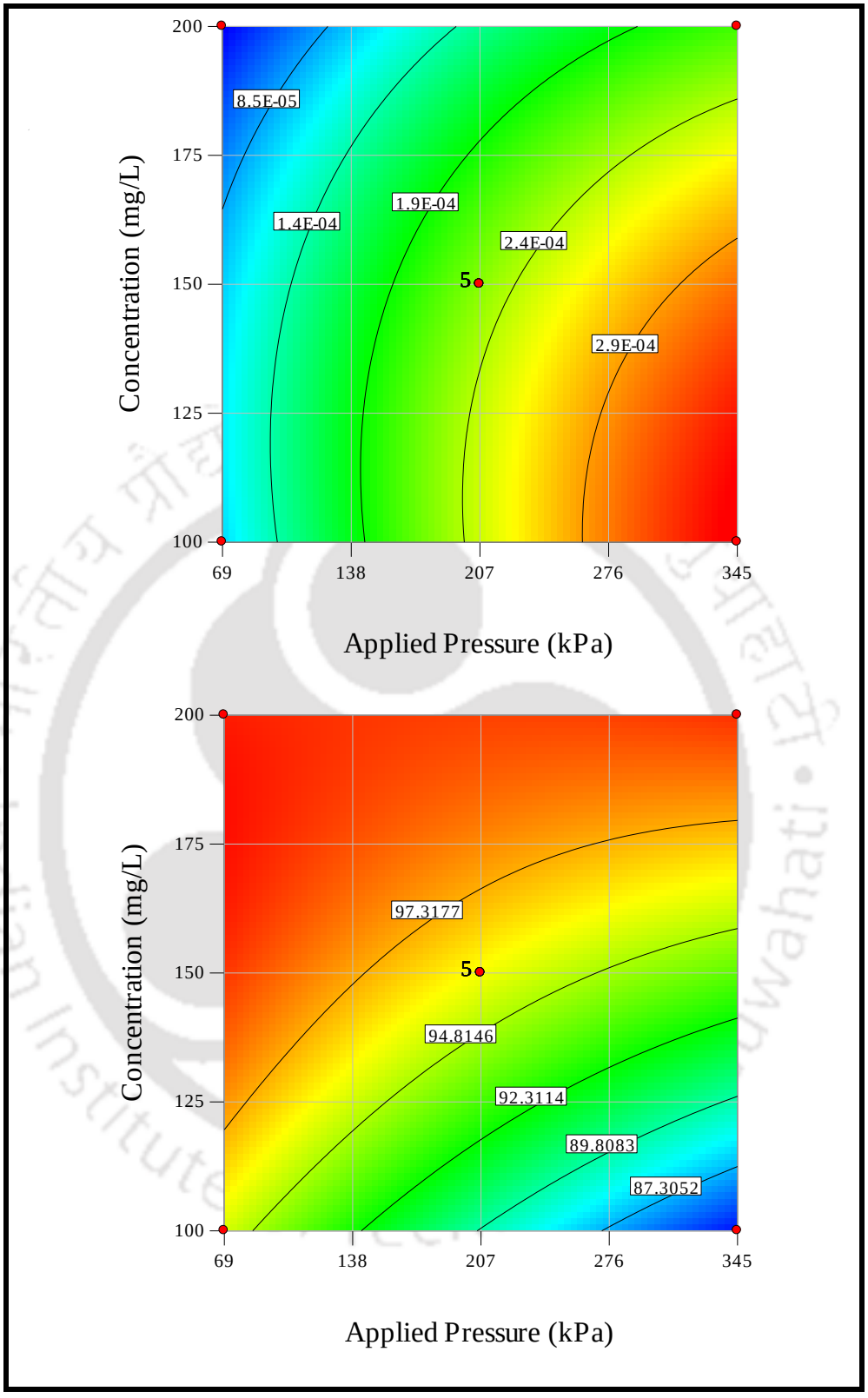

Figure 4.8: Contour plots for combined effects on permeate flux and rejection of M2 membrane

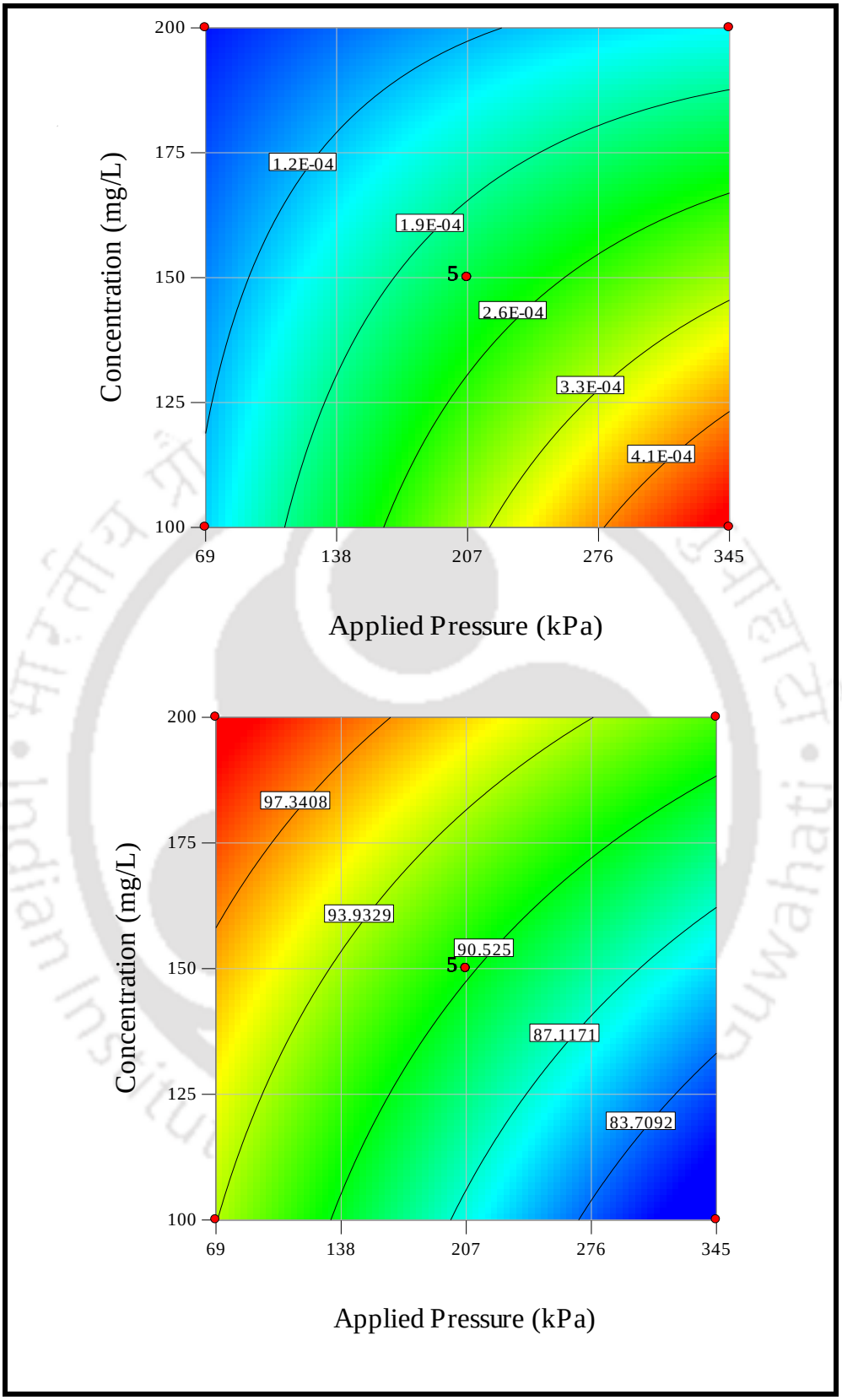

Figure 4.9: Contour plots of permeate flux and rejection for M1 membrane

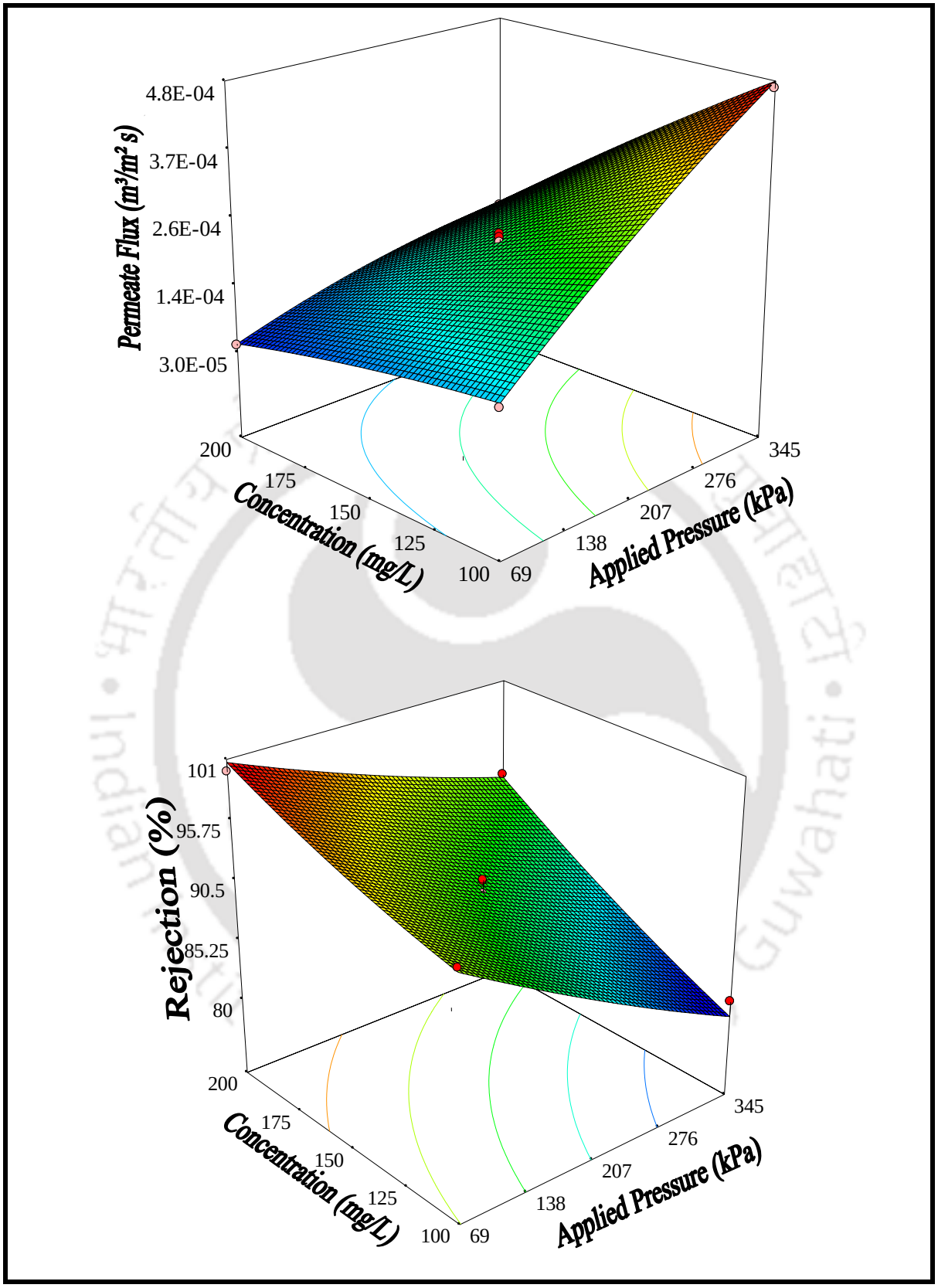

Figure 4.10: Response surface plots of permeate flux and oil rejection for M1 membrane

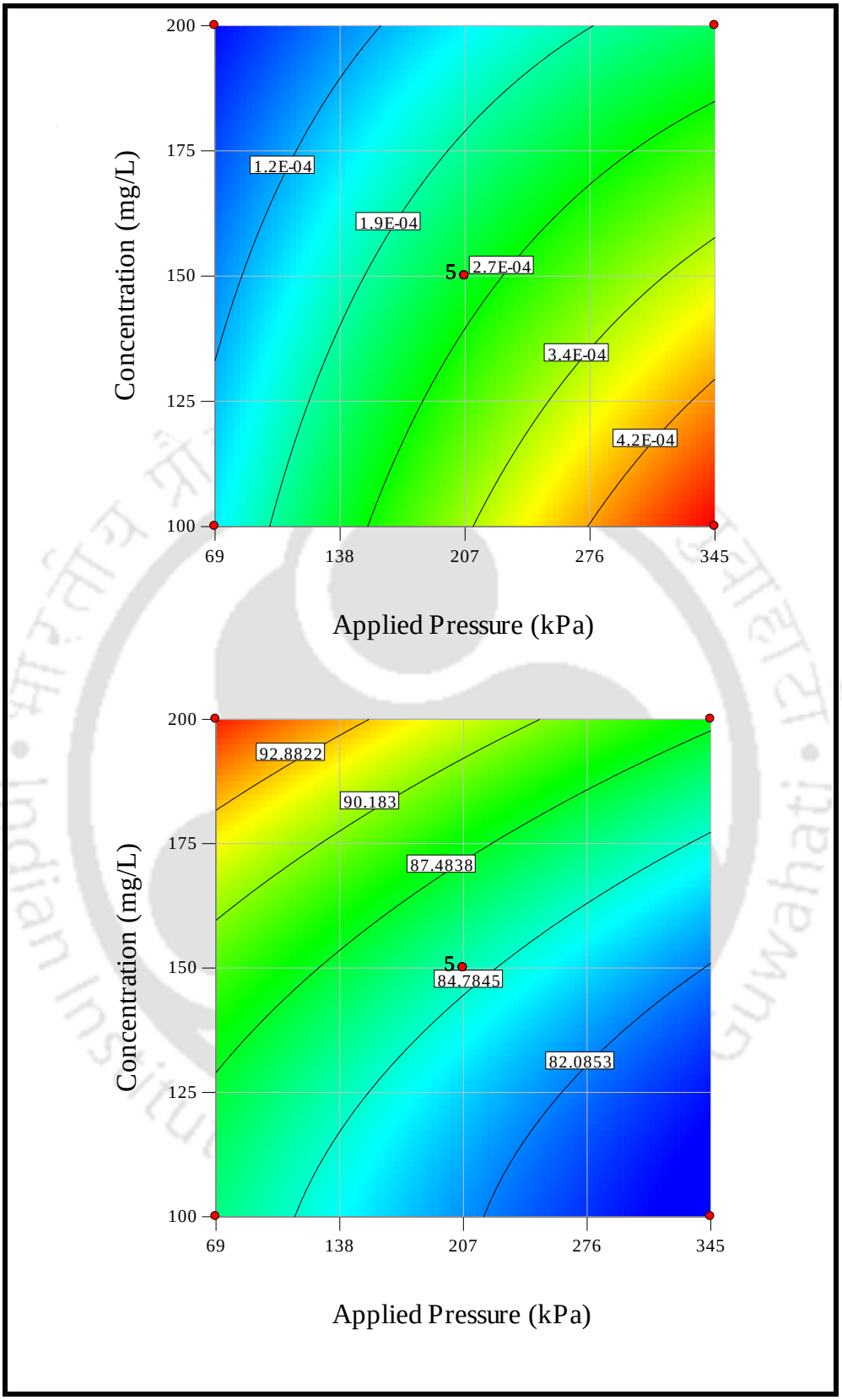

Figure 4.11: Contour plots of permeate flux and rejection for M3 membrane

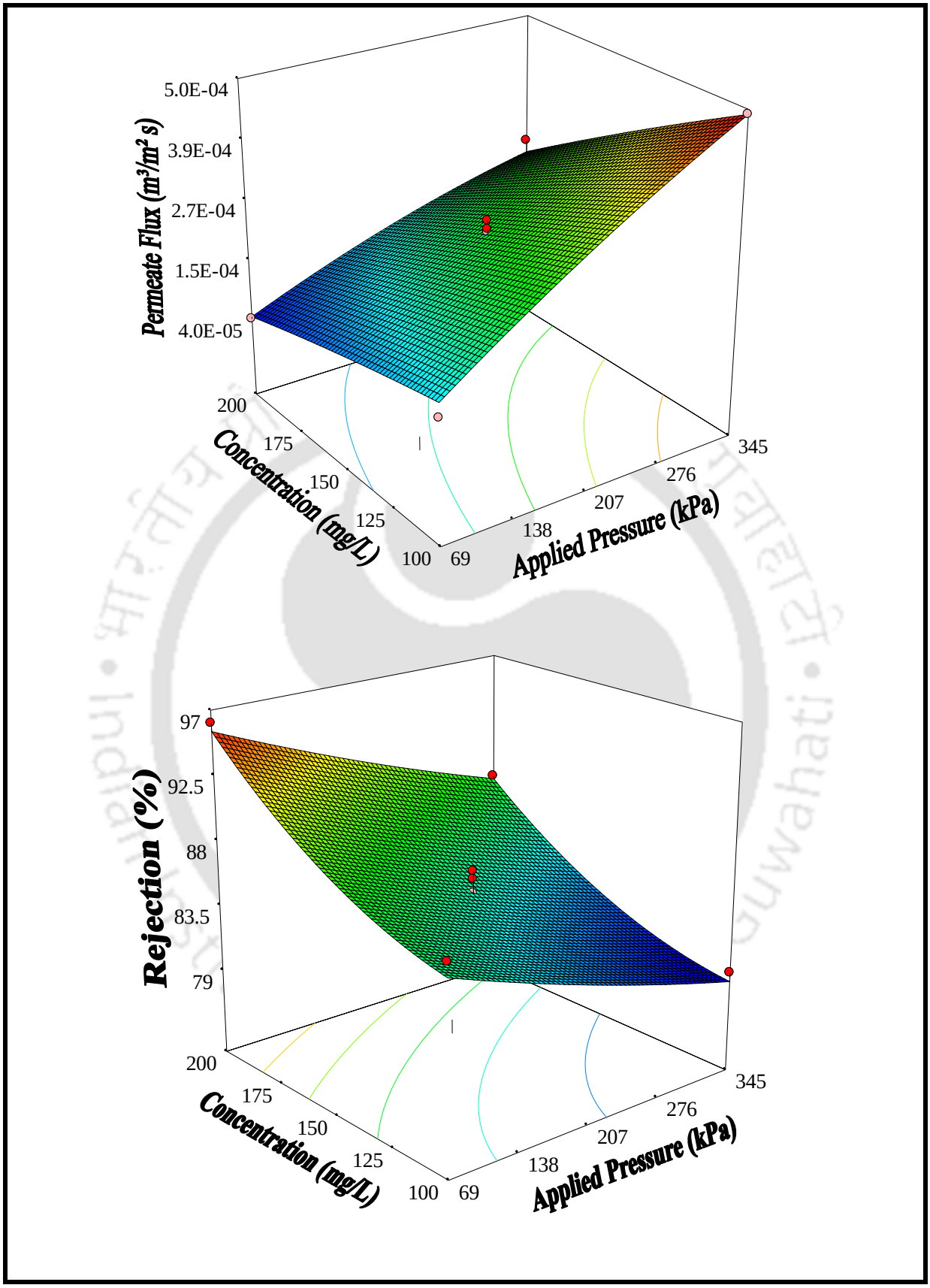

Figure 4.12: Response surface plots of permeate flux and oil rejection for M3 membrane

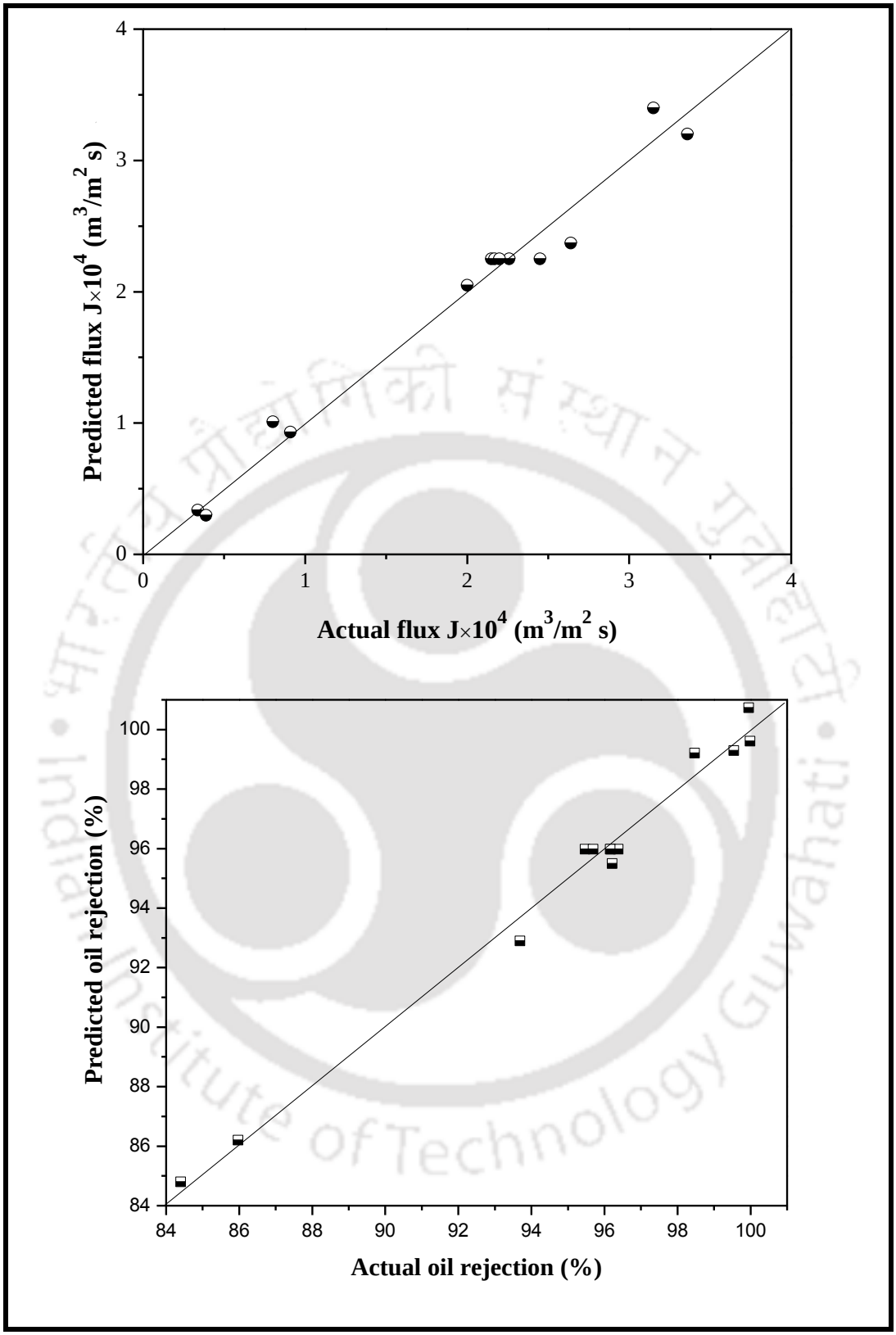

Figure 4.13: Actual versus predicted values for M2 membrane

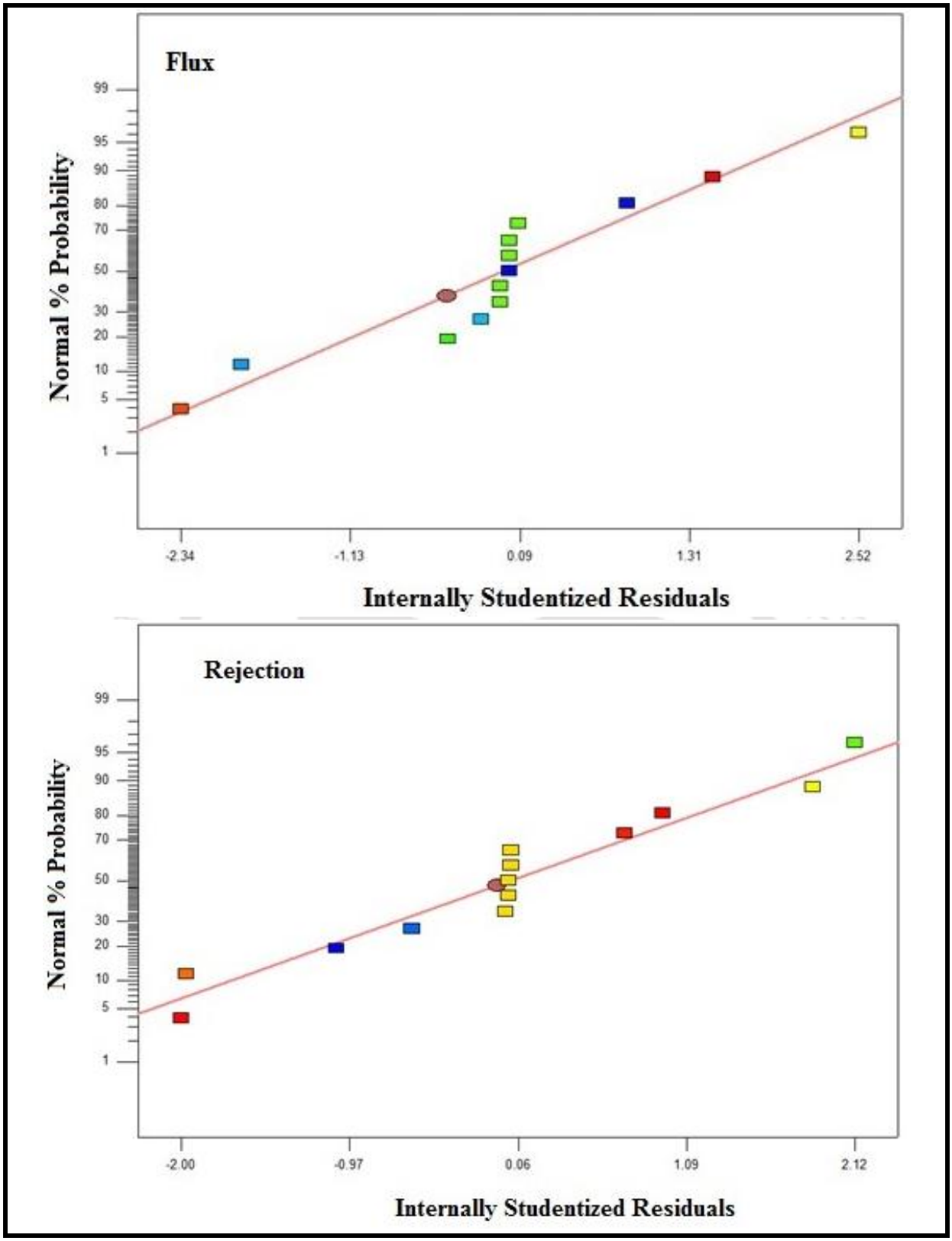

Figure 4.14: Residual plots against Normal probability for M2 membrane

4.2.11.4 Process optimization

The optimization technique is used to analyze the quadratic equation for desired features of independent and dependent variables. The design parameter values are obtained from the process optimization for either minimum and or maximum value of the response of the developed function.

The Design Expert 7.0 Model package has been used for the numerical optimization to select the required level of accuracy from each of the variable with five number of possible desired ways for responses (none, maximum, within rage, minimum and target value) and for the variable taken a fixed value. Then the optimization of numerical values are set up for the required function to maximize within the range of 69-345 kPa pressure differential and 100-200 mg/L feed concentration. The primary intention of the modeling effort is to maximize both permeate flux and oil removal by recalculating important factors from developed desirability functions. As obtained from the desirability ramp during numerical optimization, specific values for all responses are evaluated. The best local maximum is found at 345 kPa pressure, 176.07 mg/L feed concentration, 2.6×10^{-4} (m^3/m^2 s) permeate flux and 96.97% oil rejection with 0.774 desirability. Hence, Design Expert 7.0.0 software is effectively used to fit the experimental results (see Table 4.5) with a second order quadratic equation.

Multiple regression approach in Design Expert 7.0.0 software was used to fit quadratic second order model for data presented in Table 4.5. When predicted responses are relatively realistic with the experimental data, a dependable and accurate model is affirmed. Both the experimental values and predicted values of permeate flux and rejection from the statistical process model are well compared and displayed in the Fig. 4.13. In addition to this, Fig. 4.14 demonstrate the relation between the residuals values and normal probability. For the validation of the ANOVA results, it must be the case that the plot between the residuals

and normal probability is straight line to avoid any problem in the data. From Fig. 4.14, it is noticed that plot shows straight line. Therefore, these experimental investigations affirm that the empirical model is satisfactory to predict oil removal during dead end MF operation.

The perturbation plots of permeate flux and rejection versus the process variables i.e. applied pressure and feed concentration are as well important. The utility of the perturbation plot exists in terms of effects associated to relevant factors for a specific position in the design space. By maintaining all other factors constant, the response plot is achieved by varying a factor only in the set range. The Design Expert 7.0.0 sets mid-point as reference point for all factors. The sensitivity and insensitivity of a factor is sought in terms of the slope of the response. A steep slope or curvature response affirms sensitivity of response with a factor which is not the case for a relatively flat line. For the case where there are more than two factors, perturbation plots are used to find the effect of those factors on which the response is highly sensitive. This study reveals that rejection is more sensitive to feed concentration of oil-in-water emulsions and least sensitive to applied pressure while other response i.e. permeate flux is more sensitive to applied pressure and least sensitive to feed concentration.

For M1 membrane, the best local maximum is found at 188.54 kPa pressure differential, 137.32 mg/L feed concentration, 2.3060×10^{-4} (m^3/m^2 s) membrane flux, 90.44% oil rejection for 0.465 desirability. For M3 membrane, the best local maximum is found at 310.17 kPa applied pressure, 200 mg/L feed concentration, 2.1054×10^{-4} (m^3/m^2 s) permeate flux, 88.64% oil rejection at a desirability of 0.449.

4.3 Summary

This chapters summarizes the development and characterization of inexpensive ceramic membranes using fly ash as major inorganic precursor by uniaxial dry compaction method. All the membranes being sintered at 1100 ^{o}C exhibit excellent thermal, chemical and mechanical strength properties. The membranes possess porosity of 30 (M1), 39 (M2) and 43 (M3) %. The prepared membrane with different composition offers good mechanical strength (1.68, 6.99 and 9.25 MPa for mentioned membrane sequence). The permeability and average pore diameter are estimated to be 5.384×10^{-6} , 6.508×10^{-6}, 9.53×10^{-6} m/s kPa and 1.41, 1.36, 1.53 µm for said sequence of membranes. During microfiltration studies with synthetic oil-in-water emulsions, M2 membrane offered better combinations of rejection (81-99%) and membrane flux (4.42-0.337×10^{-4} m^3/m^2 s).

Dead-end flow microfiltration is an effective and prominent process for the separation of oil-in-water emulsions. For the parametric optimization, this work targeted a two-step approach in which the first step referred to experimental investigations to evaluate upon the optimality of applied pressure and feed concentration on the process variables, namely flux and rejection. The second step involved the parametric optimization RSM methodology in which central composite design approach has been followed. Using ANOVA analysis, model refinement was facilitated that allowed the identification of significant and insignificant terms for both interactive and squared terms. Both experimental and theoretical investigations are in good agreement for flux and rejection. For the M2 membrane, based on RSM, optimal process variable values of permeate flux (2.6×10^{-4} m^3/m^2s), rejection (96.94%) and desirability (0.774) have been at 345 kPa applied pressure and 176.07 mg/L feed concentration.

CHAPTER-5

Preparation, Characterization and Application of TiO_2-Fly ash Composite membranes

भारतीय प्रौद्योगिकी संस्थान गुवाहाटी
Indian Institute of Technology Guwahati

CHAPTER 5 Preparation, characterization and application of TiO_2-Fly ash composite membranes

After a brief introduction to necessity of addressing the fabrication of TiO_2-Fly ash composite membrane in section 5.1, sections 5.2.1-5.2.4 summarize the characterization results of TiO_2-Fly ash composite membrane. Eventually, sections 5.2.5 summarizes the results obtained for membranes during cross flow MF of oil-in-water emulsions. Finally the optimization of MF process by RSM for membranes and their corresponding obtained results are presented in section 5.2.6 followed with summary of the chapter in section 5.3.

5.1 Overview

In chapter 4, the results obtained from the dead end microfiltration of oil-in-water emulsions have been reported for various fly ash based ceramic membranes (M1, M2 and M3), whose average pore size is about 1.41, 1.36 and 1.53 µm, respectively. Amongst these, the M2 membrane has been identified as the optimal choice due to its good performance characteristics. While dead end microfiltration provides significantly stringent conditions of fouling for the membranes, they are not practiced regularly in the industrial scale operating systems. Typically, cross flow microfiltration is practiced on a pilot plant and industrial scale operation. Therefore, the flux and separation characteristics obtained from dead end microfiltration are not directly relevant to infer the confidence levels associated to the application of the fabricated membranes. Thus, cross flow microfiltration study has been targeted in this chapter for the developed M2 and TiO_2-Fly ash composite membranes and full details are explained in the subsequent sub-sections. In the earlier chapter 4, the separation of oil-in-water emulsions with M2 membrane in dead end mode of operation has been presented. The membrane with lowest average pore size refers to M2 membrane whose

average pore size is 1.36 µm. However, the membrane with hydrophobic nature is not favorable for the effective treatment of oil-in-water emulsions in the range of 50-200 mg/L. Thus, further engineering is targeted to achieve hydrophilic sub-micron range MF membranes. To do so, further enhancement in permeate flux, oil rejection and reduction in membrane pore size and surface modification is anticipated by coating a layer on the M2 membrane. Amongst various available materials, TiO_2 is one of the most favored choices due to its surface modification tendency. Thereby, further research has been initiated in this work to achieve hydrophilic microfiltration range ceramic membrane. For this purpose, the efficacy of the in-situ hydrothermal method is also targeted. Typically, asymmetric membranes are developed on a macroporous support with moderately higher average pore size. This is primarily due to the fact that a macroporous support with lower average pore size offers significant hydraulic resistance, which is not beneficial. Thus, considering all these issues, membrane M2 has been selected and used as the macroporous support to fabricate TiO_2-Fly ash composite membrane.

5.2 Results and discussion

5.2.1 Contact angle and FESEM micrographs

Figs. 5.1 (a) and (b) represent the images of contact angle for M2 and TiO_2-Fly ash composite membrane, respectively, with which the contact angle has been evaluated as 25.8° and 14.4°, respectively. For both membranes, the contact angle values are significantly lower than 90^o, indicating that both membranes are hydrophilic in nature. Due to this reason, it is expected that during cross flow MF of oil-in-water emulsions, the adherence of oil droplets to the membrane surface could reduce and accordingly, the membrane fouling will be lower. Further, compared to the M2 membrane, the TiO_2-Fly ash composite membrane is strongly hydrophilic and this is due to the TiO_2 layer. Thereby, TiO_2 could significantly lower the

interaction of the oil droplets with the membrane surface and strongly mitigate or weaken membrane fouling. Thus it is expected that among the asymmetric and symmetric membranes, the composite membrane would have lower fouling and greater shelf life for oil-in-water emulsion treatment.

Figs. 5.1 (c) and (d) depict the FESEM images of M2 membrane and TiO_2 composite membrane, respectively. The presence of TiO_2 nanoparticles is depicted with circle symbol and arrow mark in the FESEM image of composite membrane (Fig. 5.1(d)). It can be observed that TiO_2 nanoparticles were uniformly coated on the composite membrane and both membrane surfaces exhibit a defect free surface that is bereft of pinholes/cracks. The EDX analysis of TiO_2 composite membrane further confirms the distribution of titanium element on the membrane surface as the scan image indicated Ti element on the tiny TiO_2 porous layer prevalent on the surface (Fig. 5.1(e)). Thus, FESEM images confirmed upon greater hydrophilic nature of the composite membrane due to the presence of TiO_2 nanoparticles on the surface which contributed to pore size reduction and porosity as well.

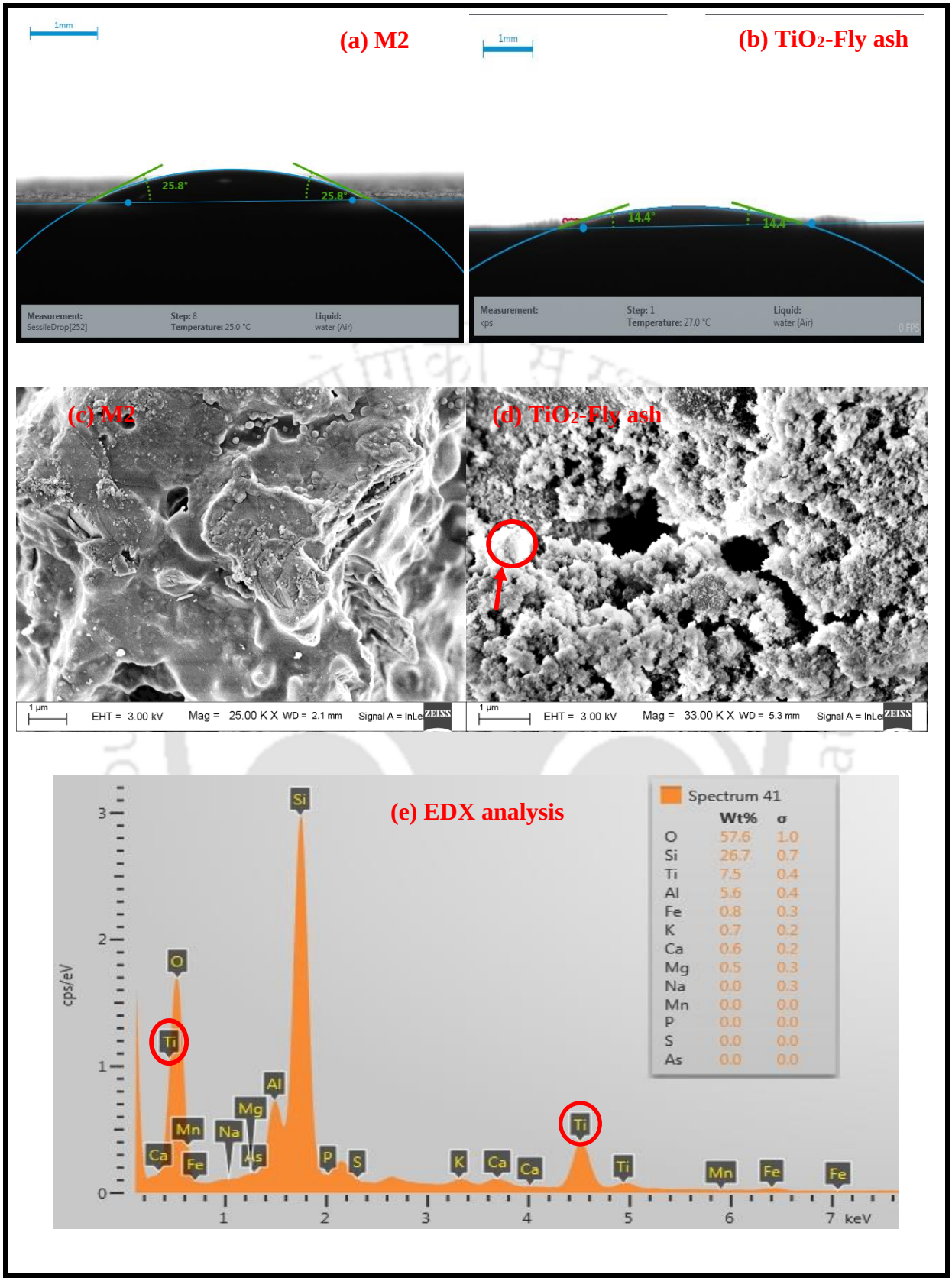

Figure 5.1: (a,b) Contact angle, (c,d) FESEM images and (e) EDX analysis of M2 membrane and TiO_2-Fly ash membrane

5.2.2 Average porosity and FESEM based pore size

TiO_2-Fly ash composite membrane and M2 membrane porosities were evaluated to be 35% and 39%, respectively. Thus, the titania coating has reduced the porosity by 4 % due to the reduction in pore volume with the coated layer. The FESEM image based average membrane pore sizes are 1.32 and 1.75 µm for TiO_2-Fly ash and M2 membrane, respectively. Hence, it is apparent that while porosity reduction is not significant with the titania coating, the same is not true for the average pore size of the membrane.

Fig. 5.2 depicts the N_2 gas permeation data based effective permeability factor variation with average pressure for both membranes. Compared to M2 membrane, the TiO_2-fly ash membrane indicated lower combinations of effective permeability factor and pore size. The N_2 permeation based average membrane pore size values are 1.12 and 1.30 µm for TiO_2-Fly ash and M2 membrane, respectively. Corresponding FESEM image analysis based mean pore size values are 1.32 and 1.75 µm, respectively. Significant variation exists in the mean pore size with FESEM analysis and with N_2 permeation data. This is due to the reason that gas permeation based data refers to open channel pores, which is not the case for FESEM based analysis in which even dead pores are also counted during pore size evaluation.

5.2.3 Droplet size distributions

Fig. 5.3 depicts the droplet size distribution of oil-in-water emulsions were evaluated at various solution concentrations. For all the concentrations, the emulsion droplet sizes varied from 0.05 - 100 µm. The average emulsion droplet size (in diameter) was evaluated to be 0.989, 5.246 and 6.716 µm for solutions with 100, 150 and 200 mg/L oil concentrations, respectively.

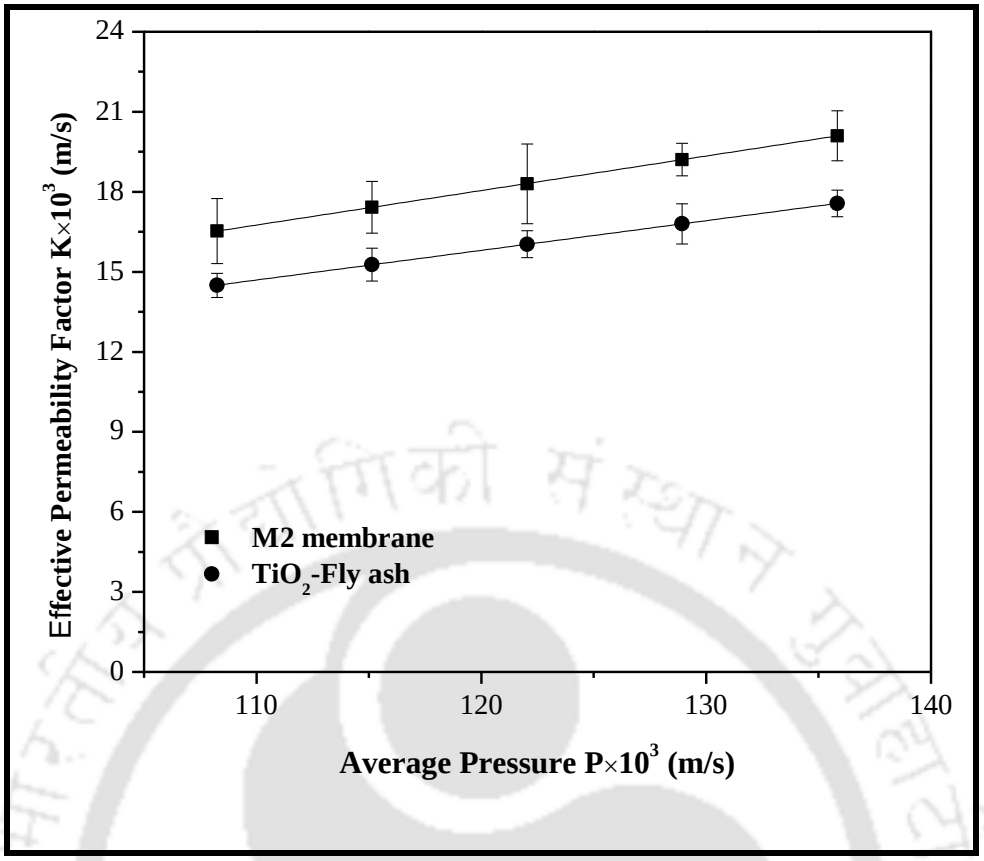

Figure 5.2: N_2 gas permeation through membranes

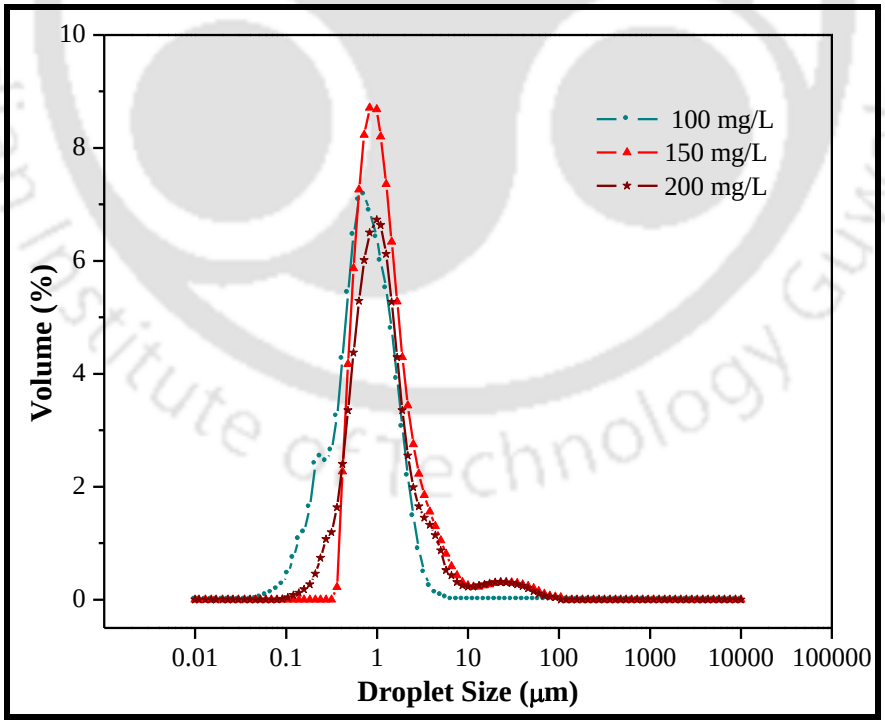

Figure 5.3: Droplet size distribution of oil-in-water emulsions

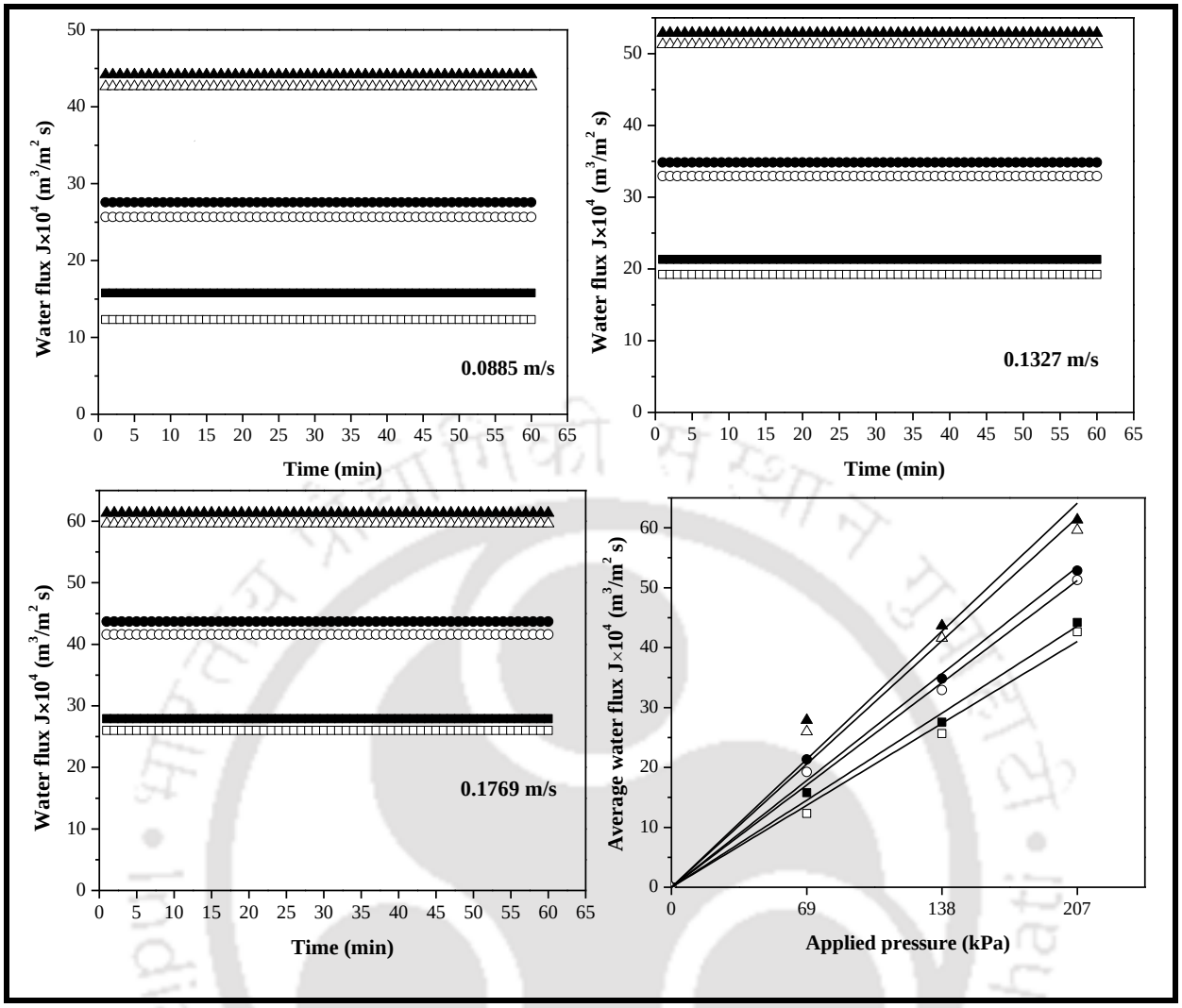

Figure 5.4: The variation of water flux of TiO_2-Fly ash composite membrane (filled symbol) and M2 (unfilled symbol**) membranes with various applied pressures at different cross flow velocities (■,□ - 69 kPa; ●,○ - 138 kPa; ▲,Δ - 207 kPa)**

5.2.4 Water flux

Fig. 5.4 illustrates the variation of membrane pure water flux with variations in cross flow velocity at variant applied pressures. Constant flux was observed during entire filtration time for all cases. Further, it was in accordance with Darcy's law and increased linearly with increasing pressure value. For all cases, the water flux values for TiO_2-Fly ash membrane are higher than those obtained for the M2 membrane due to its higher hydrophilic nature. At 207 kPa and 0.1769 m/s experimental conditions, maximum water flux value of 61.3545×10^{-4}

m^3/m^2 s and 59.6213×10^{-4} m^3/m^2 s was obtained for TiO_2-Fly ash and M2 membranes, respectively.

5.2.5 Cross-flow MF of oil-in-water emulsions

5.2.5.1 Effect of applied pressure

Fig. 5.5 depicts the variation of time dependent membrane flux at different applied pressures and cross flow velocities. Membrane flux increases with increasing applied pressure due to enhancement in driving force (Chakrabarty et al., 2008). For all cases, flux decline trends indicate that the flux reduced slightly up to 5 min and thereafter, the variation of permeate flux with time is almost negligible for 1 h operation. This may be due to the pore blocking at early stages, after that this effect is negligible (Mittal et al., 2011). Higher applied pressure contributed to membrane fouling due to which flux decline rate is slightly enhanced for all cases. This may be due to the collision between the emulsion droplets, thereby larger droplet forms which further create an oil layer just over the membrane surface. Further, the oil droplets were pressed and squeezed by higher pressure to penetrate in to the pores causing fouling (Mittal et al., 2011). For the M2 membrane, the flux decline rate is higher than that existent for the TiO_2-Fly ash membrane. This is confirmed with the maximum average permeate flux value (42.8495×10^{-4} (m^3/m^2 s) and 40.9045×10^{-4} (m^3/m^2 s) for TiO_2-Fly ash and M2 membrane, respectively) after 1 h of cross flow MF at the experimental conditions of 207 kPa, 0.1769 m/s and 200 mg/L feed concentration. This is due to the hydrophilic nature generated by TiO_2 layer, which results in reducing the effect of membrane fouling.

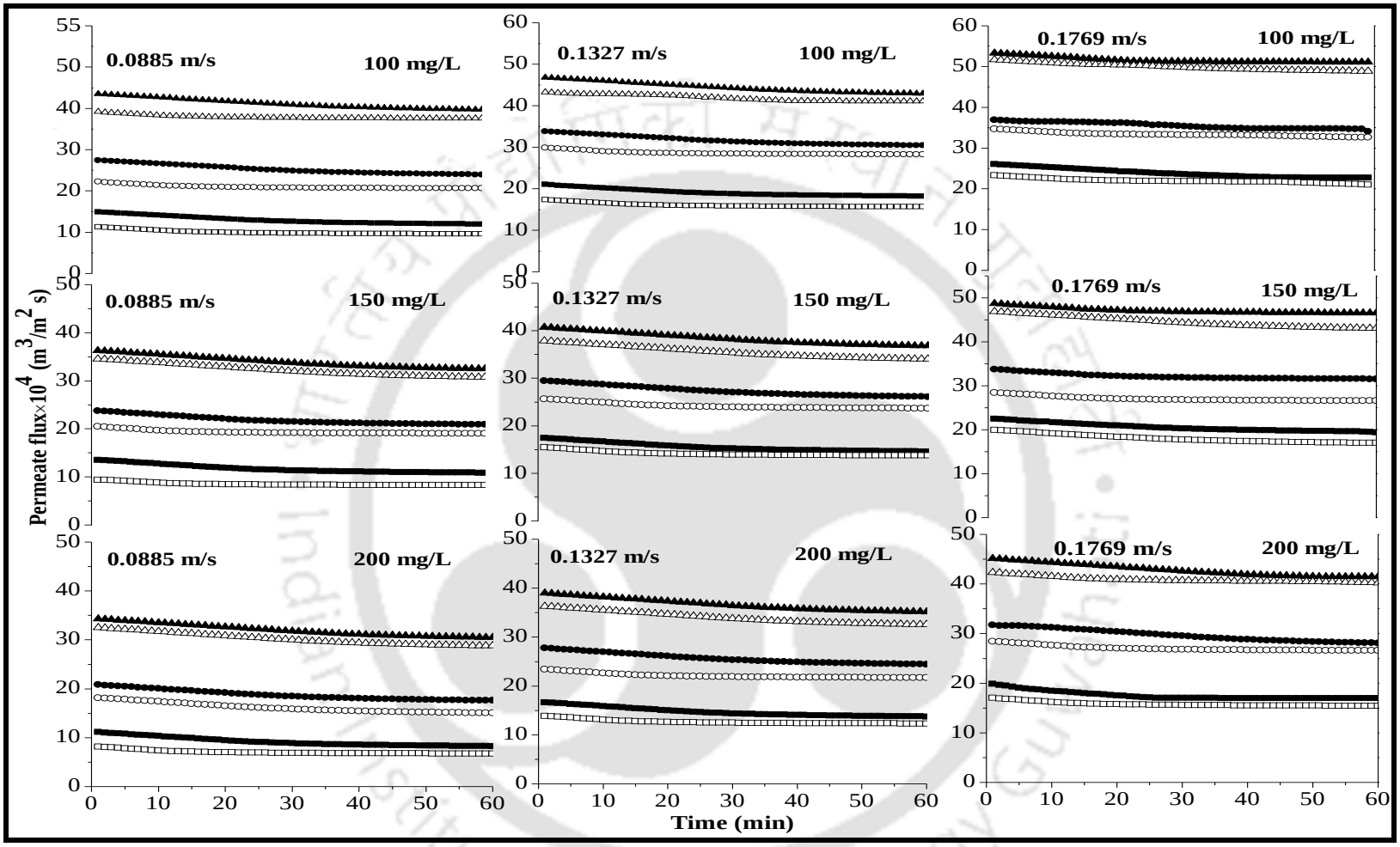

Figure 5.5: The variation of permeate flux of TiO_2-Fly ash composite membrane (filled symbol) and M2 (unfilled symbol**) membranes with various applied pressures and cross flow velocities at different feed concentrations (■,□ - 69 kPa; ●,○ - 138 kPa; ▲,Δ - 207 kPa)**

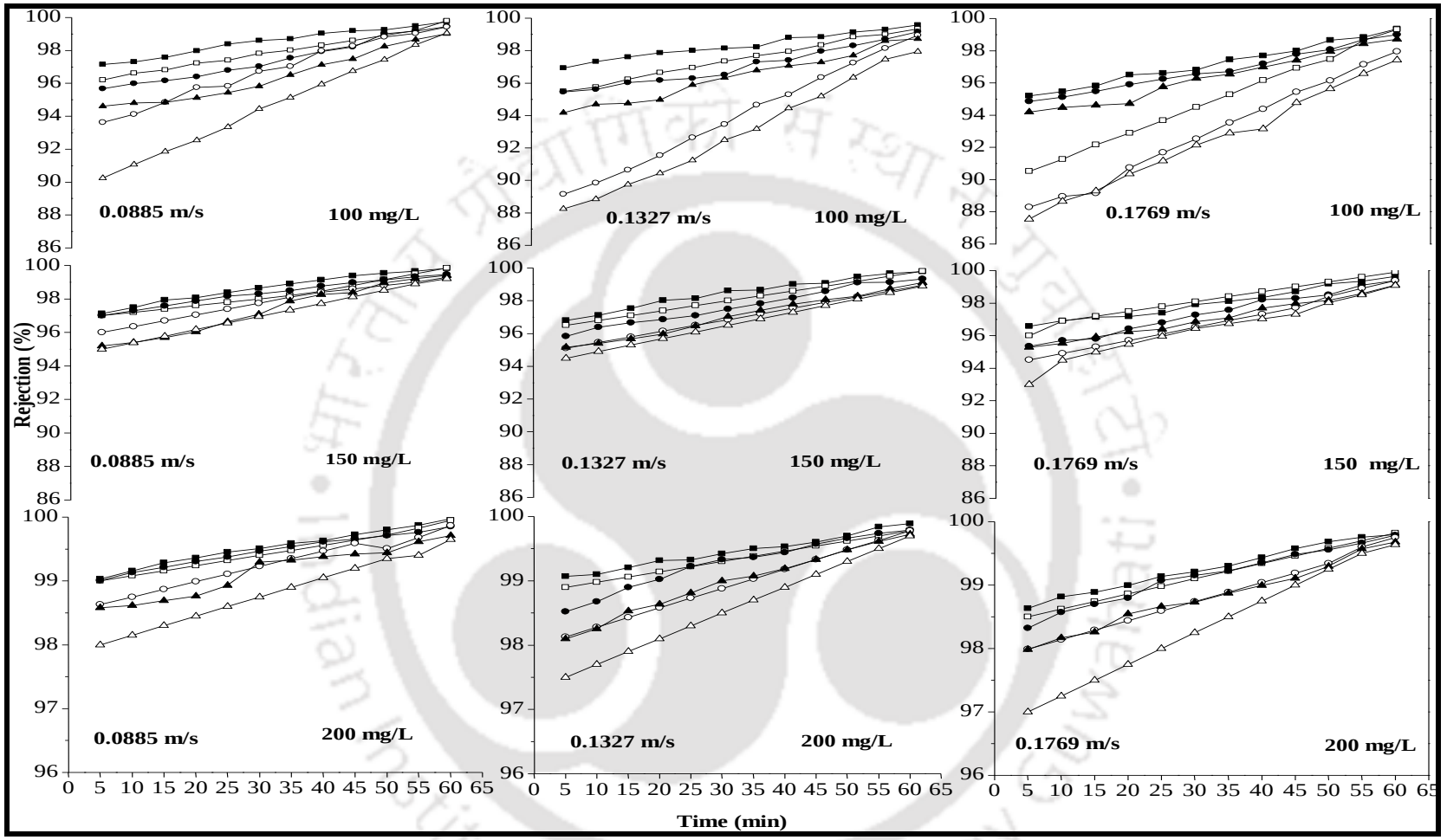

Figure 5.6: The variation of rejection of TiO_2-Fly ash composite membrane (filled symbol) and M2 (unfilled symbol**) membranes with various applied pressures and cross flow velocities at different feed concentrations (■,□ - 69 kPa; ●,○ - 138 kPa; ▲,Δ - 207 kPa)**

Fig. 5.6 depicts of time dependent variation of oil rejection with applied pressure. At 0.0885 m/s cross flow velocity, for M2 membrane, the average rejection values varied from 97.91-94.68%, 98.24-97.14% and 99.45-98.82% for three feed concentrations (100-200) at different applied pressures (69-207 kPa). However, for same experimental conditions, the TiO_2-fly ash membrane exhibited the rejection variations of about 98.53-96.48%, 98.67-97.35% and 99.53-99.15%. The higher applied pressure facilitated greater wetting and coalescence of oil droplets and hence, greater permeate concentrations due to significant passage of oil droplets through the ceramic membranes. The enhancement in the rejection rate with time is due to pore blocking that occurred after a certain time frame during the cross flow MF run. The oil rejection has been evaluated to be a highly dependent upon membrane pore size and applied pressure with higher rejection obtained for the TiO_2-fly ash composite membranes in comparison with those obtained for the M2 membrane (99.53% for composite membrane and 99.45% for M2 membrane at 69 kPa, 0.0885 m/s, and 200 mg/L solution concentration). From this study, it was known that the oil rejection depends on membrane pore size and the best operating applied pressure for obtaining better permeate flux and oil rejection was 207 kPa.

5.2.5.2 Effect of cross flow rate

The variations in trans-membrane flux and rejection with variations in cross flow velocities (0.0885-0.1769 m/s) and applied pressure (69-207 kPa) are shown in Figs. 5.5 and 5.6. As expected, higher membrane flux was obtained at higher cross flow velocity due to reduction in concentration polarization. Further, an enhancement in the cross flow velocity enabled an increase in the shear stress on the surface and thereby reduces the thickness of oil layer that adheres on the membrane surface. Further, flux decline rate reduced with increasing cross flow velocity. This is due to the lower cake layer formation on the membrane surface, which

reduces permeation resistance and hence higher flux (Chakrabarty et al., 2008; Mittal et al., 2011); Mueller et al., 1997; Vasanth et al., 2013; Jonsson and Tragardh, 1990). For TiO_2-Fly ash membrane, the maximum average permeate flux (51.6372×10^{-4} m^3/m^2 s) was evaluated at experimental conditions of 0.1769 m/s cross flow velocity (highest value), 207 kPa applied pressure (highest value) and 100 mg/L feed concentration (lowest value). Corresponding membrane flux value for M2 membrane was 49.9712×10^{-4} m^3/m^2 s.

The M2 membrane rejection has been found to decrease (94.69-92.47%, 97.14-96.42% and 98.82-98.37% for 100, 150 and 200 mg/L of feed, respectively at 207 kPa) with increasing cross flow velocity (0.0885-0.1769 m/s). On the other hand, TiO_2-Fly ash membrane exhibited maximum rejection (96.48-96.35%, 97.35-97.07% and 99.15-98.82%). At higher cross flow velocities, oil emulsion droplet sizes are reduced significantly and finer droplets are facilitated to enter the permeate stream significantly to reduce the rejection. For M2 membrane, the maximum oil rejection of 98.82% has been obtained at lower cross flow velocity (0.0885 m/s), higher feed concentration (200 mg/L) and higher pressure of 207 kPa. Corresponding rejection value for TiO_2-fly ash membranes is 99.15%. At higher cross flow velocity values, rejection values are lower but flux values are higher and hence if maximum membrane flux is to be considered, the higher cross flow velocity (0.1769 m/s) is the optimal cross flow velocity. In general, ceramic membranes for application towards industrial scale separation should provide higher combination of rejection efficiency and permeate flux. Therefore, the optimal cross flow velocity of 0.1789 m/s is justified. At this condition, the TiO_2-Fly ash membrane provided about 98.82% of rejection with 42.8495×10^{-4} (m^3/m^2 s) flux and M2 membrane provided 98.37% of rejection (permeate flux of 40.9045×10^{-4} (m^3/m^2 s)) at a pressure of 207 kPa and 200 mg/L feed concentration.

Further, as shown in Fig. 5.5, the application of a thin hydrophilic TiO_2 coating did increase membrane flux at the very beginning of the cross flow MF run. The fluxes of TiO_2-Fly ash composite membrane were higher than those of M2 membrane for all MF runs. Fig. 5.5 shows that during the MF process, a small variation in flux was observed for M2 membrane thereby confirming that M2 underwent minimal fouling due to concentration polarization effect under these conditions. This is also due to the fact that higher feed concentration allows quicker formation of oil layer on the membrane surface that hinders water transport. The fouling of fly ash membrane was typically due to the adherence of formed oil droplets to the surface and membrane pores to deteriorate the membrane flux. However, for the TiO_2-Fly ash composite membrane, flux decline was slower than that observed for the M2 membrane (only 1% flux decline for TiO_2-Fly ash composite membrane). A small reduction in initial flux was due to rapid oil layer formation on the membrane surface. However, significant increase in concentration polarization did not occur with time due to hydrodynamic flow action and hence a constant flux was observed with time after the initial small reduction in flux.

It is further interesting to note that the TiO_2 thin layer coating altered the rejection characteristics due to alterations in the interaction between oil droplets and membrane surface. The hydrophilicity of the TiO_2-Fly ash composite microfiltration membrane was nominally improved, which was expected to repel the hydrophobic oil droplets from adhering to membrane surface. Thus, the pore blocking tendencies of the membrane was avoided due to high capillary repulsion force present in the hydrophilic membrane pores, which prevents oil droplets to transport across the membrane (Zhu et al., 2016). After modification, the TiO_2-Fly ash composite membrane pores became smaller and enhanced the hydrophilic nature of the M2 membrane. The repulsing force that generated during the process was high enough to

reject oil droplets, thus weakening membrane fouling, which directly minimized the influence of surface adsorption and irreversible membrane fouling (Srijaroonrat et al., 1999; Zhou et al., 2010).

Membrane fouling, which results from specific interactions between membrane pore surface and oil droplets, caused a rapid (sometimes irreversible) flux decline of the whole membrane. In order to reduce the effect of membrane fouling and to recover membrane flux, a periodic cleaning process with detergent solution was employed in our study. During this step, detergent solution flowed through the membrane pore structure, resulting in an effective removal of oil droplets that adhered on membrane surface. Compared to M2 membrane, higher flux restoration efficiency was observed for the TiO_2-Fly ash composite membrane in each run. It is realized that over 99.9% of the original flux (61.3545×10^{-4} m^3/m^2 s at 207 kPa and 0.1769 m/s) was recovered by washing in the first cycle itself. This confirms that the TiO_2-Fly ash membrane has greater hydrophilic nature than the M2 membrane. The oil-in-water emulsion might be barely adsorbed on the TiO_2-Fly ash composite membrane surface, and the bonding between hydrophilic TiO_2 and hydrophobic oil layer could be weak and facilitates rapid detachment. The oil droplets in the porous structure and those adhering to the membrane surface could be readily washed with an appropriate cross-flow velocity and washing with detergent solution. This is not the case for M2 membrane. For M2 membrane, washing with detergent solution was not so effective for flux restoration and only 95-98% flux recovery efficiency of the original flux (59.6213×10^{-4} m^3/m^2 s at 207 kPa and 0.1769 m/s) was observed. This indicated severity in membrane fouling. In this case, membrane fouling was partially recoverable. This is likely due to unfavorable interaction between oil droplets and M2 membrane surface with relatively poor hydrophilicity. Thereby, M2

membrane could have a progressive deterioration of membrane permeation performance with repetitive usage for oil-in-water emulsion separation.

5.2.5.3 Performance indices

For each case, the performance indices of membrane were evaluated by multiplying the average permeate flux with corresponding average rejection after 1 h MF operation. For a variation in cross flow velocity from 0.0885-0.1769 m/s and applied pressure from 69-207 kPa at a feed concentration of 100 mg/L, the performance indices were evaluated to vary from 973.7939×10^{-4}-4620.751×10^{-4} (%. m^3/m^2 s) for M2 membrane and 1273.715×10^{-4}-4974.97×10^{-4} (%. m^3/m^2 s) for TiO_2-fly ash membrane. The highest performance indices have been observed for TiO_2-fly ash membrane in all cross flow MF runs. This indicates that surface hydrophilic nature enhanced with coating of TiO_2 material on the surface. For the M2 membrane, the performance indices varied from 973.7939×10^{-4}-3592.255×10^{-4} (%. m^3/m^2 s) for a variation in applied pressure from 69 to 207 kPa, at 0.0885 m/s of cross flow velocity and 100 mg/L of feed concentration. Thus it can be observed that applied pressure significantly influence the performance index for M2 membrane.

The variation of membrane performance indices with cross flow velocity for fly ash membrane (M2) and TiO_2-fly ash membrane has been presented in Fig. 5.7. As shown in Fig 5.7, for TiO_2-fly ash membrane, at an applied pressure of 207 kPa, the performance index varied from 3977.025×10^{-4}-4974.97×10^{-4}, 3310.996×10^{-4}-4576.418×10^{-4} and 3174.977×10^{-4}-4234.509×10^{-4} (%. m^3/m^2 s), with increasing cross flow velocities from 0.0885-0.1769 m/s, at 100, 150 and 200 mg/L, respectively [3592.255×10^{-4}-4620.751×10^{-4}, 3135.382×10^{-4}-4299.212×10^{-4} and 2988.133×10^{-4}-4023.602×10^{-4} (%. m^3/m^2 s) for fly ash membrane (M2)].

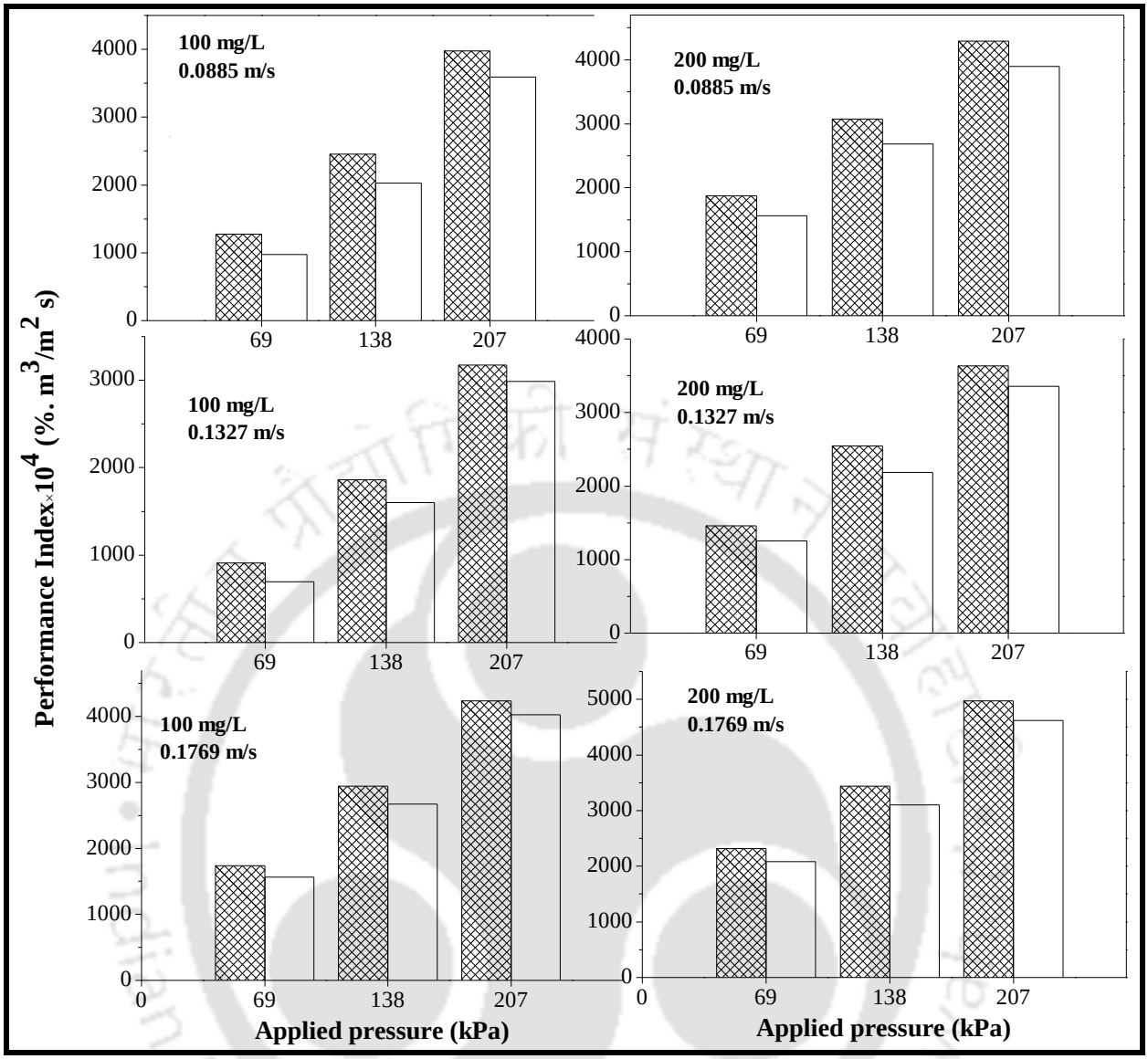

Figure 5.7: The performance indices for TiO_2-Fly ash composite membrane (Filled symbol) and M2 membrane (unfilled symbol**) at different feed concentrations (100-200 mg/L) with various cross flow velocities (0.0885-0.1768 m/s)**

Thus, it can be inferred that substantial fouling occurred for fly ash membrane (M2) even for cross flow microfiltration. This was not the case for TiO_2-Fly ash membrane. Thus, TiO_2 based modification of ceramic membrane is an important step to enhance membrane shelf life. Also, an enhancement in cross flow velocity results in an improvement in the performance index values for both membranes. This indicates that higher turbulence

promoted prohibition of membrane fouling (Sriharsha et al., 2014). However, the enhancement in the performance index is significant for the TiO_2-fly ash membrane case. This is due to greater hydrophilic nature of the membrane in comparison with M2 membrane.

For both the membranes, the variation of performance indices with applied pressure for maximum cross flow velocity case (0.1769 m/s) with 100 mg/L feed is depicted in Fig. 5.7. As shown in Fig. 5.7, for an applied pressure variation from 69-207 kPa, the performance indices varied from 2082.534×10^{-4}-4620.751×10^{-4} (%. m^3/m^2 s) for M2 membrane and 2317.593×10^{-4}-4974.97×10^{-4} (%. m^3/m^2 s) for TiO_2-fly ash membrane. This indicates that higher applied pressure minimizes membrane fouling. This is possibly due to the alteration of pore blocking phenomena and dynamic cake filtration layer characteristics with variations in applied pressure (Sriharsha et al., 2014). On the other hand, as shown in Fig. 5.7, at 0.1769 m/s, for a variation of applied pressure from 69-207 kPa, the performance indices varied from 1562.167×10^{-4}-4023.602×10^{-4} (%. m^3/m^2 s) for M2 membrane and 1737.488×10^{-4}-4234.509×10^{-4} (%. m^3/m^2 s) for TiO_2-Fly ash membrane, respectively using 200 mg/L feed concentration. Once again, it can be confirmed that higher applied pressure and maximum cross flow velocity and surface modification are most favorable choices to maximize the shelf life of the developed membranes.

Amongst both the membranes, TiO_2-fly ash membrane provided better performance in terms of average permeate flux (9.1634×10^{-4}-51.6372×10^{-4} m^3/m^2 s for TiO_2-fly ash membrane and 7.0086×10^{-4}-49.9712×10^{-4} m^3/m^2 s for M2 membrane) and performance indices (912.0626×10^{-4}-4974.97×10^{-4} (%. m^3/m^2 s) for TiO_2-fly ash membrane and 696.9989×10^{-4}-4620.751×10^{-4} (%. m^3/m^2 s) for M2 membrane). The above mentioned minimum value (at 69 kPa, 0.0885 m/s, 200 mg/L condition) and maximum value (at 207 kPa, 0.1769 m/s, 100 mg/L condition) are obtained for entire MF study. Thus, it is apparent that the cross flow

microfiltration operation achieved the desired objective to reduce oil content in the permeate samples and minimize the membrane fouling. Further, it is interesting to note that only when TiO_2-fly ash membrane was considered, the oil content in the permeate samples reduced to negligible value. Thus the MF of oil-in-water emulsions with TiO_2-fly ash membrane provided high quality water which might be used for domestic usage as well with minimal further treatment.

The obtained results in this work have been compared with the data reported in the literature. A comparative summary of the data is presented in Table 5.1. In this regard, it can be observed that Li et al., (2006) used surface modified Al_2O_3 membrane for the treatment of (15.5 mg/L) oil-in-water emulsion to obtain 98.04% rejection, 4.1614×10^{-7} m^3/m^2 s kPa normalized flux at 100 kPa and 7.8 m/s cross flow velocity. Similarly, Zhou et al., (2010) achieved 98.7% of oil rejection with ZrO_2-Al_2O_3 composite membrane for the separation of 1000 mg/L oil-in-water emulsion at 179 kPa and 5 m/s of cross flow velocity. In another work, Zhu et al., (2016) applied TiO_2-Mullite composite membrane for the treatment of 200 mg/L oil-in-water emulsion to obtain 4.1667×10^{-7} m^3/m^2 s kPa membrane normalized flux and 97% rejection at 2.5 kPa and 0.15 m/s cross flow velocity. In the present work, TiO_2-Fly ash membrane provided maximum rejection (98.82%) and permeate flux (2.07×10^{-5} m^3/m^2 s kPa) than that provided by the M2 membrane (98.37% rejection; 1.98×10^{-5} m^3/m^2 s kPa) at 0.1769 m/s, 207 kPa, 200 mg/L. Therefore, the results obtained in this work is comparably better than the results reported in the literature

Table 5.1: Comparison between permeate flux and rejection of the TiO_2-Fly ash composite membrane and M2 membrane in this work and those reported in the literature.

Author	Material	Pore size (μm)	Type of oil	Applied pressure (kPa)	Feed Concentration (mg/L)	Oil droplet size (μm)	Cros flow velocity (m/s)	Permeability (m^3/m^2 s kPa)	Rejection (%)
Li et al., (2006)	Al_2O_3-PVDF	-	Oil field wastewater	100	15.5	-	7.8	4.1614×10^{-7}	98.04
Hua et al., (2007)	α- Al_2O_3	0.05	Edible oil	100	500	-	1.68	1.775×10^{-7}	98.1
Zhou et al., (2010)	ZrO_2-Al_2O_3	0.2	Engine oil	16	1000	1.79	5	-	98.7
Chang et al., (2014)	TiO_2- Al_2O_3	6	Hydraulic oil	16	<4000	0.7-20	-	8.8889×10^{-7}	>99.9
Zhu et al., (2016)	TiO_2-Mullite	0.11	Soybean oil	2.5	200	1.09	0.15	4.1667×10^{-7}	97_{TOC}
This work	TiO_2-Fly ash	1.12	Crude oil	207	200	6.716	0.1769	2.07×10^{-5}	98.8227
This work	M2	1.30	Crude oil	207	200	6.716	0.1769	1.98×10^{-5}	98.3658

5.2.6 ANOVA analysis

Tables 5.2 and 5.3 demonstrate the obtained response values (permeate flux and rejection) from the three level-three factor CCD design for TiO_2-Fly ash membrane and M2 membrane, respectively. The statistically significance of the model fit revealed that the obtained response values fit well with the quadratic model. Table 5.4 summarizes the ANOVA results obtained for second-order polynomial model of permeate flux. The ANOVA results are highly satisfactory and promising given the fact that F value is high (128.79) to indicate model significance and p value is low i.e., (p–value > F) = <0.0001. This confirms that there is only 0.01% chance for model F value to have larger noise. Further, the applied pressure (X_1), concentration (X_2) and cross flow velocity (X_3) are the most significant terms on permeate flux as they have p-value < 0.05. The value for lack of fit of F is 3.63 and this confirms as well upon model significance. The model acceptability is further confirmed with the evaluated regression coefficient (R^2 = 0.99), which is in agreement with the adjusted regression coefficient (adj R^2 = 0.98) and predicted regression coefficient (pred R^2 = 0.94). The ANOVA results for rejection are summarized in Table 5.5. In case of rejection, the quadratic model is observed as significant model with F-value of 8.86; p-value <0.001; lack of fit F value as 0.41; model R^2 of 0.8886; predicted R^2 value of 0.6270 (poor but reasonable); "adj R-squared" value of 0.7883. The model has once again confirmed that all terms, namely applied pressure (X_1), feed concentration (X_2) and cross flow velocity (X_3) are significant terms.

For the TiO_2-fly ash composite membrane, the regression model from ANOVA analysis in terms of coded factors for membrane flux and rejection are presented as follows:

$$\text{Flux}\left(m^3/m^2\ s\right) = 26.85 + 12.38\ X_1 - 3.30\ X_2 + 4.95\ X_3 - 0.99\ X_1X_2 + 0.25\ X_1X_3 - 0.27\ X_2X_3 + 0.37\ X_1^2 + 0.78\ X_2^2 + 0.29\ X_3^2 \quad (5.1)$$

$$\text{Rejection}\ (\%) = +97.60 - 0.56\ X_1 + 1.06\ X_2 - 0.36\ X_3 + 0.26\ X_1X_2 + 0.14\ X_1X_3 + 0.11\ X_2X_3 + 0.12\ X_1^2 + 0.21\ X_2^2 + 0.13\ X_3^2 \quad (5.2)$$

Similar expressions exist for M2 membrane and are presented as follows:

$$\text{Flux}\left(m^3/m^2\ s\right) = 24.18 + 12.10\ X_1 - 4.46\ X_2 + 5.30\ X_3 - 0.95\ X_1X_2 + 0.24\ X_1X_3 - 0.58\ X_2X_3 + 0.72\ X_1^2 + 0.14\ X_2^2 + 1.60\ X_3^2 \quad (5.3)$$

$$\text{Rejection}\ (\%) = 97.07 - 0.80\ X_1 + 2.11\ X_2 - 0.64\ X_3 + 0.53\ X_1X_2 + 0.079\ X_1X_3 + 0.079\ X_2X_3 + 0.12\ X_1^2 - 0.31\ X_2^2 + 0.065\ X_3^2 \quad (5.4)$$

where, X_1, X_2 and X_3 are the coded factors of applied pressure, feed concentration and cross flow velocity, respectively.

The ANOVA results for M2 membrane flux and rejection are presented in Tables 5.6 and 5.7. Their analysis is similar to that presented earlier and is therefore not elaborated further.

Table 5.2: RSM design and its actual and predicted values for TiO_2-Fly ash membrane

Run order	Pressure (kPa)	Concentration (mg/L)	Cross Flow Velocity (m/s)	Permeate flux $J\times10^4$ (m^3/m^2s)		Rejection (%)	
	X1	X2	X3	Actual	Predicted	Actual	Predicted
1	69	100	0.0885	12.93	13.26	98.53	98.43
2	207	100	0.0885	41.22	39.50	96.48	96.5
3	69	200	0.0885	9.16	9.17	99.53	99.8
4	207	200	0.0885	32.02	31.47	99.15	98.91
5	69	100	0.1769	23.84	23.21	97.2	97.21
6	207	100	0.1769	51.64	50.44	96.34	95.85
7	69	200	0.1769	17.50	18.04	99.27	99.02
8	207	200	0.1769	42.85	41.33	98.82	98.7
9	21.96	150	0.1327	7.81	7.08	98.94	98.87
10	254.04	150	0.1327	46.33	48.73	96.59	96.98
11	138	65.91	0.1327	33.28	34.62	96.17	96.4
12	138	234.09	0.1327	23.18	23.52	99.86	99.96
13	138	150	0.0584	18.77	19.35	98.65	98.58
14	138	150	0.207	34.92	36.02	96.98	97.37
15	138	150	0.1327	27.33	26.85	97.71	97.6
16	138	150	0.1327	26.09	26.85	97.69	97.6
17	138	150	0.1327	25.47	26.85	97.07	97.6
18	138	150	0.1327	27.26	26.85	96.81	97.6
19	138	150	0.1327	28.25	26.85	97.71	97.6
20	138	150	0.1327	26.99	26.85	98.65	97.6

Table 5.3: RSM design and its actual and predicted values for M2 membrane

Run order	Pressure (kPa)	Concentration (mg/L)	Cross Flow Velocity (m/s)	Permeate flux $J\times10^4$ (m^3/m^2s)		Rejection (%)	
	X1	X2	X3	Actual	Predicted	Actual	Predicted
1	69	100	0.0885	9.95	11.4	97.91	97.44
2	207	100	0.0885	37.94	37.03	94.69	94.62
3	69	200	0.0885	7.01	5.54	99.45	99.48
4	207	200	0.0885	30.24	27.35	98.82	98.77
5	69	100	0.1769	21.94	22.67	94.9	94.89
6	207	100	0.1769	49.97	49.28	92.47	92.38
7	69	200	0.1769	15.75	14.5	99.16	99.16
8	207	200	0.1769	40.9	37.28	98.37	98.77
9	21.96	150	0.1327	6.58	5.85	98.52	98.76
10	254.04	150	0.1327	42.78	46.56	96.2	96.05
11	138	65.91	0.1327	33.47	32.08	92.29	92.64
12	138	234.09	0.1327	12.61	17.06	99.99	99.73
13	138	150	0.0584	15.73	16.95	98.03	98.32
14	138	150	0.207	32.95	34.78	96.39	96.18
15	138	150	0.1327	24.17	24.18	97.03	97.07
16	138	150	0.1327	25.17	24.18	96.22	97.07
17	138	150	0.1327	23.17	24.18	98.18	97.07
18	138	150	0.1327	24.17	24.18	97.03	97.07
19	138	150	0.1327	24.77	24.18	96.94	97.07
20	138	150	0.1327	24.17	24.18	97.03	97.07

Table 5.4: ANOVA for the permeate flux response surface quadratic model of TiO_2-Fly ash membrane

Source	Sum of Squares	df	Mean Square	F Value	p-value Prob > F
Model	2596.89	9	288.54	128.79	< 0.0001
X_1-Pressure (kPa)	2093.46	1	2093.46	934.41	< 0.0001
X_2-Conc. (mg/L)	148.69	1	148.69	66.37	< 0.0001
X_3-CFV (m/s)	335.25	1	335.25	149.64	< 0.0001
X_1X_2	7.77	1	7.77	3.47	0.0922
X_1X_3	0.49	1	0.49	0.22	0.6491
X_2X_3	0.59	1	0.59	0.26	0.62
X_1^2	2	1	2	0.89	0.3667
X_2^2	8.85	1	8.85	3.95	0.075
X_3^2	1.24	1	1.24	0.56	0.4733
Residual	22.4	10	2.24		
Lack of Fit	17.57	5	3.51	3.63	0.0916
Pure Error	4.84	5	0.97		
Cor Total	2619.3	19			
Std. Dev.	1.5			R^2	0.9914
Mean	27.84			Adj R^2	0.9837
C.V. %	5.38			Pred R^2	0.9459
PRESS	141.82			Adeq Precision	40.965

C.V. % =Coefficient of variation; PRESS=Predicted Residual Sum of Squares; Cor Total=Corrected total sum of squared deviations from the grand mean; df=Degree of freedom.

Table 5.5: ANOVA for the rejection response surface quadratic model of TiO_2-Fly ash membrane

Source	Sum of Squares	df	Mean Square	F Value	p-value Prob > F
Model	23.0141	9	2.55712	8.862263	0.0010
X_1-Pressure (kPa)	4.33982	1	4.33982	15.04061	0.0031
X_2-Conc. (mg/L)	15.2291	1	15.2291	52.77981	< 0.0001
X_3-CFV (m/s)	1.74106	1	1.74106	6.034037	0.0339
X_1X_2	0.54122	1	0.54122	1.875705	0.2008
X_1X_3	0.16273	1	0.16273	0.56397	0.4700
X_2X_3	0.09676	1	0.09676	0.335342	0.5753
X_1^2	0.19148	1	0.19148	0.663617	0.4343
X_2^2	0.61177	1	0.61177	2.120232	0.1760
X_3^2	0.2576	1	0.2576	0.892758	0.3670
Residual	2.8854	10	0.28854		
Lack of Fit	0.84563	5	0.16913	0.41457	0.8220
Pure Error	2.03977	5	0.40795		
Cor Total	25.8995	19			
Std. Dev.	0.54			R^2	0.8886
Mean	97.91			Adj R^2	0.7883
C.V. %	0.55			Pred R^2	0.627
PRESS	9.66			Adeq Precision	10.815

C.V. % =Coefficient of variation; PRESS=Predicted Residual Sum of Squares; Cor Total=Corrected total sum of squared deviations from the grand mean, df=Degree of freedom.

Table 5.6: ANOVA for the permeate flux response surface quadratic model of M2 membrane

Source	Sum of Squares	df	Mean Square	F Value	p-value Prob > F
Model	2678.42	9	297.6	40.8	< 0.0001
X_1-Pressure (kPa)	2000.49	1	2000.49	274.28	< 0.0001
X_2-Conc. (mg/L)	272.16	1	272.16	37.32	0.0001
X_3-CFV (m/s)	383.89	1	383.89	52.63	< 0.0001
X_1X_2	7.29	1	7.29	1	0.3409
X_1X_3	0.48	1	0.48	0.065	0.8033
X_2X_3	2.67	1	2.67	0.37	0.5587
X_1^2	7.41	1	7.41	1.02	0.3374
X_2^2	0.27	1	0.27	0.037	0.8504
X_3^2	5.13	1	5.13	0.7	0.4213
Residual	72.94	10	7.29		
Lack of Fit	70.64	5	14.13	30.7	0.0009
Pure Error	2.3	5	0.46		
Cor Total	2751.36	19			
Std. Dev.	2.7			R^2	0.9735
Mean	25.17			Adj R^2	0.9496
C.V. %	10.73			Pred R^2	0.8039
PRESS	539.44			Adeq Precision	22.904

C.V. % =Coefficient of variation; PRESS=Predicted Residual Sum of Squares; Cor Total=Corrected total sum of squared deviations from the grand mean, df= Degree of freedom.

Table 5.7: ANOVA for the rejection response surface quadratic model of M2 membrane

Source	Sum of Squares	df	Mean Square	F Value	p-value Prob > F
Model	81.7	9	9.08	32.83	< 0.0001
X_1-Pressure (kPa)	8.84	1	8.84	31.96	0.0002
X_2-Conc. (mg/L)	60.65	1	60.65	219.32	< 0.0001
X_3-CFV (m/s)	5.57	1	5.57	20.15	0.0012
X_1X_2	2.24	1	2.24	8.09	0.0174
X_1X_3	0.05	1	0.05	0.18	0.6805
X_2X_3	2.52	1	2.52	9.11	0.0129
X_1^2	0.21	1	0.21	0.74	0.4085
X_2^2	1.41	1	1.41	5.08	0.0478
X_3^2	0.061	1	0.061	0.22	0.6481
Residual	2.77	10	0.28		
Lack of Fit	0.8	5	0.16	0.41	0.825
Pure Error	1.96	5	0.39		
Cor Total	84.47	19			
Std. Dev.	0.53			R^2	0.9673
Mean	96.98			Adj R^2	0.9378
C.V. %	0.54			Pred R^2	0.8922
PRESS	9.11			Adeq Precision	19.767

C.V. % =Coefficient of variation; PRESS=Predicted Residual Sum of Squares; Cor Total=Corrected total sum of squared deviations from the grand mean, df=Degree of freedom.

The 3D response surface interaction effect of independent variables on the response variables is presented in Fig. 5.8. The 3D surface and contour plots of RSM have been prepared by varying two factors at a time and maintaining the other factor constant (at zero level). These plots thereby allow a deeper insight into the interaction effect of two variables on the response variables. Fig. 5.8a shows that the permeate flux increases from the low level region to high level region. This confirms that there is significant interaction between the applied pressures (69-207 kPa) with feed concentration (100-200 mg/L). Fig. 5.8(a) depicts that the effect of applied pressure and feed concentration on permeate flux. It can be observed that applied pressure has a positive effect on permeate flux in terms of driving force enhancement. On the other hand, the feed concentration has a negative effect for permeate flux. This is probably due to the formation of cake layer containing oil droplets that offers higher resistance to the fluid transport. At higher feed concentration, the cake layer formation is expected to happen at a higher rate and this enhances pore blocking and fouling at higher rates (Salahi et al., 2013; Wang et al., 2000). Thus, the effect of applied pressure at lower oil concentration is significant. Similar observations were also reported by Salahi et al. (2013) in cross flow microfiltration of oily wastewater using nano-porous membrane. For example, at feed concentration of 100 mg//L, for an enhancement of applied pressure from 69 kPa to 207 kPa, the permeate flux increased significantly. However, for the higher feed concentration at 200 mg/L, similar applied pressure variations allowed lower permeate flux. Therefore, it can be concluded that at high feed concentration and lower pressure levels, more oil droplets get formed on the surface and at higher pressure levels, these droplets are pushed and pressed into the membrane surface to eventually decrease the droplet size. This may get deformed subsequently in the constricted portions of the membrane to enforce pore blocking. Jokic et al., (2010) reported higher flux values with an increase in the trans-membrane pressure in cross flow microfiltration of yeast suspensions.

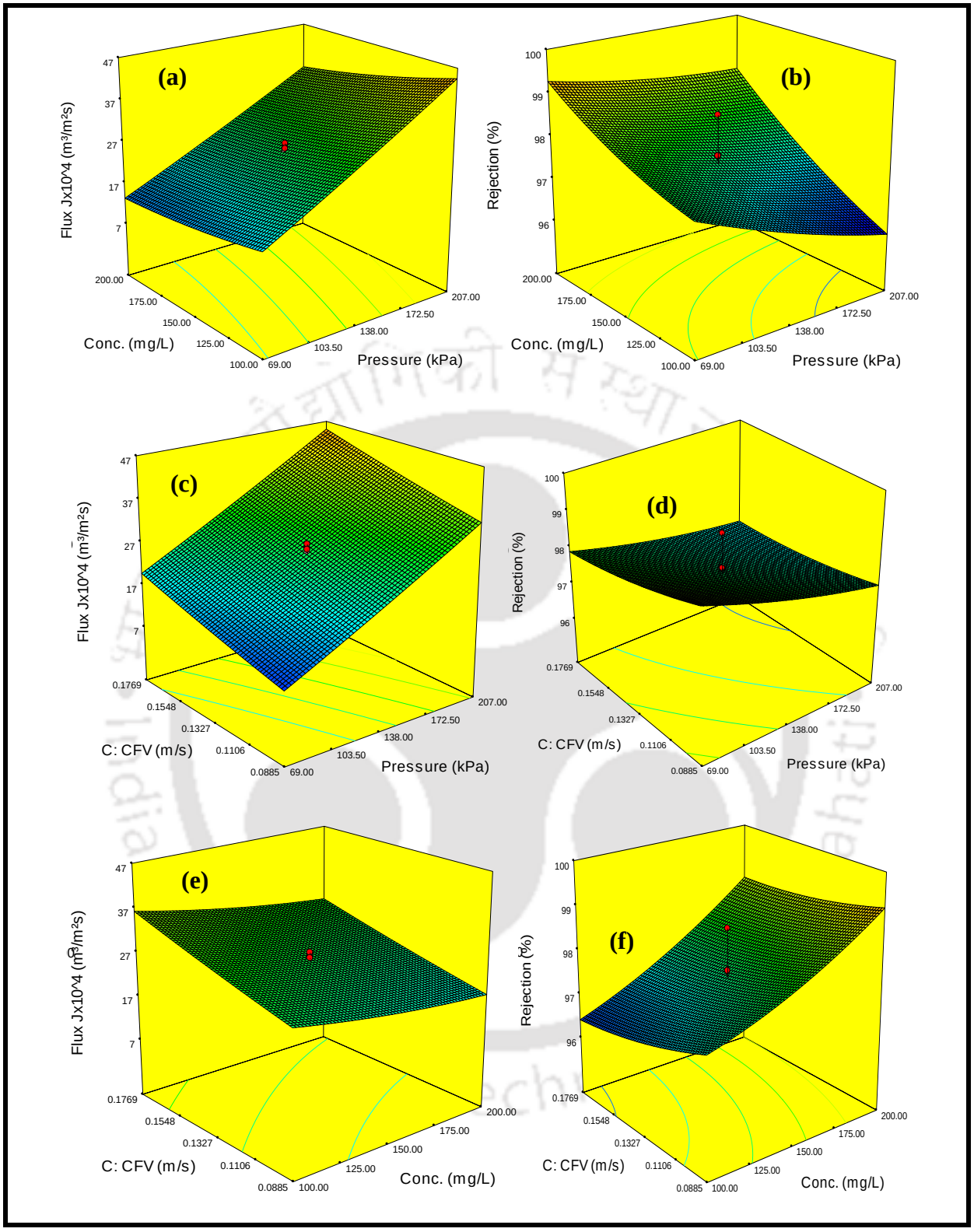

Figure 5.8: Permeate flux and rejection surface plots as a function of (a,b) pressure and concentration, (c,d) pressure and cross flow velocity, and (e,f) concentration and cross flow velocity for the TiO_2-Fly ash composite membrane

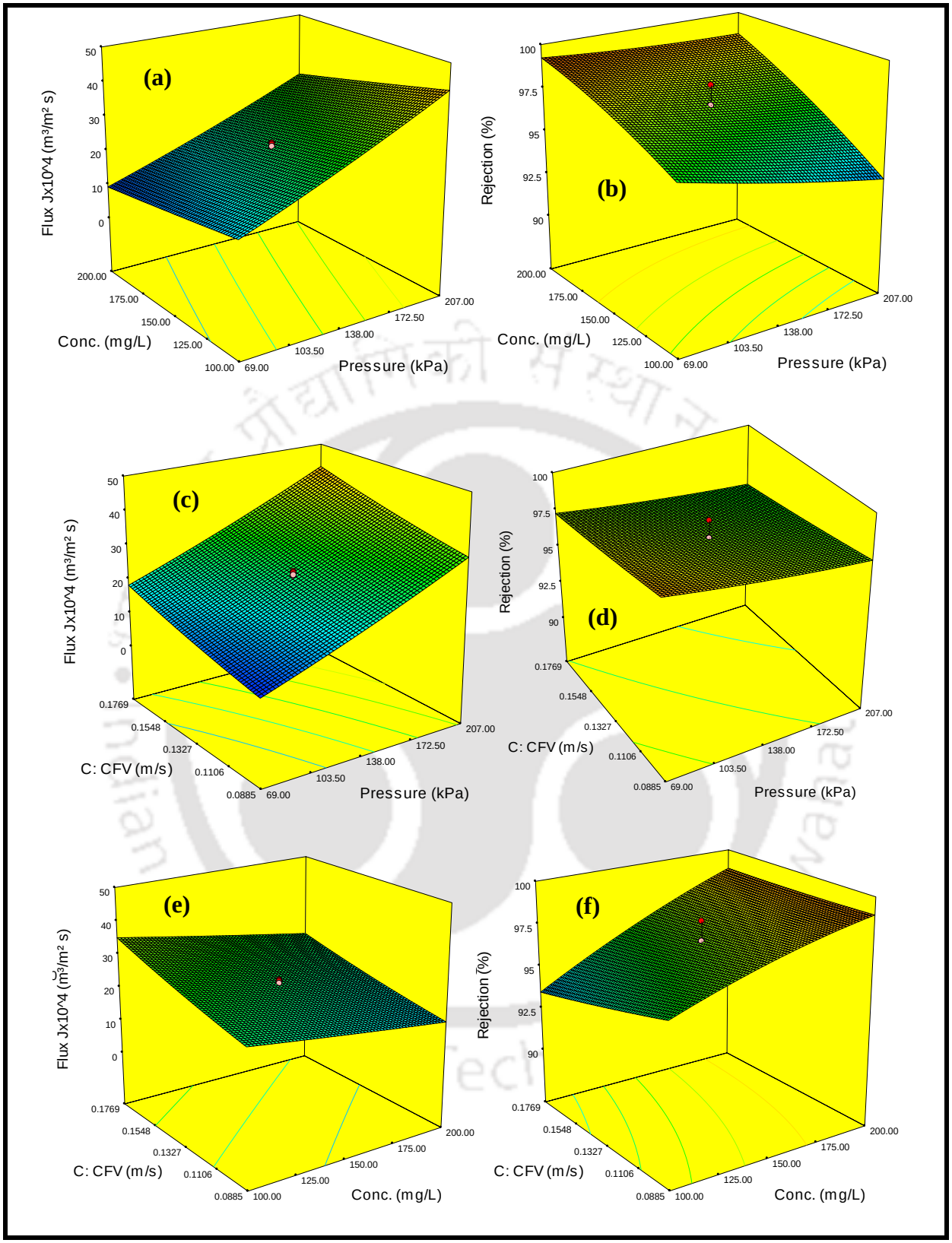

Figure 5.9: Permeate flux and rejection surface plots as a function of (a,b) pressure and concentration, (c,d) pressure and cross flow velocity, and (e,f) concentration and cross flow velocity for the M2 membrane

From Fig. 5.8e, it is apparent that the interaction between feed concentration and cross flow velocity is the best significant interaction. The plot indicates that with an increase in feed concentration and cross flow velocity, the membrane flux is reduced. Further, the effect of cross flow velocity is significant at lower feed concentration level. This is due to lower concentration polarization at lower feed concentration and higher cross flow velocity. Thus, both cross flow velocity and applied pressure are most important parameters for enhancement in permeate flux. As shown in Fig. 5.8c the membrane flux increases with increasing pressure. In addition, higher permeate flux is observed at higher cross flow velocity level. This indicates that higher cross flow velocity enhances shear stress on the membrane surface (Mueller et al., 1997). Conversely, it is alleged that oil droplets are broken into smaller droplets under higher pressure and higher cross flow velocity condition.

Fig. 5.8 illustrates upon the rejection dependence on the interaction between feed concentration and applied pressure (5.8b), cross flow velocity and applied pressure (5.8d) and cross flow velocity and feed concentration (5.8f). As evidenced in Fig. 5.8(b), the percentage of oil rejection increases when the feed concentration changes from low level to high level at a fixed zero level of applied pressure. Similarly, at a fixed zero level of cross flow velocity, the rejection improves with increasing feed concentration (from low level to high level) (see 5.8(f)). However, the variation in the levels of these variables (for instance cross flow velocity (high level) and applied pressure (high level) at a fixed zero level of feed concentration) consequences in reduction of the oil rejection percentage. This may be due to two reasons. The first reason is that there is a reduction in formation of cake layer on membrane surface at a higher level. Secondly, oil droplets of smaller size are prevalent at lower level of feed concentration. From Fig. 5.9, it can be concluded that the M2 membrane also exhibits similar behaviour to those presented for the TiO_2-Fly ash composite membrane.

Moreover, Fig. 5.10 demonstrates the relationship between the predicted and experimental flux values, which gave satisfactory correlation ($R^2 = 0.99$). It can be seen that the location of the points around the diagonal line affirm that the deviation is not significant (Fig. 5.10). The predicted values of the response of these conditions using eqns 5.1 and 5.2 are given together with the experimental data (Table 5.2). For M2 membrane, the experimental data and the corresponding predicted values of permeate flux and rejection are determined from eqn 5.3 and eqn 5.4 (see Table 5.3).

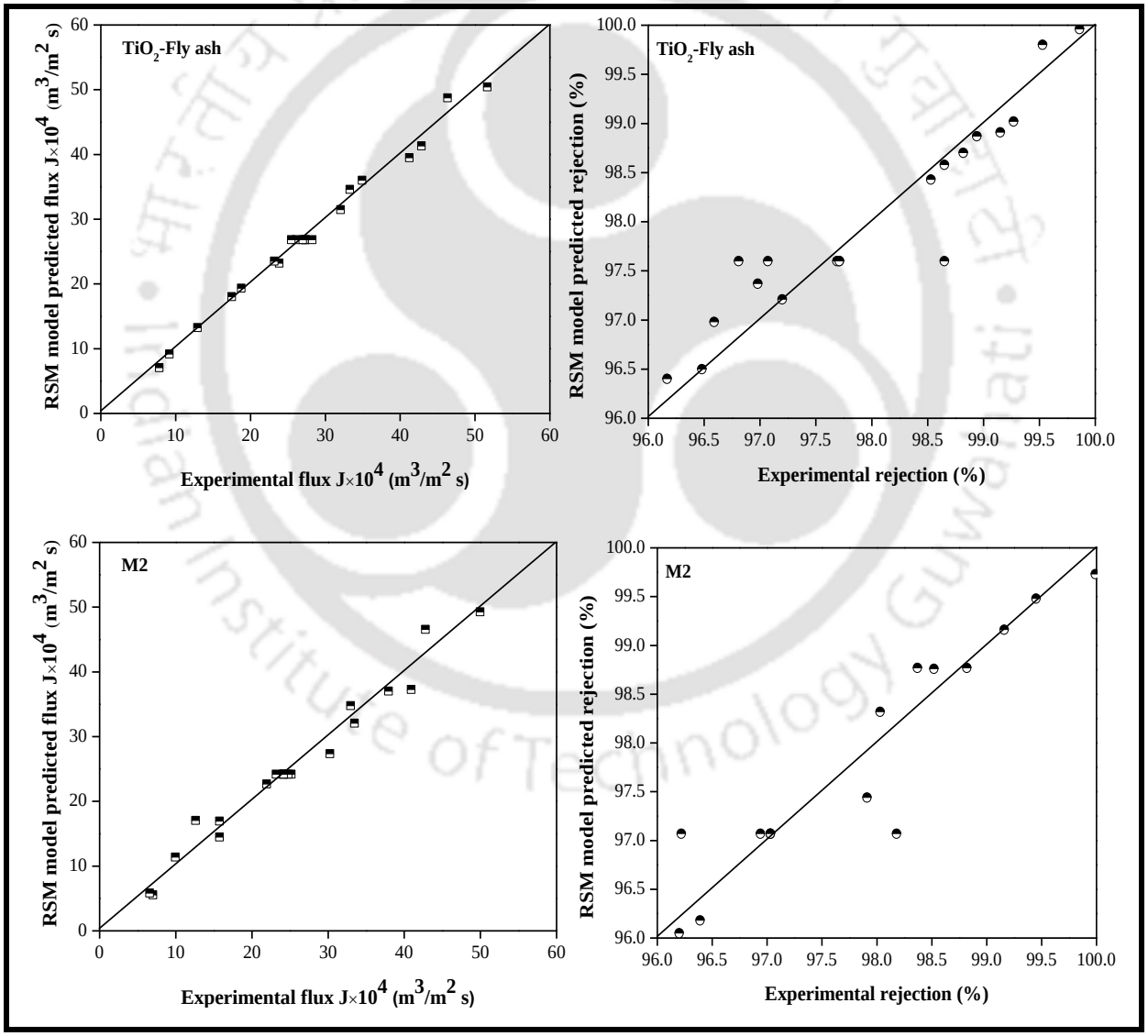

Figure 5.10: RSM model predicted values vs experimental values

5.2.6.1 Validation of predicted response at the optimum condition

The optimum condition for the TiO_2-Fly ash membrane to obtain the maximum permeate flux and rejection are applied pressure = 207 kPa, feed concentration= 200 mg/L and cross flow velocity = 0.1769 m/s. At this condition, the predicted responses were found to be 41.3301×10^{-4} (m^3/m^2 s) for membrane flux and 98.7% rejection. Additional experiments were performed at the model predicted optimum conditions to examine the suitability of the model equation. The permeate flux and rejection values obtained through the experimental result were 42.8495×10^{-4} (m^3/m^2 s) and 98.82%, respectively, and these values are in good agreement with the model predicted values for TiO_2-Fly ash membrane. The same optimum conditions are obtained for the M2 membrane through ANOVA study at which the maximized predicted permeate flux (37.284×10^{-4} m^3/m^2 s) and rejection (98.77%) were observed. From experimental investigations, these correspond to 40.9045×10^{-4} m^3/m^2 s, 98.37%, respectively. Hence, the developed model is expected to be effective for implemented in process simulation, and modelling studies involving the integration of membrane processes with other processes.

5.3 Summary

In this work, a low-cost TiO_2-Fly ash composite membrane was fabricated and then utilized to efficiently remove oil from oil-in-water emulsions. Fly ash, a bulk waste material with limited uses, was used as main starting materials to fabricate fly ash ceramic membrane (M2), on which a more hydrophilic TiO_2 layer deposited via hydrothermal method using $TiCl_4$ as titania source. The TiO_2-Fly ash composite membrane is more hydrophilic, which is evident from the lower contact angle value (14.4°) than (M2) fly ash membrane (25.8°). The enhanced hydrophilic composite membrane has prevented oil droplets to adhere with the membrane surface and hence less membrane fouling. Amongst both the membranes, TiO_2-fly

ash membrane provided better performance in terms of average permeate flux 51.6372×10^{-4} m^3/m^2 s (49.9712×10^{-4} m^3/m^2 s for M2 membrane) and performance indices 4974.97×10^{-4} (%. m^3/m^2 s) (4620.751×10^{-4} (%. m^3/m^2 s) for M2 membrane). From RSM study, the optimum conditions to obtain the maximum permeate flux and rejection for the TiO_2-Fly ash membrane are applied pressure (207 kPa), feed concentration (200 mg/L) and cross flow velocity (0.1769 m/s) at which condition, the predicted responses are evaluated to be 41.3301×10^{-4} (m^3/m^2 s) (permeate flux) and 98.7% (rejection). At the same optimum experimental conditions, the experimental results are 42.8495×10^{-4} (m^3/m^2 s), 98.82%, respectively. In summary, a low-cost and good performance TiO_2-Fly ash composite membrane has been prepared, which can be highly competitive for the treatment of oil-in-water emulsions. This study is expected to outline upon an effective route to reuse waste coal fly ash and mitigate environmental hazards associated to its disposal. The outlined methodology in this work is to produce a value added product such as fly ash based membrane for wastewater treatment applications. Thereby, this work is expected to envisage upon newer options to recycle industrial solid waste coal fly ash by targeting value added products for separation process industries.

CHAPTER-6

Preparation, Characterization and Application of TiO_2-Clay, γ-Al_2O_3-Clay Composite and Clay Membranes

भारतीय प्रौद्योगिकी संस्थान गुवाहाटी
Indian Institute of Technology Guwahati

CHAPTER 6 Preparation, characterization and application of TiO_2-clay, γ-Al_2O_3-clay composite and clay membranes

Along with the comparative assessment with ceramic membranes, this chapter summarizes the separation efficiency results obtained during dead end microfiltration performance of TiO_2-clay, γ-Al_2O_3-clay and clay membranes using synthetic oil-in-water emulsions. Section 6.1 presents an overview of the chapter. Eventually, the characterization results and the comparative microfiltration performance of composite membranes and clay membranes are presented for various feed concentration in section 6.2. Based on the research findings, the summary of the chapter is presented in section 6.3.

6.1 Overview

This chapter explains the surface modification of clay membrane by TiO_2 and γ-Al_2O_3 coating. It is the very first step towards the development of TiO_2-clay and γ-Al_2O_3-clay composite membrane. The materials used for sol preparation and the corresponding coating conditions are discussed in the chapter 2. In the experiment, clay membrane is used as the base support, which is fabricated using low cost clay by uni-axial pressing method.

6.2 Results and discussion

6.2.1 Particle size distribution (PSD)

Fig. 6.1 demonstrates the particle size distribution of synthesized sols (TiO_2 and γ-Al_2O_3). Generally, smaller sized particles deposite uniformly on the support in more quantity and block the pores of the support and even some particles may penetrate through larger pores

(Steenkiste et al., 2002). Sols with larger size particles may not form uniformly on the support and mostly create patches on the surface of the support (Saleh and Guigon, 2007). It can be noticed from Fig. 6.1 that the particle sizes of the TiO_2 and γ-Al_2O_3 sol are in the range of 0.3382-0.4777 µm, and 7.192-16.912 µm, respectively, while the volume median diameter is found to be 0.016225 and 0.001698 µm for TiO_2 and γ-Al_2O_3, respectively. The preparation of composite ceramic membrane would be satisfied using the particle sizes of aforesaid range.

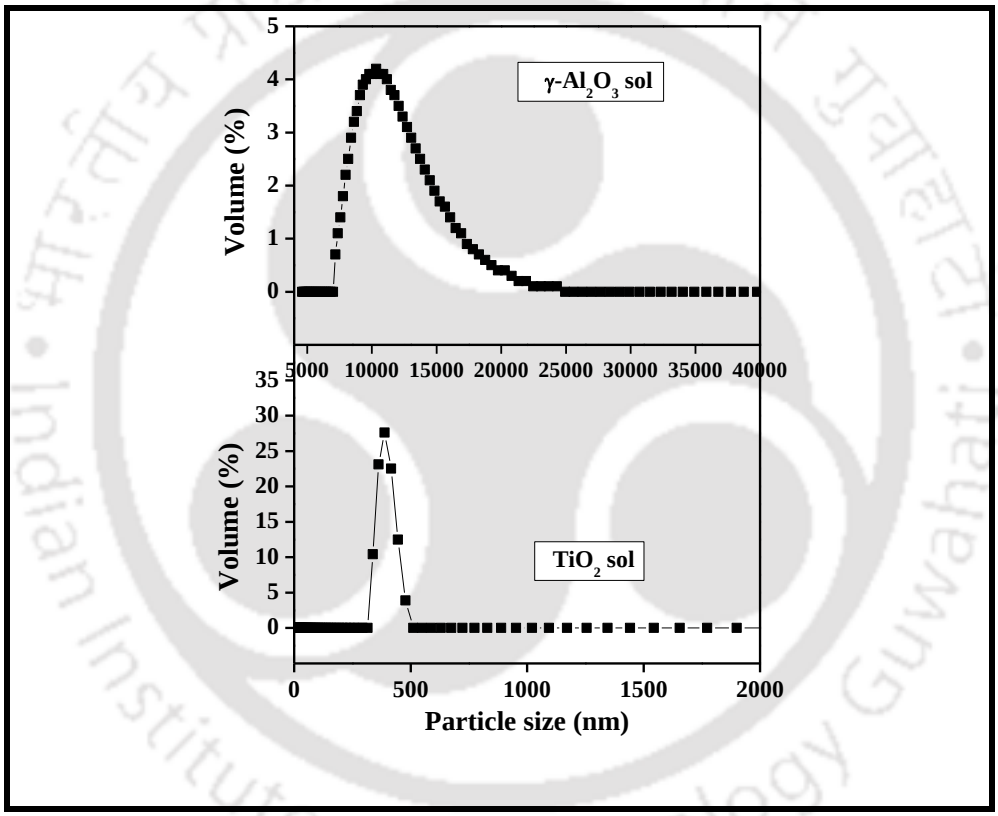

Figure 6.1: Particle size distribution of synthesized sols (TiO_2 and γ-Al_2O_3)

6.2.2 N_2 adsorption-desorption isotherm

Nitrogen adsorption-desorption isotherm and BJH pore size distributions of γ-Al_2O_3 and TiO_2 powder are shown in Fig. 6.2. According to the IUPAC classification, isotherm of mesoporous TiO_2 and γ-Al_2O_3 powder matches with a type IV group (with an H2 hysteresis

loop). It also displays that particles of TiO_2 and γ-Al_2O_3 possess complex and interconnected pores of different size and shape (Wang et al., 2007). The pore size distributions of TiO_2 and γ-Al_2O_3 are measured based on the desorption isotherm data by using the technique of BJH as depicted in Fig. 6.2. From these plots, it is evident that the TiO_2 and γ-Al_2O_3 particles contain only mesopores. These also show a unimodel distribution with pore radius of 1.54-73.85 nm for γ-Al_2O_3 and 0.15-7.36 nm for TiO_2. Moreover, 90 % of pores are having the size less than 10 nm for γ-Al_2O_3 (1.5 nm for TiO_2). BET surface area (SA) along with pore volume (PV) of TiO_2 is evaluated as 105.7 m^2/g (200.3 m^2/g for γ-Al_2O_3) and 0.4037 ml/g (0.4495 ml/g for γ-Al_2O_3), respectively.

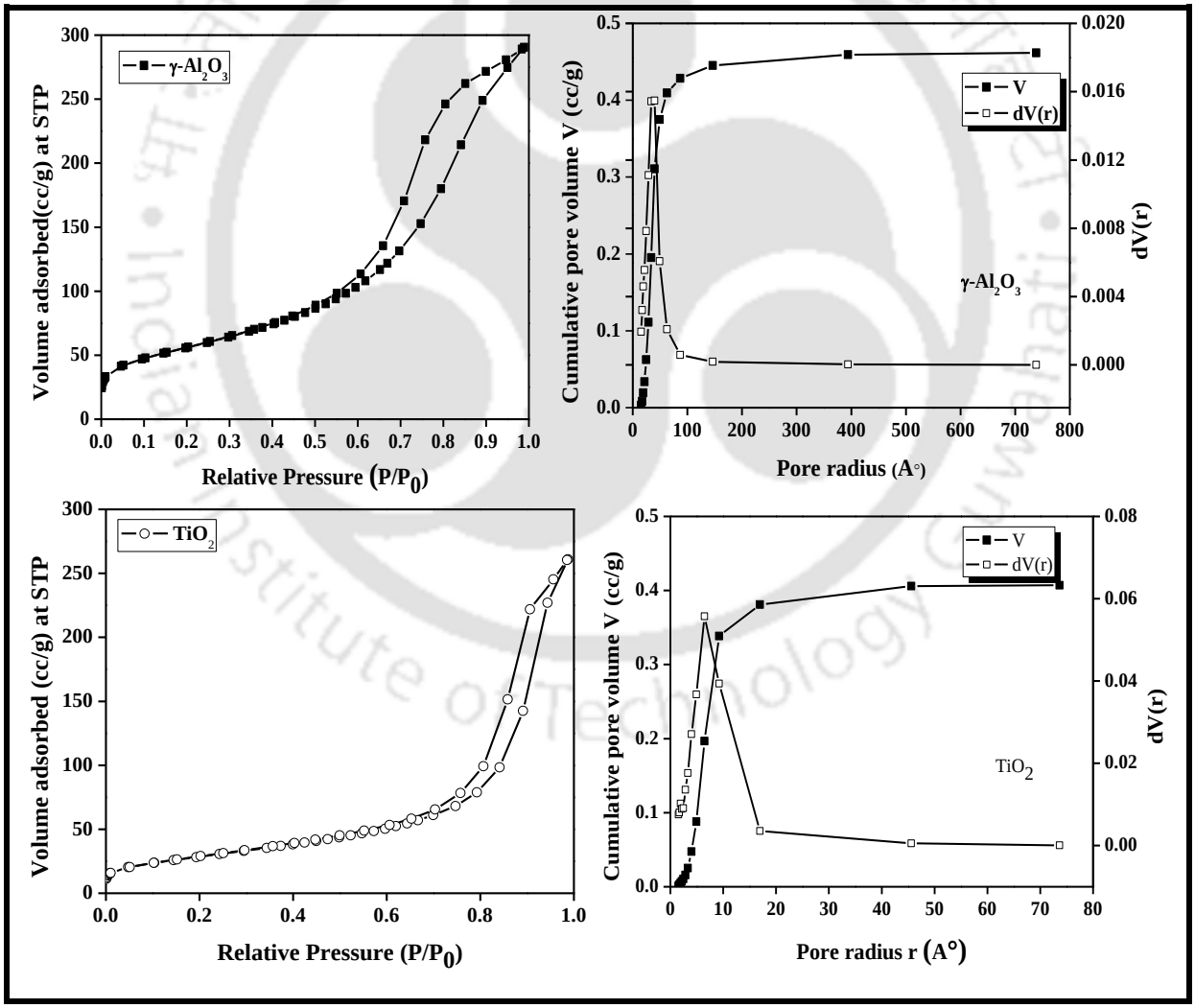

Figure 6.2: N_2 adsorption and desorption isotherms and BJH pore size distributions of TiO_2 and γ-Al_2O_3 powders

6.2.3 Thermo gravimetric analysis (TGA)

Fig. 6.3 illustrates the differential thermogravimetric (DTG) and thermogravimetric (TG) plots for the TiO_2 and γ-Al_2O_3 powder samples. TiO_2 powder (before calcination) seems to undergo two different stages of weight loss during heating. The weight loss at <195 °C is due to the deliverance of physically adsorbed water present inside pores of the powder. The second step of weight loss at temperature range of 195-350 °C is attributed to the structural change of the powder from $Ti(OH)_4$ to TiO_2. After 350 °C the weight loss is negligible and hence, the calcination temperature for the fabrication of the membrane is fixed as 400 °C. In the DTG plot, an endothermic peak noticed around the temperature of 290 °C represents the loss of crystallization of the TiO_2 powder by changing its structure from titanium hydroxide to TiO_2. γ-Al_2O_3 (before calcination) sample undergoes step by step of weight loss in three stages during the heating process. The first stage of weight loss at less than 70 °C is due to the liberation adsorbed water existing inside the powder and the second step of weight loss noticed between 70 °C and 250 °C corresponds to the evaporation of crystal water present in the powder, which is also clearly evidenced in the DTG curve around 125.5 °C. The third stage of weight loss observed from 250 °C to 550 °C is due to the dehydroxylation of the sample to γ-Al_2O_3 structural change. In the DTG graph, a peak (an endothermic) at 334 °C corresponds to the decomposition of the sample to γ-Al_2O_3 powder (Jones and Barron, 2007). The weight loss at >550 °C is negligible and therefore, the optimized calcination temperature is selected as 600 °C for the preparation of γ-Al_2O_3 membrane.

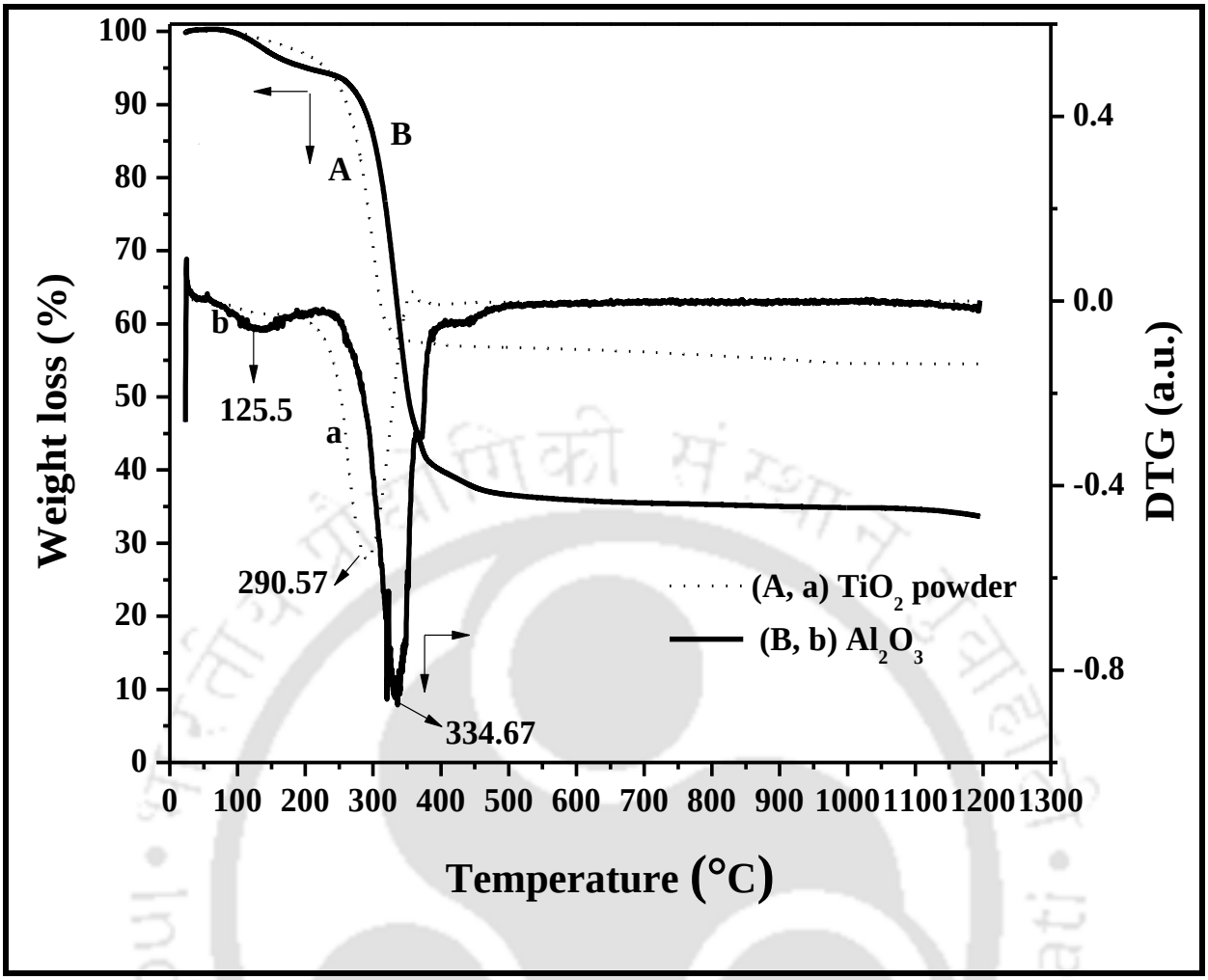

Figure 6.3: TGA and DTG curves of as synthesized (before calcination) TiO_2 (A, a), and γ-Al_2O_3 (B, b) powder

6.2.4 FTIR

FTIR spectra of Al_2O_3 and TiO_2 powders (before and after calcination) are shown in Fig. 6.4. For as-synthesized Al_2O_3 powder (before calcination), bands at 744, 628 and 1070 cm^{-1} are allotted to boehmite, and similar kind of characteristic results are reported in the literature (Majhi et al., 2009). Bending modes of Al-O-H is observed at 1070 cm^{-1} for symmetric and 1160 cm^{-1} for asymmetric (Frost et al., 1999). The OH torsional mode is not identified at 750 cm^{-1} due to overlap of stretching vibrations of Al-O with OH. The intense band at 1402 cm^{-1}

and 1722 cm^{-1} represents bending of physically presented water and the stretching mode of adsorbed water molecule can be seen at 3118 cm^{-1} (Colomban, 1988).

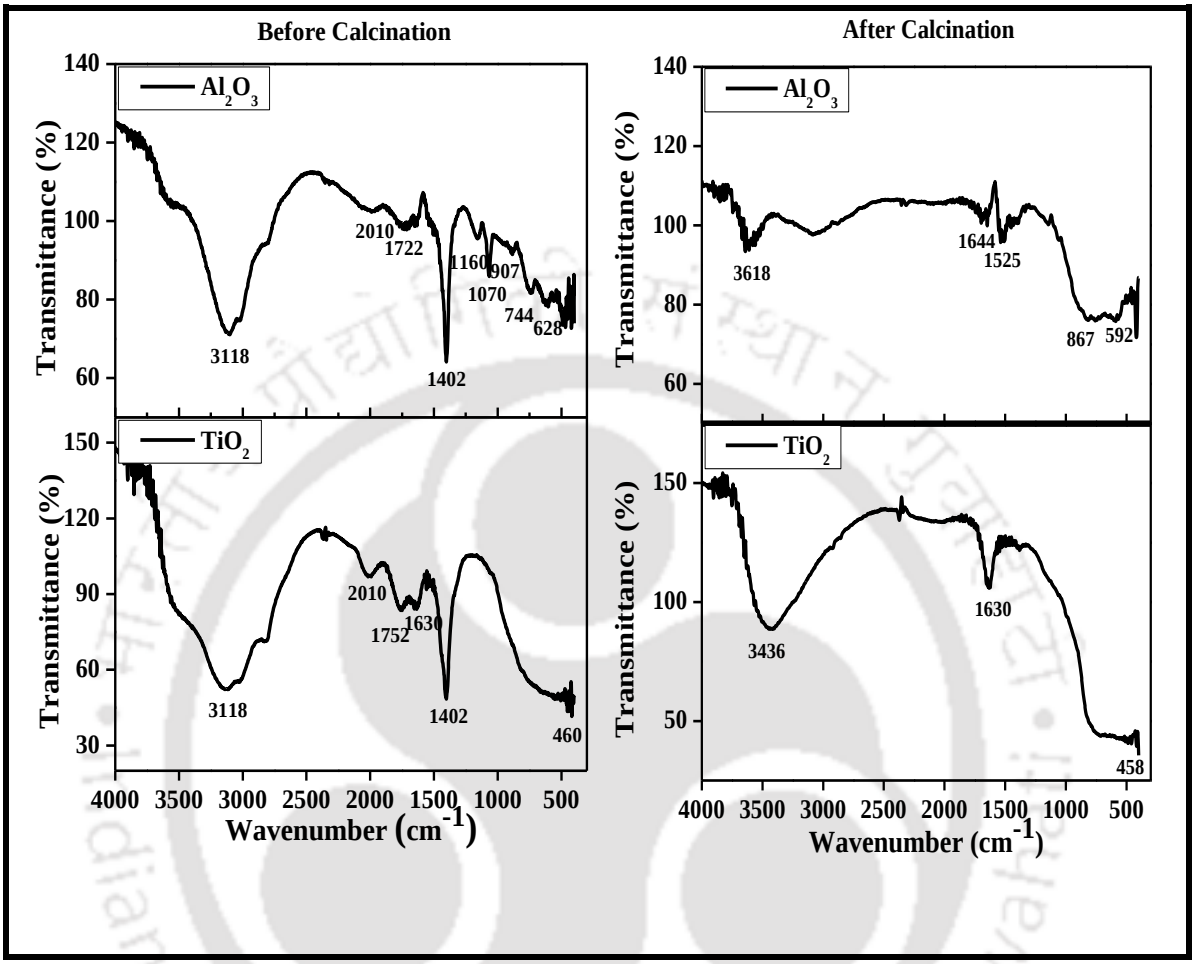

Figure 6.4: FTIR analysis of TiO_2 powder and γ-Al_2O_3 powder

The weak band observed at 2010 cm^{-1} corresponds to a combination band in boehmite, which is not observed in the calcined sample (see Fig.6.4, after calcination). In general, alumina can exhibit various kinds of coordination with an oxygen molecule from its oxides. In the as-synthesized γ-Al_2O_3 (before calcination), the bands of stretching modes for AlO_6 are observed at 744 and 628 cm^{-1} (McMillan and Piriou, 1982). After calcination of γ-Al_2O_3 sample at 600 °C, the bands at 1070 and 2010 cm^{-1} are disappeared, which confirms the formation of γ-Al_2O_3 (see Fig.4). For γ-Al_2O_3 (after calcination), the narrow bands identified

at 1644, 1525, and 3618 cm^{-1} are because of the adsorbed water present in the sample. The peaks observed at 592 and 867 cm^{-1} correspond to AlO_6 and AlO_4, respectively. The above result corroborates that γ-Al_2O_3 (Al_2O_3 after calcination sample) presents two kinds of Al-O structures i.e tetrahedral and octahedral, while γ-Al_2O_3 powder before calcination is purely octahedral in nature (Cross, 1964). In the case of TiO_2 samples, the band appeared around 460 cm^{-1} corresponds to the Ti-O stretching (Li et al., 2010). IR bands observed for sample TiO_2 (before calcination) at 1402, 1630, 1752 cm^{-1} are ascribed to stretching mode and the bands appeared at 3118, and 3436 cm^{-1} represent bending modes of a physically adsorbed water molecule. The weak band observed at 2010 cm^{-1} for TiO_2 sample (before calcination) is attributed to Ti-OH bond of the $Ti(OH)_4$ functional group, which disappears after calcination at 400 °C.

6.2.5 XRD analysis

The XRD analysis was carried out to recognize whether any phase transformation occured during the course of sintering. The XRD patterns of powders (TiO_2, and γ -Al_2O_3) and the membrane support (before and after sintering) are presented in Fig. 6.5. During sintering, phase transformations usually occur due to a series of reactions, and also caused by the formation of new phases. Prior to sintering, there are few major phases seen in the support, which are pyrophyllite, kaolin, calcium carbonate, feldspar, and quartz. Several phase changes take place within the support at the time of sintering. However, the important phase conversion is the change of kaolinite to mullite through metakaolinite. It is ensured from the XRD patterns of sintered support, in which kaolin peaks are disappeared. The consistent peaks corresponding to the quartz appear in both the support (before and after sintering). This clearly indicates that quartz is thermally stable phase. Moreover, no significant weight loss is observed for quartz in TGA analysis (Ezzati et al., 2005). During

sintering process, $CaCO_3$ is converted to CaO and CO_2, which is reflected in the XRD profile of after sintering sample. The new phase, wollastonite ($CaSiO_3$) is alse observed, that may be formed due to the reaction of amorphous silica with CaO (Gualtieri, 1995).

The XRD patterns of γ-Al_2O_3 powder (before and after calcination) are illustrated in Fig. 6.5. XRD peaks of γ-Al_2O_3 powder are well matched with JCPDS PDF (File No. 21-1307), corresponding to the boehmite powder. The diffraction analysis of Al_2O_3 powder (after calcination) is observed as γ-Al_2O_3 phase, which is concurrence with the standard γ-Al_2O_3 phase of JCPDS PDF (File No. 10-0425). The presence of (311), (400), (440) peaks in the calcined sample of Al_2O_3 confirm the existence of γ-Al_2O_3 nanocrystallites (Liu et al., 2008). In order to determine the crystallite size of γ-Al_2O_3 powder samples (before and after calcination), three measurements were carried out for each sample synthesized in a single batch and the average value was reported with standard deviation. The crystaline size of γ-Al_2O_3 (after calcination) from (400) peak is found to be 3.5±1.03 nm, while the crystalline size of before calcination sample is 2.3±0.92 nm, which is obtained from (020) peak. These values reveal the existence of nano γ-Al_2O_3 phase (Padmaja, 2004). The XRD patterns of TiO_2 powder (before and after calcination) are also shown in Fig. 6.5. After calcination, XRD peaks of TiO_2 sample such as (101), (004), (020), (015), (024) match with JCPDS PDF File No. 21-1272 for anatase. This reveals the formation of the nano-TiO_2 powder (Wang et al., 2010).

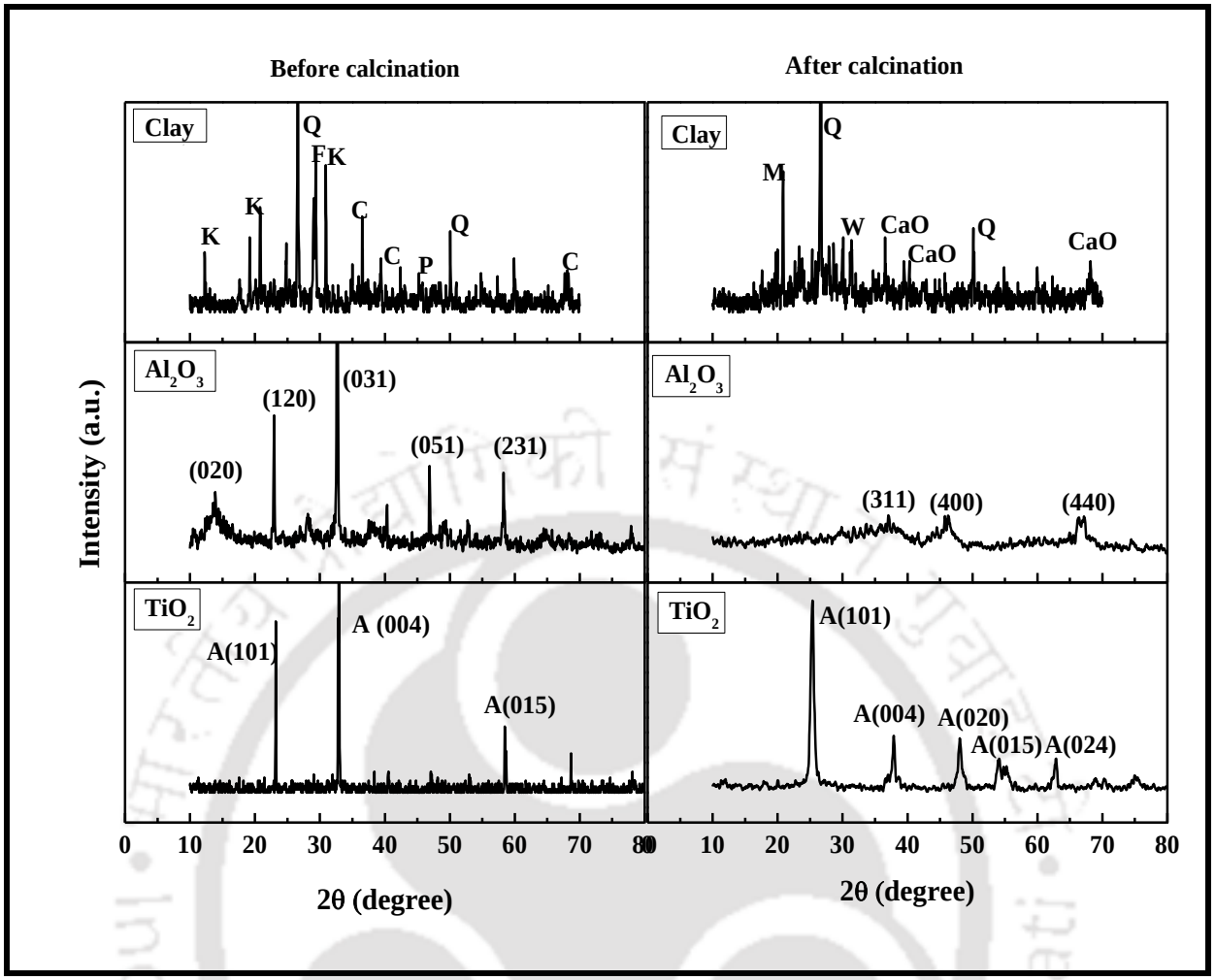

Figure 6.5: XRD profiles of the clay, TiO_2, and Al_2O_3 powders before and after calcination (P-Pyrophyllite, M-Mullite, C-Calcium carbonate, F-Feldspar, CaO-Calcium oxide, W-Wollastonite, K-Kaolin and A-Anatase)

6.2.6 Porosity

For every membrane, five experiments were conducted using same composition membranes prepared at different batches and the average value was reported with standard error. The porosity of the clay, TiO_2–clay and γ-Al_2O_3–clay membranes is found to be 45.57±0.65, 43.32±0.35 and 42.29±0.62%, respectively. These results elucidate that there is no significant difference in the porosity of the membranes. However, there is a variation between clay and

composite membranes, which is due to the formation of TiO_2 and γ-Al_2O_3 layers on the clay membrane.

6.2.7 FESEM images of the membrane

FESEM images of clay and composite membranes were depicted in Fig. 6.6 (a-c). It is clearly visible that surface of clay membrane is coated with TiO_2 and γ-Al_2O_3 particles. The rough morphology resembles that there are no cracks and pin holes on the surface. In the images, TiO_2 nanoparticles deposited on the clay membrane are shown in a circle symbol with arrow mark and γ-Al_2O_3 layers are shown in rectangular symbol with arrow mark. Images with different magnifications display uniform coating of TiO_2 and γ-Al_2O_3 on the clay membrane. These layers change the surface character of the clay membrane from hydrophobic to hydrophilic nature. Therefore, it is useful to separate oil from oily wastewater. The hydrophilic membrane surface contributes to repel oil droplets from adhering to the membrane surface, thus reduces the membrane fouling.

The pore size distribution of membranes was estimated from FESEM images using ImageJ software (http:// rsbweb.nih.gov/ij/download.html) and the obtained results are presented in the Fig. 6.7. It is apparent from Fig. 6.7 that the clay and composite membranes have different porous structure with pore sizes ranging between 0.001 and 2.75 μm. From these pore size distributions, the average pore diameter of the clay, TiO_2-clay and γ-Al_2O_3-clay membranes is estimated to be 1.01±0.036, 0.98±0.021 and 0.97±0.017 μm, respectively.

Pore size of the clay and composite membranes was also determined by N_2 gas permeation study. Fig. 6.8 depicts the effective permeability factor versus average pressure for clay and composite membranes. The smallest pore size and the lowest value of effective permeability factor are noticed for the TiO_2-clay membrane. The average pore size obtained from N_2 gas permeation is 0.981±0.014, 0.877±0.029 and 0.786±0.041 μm for clay, TiO_2-

clay and γ-Al_2O_3-clay membrane, respectively, whereas the mean pore size of clay, TiO_2-clay and γ-Al_2O_3-clay membrane determined from FESEM analysis is 1.01±0.036, 0.98±0.021 and 0.97±0.017 μm, respectively. The difference might be due to the fact that the FESEM analysis deals only with the surface pores of the membrane, while gas permeation study provides the size of inner pore channels (minimum passage, which is the neck of a funnel like shape, to pass through the gas) of the membrane. The decrease in pore sizes with coating of TiO_2 and γ-Al_2O_3 particles on clay membrane is observed from both N_2 gas permeation and FESEM image analysis.

Fig. 6.6 (d-f) shows the contact angle of the clay, TiO_2-clay and γ-Al_2O_3-clay membrane. Five measurements were carried out for each membrane at different locations and the average value was reported with standard error. The contact angle measurement was done to know the wettability and surface interaction of the membrane with liquid. The contact angle indicates the degree of wetting when a solid and liquid interact. A small contact angle (<< 90°) corresponds to high wettability, while a larger contact angle value (>> 90°) corresponds to low wettability. Generally, for super hydrophilic surfaces, the water contact angle (CA) is less than 0° and at this condition, the solid surface exhibits the droplet shape into flat puddle due to complete wetting of the surface. It is well documented in the literature that for super hydrophobic surfaces, water contact angles are usually greater than 150°, and it will show almost no contact between the water droplet and the solid surface (Arkles, 2006; Yuan, 2013; Adamson and Gast, 1976; Feng et al., 2002; Chinnam, 2015). The contact angle of the clay, TiO_2-clay and γ-Al_2O_3-clay membrane is found to be 77.07±2.37°, 14.57±0.54° and 19.43±1.13°, respectively. The obtained results clearly point out that the prepared TiO_2 membrane is more hydrophilic in nature. Fig. 6.6 (d-f) shows that a small contact angle is observed when the water spreads on the TiO_2 membrane, while a larger contact angle is

observed when the water spreads on the clay membrane. Moreover, the contact angle of TiO_2-clay membrane is 14.57±0.54°, indicating that the wetting of the surface is favorable, and the fluid will spread over a large area on the surface of TiO_2-clay membrane. In contrary, the contact angle of clay membrane is 77.07±2.37°, signifying that the wetting of surface of clay membrane is unfavorable. Therefore, the fluid will minimize its contact with clay membrane surface and form a compact liquid droplet. The contact angle of clay membrane is more than that of the prepared composite membranes; hence the clay membrane has less hydrophilic in nature compared to TiO_2-clay and γ-Al_2O_3-clay membranes. The hydrophilicity of the prepared membranes varies in the following trend: TiO_2-clay > γ-Al_2O_3-clay > Clay membrane.

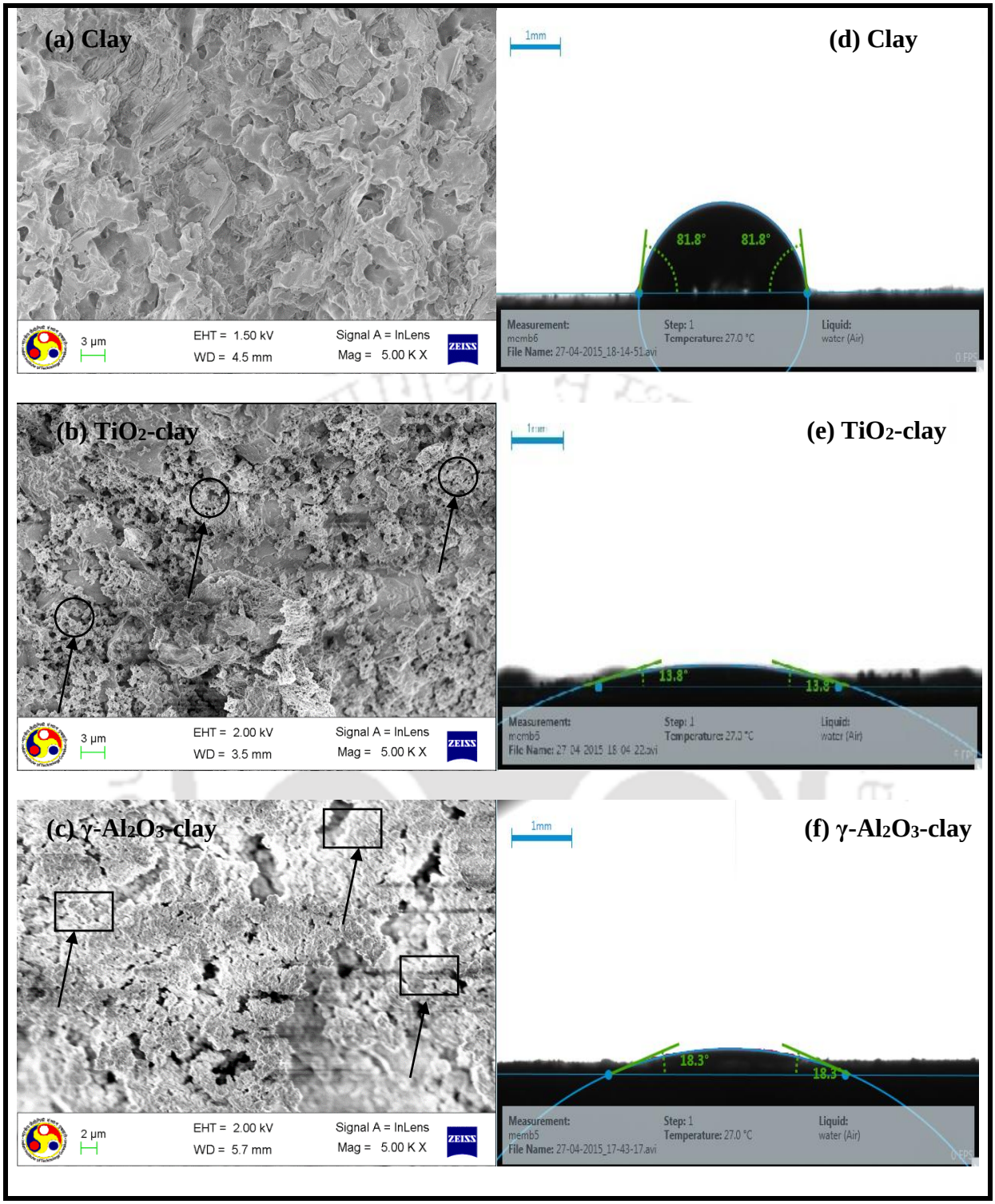

Figure 6.6: FESEM images (a,b,c) and contact angle (d,e,f) of clay, TiO_2-clay and γ-Al_2O_3-clay membrane (○-TiO_2 layer; □-γ-Al_2O_3 layer)

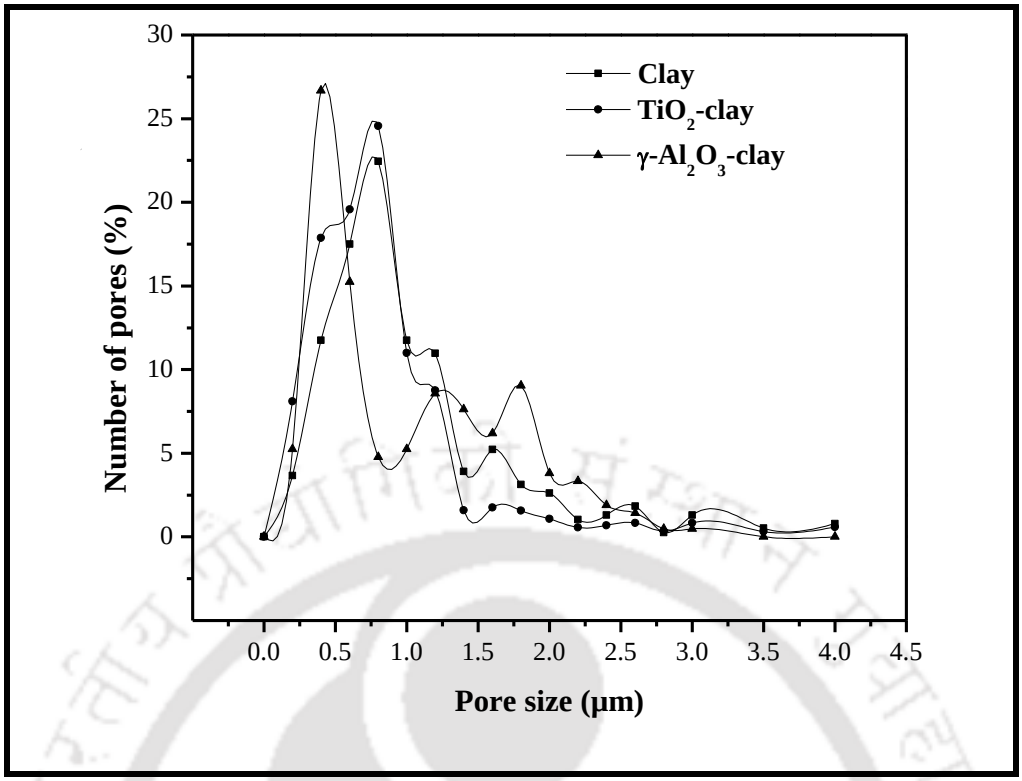

Figure 6.7: Pore size distribution of the clay and composite membranes

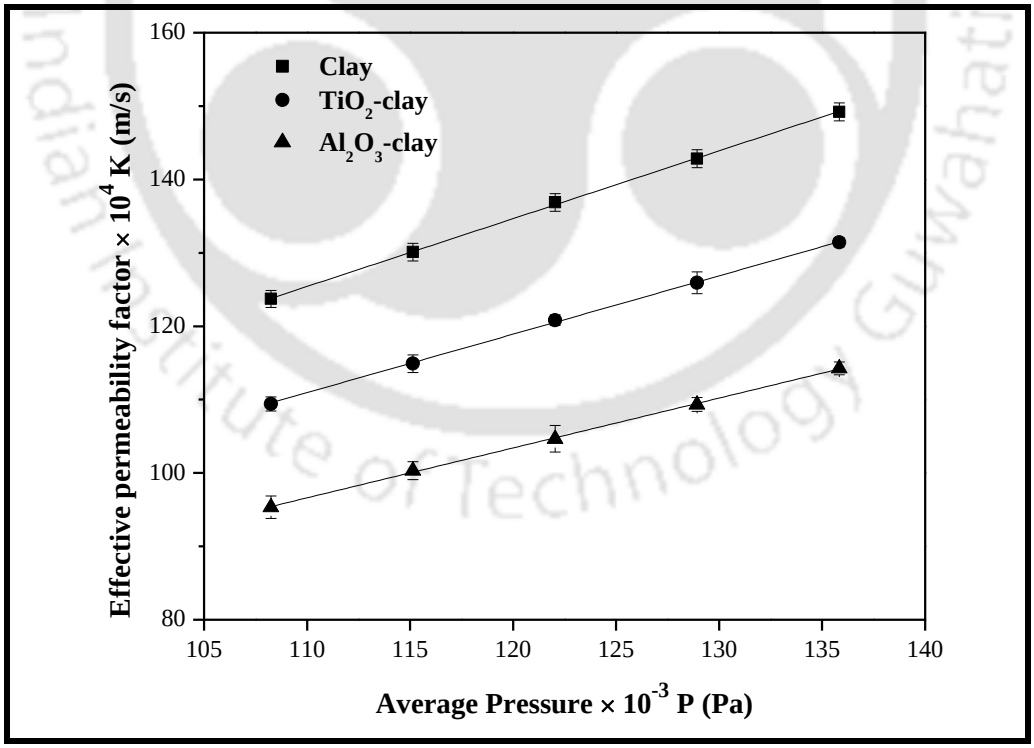

Figure 6.8: Effect of pressure on N_2 gas permeability of clay and composite membranes.

6.2.8 Water flux and hydraulic permeability

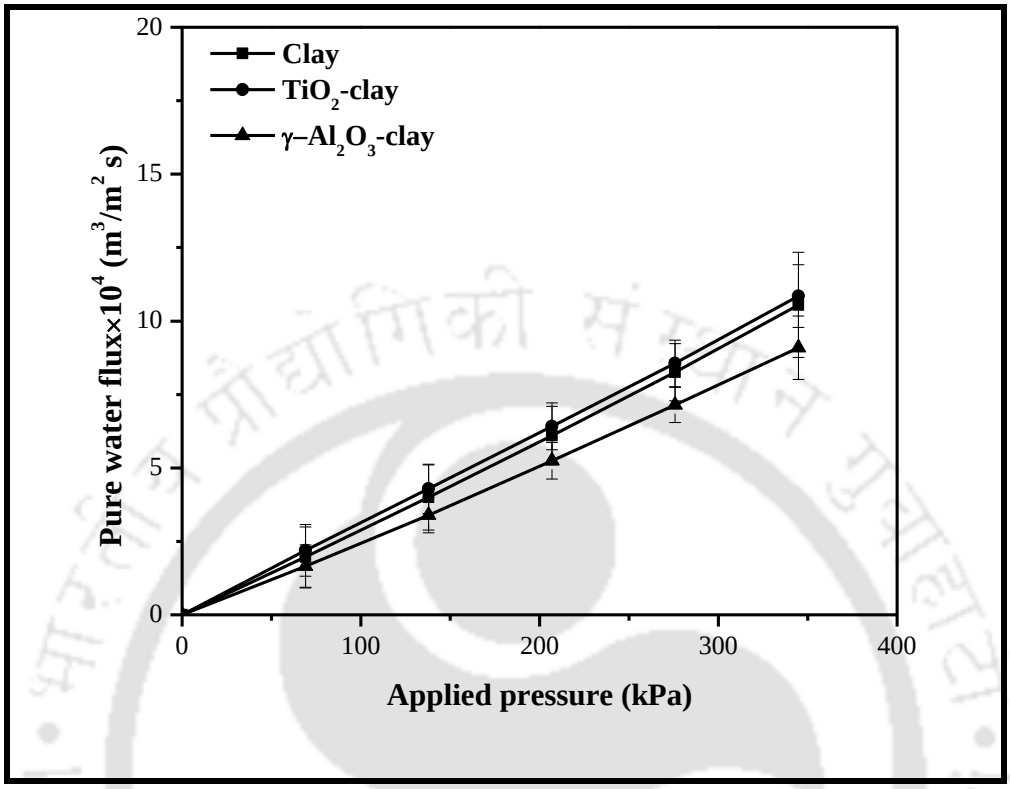

Figure 6.9: Effect of pressure on pure water flux of clay and composite membranes.

The water flux or hydraulic permeability of the membrane will depend on three factors such as hydrophilic nature of the membrane surface, pore size and porosity (Ochoa et al., 2003). Fig. 6.9 shows the effect of applied pressure on the water flux. Despite the fact that, the pure water flux of the clay and composite membranes increases proportionately with an increment in the applied pressure, which is consistent with the results obtained by Shokrkar et al., (2012). The flux of TiO_2 coated membrane is higher than that of the clay membrane. This is mostly because of changes in the hydrophilic nature of the surface of clay membrane by TiO_2 coating. Similar result was also reported in the literature (Hua et al., 2007; Zhou et al., 2010; Yan et al., 2006). TiO_2 nanoparticles coating did not decrease the water flux, but increased the hydrophilic character of the clay surface. The water flux of the TiO_2-clay membrane is

more than that of the γ-Al_2O_3-clay membrane because the hydrophilic nature of the TiO_2 coating is more than that of γ-Al_2O_3 coating and also pore size reduction is more in the γ-Al_2O_3-clay membrane. The hydraulic permeability value is estimated to be 3.12×10^{-9}, 2.59×10^{-9} and 3.003×10^{-9} (m^3/m^2 s Pa) for TiO_2-clay, γ-Al_2O_3-clay and clay membrane, respectively. It is worth to mention that the average pore diameter of the clay, TiO_2-clay and γ-Al_2O_3-clay membrane is 0.981±0.014, 0.877±0.029 and 0.786±0.041 μm, respectively, which is determined from N_2 gas permeation experiments. The variation in water permeability of the membranes is due to hydrophilic modification of the surface of the clay membrane.

6.2.9 Dead end MF of oil-in-water emulsions

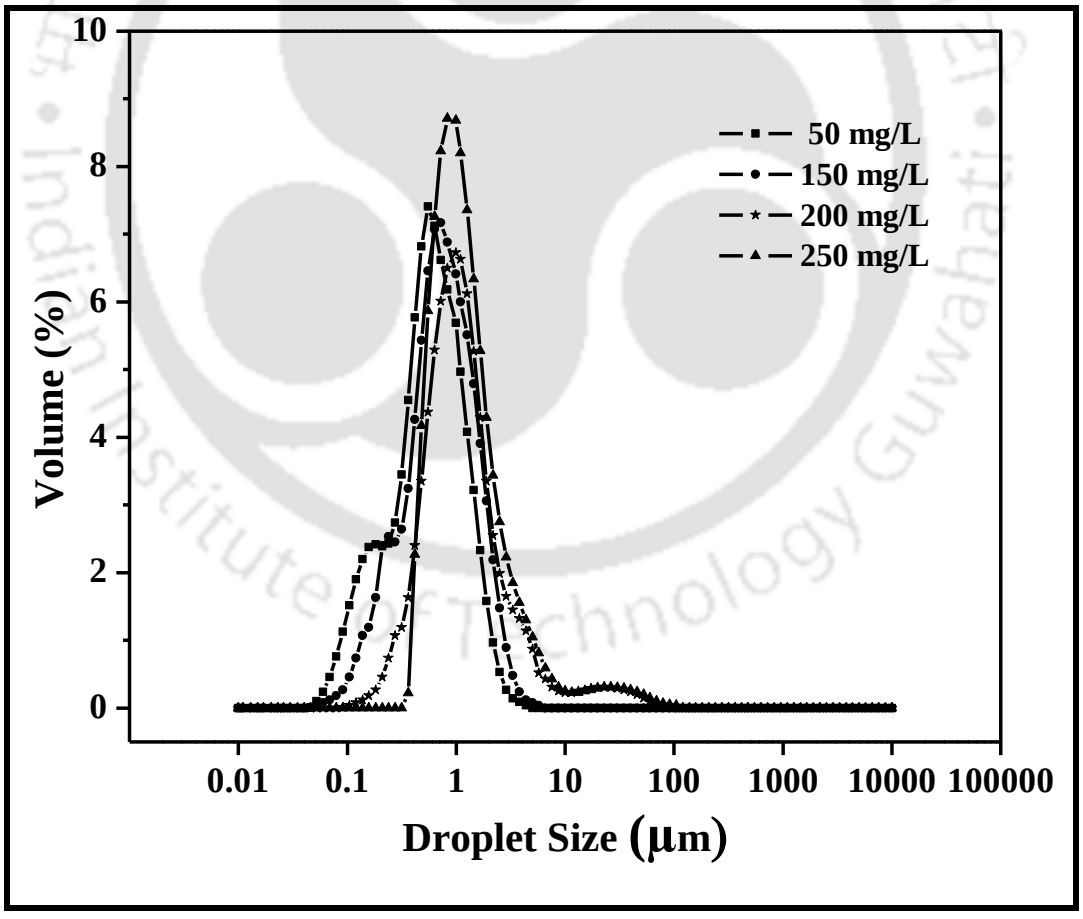

Figure 6.10: Droplet size distribution of oil-in-water emulsions

Fig. 6.10 demonstrates the droplet size distribution of oil-in-water emulsion at different feed concentrations. For all the concentrations, it can be noticed that the droplet size of emulsion varies in the range of 0.05-100 μm. The average droplet size (in diameter) of emulsion is determined as 0.771, 0.989, 6.037 and 6.928 μm of 50, 150, 200 and 250 mg/L of oil concentration, respectively.

6.2.9.1 Effect of applied pressure on oil separation

The performance of the membranes was tested at various applied pressures ranging from 69 to 345 kPa for a fixed concentration of 200 mg/L. Fig. 6.11 reveals that the rejection decreases with increasing applied pressure for all the membranes. The reason for this trend is that higher pressures facilitate the enhancement of wetting and coalescence of oil droplets by increasing forced convection. This possibly allows a few oil droplets to elapse all the way through the pores of the membrane to arrive at the permeate stream side resulting decreased rejection. This kind of results is well documented in the literature (Monash and Pugazhenthi, 2011b; Srijaroonrat et al., 1999; Salahi et al., 2010). All the membranes display around 96-99% rejection and the maximum rejection is obtained with TiO_2-clay membrane when compared to the γ-Al_2O_3-clay membrane and clay membrane.

The hydrophilic membranes show more selectivity towards water due to which the permeability of the TiO_2-clay and γ-Al_2O_3-clay membrane is found to be higher when compared with the hydrophobic clay membrane (Olegovich et al., 2013). This reveals that the hydrophilic character and nanoparticles coating on the clay membrane are responsible for both permeate flux and oil removal (%) in the treatment of oily wastewater. Among all the studied membranes, TiO_2-clay membrane is better with respect to permeate flux and rejection.

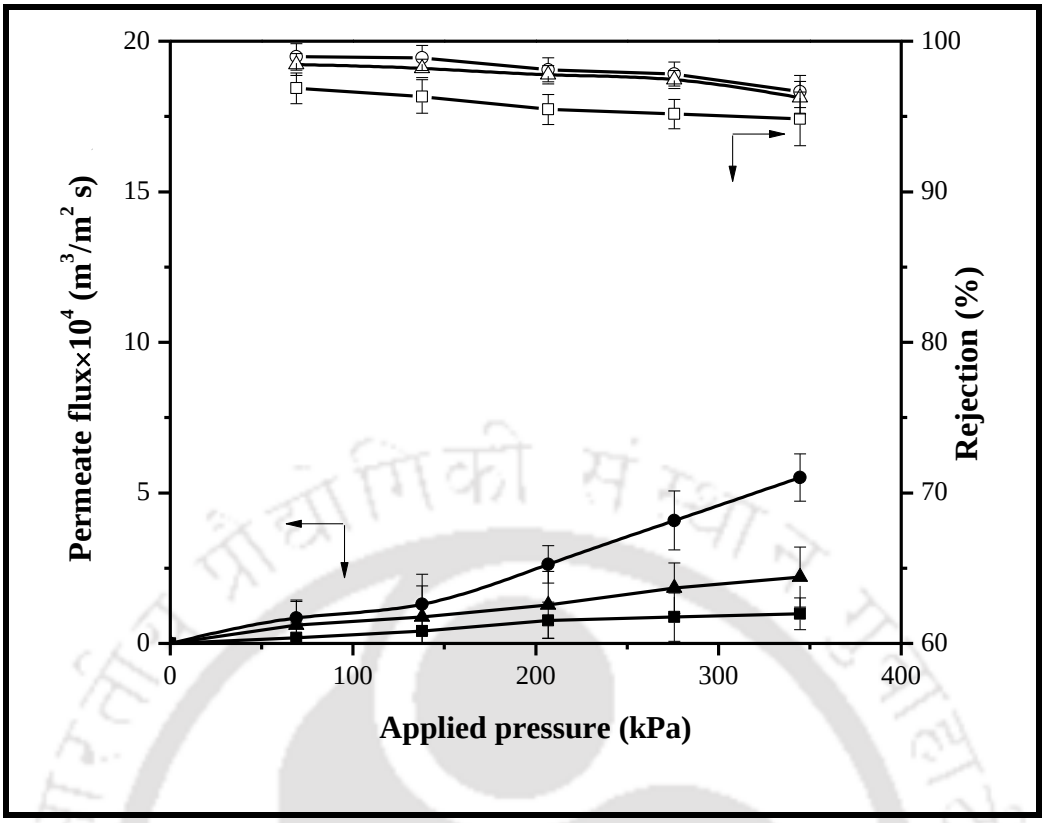

Figure 6.11: Variation of permeate flux and rejection of oil with applied pressure for clay (■, □), TiO_2–clay membrane (●, ○) and γ-Al_2O_3–clay membrane (▲, Δ)

6.2.9.2 Effect of feed concentration on oil separation

The potential of the TiO_2-clay and γ-Al_2O_3-clay membranes was investigated by treating synthetic oil-in-water emulsions with oil concentrations of 50, 150, 200 and 250 mg/L at an applied pressure of 207 kPa. Fig. 6.12 depicts the effect of oil concentration on permeate flux and rejection of the TiO_2-clay and γ-Al_2O_3-clay membranes. In general, the oil droplet size and density increase with increasing feed concentration. This is a reason for the increased rejection at a higher concentration. The droplet size of the emulsion varies between 0.05 to 100 μm for all the studied concentrations (50-250 mg/L). Then the resulted average droplet size of oil (in diameter) is determined as 0.771, 0.989, 6.037 and 6.928 μm for oil concentration of 50, 150, 200 and 250 mg/L, respectively.

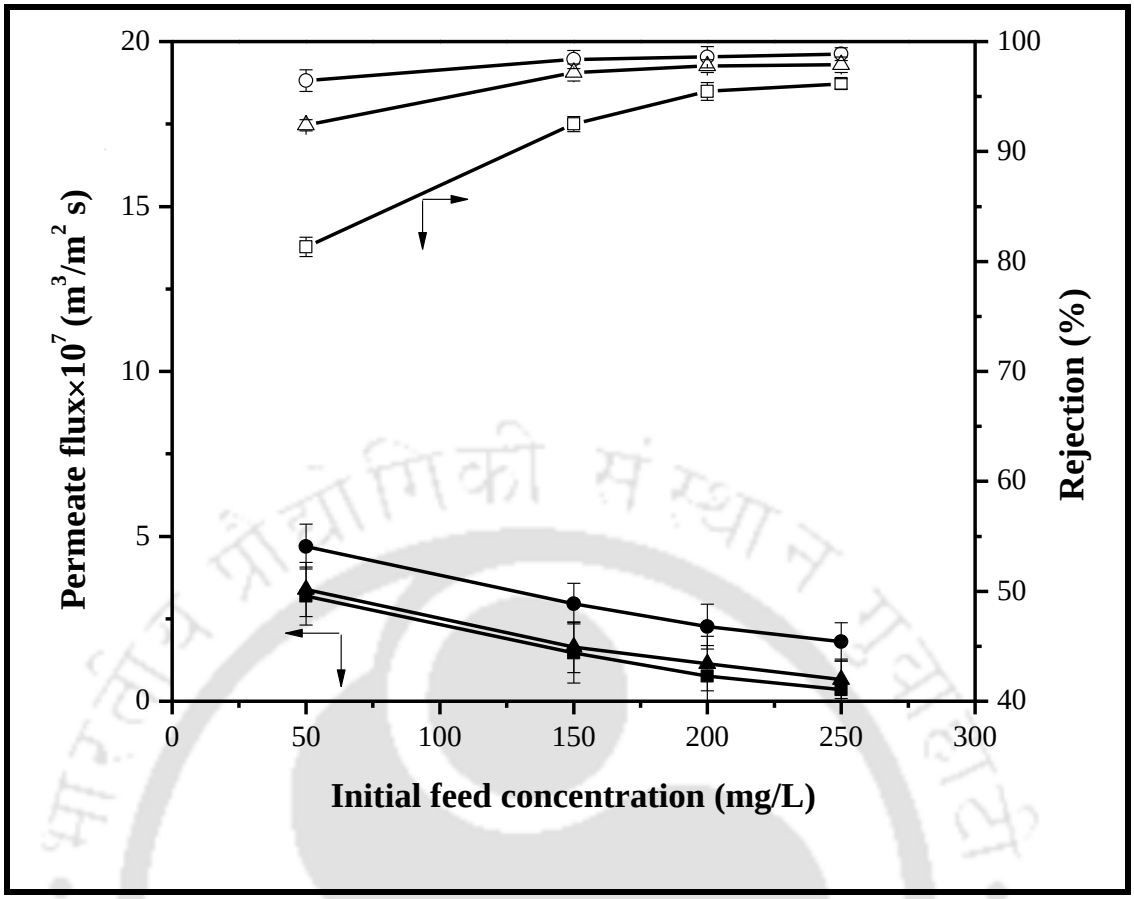

Figure 6.12: Variation of permeate flux and rejection (%) of oil with feed concentration for clay (■, □), TiO_2–clay membrane (●, ○) and γ-Al_2O_3–clay membrane (▲, Δ)

It is clear from Fig. 6.7 that the clay membrane and composite membranes have different porous structure with pore sizes ranging between 0.001 and 2.75 μm. From these pore size distributions (Fig. 6.7), the average pore diameter of the clay, TiO_2-clay and γ-Al_2O_3-clay membranes is estimated to be 1.01±0.036, 0.98±0.021 and 0.97±0.017 μm, respectively. The average pore size obtained from N_2 gas permeation is 0.981±0.014, 0.877±0.029 and 0.786±0.041 μm for clay membrane, TiO_2-clay and γ-Al_2O_3-clay membrane, respectively. The volume median diameter of the oil droplet (0.771-6.928 μm) is higher than the pore diameter of the clay membrane (0.981±0.014 μm) and composite membranes (0.877±0.029, 0.786±0.041 μm), suggesting a greater possibility for the rejection

of oil droplets. The oil droplet sizes greater than the pore sizes of the membrane are retained on the membrane surface during microfiltration of oil-in-water emulsion according to sieving mechanism. In general, the permeability depends on the pore diameter as well as surface characteristics of the membrane pores. If the membrane possesses superior percentage of pore sizes that are larger than the emulsion droplet sizes along with greater hydrophilic surface, then the membrane will display better removal efficiency with good permeate flux, which is highly essential for industrial point of view. Higher concentration of the oil leads to coalescence of the oil droplets forming a bigger droplet that result in a higher rejection. When oil concentration increases from 50 to 250 mg/L, the permeate flux decreases because the size of oil droplet is higher than the pore diameter of the membranes at higher concentrations. Also, this may be due to the pore blocking mechanism of oil with the membrane (Mittal et al, 2011; Vasanth et al., 2013). For hydrophilic membranes, the bond between the oil droplets and membrane surface is weak and can be broken easily because of hydrophilic nature of the membrane surface. Therefore, the oil rejection and flux of the TiO_2-clay and γ-Al_2O_3-clay membranes are higher than that of the clay membrane having a hydrophobic surface (Abbasi et al., 2010).

The performance of the TiO_2-clay membrane (98.95% of oil rejection as well as 8.481×10^{-5} m^3/m^2 s of permeate flux for the feed oil concentration of 200 mg/L at 69 kPa) and γ-Al_2O_3-clay membrane (oil rejection of 98.46 % with permeate flux of 6.1185×10^{-5} m^3/m^2 s for the feed oil concentration of 200 mg/L at an applied pressure of 69 kPa) is comparable with the available literature data (Vasanth et al., 2013). A clay based ceramic membrane developed by Vasanth et al., (2013) showed about 96% rejection with permeate flux of 0.006×10^{-5} m^3/m^2 s for the feed oil concentration of 200 mg/L at an applied pressure of 69 kPa. A maximum oil removal of 92.54% was obtained using cellulose acetate membrane having pore size of 0.028 µm at an applied pressure of 138 kPa for the oil-in-water

emulsion concentration of 200 mg/L (Mittal et al., 2011). In the work reported by Singh et al., (2011), the polyamide membrane with the mean pore size of 1.116 µm displayed ~ 97.80% removal efficiency of oil with permeate flux of 0.0335×10^{-4} m^3/m^2 s. Salahi et al., (2010) investigated the ability of the polysulfone membrane (with an average pore diameter of 0.1 µm) to remove oil from oil-in-water emulsion (200 mg/L) and the membrane demonstrated about 95% oil rejection. Till date, only few researchers have investigated upon the performance of ceramic membrane technology for the separation of oil from its emulsions. A critical analysis of the available literature provides several insights. Firstly, the literature is highly focused towards higher concentration oil-in-water emulsions treatment applications but not lower concentration, which are also important from the perspective of industrial waste disposal. Therefore, low cost ceramic membrane technology might be promising in such scenarios. Cui et al., (2008) studied upon the efficacy of α-Al_2O_3 membrane with pore size of 1.2 µm for oil-in-water emulsion applications. They presented a detailed investigation with respect to oil removal from oil-in-water emulsions (100 mg/L) at applied pressure of 100 kPa. Then they achieved 98.80% of oil rejection with 0.1667×10^{-4} m^3/m^2 s of permeate flux. The research work of Song et al., (2006) has proven that coal membrane with a pore size 1 µm was also efficient for treatment of 120 mg/L feed oil at an applied pressure of 100 kPa. The permeate flux of 0.1786×10^{-4} m^3/m^2 s and oil removal of 97.80% were observed. In work of chakrabarty et al., (2008), the polysulfone membrane (average pore size 0.00362 µm) displayed oil separation efficiency was 97.57% and permeate flux of 0.2399×10^{-4} m^3/m^2 s for a feed oil concentration of 100 mg/L and applied pressure of 69 kPa.

A vital concern of the fabricated ceramic membranes is to achieve 100% separation efficiency with good flux, which is very much dependent on pore size distributions,

morphologies, surface characteristics (hydrophilic/hydrophobic) and feed concentration of the oil-in-water emulsions. Thus, it is apparent that significant amount of research activity needs to be dovetailed towards the development and application of ceramic membranes for oil-in-water emulsion filtration applications. In view of this, a systematic investigation that accounts for the modification of surface characteristics of the membrane to suite the desired application is very important.

The resistances of different membranes to survive in severe ecological surroundings and possessing extensive serviceable life are of important task. In this context, clay based membrane is unique choice that can be used for many industrial applications, since it was tested and justified to have a superior serviceable life and endurance for the treatment of wastewater. However for comparable view point, it can be noticed that the highest oil removal ability of fly ash membrane recorded by Fang et al., (2013) was 95.30% with permeate flux of 0.4417×10^{-4} m^3/m^2 s, which is very low. Therefore, this effort involved to concentrate on productive and economical manufacturing methods as well as coating materials to attain excellent quality of membrane, which can provide better separation efficiency and superior permeate flux than the published data are highly valuable.

It can be concluded that the studied membranes demonstrate better performance on the basis of rejection and flux as compared to other membranes listed in literature. Table 6.1 summarizes the comparison of present membrane performance for the separation of oil from the oil-in-water emulsions with the data available for different membranes listed in the literature (Cui et al., 2008; Monash and Pugazhenthi, 2011; Adamson and Gast, 1976; Suresh and Pugazhenthi, 2016; Ochoa et al., 2003; Shokrkar et al., 2012; Yan et al., 2006; Srijaroonrat et al., 1999; Salahi et al., 2010; Olegovich et al., 2013; Abbasi et al., 2010). It can be observed that the rejection values of the membranes are comparable with those

membranes reported in the literature. In comparison with clay membrane, TiO_2-clay and Al_2O_3-clay membranes display the highest oil removal efficiency along with good flux owing to the enhanced hydrophilic characteristics of the surface modified membrane. Amongst the available data, the result obtained for the TiO_2-clay membrane is the finest in terms of superior permeate flux (0.8481×10^{-4} m^3/m^2 s) and maximum oil rejection (98.96%) for the feed oil concentration of 200 mg/L at an applied pressure of 69 kPa. The membrane performance ability is estimated on the basis of it's permeate flux and rejection values, which are found to be acceptable range and hence, the fabricated composite membranes are opined to be chosen for more efficient in separation of oil from oil-in-water emulsions.

Table 6.1: Comparison of membrane performance with other reported membranes

Membrane materials	Average pore size (μm)	Type of oil	Applied pressure (kPa)	Feed oil concentration (mg/L)	Permeate flux×10^4 (m^3/m^2 s)	Oil rejection (%)	Author
Clay materials	1.21	Crude oil	69	200	0.0006	96.00	Vasanth et al., (2013a)
Cellulose Acetate	0.028	Crude oil	138	200	0.389	92.54	Mittal et al., (2011)
Clay materials	0.98	Crude oil	345.4	200	0.7978	96.00	Monash and Pugazhenthi, (2011b)
Polyamide	1.16	Crude oil	207	192	0.0335	97.80	Singh et al., (2011)
Clay materials	0.285	Crude oil	69	125	0.054	98.40	Nandi et al., (2009)
Clay materials	1.3	Crude oil	276.4	125	6.1084	85.00	Vasanth et al., (2011b)
Coal	1	Crude oil	100	120	0.1786	97.80	Song et al., (2006)
NaA1/α-Al_2O_3	1.2	Lubricant oil	100	100	0.1667	98.80	Cui et al., (2008)
Polysulfone	0.00362	Crude oil	69	100	0.2399	97.57	Chakrabarty et al. (2008)
Clay materials	1.06	Crude oil	207	100	0.554	87.00	Vasanth et al., (2013b)
Polysulfone	0.1	Gas-oil	300	78	0.2111	95.00	Salahi et al., (2010)
Fly ash	0.77	Crude oil	100	75	0.4417	95.30	Fang et al., (2013)
α-Al_2O_3	0.2	Refinery oil	125	26	0.6944	84.61	Abadi et al., (2011)
TiO_2-clay	0.98	Crude oil	69	200	0.8481	98.96	Present work
γ-Al_2O_3-clay	0.97	Crude oil	69	200	0.6119	98.46	Present work

6.3 Summary

Clay based ceramic membrane has been successfully fabricated by a uniaxial pressing method and sintered at 950 ^{o}C. TiO_2-clay and γ-Al_2O_3-clay composite membranes were fabricated using inexpensive titanium tetrachloride and aluminium chloride as source material, respectively. Hydrothermal method was adopted to coat the TiO_2 and γ-Al_2O_3 nanoparticles on the clay membrane and modified the surface character of the clay membrane from hydrophobic to hydrophilic. The porosity of clay, TiO_2-clay and γ-Al_2O_3-clay membranes is found to be 45.57±0.65, 43.32±0.35 and 42.29±0.62%, respectively. The average pore diameter of the clay, TiO_2-clay and γ-Al_2O_3-clay membranes is estimated to be 0.981±0.014, 0.877±0.029, 0.786±0.041 µm, respectively. The above prepared TiO_2-clay and γ-Al_2O_3-clay membranes show better rejection and permeate flux in separation of oil-in-water emulsions than that of the clay membrane.

भारतीय प्रौद्योगिकी संस्थान गुवाहाटी
Indian Institute of Technology Guwahati

CHAPTER-7

Cross Flow Microfiltration Studies for TiO_2-clay and Clay membranes

भारतीय प्रौद्योगिकी संस्थान गुवाहाटी
Indian Institute of Technology Guwahati

CHAPTER 7 Cross flow microfiltration studies for TiO_2-clay and clay membranes

After a brief overview of cross flow MF of oil-in-water emulsion with TiO_2-clay and clay membranes in section 7.1, Section 7.2 summarizes the flux profiles and fouling analysis using the pore blocking models. Finally, section 7.3 presents a summary of the cross flow microfiltration data.

7.1 Overview

This chapter presents studies upon the application of prepared TiO_2-clay composite membrane for the treatment of oil-in-water emulsions. Synthetic oil-in-water emulsions were subjected to microfiltration in cross flow mode of operation. The aim of these experiments was to evaluate the effect of applied pressure as well as cross flow velocity on the permeate flux and oil rejection of both clay and TiO_2-clay composite membrane. Subsequently, the fouling analysis was done using different pore blocking models such as standard pore blocking, complete pore blocking, intermediate pore blocking and cake filtration to gain insights into the nature of membrane fouling during permeation studies.

7.2 Results and discussion

7.2.1 Determination of pure water flux in cross flow mode

Both clay and TiO_2–clay membrane were subjected to evaluate their pure water permeate flux in cross flow mode. The permeated pure water flux was calculated at different applied pressures (69-207 kPa) with cross flow velocity of 0.0885 m/s for 30 min. Fig. 7.1 depicts the effect of applied pressure on the water flux of clay and TiO_2–clay membrane. As can be seen, the flux increases linearly with an increase in the applied pressure, which is due to an

enhancement of driving force with increasing pressure. The variation in pure water flux depends on physical properties of the membrane, such as hydrophilic nature of the membrane surface, pore size and porosity (Shokrkar et al., 2012; Ochoa, 2003). The water flux of the TiO_2–clay membrane is more than that of clay membrane, which is due to modification of the surface of the clay membrane from hydrophobic to hydrophilic by TiO_2 coating. Similar observations were also reported in literature for TiO_2-Al_2O_3 and Al_2O_3-PVDF composite membranes (Chang et al., 2014; Yan et al., 2006).

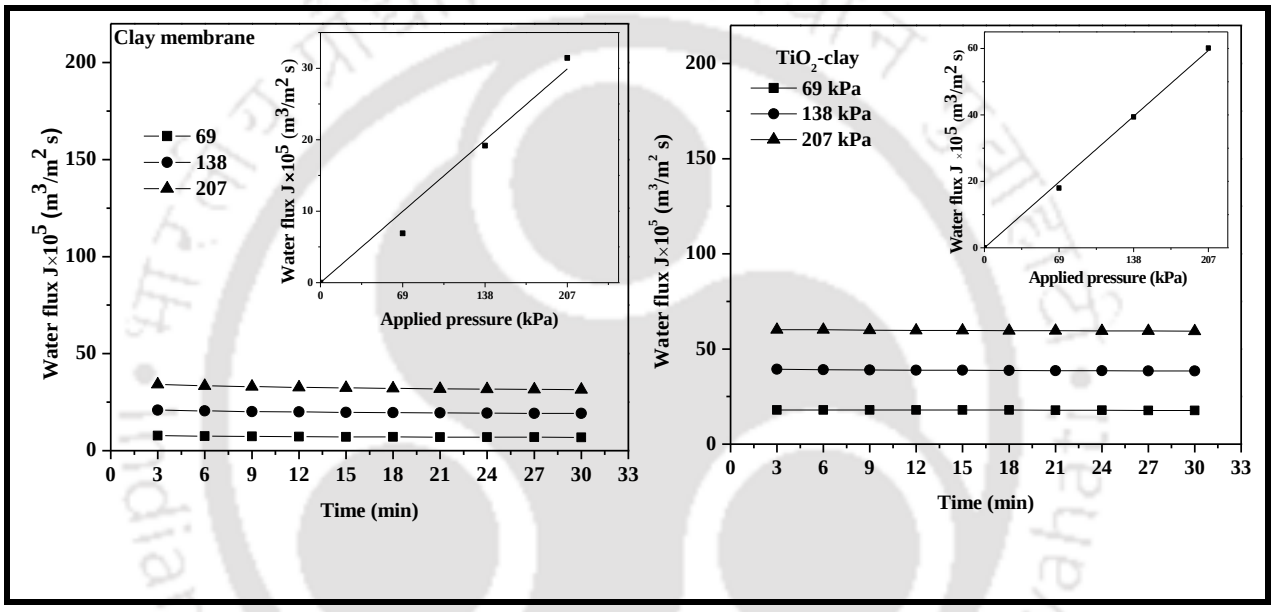

Figure 7.1: Variation of pure water flux of clay and TiO_2-clay membrane in cross flow mode with applied pressures (69-207 kPa) at cross flow velocity of 0.0885 m/s

In the work of Yan et al., (2006), the modified PVDF membrane demonstrated superior water flux (123.547 L/m^2 h at 0.1 MPa) than that of unmodified membrane (31.9767 L/m^2 h at 0.1 MPa). It is apparent that the coating of TiO_2 nanoparticles on the support does not reduce the water flux but increased the hydrophilic character of the surface of the clay membrane. This hydrophilic nature contributes to increase the flux of the composite membrane as compared to clay membrane. This type of TiO_2–clay membrane with high water flux is quite useful for industrial applications (Zhou et al., 2009). It is worth to mention that there is a difference in

the average pore size of the clay and composite membrane as evidenced from N_2 gas permeation analysis, however, an increment in the water flux is due to the hydrophilic nature of the membrane.

7.2.2 Cross- flow microfiltration of oil-in-water emulsions

Oil-in-water emulsion with concentration of 200 mg/L was prepared and utilized for microfiltration experiments. The droplet size of emulsion is in the ranges of 0.05 - 100 µm for the concentration of 200 mg/L and the average diameter of droplet is found to be 6.928 µm. The separation potential of the clay and TiO_2-clay membrane was tested with the oil-in-water emulsion concentration of 200 mg/L at various applied pressures ranging between 69 and 207 kPa and different cross flow velocities in the ranges of 0.0885-0.1769 m/s.

The variations of the permeate flux of clay membrane and TiO_2-clay membrane with time for three different applied pressures and three cross flow velocities (0.0885-0.1769 m/s) are shown in Figs. 7.2 and 7.3, respectively. The transport resistance, which arises as a result of concentration polarization and adsorption, leads to the decline of permeate flux with an increment in filtration time. The membrane fouling arises due to the thin layer of oil which sticks to the surface of the membrane. The rate of flux decline is comparatively slow, due to the fact that slow concentration polarization influences the rejection during the process. The permeate flux increases with increasing applied pressure, which is due to an enhancement of the driving force across the membrane with increasing pressure.

At higher pressures, the decline rate of flux is more, which can be seen in the obtained results. The reason for this trend is quick formation of oil layer over the surface, which leads to the fouling of the membrane. It is also evident from Figs. 7.2 and 7.3 that the flux decline increases with an increase in separation time, which is due to the formation of oil layer and

blocking of the membrane pores. The rate of flux decline is lower for TiO_2-clay membrane in comparison with clay membrane as evidenced from Figs. 7.2 and 7.3. This is mainly due to the hydrophilic nature of the TiO_2-clay membrane surface that prevents the oil droplets penetrating into the membrane pores. At an applied pressure of 207 kPa, the maximum permeate flux of clay membrane and TiO_2-clay membrane after 30 min of operation is found to be 8.70×10^{-5} and 18.66×10^{-5} m^3/m^2 s, respectively. This result proves the surface modification of the TiO_2-clay membrane with more hydrophilic characteristics.

The influence of cross flow velocity on permeate flux is measured by considering three different cross flow velocities viz. 0.0885, 0.1327 and 0.1769 m/s as shown in Figs. 7.2 and 7.3. It is apparent that an increase in the cross flow velocity leads to an improvement in permeates flux. An increment in the cross flow velocity reduces the concentration polarization, and also adds to enhance the shear stress on the surface of the membrane, which diminishes the profundity of the oil layer on the membrane surface. The permeate flux of clay membrane is inferior as compared to the TiO_2-clay membrane during the entire cross flow velocity investigation due to its hydrophobic nature. It is seen from this pattern that an increment in the cross flow velocity decreases the development of cake layer on the surface of the membrane. The highest permeate flux of 10.36×10^{-5} and 19.35×10^{-5} m^3/m^2 s is obtained at the beginning of the filtration process for the clay membrane and TiO_2-clay membrane, respectively, with the cross flow velocity of 0.1769 m/s and an applied pressure of 207 kPa.

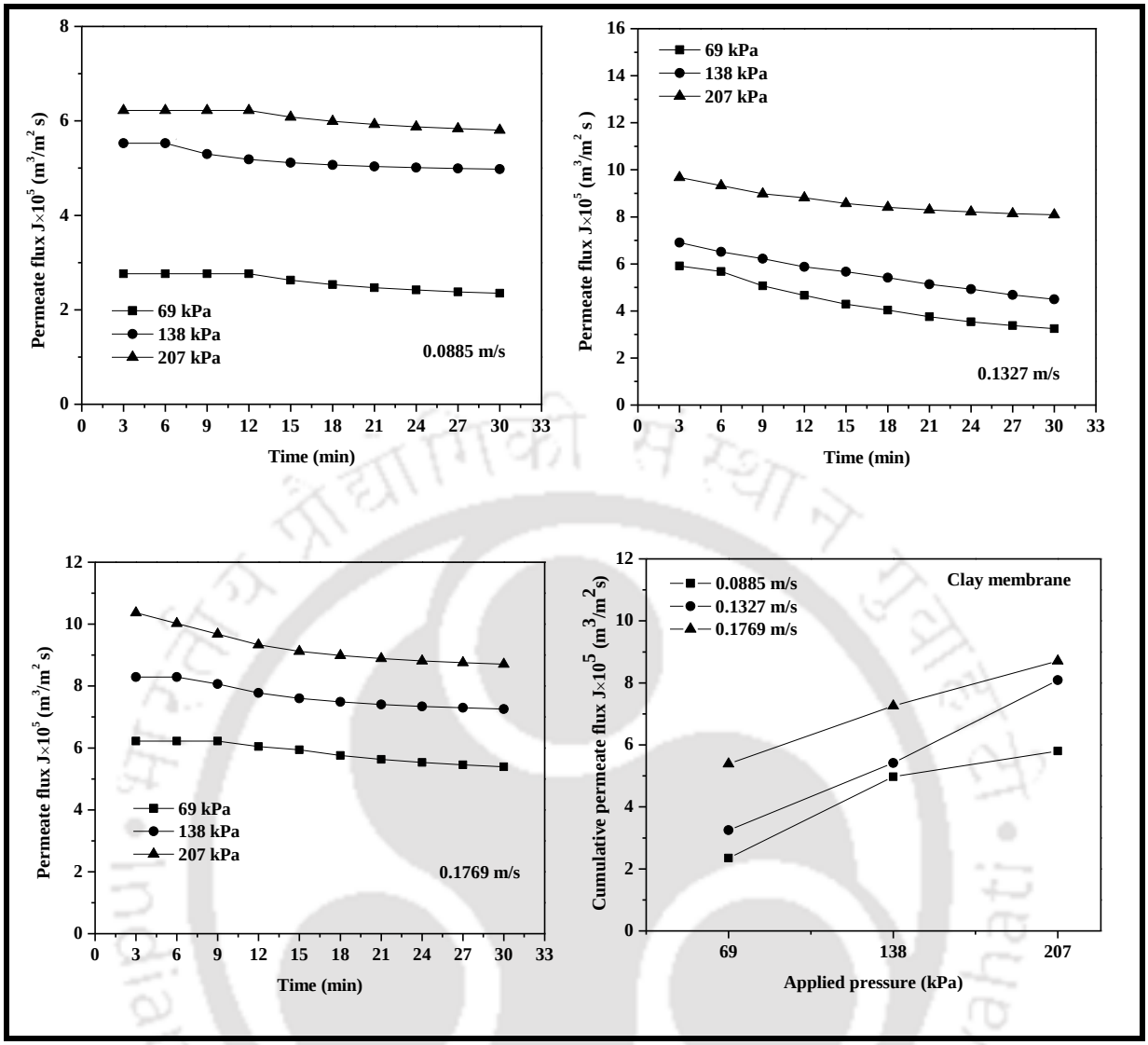

Figure 7.2: Variation of permeate flux of clay membrane at three cross flow velocities and applied pressures

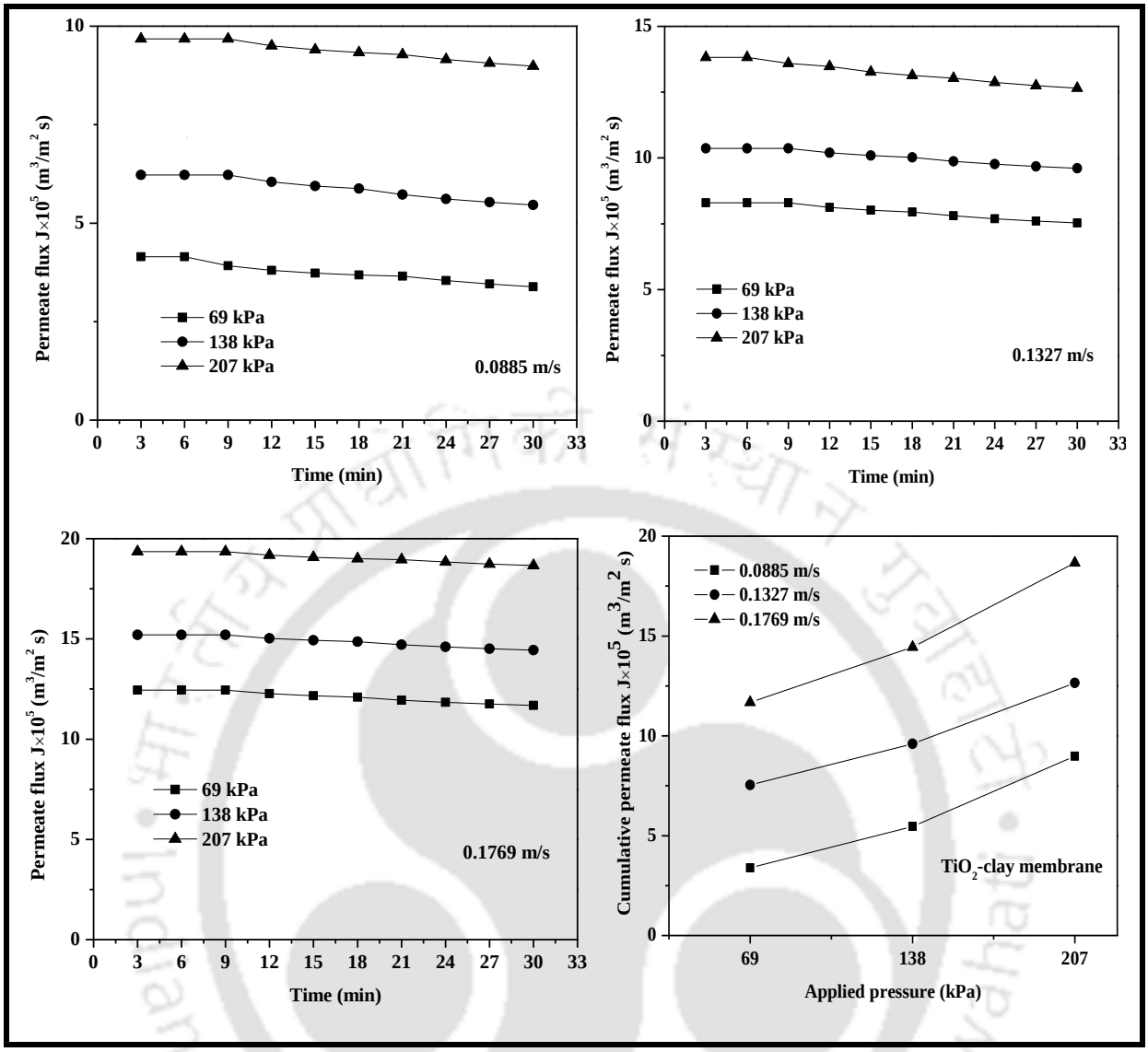

Figure 7.3: Variation of permeate flux of TiO_2–clay membrane at three cross flow velocities and applied pressures

The variation of oil rejection with increasing applied pressure is presented in Fig. 7.4. As evidenced from Fig. 7.4, the rejection of clay membrane is found to be reduced marginally with augmenting cross flow velocity. This is due to the fact that increasing cross flow velocity reduces the formation of cake layer on the surface of clay membrane. Therefore, the resistance to the permeate flow decreases. When the cross flow velocity increased, it leads to increase in the surface shear stress, which in turn caused to decrease the surface cake layer

formation. This results in the reduction of the resistance to the permeate flow. Owing to above reasons, some oil droplets pass through the pores to reach the permeate stream, which results in the decreased oil rejection. Similar observations were also reported in the literature (Monash and Pugazhenthi et al., 2011b; Chinnam et al., 2015). Additionally, a higher cross flow velocity empowers droplets of the oil to deform its shape due to flush of the feed.

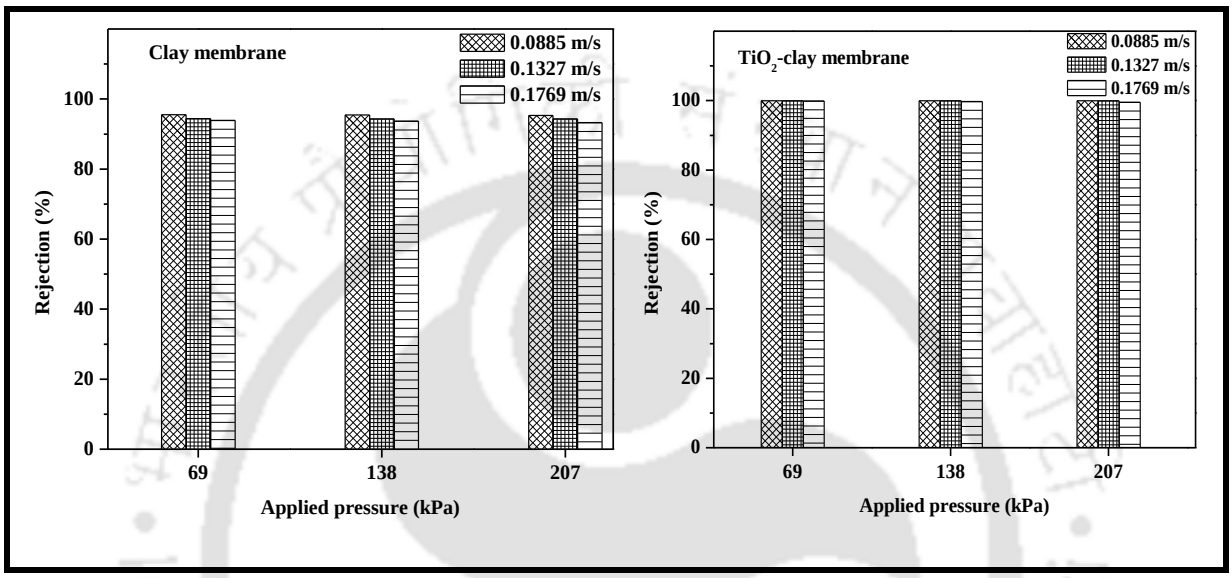

Figure 7.4: The effect of applied pressure and cross flow velocity on rejection for clay and TiO_2-clay membrane

On the other hand, no significant variation in the rejection is observed with increasing applied pressure for the TiO_2-clay membrane. This is because of the impact of higher hydrophilic nature of the surface of the TiO_2-clay membrane when compared to clay membrane. This helps to repel the oil droplets from the membrane surface (Chang et al., 2014; Salahi et al., 2010). As per the outcomes indicated in Fig. 7.4, the fabricated TiO_2-clay membrane offers better values of oil rejection. A maximum oil rejection of 99.94% is achieved at an applied pressure of 69 kPa with TiO_2 membrane. The acquired results demonstrate that the dismissal of oil relies on the pore size of the membrane and surface tendency. The hydrophilic membrane shows more selectivity towards water due to which, the permeate flux of the hydrophilic TiO_2-clay membrane is higher as compared to the

hydrophobic clay membrane (Olegovich et al., 2013). This reveals that the hydrophilic character and nanoparticles coating on the clay membrane are responsible for both improved permeate flux and rejection of oil in the treatment of oil-in-water emulsion. Extensive lab scale investigations were conducted to evaluate cross flow microfiltration of oil-in-water emulsions using clay membrane and TiO_2-clay membrane with synthetic oil-in-water emulsions. Overall summary is presented in Table 7.1.

Table 7.1 summarizes the most appropriate research findings of this work along with the few competent literature data. With careful observation of the table, the following can be outlined as the promising output of the work. It can be seen that the permeate flux and oil removal efficiency for clay membrane varied from 2.3498-8.708×10^{-5} m^3/m^2 s and 99.55-93.24%, respectively. Similarly for TiO_2-clay membrane, these parameters vary from 3.386-18.660×10^{-5} (m^3/m^2 s) and 99.94-99.56%, respectively. Thus, it is apparent that the microfiltration of oil using clay membrane provides lower permeate flux and oil removal (%) in comparison with TiO_2-clay membrane. This is due to the surface nature of the TiO_2-clay membrane and hydrophilic character influences the separation characteristics. A comparative assessment of permeate flux and oil rejection obtained for clay membrane and TiO_2-clay membrane as well as literature data is presented in Table 7.1. Various clay membranes have used for the oil removal from synthetic oil-in-water emulsions (Vasanth et al., 2013b; Nandi et al., 2010; Song et al., 2006; Cui et al., 2008; Abbasi et al., 2010; Mueller et al., 1997). Also, existing literature have focused towards the synthetic oil-in-water emulsions whose chemical constitution is simpler in comparison with the real industrial oily wastewater streams where solution chemistry is bound to be complex (Wang et al., 2008). Two important studies in the literature have elaborated upon the application of fly ash (Fang et al., 2013) and ZrO_2 membrane (Yang et al., 1998). For ZrO_2 membrane, the oil rejection (94.3%) has been

reported to have lower than that of the fly ash membrane (98.2%). This was not the case for the clay membranes. However, despite having the lower rejection (87 and 88.35%) than fly ash membrane (98.2%), clay membranes (Vasanth et al., 2013; Emani et al., 2014) were able to provide better permeate flux (55.4×10^{-6}, 44.1×10^{-6} m^3/m^2 s) than those obtained with the fly ash membrane (25.83×10^{-6} m^3/m^2 s). However, the same has not been studied for the feed oil concentration. This work summarizes the results obtained during the cross flow microfiltration of oil-in-water emulsions for various membranes. It is evident that the separation characteristics of TiO_2-clay membrane are more than those evaluated for other membranes (ZrO_2, fly ash and clay membranes). For the optimized choice of cross flow microfiltration parameters (cross flow velocity of 0.1769 m/s, applied pressure of 207 kPa and operation time of 0.5 h), the TiO_2-clay membrane provides permeate flux and oil removal efficiency of 186.60×10^{-6} m^3/m^2 s and 99.56 %, respectively for the feed oil concentration of 200 mg/L using cross flow microfiltration.

Table 7.1: Comparison study of permeate flux and rejection data of present work with other membranes published in literature for separation of oil-in-water emulsion.

Material	Pore size (μm)	Type of oil	Oil Conc. (mg/L)	Pressure (kPa)	Cross flow velocity (m/s)	Time (h)	Permeate flux×10^6 (m^3/m^2 s)	Oil Rejection (%)	Author
Carbon membrane	1.0	Crude oil	120	100	0.1	1.67	17.86	97.8	Song et al., (2006)
NaAl/α-Al_2O_3	1.20	Lubricant oil	100	100	0.01	10	16.67	98.8	Cui et al., (2008)
Mullite membrane	0.289	Condensate gas (C_8-C_{12})	1000	300	1	2	11.11	94	Abbasi et al., (2010)
Kaolin, quartz, etc.	0.285	Crude oil	125	69	-	1	5.40	98.4	Nandi et al., (2010)
α-Al_2O_3 membrane	0.80	Crude oil	250	69	0.24	2	8.33	99.9	Mueller et al., (1997)
ZrO_2/α-Al_2O_3	1.0	Vegetable oil	5500	100	3-5	4	7.50	94.3	Yang et al., (1998)
α-Al_2O_3 membrane	0.20	Refinery oil	141	125	2.25	1.5	80.55	97.8	Abadi et al., (2011)
Fly ash membrane	0.77	Crude oil	2000	100	4	10	25.83	98.2	Fang et al., (2013)
Clay membrane	3.06	Crude oil	400	207	0.2688	0.5	44.1	88.35	Emani et al., (2014)
Clay membrane	1.06	Crude oil	100	207	13.9×10^{-7} (m^3/s)	1	55.4	87	Vasanth et al., (2013)
Clay membrane	1.00	Crude oil	200	207	0.1769	0.5	87.08	93.24	This work
TiO_2–clay	0.9	Crude oil	200	207	0.1769	0.5	186.60	99.56	This work

7.2.3 Analysis of fouling

Four distinctive filtration models were utilized to study the flux decline of clay membrane and TiO_2-clay composite membrane in the cross flow microfiltration of oil-in-water emulsions. These models were fitted utilizing the filtration data obtained from clay membrane and TiO_2-clay membrane. Fig. 7.5 displays the correlation of the distinctive pore blocking models for clay membrane and TiO_2-clay membrane at three applied pressures (69-207 kPa) and a constant cross flow velocity of 0.0885 m/s. As evidenced, the cake filtration model furnishes great concurrence with experimental results at all applied pressures when contrasted with alternate models for clay membrane. In the case of TiO_2-clay membrane, it is observed that the cake filtration model is well fitted at lower pressure, while at higher applied pressures, complete pore blocking model provides good agreement with experimental values.

The model parameters, for example, permeate flux values (J_0 at t=0), slope, correlation coefficient (R^2) obtained with various models for clay membrane and TiO_2-clay composite membrane are presented in Table 7.2. It is noteworthy to mention that the cake filtration model offers the highest R^2 value for ceramic support at all applied pressure. In case of TiO_2-clay membrane, the cake filtration model provides the highest R^2 value at lower pressure, and the complete pore blocking model gives the best R^2 value with increasing pressure. In this manner, it can be presumed that the cake filtration model depicts well the fouling mechanism for clay membrane and complete pore blocking model for TiO_2-clay membrane.

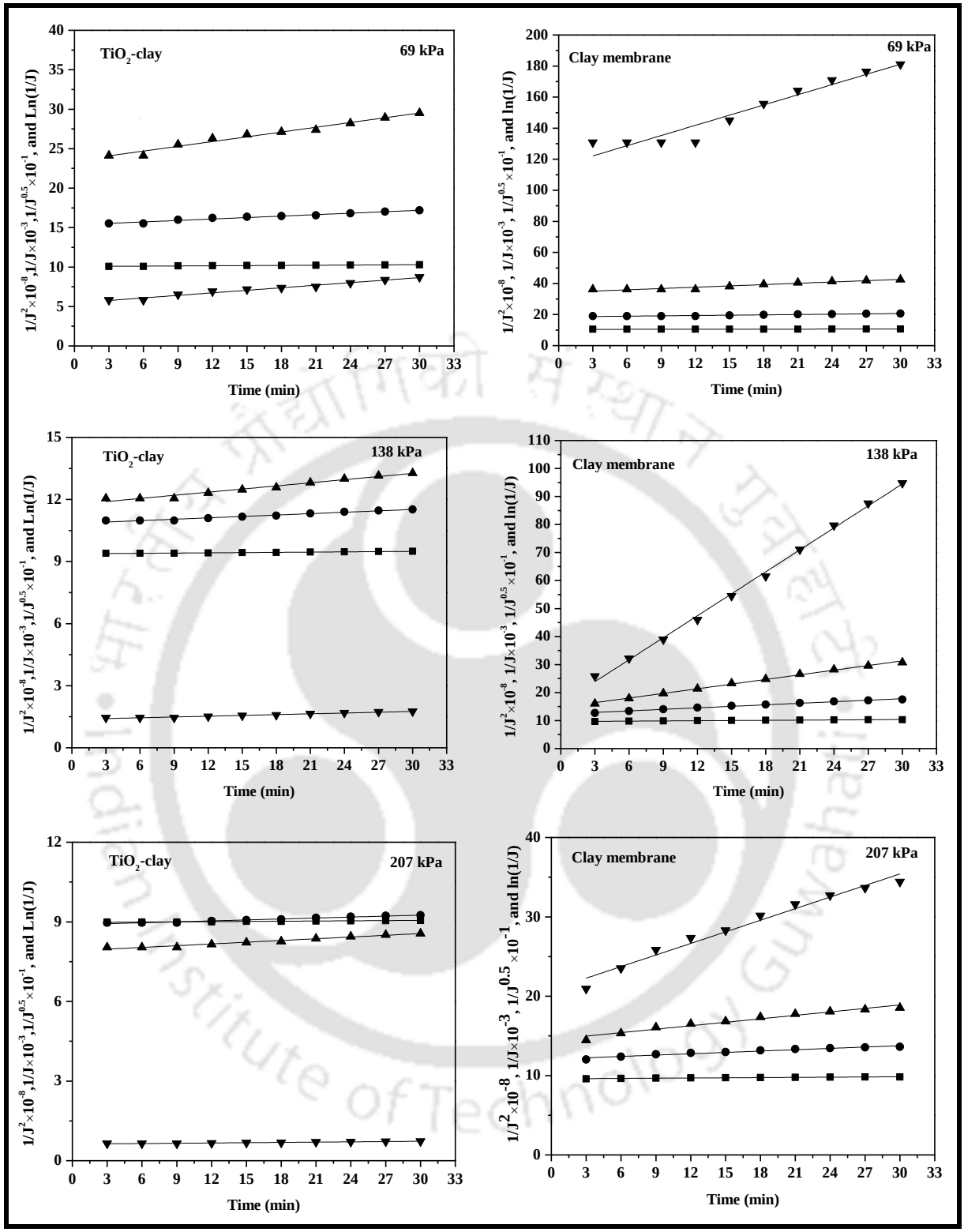

Figure 7.5: Effect of pressure on four different pore blocking models. (■ Complete pore blocking, ● Standard pore blocking, ▲ Intermediate pore blocking, ▼ Cake filtration)

As per Emani et al., (2014) observation, the cake filtration model produced the highest R^2 values to address the reduction of flux values in the treatment of oil-in-water emulsions. In the work reported by Vasanth et al., (2013) four different models were used for analyzing the experimental results and it was found that the cake filtration model with kaolin based membrane was considered to be the best model for representing the experimental data.

Table 7.2 also illustrates the value of model parameters (k) determined from various filtration models for clay and TiO_2–clay membrane. According to the definition and physical meaning of Hermia's model parameters, the value of 'k' represents the severity of fouling. It can be understood from Table 7.2 that for all the model fittings, the value of 'k' is higher for clay membrane compared to TiO_2–clay membrane. This can be explained by higher rate of fouling in clay membrane.

Table 7.2: Model parameters acquired for distinctive pore blocking models with clay and TiO_2–clay composite membrane at three pressures. (Coefficient of correlation (R^2), initial permeate flux (J_0) and slopes (k))

Clay	69 kPa			138 kPa			207 kPa		
Model	**Correlation coefficient (R^2)**	**Slope (k)**	**Initial permeate flux, J_0 m/s**	**Correlation coefficient (R^2)**	**Slope (k)**	**Initial permeate flux, J_0 m/s**	**Correlation coefficient (R^2)**	**Slope (k)**	**Initial permeate flux, J_0 m/s**
Complete	0.924	0.00718 s^{-1}	2.90×10^{-5}	0.979	0.02396 s^{-1}	6.35×10^{-5}	0.942	0.00874 s^{-1}	6.84×10^{-5}
Standard	0.924	0.07805 $s^{0.5}\ m^{-0.5}$	2.91×10^{-5}	0.990	0.18136 $s^{0.5}\ m^{-0.5}$	6.53×10^{-5}	0.951	0.05635 $s^{0.5}\ m^{-0.5}$	6.86×10^{-5}
Intermediate	0.925	0.27987 m^{-1}	2.92×10^{-5}	0.997	0.55274 m^{-1}	6.78×10^{-5}	0.958	0.14554 m^{-1}	6.88×10^{-5}
Cake filtration	0.926	2.18682 $s\ m^{-2}$	2.94×10^{-5}	0.997	2.61507 $s\ m^{-2}$	7.89×10^{-5}	0.972	0.48678 $s\ m^{-2}$	6.93×10^{-5}

TiO_2-clay	69 kPa			138 kPa			207 kPa	
Model	**Correlation coefficient (R^2)**	**Slope (k)**	**Initial permeate flux, J_0 m/s**	**Correlation coefficient (R^2)**	**Slope (k)**	**Initial permeate flux, J_0 m/s**	**Correlation coefficient (R^2)**	**Slope (k)**	**Initial permeate flux, J_0 m/s**
Complete	0.966	0.00754 s^{-1}	4.23×10^{-5}	0.967	0.00401 s^{-1}	8.5×10^{-5}	0.968	0.00263 s^{-1}	12.6×10^{-5}
Standard	0.969	0.07805 $s^{0.5}\ m^{-0.5}$	4.24×10^{-5}	0.967	0.02248 $s^{0.5}\ m^{-0.5}$	8.51×10^{-5}	0.967	0.01196 $s^{0.5}\ m^{-0.5}$	12.6×10^{-5}
Intermediate	0.972	0.27987 m^{-1}	4.26×10^{-5}	0.966	0.05049 m^{-1}	8.51×10^{-5}	0.967	0.02177 m^{-1}	12.6×10^{-5}
Cake filtration	0.976	2.18682 $s\ m^{-2}$	4.29×10^{-5}	0.965	0.01274 $s\ m^{-2}$	8.53×10^{-5}	0.966	0.0036 $s\ m^{-2}$	12.7×10^{-5}

7.3 Summary

The uniaxial pressing method has been applied for the fabrication of porous clay membrane using clay mixture composition of kaolin, quartz, ball clay, pyrophyllite, calcium carbonate and feldspar. It was sintered at 950 °C to examine the performance by separation of oil-in-water emulsions. TiO_2 composite membrane was fabricated using inexpensive titanium tetrachloride by hydrothermal method. The surface character of the clay membrane was modified from hydrophobic to hydrophilic, which was verified by the contact angle measurements. The above prepared TiO_2-clay membrane showed better rejection and permeate flux in separation of oil-in-water emulsions than that of the clay membrane in cross flow mode.

CHAPTER-8

Conclusions and Future Work

भारतीय प्रौद्योगिकी संस्थान गुवाहाटी
Indian Institute of Technology Guwahati

CHAPTER 8 Conclusions and Future work

Section 8.1 summarizes conclusions obtained from the research findings of the thesis. Section 8.2 presents possible scope for the future research work.

8.1 Conclusion

In this work, the inexpensive ceramic membrane fabrication involved three stages. The first stage involved the development of low cost ceramic membranes. During this phase, new inexpensive compositions were identified by trial and error based approach to prepare ceramic membranes SP1-SP4 (2.97-1.32 µm average pore size) and sub-micron range microfiltration membranes M1-M3 (1.36-1.44 µm average pore size). Morphological and structural characterization have affirmed that the membranes possess desired properties and are effective for oil-in-water emulsion treatment application. The second stage involved the preparation of TiO_2-Fly ash composite membrane using in-situ hydrothermal crystallization method and subsequent application of this membrane for the cross flow microfiltration of oil-in-water emulsions and process parametric optimization using response surface methodology. Finally, the last stage involved the fabrication of clay membrane and its surface nature was modified by coating of TiO_2 and γ-Al_2O_3 materials via hydrothermal method. The performance of the TiO_2 and γ-Al_2O_3 composite membranes was carried out by conducting separation studies on oil-in-water emulsions. In these studies, the effect of process parameters on permeates flux and oil rejection was evaluated. The conclusions drawn from experimental investigations are presented as follows:

- Among SP1-SP4 inexpensive membranes, SP4 membrane (48% porosity, 1.32 µm average pore size and 13.82 MPa mechanical strength) provided optimal performance for oil-in-water emulsion treatment to obtain 4.1×10^{-8} (m^3/m^2 s) membrane flux and 99.2% rejection at 69 kPa and 200 mg/L initial oil concentration.

- Among M1-M3 membranes that were prepared with maximum constitution of fly ash, M2 membrane provided optimal combinations of rejection (81-99%) and membrane flux (4.42-0.337×10^{-4} (m^3/m^2 s)). Further, the RSM based assessment of optimal parameters and variables corresponds to 345 kPa applied pressure, 176.07 mg/L feed concentration, 2.6×10^{-4} m^3/m^2 s membrane flux, 96.97% rejection and 0.77 desirability.
- The TiO_2-fly ash composite membrane prepared with the M2 membrane support provided optimal performance during oil-in-water emulsion treatment with cross-flow microfiltration. The membrane provided an 51.6372×10^{-4} m^3/m^2 s average membrane flux, 0.4974 m^3/m^2 s performance index which was better than those obtained for the M2 membrane (49.9712×10^{-4} m^3/m^2 s and 0.4620 (m^3/m^2 s) (%)). For the titania-fly ash composite membrane, the RSM based optimal parameters and variables correspond to 207 kPa applied pressure, 200 mg/L feed concentration, 0.1769 m/s cross flow velocity, 41.3301×10^{-4} (m^3/m^2 s) membrane flux and 98.7% rejection. Corresponding optimal flux and rejection based on experimental investigations are 42.74×10^{-4} m^3/m^2.s and 98.5% respectively.
- In view to compare fly ash membranes and clay membranes, the clay membrane was manufactured by means of a uniaxial dry pressing technique with clay powders available locally. TiO_2–clay and γ-Al_2O_3-clay membranes were prepared on the clay membrane by in-situ hydrothermal crystallization technique using $TiCl_4$ and $AlCl_3$ as a source material, respectively. It was observed that the surface character of the clay membrane was modified from hydrophobic to hydrophilic. Clay, TiO_2-clay and γ-Al_2O_3-clay membranes were subjected to dead end flow microfiltration of oil-in-water emulsions. Amongst the studied membranes, the result obtained for the TiO_2 membrane is the finest in terms of superior permeate flux (0.8481×10^{-4} m^3/m^2 s) and

maximum oil rejection (98.96%) for the feed oil concentration of 200 mg/L at an applied pressure of 69 kPa.

- Among TiO_2–clay and clay membranes tested for MF of oil-in-water emulsion in cross flow mode, the separation characteristics of TiO_2-clay membrane in terms of permeate flux (1.866×10^{-4} $m^3/m^2.s$) and rejection (99.56%) are found to be better for the feed oil concentration of 200 mg/L at an applied pressure of 207 kPa with cross flow velocity of 0.1769 m/s. Further, complete pore blocking is found to be best fit model to represent pertinent flux decline at higher applied pressures.
- Among all the membranes, TiO_2-Fly ash composite membrane provided best combinations of membrane flux and rejection for oil-in-water emulsion treatment.

In summary, the membrane reported in the thesis along with identified novel precursor formulations for inexpensive MF membranes provided satisfactory and comparatively better performance than those reported in the literature for oil-in-water emulsion separation.

8.2 Future work

Based on the conclusions of this work, few proposals for future research have been presented as follows:

Ceramic membrane fabrication and characterization

- Develop fly ash based tubular ceramic membranes with significantly higher constitution of fly ash by adopting extrusion method.
- Investigate upon the effect of extrusion process parameters (such as velocity) on the morphology and structural properties of membranes.
- Investigate upon the role of various binders (polyvinyl alcohol, polyethylene glycol and carboxy methyl cellulose) on the membrane morphological properties and separation efficacy.

- ❖Evaluate average membrane pore size using either mercury porosimetry approach or molecular weight cutoff (MWCO) characterization methods.
- ❖Target the fabrication of multi-layered asymmetric tubular ceramic composite membranes with fly ash as a skin layer.

Microfiltration applications of fly ash based tubular and multi-layered ceramic membranes

- Treatment of real oil-in-water emulsion effluents produced from industries to obtain confidence levels for the commercial application of low cost ceramic membranes.
- Pilot plant studies for oil-in-water emulsion treatment using low cost ceramic MF and UF membranes.

REFERENCES

भारतीय प्रौद्योगिकी संस्थान गुवाहाटी
Indian Institute of Technology Guwahati

References

Abadi, S. R. H., Sebzari, M., Hemati, M., Rekabdar, F., Mohammadi, T., Ceramic membrane performance in microfiltration of oily wastewater, *Desalination* 265 (2011) 222-228.

Abadikhah, H., Ashtiani, F. Z., Fouladitajar, A., Nanofiltration of oily wastewater containing salt; experimental studies and optimization using response surface methodology, *Desalination Water Treatment* 56 (2015) 2783-2796.

Abbasi, M., Mirfendereski, M., Nikbakht, M., Golshenas, M., Mohammadi, T., Performance study of mullite and mullite-alumina ceramic MF membranes for oily wastewaters treatment, *Desalination* 259 (2010) 169-178.

Abbasi, M., Salahi, A., Mirfendereski, M., Mohammadi, T., Park, A., Dimensional analysis of permeation flux for microfiltration of oily wastewaters using mullite ceramic membranes, *Desalination* 252 (2010) 113-119.

Adamson, A.W., Gast, A. P., Physical Chemistry of Surfaces, John Wiley & Sons, Inc., New York, USA, 1976.

Ahmad, A., Majid, M., Ooi, B., Functionalized PSf/SiO_2 nanocomposite membrane for oil-in-water emulsion separation, *Desalination* 268 (2011) 266-269.

Ahmadun, F. R., Pendashteh, A., Abdullah, L. C., Biak, D. R. A., Madaeni, S. S., Abidin, Z. Z., Review of technologies for oil and gas produced water treatment, *Journal of Hazardous Materials* 170 (2009) 530-551.

Ahmaruzzaman, M., A review on the utilization of fly ash, *Progress in Energy Combustion Science* 36 (2010) 327-363.

Akgerman, A., Zardkoohi, M., Adsorption of phenolic compounds on fly ash, *Journal of Chemical Engineering Data* 41 (1996) 185-187.

Aleboyeh, A., Daneshvar, N., Kasiri, M. B., Optimization of C.I. Acid Red 14 azo dye removal by electrocoagulation batch process with response surface methodology, *Chemical Engineering and Processing: Process Intensification* 47 (2008) 827-83.

Alem, A., Sarpoolaky, H., Keshmiri. M., Sol gel preparation of titania multilayer membrane for photocatalytic applications, *Ceramics International* 35 (2009b) 1837-1843.

Alem, A., Sarpoolaky, H., Keshmiri, M., Titania ultrafiltration membrane: Preparation, characterization and photocatalytic activity, *Journal of the European Ceramic Society* 29 (2009a) 629-635.

Almandoza, M. C., Marchese, J., Prádanos, P., Palacio, L., Hernández, A., Preparation and characterization of non-supported micro-filtration membranes from alumino silicates, *Journal of Membrane Science* 241 (2004) 95-103.

Al-Shamrani, A. A., James, A., Xiao, H., destabilization of oil-water emulsions and separation by dissolved air flotation, *Water Research* 36 (2002) 1503-1512.

Alzahrani, S., Mohammad, A.W., Challenges and trends in membrane technology implementation for produced water treatment: A review, *Journal of Water Process Engineering* 4 (2014) 107-133.

Apak, R., Tutem, E., Hugul, M., Hizal, J., Heavy metal cation retention by unconventional sorbents (red muds and fly ashes), *Water Research* 32 (1998) 430-440.

Arkles, B., Hydrophobicity, Hydrophilicity and Silanes, Paint & Coatings Industry magazine, Gelest Inc., Morrisville, PA, USA, 2006.

Arnot, A., Field, R. W., Koltuniewicz, A. B., Cross-flow and dead-end microfiltration of oily-water emulsions part II. Mechanisms and modelling of flux decline, *Journal of Membrane Science* 169 (2000) 1-15.

Arzani, M., Mahdavi, H .R., Bakhtiari, O., Mohammadi, T., Preparation of mullite ceramic microfilter membranes using Response surface methodology based on central composite design, *Ceramics International* 42 (2016) 8155-8164.

Baker, R. W., Membrane technology and applications, *John Wiley & Sons Ltd*, West Sussex, England, (2004).

Banerjee, S. S., Jayaram, R. V., Joshi, M. V., Removal of nickel (II) and zinc (II) from wastewater using fly ash and impregnated fly ash, *Separation Science Technology* 38 (2003) 1015-1032.

Banerjee, S. S., Joshi, M. V., Jayaram, R. V., Removal of Cr(VI) and Hg(II) from aqueous solutions using fly ash and impregnated fly ash, *Separation Science Technology* 39 (2004) 1611-1629.

Bashir, M. J. K., Aziz, H. A., Yusoff, M. S., Adlan, M. N., Application of response surface methodology (RSM) for optimization of ammonical nitrogen removal from semi-aerobic landfill leachate using ion exchange resin, *Desalination* 254 (2010) 154-161.

Bashir, M. J. K., Aziz, H. A., Yusoff, M.S., Aziz, S. Q., Mohajeri, S., Stabilized sanitary landfill leachate treatment using anionic resin: Treatment optimization by response surface methodology, *Journal of Hazardous Materials* 182 (2010) 115-122.

Basumatary, A. K., Kumar, R.V., Ghoshal, A. K., Pugazhenthi, G., Crossflow ultrafiltration of Cr (VI) using MCM-41, MCM-48 and Faujasite (FAU) zeolite ceramic composite membranes, *Chemosphere* 153 (2016) 436-446.

Basumatary, A. K., Kumar, R.V., Ghoshal, A. K., Pugazhenthi, G., Removal of $FeCl_3$from aqueous solution by ultrafiltration using ordered mesoporous MCM-48 ceramic composite membrane, *Separation Science and Technology* 51 (2016) 2038-2046

Benito, J. M., Conesa, A., Rubio, F., Rodriguez, M. A., Preparation and characterization of tubular ceramic membranes for treatment of oil emulsions, *Journal of European Ceramic Society* 25 (2005) 1895-1903.

Bensadok, K., Benammar, S., Lapicque, F., Nezzal, G., Electrocoagulation of cutting oil emulsions using aluminium plate electrodes, *Journal of Hazardous Materials* 152 (2008) 423-430.

Berg, G. B. V. D., Smolders, C. A., Flux decline in ultrafiltration processes, *Desalination* 77 (1990) 101-133.

Blissett, R. S., Rowson, N. A., A review of the multi-component utilization of coal fly ash, *Fuel* 97 (2012) 1-23.

Boudaira, B., Harabia, A., Bouzerara, F., Condom, S., Preparation and characterization of microfiltration membranes and their supports using kaolin (DD2) and $CaCO_3$, *Desalination and Water Treatment* 9 (2009) 142-148.

Bouzerara, F, Harabi, A, Achour, S, Larbot, A, Porous ceramic supports for membranes prepared from kaolin and doloma Mixtures, *Journal of European Ceramic Society* 26 (2006) 1663-1671.

Bruggen, B. V. D., Manttari, M., Nystrom, M., Drawbacks of applying nanofiltration and how to avoid them: A review, *Separation and Purification Technology* 63 (2008) 251-263.

Ceramiques techniques & industrielles, SA, France, 2007.http://perso.orange.fr/ctisa.

Chakrabarty, B., Ghoshal, A. K., Purkait, M. K., Ultrafiltration of stable oil-in-water emulsion by polysulfone membrane, *Journal of Membrane Science* 325 (2008) 427-437.

Chang, Q., Zhou, J., Wang, Y., Liang, J., Zhang, X., Cdfneaux, S., Wang, X., Zhu, Z., Dong, Y., Application of ceramic microfiltration membrane modified by nano-TiO_2 coating

in separation of a stable oil-in-water emulsion, *Journal of Membrane Science* 456 (2014) 128-133.

Chavalparit, O., Ongwandee, M., Optimizing electrocoagulation process for the treatment of biodiesel wastewater using response surface methodology, *Journal of Environmental Sciences* 21 (2009) 1491-1496.

Cheryan, M., Ultrafiltration and microfiltration handbook, Technomic publishing company, Basel, Switzerland, 1998.

Chinnam, J., Das, D., Vajjha, R., Satti, J., Measurements of the contact angle of nanofluids and development of a new correlation, *International Communication in Heat and Mass Transfer* 62 (2015) 1-12.

Chou, K. S., Kao, K. B., Huang, C. D., Chen, C. Y., Coating and characterization of titania membrane on porous ceramic supports, *Journal of Porous Materials* 6 (1999) 217-225.

Chowdhury, S. R, Schmuhl, R., Keizer, K., Elshof, J. E. T., Blank, D. H., Pore size and surface chemistry effects on the transport of hydrophobic and hydrophilic solvents through mesoporous γ-alumina and silica MCM-48, *Journal of Membrane Science* 225 (2003) 177-186.

Colomban, P. H., Raman study of the formation of transition alumina single crystal from protonic β/β`` aluminas, *Journal of Materials Science Letters* 7 (1988) 1324-1326.

Cross, A. D., *An Introduction to practical IR Spectroscopy,* 2nd edition, Butterworth, London, 1964.

Cui, J., Zhang, X., Liu, H., Liu, S., Yeung, K. L., Preparation and application of zeolite/ceramic microfiltration membranes for treatment of oil contaminated water, *Journal of Membrane Science* 325 (2008) 420-426.

Cultrone, G., Navarro, C. R., Sebastian, E., Cazalla, O., Torre, M. J., Carbonate and silicate phase reactions during ceramic firing, *European Journal of Mineralogy* 13 (2001) 621-634.

Cumming, I. W., Holdich, R. G., Smith, I. D., The rejection of oil by microfiltration of a stabilized kerosene/water emulsion, *Journal of Membrane Science* 169 (2000) 147-155.

Daifullah, A. E. H., Gad, H., Sorption of semi-volatile organic compounds by bottom and fly ashes using HPLC. *Adsorption Science Technology* 16 (1998) 273-283.

Davini, P., Flue gas treatment by activated carbon obtained from oil-fired fly ash. Carbon 40 (2002) 1973-1979.

DeFriend, K. A., Wiesner, M. R., Barron, A. R., Alumina and aluminate ultrafiltration membranes derived from alumina nanoparticles, *Journal of Membrane Science* 224 (2003) 11-28.

Delagrave, A., Marchand, J., Pigeon, M., Boisvert, J., Deicer salt scaling resistance of roller compacted concrete pavements. *ACI Materials Journal* 96 (1997) 164-169.

Dong, Y. C., Liu, X. Q., Ma, Q. L., Meng, G.Y., Preparation of cordierite-based porous ceramic micro-filtration membranes using waste fly ash as the main raw material, *Journal of Membrane Science* 285 (2006) 173-181.

Dong, Y., Feng, X., Dong, D., Wang, S., Yang, J., Gao, J., Liu, X., Meng, G., Elaboration and chemical corrosion resistance of tubular macro-porous cordierite ceramic membrane supports, *Journal of Membrane Science* 304 (2007) 65-75.

Dong, Y., Hampshire, S., Zhou, J., Ji, Z., Wang, J., Meng, G., Sintering and characterization of fly ash based mullite with MgO addition, *Journal of the European Ceramic Society* 31 (2011) 687-695.

Dong, Y., Hampshire, S., Zhou, J., Lin, B., Ji, Z., Zhang, X., Meng, G., Recycling of fly ash for preparing porous mullite membrane supports with titania addition, *Journal of Hazardous Materials* 180 (2010) 173-180.

Ebrahimi, M., Ashaghi, K. S., Engel, L., Willershausen, D., Mund, P., Bolduan, P., Czermak, P., Characterization and application of different ceramic membranes for the oil-field produced water treatment, *Desalination* 245 (2009) 533-540.

Ebrahimi, M., Willershausen, D., Ashaghi, K. S., Engel, L., Placido, L., Mund, P., Bolduan, P., zermak, P.C., Investigations on the use of different ceramic membranes for efficient Oil-field produced water treatment, *Desalination* 250 (2010) 991-996.

Emani, S., Uppaluri, R., Purkait, M. K., Cross flow microfiltration of oil-water emulsions using kaolin based low cost ceramic membranes, *Desalination* 341 (2014) 61-71.

Emani, S., Uppaluri, R., Purkait, M. K., Preparation and characterization of low cost ceramic membranes for mosambi juice clarification, *Desalination* 317 (2013) 32-40.

Erdem, I., Ciftcioglu, M., Harsa, S., Separation of whey components by using ceramic composite membranes. *Desalination* 189 (2006) 87-91.

Ezzati, A., Gorouhi, E., Mohammadi, T., Separation of water in oil emulsions using microfiltration, *Desalination* 185 (2005) 371-382.

Falamaki, C., Afarani, M. S., Aghaie, A., Initial sintering stage pore growth mechanism applied to the manufacture of ceramic membrane supports, *Journal of European Ceramic Society* 24 (2004) 2285-2292.

Falamaki, C., Naimi, M., Aghaie, A., Dual behavior of $CaCO_3$ as a porosifier and sintering aid in the manufacture of alumina membrane/catalyst supports, *Journal of the European Ceramic Society* 24 (2004) 3195-3201.

Fang, J., Qin, G. T., Wei, W., Zhao, X. Q., Preparation and characterization of tubular supported ceramic microfiltration membranes from fly ash, *Separation and Purification Technology* 80 (2011) 585-591.

Fang, J., Qin, G., Wei, W., Zhao, X., Jiang, L., Elaboration of new ceramic membrane from spherical fly ash for microfiltration of rigid particle suspension and oil-in-water emulsion, *Desalination* 311 (2013) 113-126.

Feng, L., Li, S., Li, Y., Li, H., Zhang, L., Zhai, J., Song, Y., Liu, B., Jiang, L., Zhu, D., Super-hydrophobic surfaces: From natural to artificial, *Advanced Materials* 4 (2002) 1857-1860.

Frost, R. L., Kloprogge, J., Russell, S. C., Szetu, J. L., Dehydroxylation and structure of alumina gels prepared from trisecbutoxyaluminium, *Thermochimica Acta* 329 (1999) 47-56.

Fukui, K., Arimitsu, N., Jikihara, K., Yamamoto, T., Yoshida, H., Performance of fuel cell using calcium phosphate hydrogel membrane prepared from waste incineration fly ash and chicken bone powder, *Journal of Hazardous Materials* 168 (2009) 1617-1621.

Gao, P., Lu, X., Lin, H., Li, X., Hou, J., Effects of fly ash on the properties of environmentally friendly dam concrete, *Fuel* 861 (2007) 208-211.

Garcia, C., Hernandez, E. R., Lopez, L. Z. F., Gomez, H. E., Effect of the membrane characteristics and operation modes, in the fouling of ultrafiltration membranes by natural organic matter (NOM), *Journal of the Chilean Chemical Society* 57 (2012) 1083-1086.

Gengec, E., Kobya, M., Demirbas, E., Akyol, A., Oktor, K., Optimization of baker's yeast wastewater using response surface methodology by electrocoagulation, *Desalination* 286 (2012) 200-209.

Ghaedi, M., Kokhdan, S. N., Removal of methylene blue from aqueous solutions by wood millet carbon optimization using response surface methodology, *Spectrochimica Acta Part A: Molecular and Biomolecular Spectroscopy* 136 (2015) 141-148.

Ghafari, S., Aziz, H. A., Isa, M. H., Zinatizadeh, A. A., Application of response surface methodology (RSM) to optimize coagulation-flocculation treatment of leachate using poly-aluminum chloride (PAC) and alum, *Journal of Hazardous Materials* 163 (2009) 650-656.

Gonzalez, A., Navia, R., Moreno, N., Fly ashes from coal and petroleum coke combustion: current and innovative potential applications, *Waste Management and Research* 27 (2009) 976-987.

Gualtieri, A., Bellotto, M., Artioli, G., Clark, S. M., Kinetic study of the kaolinite-mullite reaction sequence. Part II: mullite formation, *Physics and Chemistry of Minerals* 22 (1995) 215-222.

Hansen, K. D., Reinhardt, W. G., Roller-compacted concrete dams. New York: McGraw-Hill; 1991.

Hsieh, H. P., Inorganic membranes for separation and reaction, *Elsevier*, Amsterdam, (1996).

Hu, X., Yu, Y., Zhou, J., Wang, Y., Liang, J., Zhang, X., Chang, Q., Song, L., The improved oil-water separation performance of graphene oxide modified Al_2O_3 microfiltration membrane, *Journal of Membrane Science* 476 (2015) 200-204.

Hua, F. L., Tsang, Y. F., Wang, Y. J., Chan, S. Y., Chuand, H., Sin, H. N., Performance study of ceramic microfiltration membrane for oily wastewater treatment, *Chemical Engineering Journal* 128 (2007) 169-175.

Hyun, S. H., Kim, G. T., Synthesis of ceramic microfiltration membranes for oil-water separation, *Separation Science and Technology* 32 (1997) 2927-2943.

Illic, M., Cheeseman, C., Sollars, C., Knight, J., Mineralogy and microstructure of sintered lignite coal fly ash, *Fuel* 82 (2003) 331-336.

Iyer, R. S., Scott, J. A., Power station fly ash- a review of value-added utilization outside of the construction industry, *Resources, Conservation and Recycling* 31 (2011) 217-228.

Jadhav, M. V., Mahajan, Y. S., Application of response surface methodology to water/wastewater treatment using Cocconia indica, *Desalination and Water Treatment* 52 (2014) 6403-6411.

Jamaly, S., Darwish, N. N., Ahmed, I., Hasan, S. W., A short review on reverse osmosis pretreatment technologies, *Desalination* 354 (2014) 30-38.

Jana, S., Purkait, M. K., Mohanty, K., Preparation and characterization of low-cost ceramic microfiltration membranes for the removal of chromate from aqueous solutions, *Applied Clay Science* 47 (2010) 317-324.

Jedidi, I., Khemakhem, S., Larbot, A., Ben, A. R., Elaboration and characterization of fly ash based mineral supports for microfiltration and ultrafiltration membranes, *Ceramic Internationals* 35 (2009) 2747–2753.

Jedidi, I., Khemakhem, S., Saidi, S., Larbot, A., Ammar, N. E., Fourati, A., Charfi, A., Salah, A. B., Amar, R. B., Preparation of a new ceramic microfiltration membrane from mineral coal fly ash: Application to the treatment of the textile dying effluents, *Powder Technology* 208 (2011) 427-432.

Jedidi, I., Saidi, S., Khmakem, S., Larbot, A., Elloumi-Ammar, N., Fourati, A., Charfi, A., Amar, R.B., New ceramic microfiltration membranes from mineral coal fly ash, *Arabian Journal of Chemistry* 2 (2009) 31-39.

Jo, Y. M., Hutchison, R., Raper, J. A., Characterization of ceramic composite membrane filters for hot gas cleaning, *Powder Technology* 91 (1997) 55-62.

John, D., Nanotechnology-A new way to do oil skimming?, *Metal finishing* 108 (2010) 35-36.

Jokic, A., Zavargo, Z., Seres, Z., Tekic, M., The effect of turbulence promoter on cross-flow microfiltration of yeast suspensions: A response surface methodology approach, *Journal of Membrane Science* 350 (2010) 269-278.

Jones, C. D., Barron, A. R., Porosity, crystal phase, and morphology of nanoparticle derived alumina as a function of the nanoparticle's carboxylate substituent, *Materials Chemistry and Physics* 104 (2007) 460-471.

Jonsson, A. S., Tragardh, G., Ultrafiltration applications, *Desalination* 77 (1990) 135-179.

Judd, S., B. Jefferson, Membranes for industrial wastewater recovery and re-use, *Elsevier*, Oxford OX5 IGB, UK, 2003.

Kang, W., Guo, L., Fan, H., Meng, L., Li, Y., Flocculation, coalescence and migration of dispersed phase droplets and oil-water separation in heavy oil emulsion, *Journal of Petroleum Science and Engineering* 81 (2012) 177-181.

Kazemimoghadam, M., Pak, A., Mohammadi, T., Dehydration of water/1-1-dimethy hydrazine mixtures by zeolite membranes, *Microporous and Mesoporous Materials* 70 (2004) 127-134.

Kelleher, B. P., O'Callaghan, M. N., Leahy, M. J., O'Dwyer, T. F., Leahy, J. J., The use of fly ash from the combustion of poultry litter for the adsorption of chromium (III) from aqueous solution, *Journal of Chemical Technology and Biotechnology* 77 (2002) 1212-1218.

Khataee, A. R., Dehghan, G., Optimization of biological treatment of a dye solution by macro algae Cladophora sp. using response surface methodology, *Journal of the Taiwan Institute of Chemical Engineers* 42 (2011) 26-33.

Khemakhem, S., Larbot, A., Amara, R. B., Study of performances of ceramic microfiltration membrane from Tunisian clay applied to cuttlefish effluents treatment, *Desalination* 200 (2006) 307-309.

Khider, K., Akretche, D. E., Larbot, A., Purification of water effluent from a milk factory by ultrafiltration using Algerian clay support. *Desalination* 167 (2004) 147-151.

Korbahti, B. K., Tanyolac, A., Electrochemical treatment of simulated textile wastewater with industrial components and Levafix Blue CA reactive dye: Optimization through response surface methodology, *Journal of Hazardous Materials* 151 (2008) 422-431.

Koros, W. J., Mahajan, R., Pushing the limits on possibilitie for large scale gas separation: Which strategies, *Journal of Membrane Science* 172 (2000) 181-196.

Krauczyk, J. A. S., The influence of feed flow channel diameter on frictional pressure drop, membrane performance and process cost in full-scale tubular membranes, *Chemical Engineering Research and Design* 92 (2014) 174-180.

Krebs, T., Schroen, C. G. P. H., Boom, R. M., Separation kinetics of an oil-in-water emulsion under enhanced gravity, *Chemical Engineering Science* 71 (2012) 118-125.

Kumar, R. V., Ghoshal, A. K., Pugazhenthi, G., Fabrication of zirconia composite membrane by in-situ hydrothermal technique and its application in separation of methyl orange, *Ecotoxicology and Environmental Safety* 121 (2015) 73-79

Kushwaha, J. P., Srivastava, V. C., Mall, I. D., Organics removal from dairy wastewater by electrochemical treatment and residue disposal, *Separation and Purification Technology* 76 (2010) 198-205.

Li, H. J., Cao, Y. M., Qin, J. J., Jie, X. M., Wang, T. H., Liu, J. H., Yuan, Q., Development and characterization of anti-fouling cellulose hollow fiber UF membranes for oil-water separation, *Journal Membrane Science* 279 (2006) 328-335.

Li, L., Ding, L., Tu, Z., Wan, Y., Clausse, D., Lanoiselle, J. L., Recovery of linseed oil dispersed within an oil-in-water emulsion using hydrophilic membrane by rotating disk filtration system, *Journal of Membrane Science* 342 (2009) 70-79.

Li, S., Shen, Q., Zong, J., Yang, H., Simple preparation of sub-micron mesoporous TiO_2 spheres consisting of anatase nanocrystals, *Journal of Alloys and Compounds* 508 (2010) 99-105.

Li, Y., Chen, H., Liu, J., Yang, W., Microwave synthesis of LTA zeolite membranes without seeding, *Journal of Membrane Science* 277 (2006) 230-239.

Li, J., Wang, X., Wang, L., Hao, Huang, Y., Zhang, Y., Sun, Liu, X., Preparation of alumina membrane from aluminium chloride, *Journal of Membrane Science* 275 (2006) 6–11.

Lin, K. L., Feasibility study of using brick made from municipal solid waste incinerator fly ash slag, *Journal of Hazardous Materials B* 137 (2006) 1810–1816.

Lin, Y. S., Burggraaf, A. J., Preparation and characterization of high-temperature thermally stable alumina composite membrane, *Journal of American Ceramic Society* 74 (1991) 219-224.

Liu, H. L., Chiou, Y. R., Optimal decolorization efficiency of Reactive Red 239 by UV/TiO_2 photocatalytic process coupled with response surface methodology, *Chemical Engineering Journal* 112 (2005) 173-179.

Liu, Y., Ma, D., Han, X., Bao, X., Frandsen, W., Wang, D., Su, D., Hydrothermal synthesis of microscale boehmite and gamma nanoleaves alumina, *Materials Letters* 62 (2008) 1297-1301.

Lobo, A., Cambiella, A., Benito, J. M., Pazos, C., Coca, J., Ultrafiltration of oil-in-water emulsions with ceramic membranes: Influence of pH and crossflow velocity, *Journal of Membrane Science* 278 (2006) 328-334.

Majhi, A., Monash, P., Pugazhenthi, G., Fabrication and characterization of γ-Al_2O_3-clay composite ultrafiltration membrane for the separation of electrolytes from its aqueous solution, *Journal of Membrane Science* 340 (2009) 181-191.

Marchese, J., Pagliero, C. L., Characterization of asymmetric polysulphone membranes for gas separation, *Gas Separation and Purification* 5 (1991) 215-221.

Masmoudi, S., Larbot, A., Feki, H. E., Amar, R. B., Elaboration and characterization of apatite based mineral supports for microfiltration and ultrafiltration membranes, *Ceramics Internationals* 33 (2007) 337-344.

Masoudnia, K., Raisi, A., Aroujalian, A., Fathizadeh, M., Treatment of oily wastewater using the microfiltration process: Effect of operating parameters and membrane fouling study, *Separation Science and Technology* 48 (2013) 1544-1555.

Mathur, A. K., Ash utilisation in NTPC. In: Proceedings of the workshop on fly ash utilisation: issues and strategies; 2000.

McMillan, P., Piriou, B., The structures and vibrational spectra of crystals and galsses in the silica-alumina system, *Journal of Non-Crystalline Solids* 53 (1982) 279-298.

Mittal, P., Jana, S., Mohanty, K., Synthesis of low cost hydrophilic ceramic-polymeric composite membrane for treatment of oily wastewater, *Desalination* 282 (2011) 54-62.

Mohajeri, S., Aziz, H. A., Isa, M. H., Zahed, M. A., Bashir, M. J. K., Adlan, M. N., Application of the central composite design for condition optimization for semi-aerobic landfill leachate treatment using electrochemical oxidation, *Water Science & Technology* 61 (2010) 1257-1266.

Mohammad, A. W., Teow, Y. H., Ang, W. L., Chung, Y. T., Radcliffe, D. L. O., Hilal, N., Nanofiltration membranes review: Recent advances and future prospects, *Desalination* 356 (2015) 226-254.

Mohammadi, T., Pak, A., Karbassian, M., Golshan, M., Effect of operating conditions on microfiltration of an oil–water emulsion by a kaolin membrane, *Desalination*, 168 (2005) 201-205.

Monash, P., Pugazhenthi, G., Development of ceramic supports derived from low cost clays for membrane applications and its optimization based on sintering temperature, *International Journal of Applied Ceramic Technology* 8 (2011a) 227-238.

Monash, P., Pugazhenthi, G., Effect of TiO_2 addition on the fabrication of ceramic membrane supports: A study on the separation of oil droplets and bovine serum albumin (BSA) from its solution, *Desalination* 279 (2011b) 104-114.

Montgomery, D. C., Response Surface Methods and other Approaches to Process Optimization Design and Analysis of Experiments, fifth ed., *John Wiley & Sons*, New York, NY, 2001.

Mott Metallurgical Corporation, USA, 2007. http://www.mottcorp.com.

Mueller, J., Cen, Y., Davis, R. H., Cross flow microfiltration of oily water, *Journal of membrane Science* 129 (1997) 221-235.

Mulder. M., Basic Principles of Membrane Technology, *Kluwer Academic* Publishers, Dordrecht, (1991).

Nandi, B. K., Moparthi, A., Uppaluri, R., Purkait, M. K., Treatment of oily wastewater using low cost ceramic membrane: Comparative assessment of pore blocking and artificial neural network models, *Chemical Engineering Research and Design* 88 (2010) 881-892.

Nandi, B. K., Uppaluri, R., Purkait M. K., Preparation and characterization of low cost ceramic membranes for microfiltration applications**,** *Applied Clay Science* 42 (2008) 102-110.

Nandi, B. K., Uppaluri, R., Purkait, M. K., Identification of optimal membrane morphological parameters during microfiltration of mosambi juice using low cost ceramic membranes, *LWT- Food Science and Technology* 44 (2011) 214 -223.

Nandi, B. K., Uppaluri, R., Purkait, M. K., Treatment of oily wastewater using low-cost ceramic membrane: Flux decline mechanism and economic feasibility, *Separation Science and Technology* 44 (2009) 2840-2869.

Nanni, A., Ludwig, D., Shoenberger, J., Roller compacted concrete for highway pavements. *Concrete International* 18 (1996) 33–38.

Neelakandan, C., Pugazhenthi, G., Kumar, A., Preparation of NOx modified PMMA–EGDM composite membrane for the recovery of chromium (VI), *European Polymer Journal* 39 (2003) 2383–2391.

Nunes, S. P., Peinemann, K.V., Membrane technology in the chemical industry, 1st ed. *Wiley*, New York, 2001.

Ochoa, N. A., Masuelli, M., Marchese, J., Effect of hydrophilicity on fouling of an emulsified oil wastewater with PVDF/PMMA membranes, *Journal of Membrane Science* 226 (2003) 203-211.

Olegovich, D. V., Gilmanovich, S. I., Bonev, B. S., Shaukatovich, A. I., Nenov, V. A., Oily wastewater treatment using membranes modified by plasma, *Energy and Environmental Engineering* 1 (2013) 105-110.

Olmez, T., The optimization of Cr (VI) reduction and removal by electrocoagulation using response surface methodology, *Journal of Hazardous Materials* 162 (2009) 1371-1378.

Padaki, M., Murali, R. S., Abdullah, M. S., Misdan, N., Moslehyani, A., Kassinm, M. A., Hilal, N., Ismail, A. F., Membrane technology enhancement in oil-water separation. A review, *Desalination* 357 (2015) 197-207.

Padmaja, P., Krishnapillai, P., Warrier, K. G. K., Adsorption isotherm and pore characteristics of nano alumina derived from sol-gel boehmite, *Journal of Porous Materials* 11 (2004) 147-155.

Pan, Y., Wang, T., Sun, H., Wang, W., Preparation and application of titanium dioxide dynamic membranes in microfiltration of oil-in-water emulsions, *Separation and Purification Technology* 89 (2012) 78-83.

Pattanayak, J., Mondal, K., Mathew, S., Lalvani, S. B., A parametric evaluation of the removal of As(V) and As(III) by carbon-based adsorbents, *Carbon* 38 (2000) 589-596.

Patterson, V. A., Krieg, H. M., Kriek, R. J., Bisset, H., Direct synthesis of a titania membrane on a centrifugally casted tubular ceramic support, *Journal of Membrane Science* 285 (2006) 1-3.

Potdar, A., Shukla, A., Kumar, A., Effect of gas phase modification of analcime zeolite composite membrane on separation of surfactant by ultrafiltration, *Journal of Membrane Science* 210 (2002) 209-225.

Pugazhenthi, G., Sachan, S., Kishore, N., Kumar, A., Separation of chromium (VI) using modified ultrafiltration chargedcarbon membrane and its mathematical modeling, *Journal of Membrane Science* 254 (2005) 229-239.

Querol, X., Alastuey, A., Jose, L. F. T., Angel, L. S., Synthesis of zeolites by alkaline activation of ferro-aluminous fly ash, *Fuel* 74 (1995) 1226-1231.

Rastegar, S. O., Mousavi, S. M., Shojaosadati, S. A., Sheibani, S., Optimization of petroleum refinery effluent treatment in a UASB reactor using response surface methodology, *Journal of Hazardous Materials* 197 (2011) 26-32.

Rezvanpour, A., Roostaazad, R., Hesampour, M., Nystrom, M., Ghotbi, C., Effective factors in the treatment of kerosene-water emulsion by using UF membranes, *Journal of Membrane Science* 161 (2009) 1216-1224.

Sadeghian, M., Sadeghi, M., Hesampour, M., Moheb, A., Application of response surface methodology (RSM) to optimize operating conditions during ultrafiltration of oil-in-water emulsion, *Desalination and Water Treatment* 55 (2015) 615-623.

Saffaj, N., Persin, M., Younsi, S. A., Albizane, A., Cretin, M., Larbot, A., Elaboration and characterization of microfiltration and ultrafiltration membranes deposited on raw support prepared from natural Moroccan clay: application to filtration of solution containing dyes and salts, *Applied Clay Science* 31 (2006) 110-119.

Saffaj, N., Persin, M., Younssi, S. A., Albiza, A., Bouhria, M., Loukili, H., Dacha, H., Larbot, A., Removal of salts and dyes by low $ZnAl_2O_4$–TiO_2 ultrafiltration membrane deposited on support made from raw clay, *Separation and Purification Technology* 47 (2005) 36-42.

Saffaj, N., Loukili, H., Younssi, S. A., Albizane, A., Bouhria, Persin, M. M., Larbot, A., Filtration of solution containing heavy metals and dyes by means of ultrafiltration membranes deposited on support made of Moroccan clay, *Desalination* 168 (2004) 301-306.

Salahi, A., Gheshlaghi, A., Mohammadi, T., Madaeni, S. S., Experimental performance evaluation of polymeric membranes for treatment of an industrial oily wastewater, *Desalination* 262 (2010) 235-242.

Salahi, A., Noshadi, I., Badrnezhad, R., Kanjilal, B., Mohammad, T., Nano-porous membrane process for oily wastewater treatment: Optimization using response surface methodology, *Journal of Environmental Chemical Engineering* 1 (2013) 218-225.

Salam, K. K., Alade, A. O., Arinkoola, A. O., Opawale, A., Improving the demulsification process of heavy crude oil emulsion through blending with diluent, *Journal of Petroleum Engineering* 2013 (2013) 6.

Saleh, K., Guigon, P., Coating and encapsulation processes in powder technology, 1st edition, *Elsevier*, Handbook of powder technology, 2007, Chapter 7, 323-375.

Santos, S. C. R., Boaventira, R. A. R., Adsorption modelling of textile dyes by sepiolite, *Applied Clay Science* 42 (2008) 137-145.

Savasari, M., Emadi, M., Bahmanyar, M. A., Biparva, P., Optimization of Cd (II) removal from aqueous solution by ascorbic acid stabilized zero valent iron nanoparticles using response surface methodology, *Journal of Industrial and Engineering Chemistry* 21 (2015) 1403-1409.

Shi, J., Wang, X., Wang, X., Optimizing oily wastewater treatment via wet peroxide oxidation using response surface methodology, *Journal of the Korean Chemical Society* 58 (2014) 80-84.

Shokrkar, H., Salahi, A., Kasiri, N., Mohammadi, T., Prediction of permeation flux decline during MF of oily wastewater using genetic programming, *Chemical Engineering Research and Design* 90 (2012) 846-853.

Shqau, K., Mottern, M. L., Yu, D., Verweij, H., Preparation and propertis of porous α-Al_2O_3 membrane supports, *Journal of the American Ceramic Society* 89 (2006) 1790-1794.

Shukla, A., Kumar, A., Separation of Cr(VI) by zeolite-clay composite membranes modified by reaction with NO_x, *Separation Purification Technology* (52) (2007) 423-429.

Singh, V., Purkait, M. K., Das, C., Cross-flow microfiltration of industrial oily wastewater: experimental and theoretical consideration, *Separation Science and Technology* 46 (2011) 1213-1223.

Singh, R., Membrane technology and engineering for water purification application, systems design and operation, 2nd edition,USA, *Elsevie*r (2015).

Song, C. W., Wang, T. H., Pan, Y. Q., Qiu, J. S., Preparation of coal-based microfiltration carbon membrane and application in oily wastewater treatment, *Separation and Purification Technology* 51 (2006) 80-84.

Sriharsha, E., Uppaluri, R., Purkait, M. K., Cross flow microfiltration of oil-water emulsions using kaolin based low cost ceramic membranes, *Desalination* 341 (2014) 61-71.

Srijaroonrat, P., Julien, E., Aurelle, Y., Unstable secondary oil/water emulsion treatment using ultrafiltration: fouling control by back flushing, *Journal of Membrane Science* 159 (1999) 11-20.

Steenkiste, T. H. V., Smith, J. R., Teets, R. E., Aluminum coatings via kinetic spray with relatively large powder particles, *Surface and Coatings Technology* 154 (2002) 237-252.

Suresh, K., Pugazhenthi, G., Development of ceramic membranes from low-cost clays for the separation of oil-water emulsion, *Desalination and Water Treatment* 57 (2016) 1927-1939.

Suresh, K., Srinu, T., Ghoshal, A. K., Pugazhenthi, G., Preparation and Characterization of TiO_2 and γ-Al_2O_3 composite membranes for the separation of oil-water emulsions, *RSC Advances* 6 (2016) 4877-4888.

Tennison, S., Current hurdles in the commercial development of inorganic membrane reactors, *Membrane Technology* 2000 (2000) 4-9.

Thirugnanasambandham, K., Sivakumar, V., Prakash M. J., Response surface modelling and optimization of treatment of meat industry wastewater using electrochemical treatment method, *Journal of the Taiwan institute of Chemical Engineers* 46 (2015) 160-167.

Tir, M., Moulai-Mostefa, N., Optimization of oil removal from oily wastewater by electrocoagulation using response surface method, *Journal of Hazardous Materials* 158 (2008) 107-115.

Trinh, T. K., Kang, L. S., Response surface methodological approach to optimize the coagulation-flocculation process in drinking water treatment, *Chemical Engineering Research and Design* 89 (2011) 1126-1135.

Tsuru, T., Narita, M., Shinagawa, R., Yoshioka, T., Nanoporous titania membranes for permeation and filtration of organic solutions, *Desalination* 233 (2008) 1-9.

Tsuru, T., Inorganic porous membranes for liquid phase separation, *Separation and Purification Methods* 30 (2001) 191-220.

Un, U.T., Kandemir, A., Erginel, N., Ocal, S. E., Continuous electrocoagulation of cheese whey wastewater: An application of Response Surface Methodology, *Journal of Environmental Management* 146 (2014) 245-250.

Vasanth, D., Pugazhenthi, G., Uppaluri, R., Influence of sintering temperature on the properties of porous ceramic support prepared by uniaxial dry compaction Method using low cost raw materials for membrane applications, *Separation Science and Technology* 46 (2011a) 1241-1249.

Vasanth, D., Pugazhenthi, G., Uppaluri, R., Fabrication and properties of low cost ceramic microfiltration membranes for separation of oil and bacteria from its solution, *Journal of Membrane Science* 379 (2011b) 154-163.

Vasanth, D., Pugazhenthi, G., Uppaluri, R., Performance of low cost ceramic microfiltration membranes for the treatment of oil-in-water emulsions, *Separation Science and Technology* 48 (2013a) 849-858.

Vasanth, D., Pugazhenthi, G., Uppaluri, R., Cross-flow microfiltration of oil-in-water emulsions using low cost ceramic membranes, *Desalination* 320 (2013b) 86-95.

Vassilev, S. V., Vassileva, C. G., A new approach for the classification of coal ashes based on their origin, composition, properties, and behavior, *Fuel* 86 (2007) 490-512.

Wang, C., Ao, Y., Hou, P., Qian, J., A facile method for the preparation of titania-coated magnetic porous silica and its photocatalytic activity under UV or visible light, *Colloids and Surfaces A: Physicochemical and Engineering Aspects* 360 (2010) 184-189.

Wang, J. P., Chen, Y. Z., Ge, X. W., Yu, H. Q., Optimization of coagulation-flocculation process for a paper-recycling wastewater treatment using response surface methodology, *Colloids and Surfaces A : Physicochemical Engineering Aspects* 302 (2007) 204-210.

Wang, J. P., Chen, Y. Z., Wang, Y., Yuan, S. J., Yu, H. Q., Optimization of the coagulation-flocculation process for pulp mill wastewater treatment using a combination of uniform design and response surface methodology, *Water Research* 45 (2011) 5633-5640.

Wang, J., Guan, J., Santiwong, S. R., Waite, T. D., Characterization of floc size and structure under different monomer and polymer coagulants on microfiltration membrane fouling, *Journal of Membrane Science* 321 (2008) 132-138.

Wang, Y. H., Tian, T. F., Liu, X. Q., Meng, G. Y., Titania membrane preparation with chemical stability for very hash environments applications, *Journal of Membrane Science* 280 (2006) 261-269.

Wang, Y., Chen, K., Mo, L., Li, J., Xu, J., Optimization of coagulation-flocculation process for papermaking-reconstituted tobacco slice wastewater treatment using response surface methodology, *Journal of Industrial and Engineering Chemistry* 20 (2014) 391-396.

Wang, Y. H., Zhang, Y., Liu, X. Q., Meng, G. Y., Sol-coated preparation and characterization of macroporous α-Al_2O_3 membrane support, *Journal of Sol-Gel Science and Technology* 41 (2007) 267-275.

Wang. P., Xu. N., Shi. J., A pilot study of the treatment of waste rolling emulsion using zirconia microfiltration membranes, *Journal of Membrane Science* 173 (2000) 159-166.

Wang, Y. H., Liu, X. Q., Meng, G. Y., Preparation of asymmetric pure titania ceramic membranes with dual functions, *Materials Science and Engineering* A 445-446 (2007) 611–619.

Weir, W. R., Rutinduka, E., Detellier, C., Feng, C. Y., Wang, Q., Matsuura, T., Le VanMao, R., Fabrication, characterization and preliminary testing of all-inorganic ultrafiltration membranes composed entirely of a naturally occurring sepiolite clay mineral, *Journal of Membrane Science* 182 (2001) 41-50.

Wijmans, J. G., Nakao, S., Smolders, C. A., Flux limitation in ultrafiltration: Osmotic pressure model and gel layer model, *Journal of Membrane Science* 20 (1984) 115-124.

Workneh, S., Shukla, A., Synthesis of sodalite octahydrate zeolite-clay composite membrane and its use in separation of SDS, *Journal Membrane Science* 309 (2008)189-195.

Xia, C., Liu, M., A Simple and Cost-Effective Approach to Fabrication of Dense Ceramic Membranes on Porous Substrates, *Journal of American Ceramic Society* 84 (2001) 1903-1905.

Yan, L., Li, Y. S., Xiang, C. B., Xianda, S., Effect of nano-sized Al_2O_3-particle addition on PVDF ultrafiltration membrane performance, *Journal of Membrane Science* 276 (2006) 162-167.

Yang, C., Zhang, G., Xu, N., Shi, J., Preparation and application in oil-water separation of ZrO_2 / α-Al_2O_3 MF membrane, *Journal of Membrane Science* 142 (1998) 235-243.

Yi, X. S., Yu, S. L., Shi, W. X., Sun, N., Jin, L. M., Wang, S., Zhang, B., Ma, C., Sun, L. P., The influence of important factors on ultrafiltration of oil/water emulsion using PVDF membrane modified by nano-sized TiO_2/Al_2O_3, *Desalination* 281 (2011) 179-184.

Yoshino, Y., Suzuki, T., Nair, B. N., Taguchi, H., Itoh, N., Development of tubular substrates, silica based membranes and membrane modules for hydrogen separation at high temperature, *Journal of Membrane Science* 267 (2005) 8-17.

Yuan, Y., Lee, T. R., Contact angle and wetting properties In: Bracco, G., Holst, B., (eds), Surface Science Techniques, *Springer*, Berlin, Heidelberg, 2013, Chapter 1, pp 3-34.

Yue, L., Wang, L., Shi, F., Guo, J., Yang, J., Lian, J., Luo, X., Application of response surface methodology to the decolorization by the electrochemical process using $FePMo_{12}O_{40}$ catalyst, *Journal of Industrial and Engineering Chemistry* 21 (2015) 971-979.

Zhang, Y., Xiong, G., Yao, N., Yang, W., Fu, X., Preparation of titania-based catalysts for formaldehyde photocatalytic oxidation from $TiCl_4$ by the sol gel method. *Catalysis Today*, 68 (2001) 89-95.

Zhong, J., Sun, X., Wang, C., Treatment of oily wastewater produced from refinery processes using flocculation and ceramic membrane filtration, *Separation and Purification Technology* 32 (2003) 93-98.

Zhou, J., Chang, Q., Wang, Y., Wang, J., Meng, G., Separation of stable oil–water emulsion by the hydrophilic nano-sized ZrO_2 modified Al_2O_3 microfiltration membrane, *Separation and Purification Technology* 75 (2010) 243–248.

Zhou, J., Zhang, X., Wang, Y., Hu, X., Larbot, A., Persin, M., Electrokinetic characterization of the Al_2O_3 ceramic MF membrane by streaming potential measurements, *Desalination* 235 (2009) 102-109.

Zhu, L., Chen, M., Dong, Y., Tang, C. Y., Huang, A., Li, L., A low-cost mullite-titania composite ceramic hollow fiber microfiltration membrane for highly efficient separation of oil-in-water emulsion, *Water Research* 90 (2016) 277-285.

Zouboulis, A. I., Avranas, A., Treatment of oil-in-water emulsions by coagulation and dissolved-air flotation, *Colloids and Surfaces A: Physicochemical Engineering Aspects* 172 (2000) 153-161.

भारतीय प्रौद्योगिकी संस्थान गुवाहाटी
Indian Institute of Technology Guwahati

List of Publications

In Journals:

1. **Kanchapogu Suresh** and G. Pugazhenthi, Development of ceramic membranes from low cost clays for the separation of oil-water emulsion, Desalination and Water Treatment, 57 (2016) 1927-1939.
2. **Kanchapogu Suresh**, Tekula Srinu, Aloke Kumar Ghoshal and G. Pugazhenthi, Preparation and characterization of TiO_2 and γ-Al_2O_3 composite membranes for the separation of oil-water emulsions, RSC advances, 6 (2016) 4877-4888.
3. **Kanchapogu Suresh,** R. Uppaluri and G. Pugazhenthi, Fly ash based ceramic microfiltration membranes for oil-water emulsion treatment: Parametric optimization using Response Surface Methodology, Journal of Water Process Engineering, 13 (2016) 27-43.
4. **Kanchapogu Suresh** and G. Pugazhenthi, Cross flow microfiltration of oil-water emulsions using clay based ceramic support and TiO_2 composite membrane, **Egyptian Journal of Petroleum** (accepted).
5. **Kanchapogu Suresh,** R. Uppaluri and G. Pugazhenthi, Preparation and characterization of hydrothermally engineered TiO_2-Fly ash composite membranes, Frontiers of Chemical Science and Engineering (accepted).

Conferences:

1. **Kanchapogu Suresh** and G. Pugazhenthi, Performance evaluation of microfiltration ceramic membrane from fly ash by treatment of oily wastewater, **DAE-BRNS Symposium on Emerging Trends in Separation Science and Technology (SESTEC-2014)**, 25-28 February 2014, Bhabha Atomic Research Center, Mumbai, Maharashtra.

2. **Kanchapogu Suresh** and G. Pugazhenthi, Treatment of oily wastewater by ceramic membrane from fly ash, **Annual Chemical Engineering Symposium (Reflux 2.0)**, 29-30 March 2014, Indian Institute of Technology Guwahati, Guwahati, Assam.
3. **Kanchapogu Suresh** and G. Pugazhenthi, Utilization of fly ash in fabrication of ceramic membrane, **Annual Symposium on Solid Waste Management (RECYCLE 2014)**, 6 April 2014, Indian Institute of Technology Guwahati, Guwahati, Assam.
4. Tekula Srinu, **Kanchapogu Suresh**, Aloke Kumar Ghoshal and G. Pugazhenthi, Treatment of Oily Wastewater using TiO_2 Microfiltration Membrane Prepared on Ceramic Support, **International Conference on Advances in Chemical Engineering & Technology (ICACE '14)**, 16-18 October 2014, Thangal Kunju Musaliar College of Engineering, Kollam, Kerala.
5. **Kanchapogu Suresh** and G. Pugazhenthi, Development and characterization of thermally stable novel ceramic membrane from inorganic clay materials for treatment of synthetic oil-water emulsions, **National Seminar on Recent Trends in Fundamental and Applied Chemical Sciences (RTFACS-2014)**, 19-21 November 2014, Dibrugarh University, Dibrugarh, Assam.
6. **Kanchapogu Suresh**, Manpadu Ramesh and G. Pugazhenthi, Low cost ceramic microfiltration membrane for treatment of oil-water emulsions in cross flow mode, **International Conference on New Frontiers in Chemical, Energy and Environmental Engineering (INCEEE-2015)**, 20-21 March 2015, National Institute of Technology Warangal, Warangal, Telangana.

APPENDIX

भारतीय प्रौद्योगिकी संस्थान गुवाहाटी
Indian Institute of Technology Guwahati

Appendix I: Detailed cost analysis of membranes (M1-M3) and Separation cost

The following calculations represent the cost of the membranes. In these cost calculations, raw materials cost, labor, sonication, electricity, equipment cost and depreciation cost have also been considered.

(1)Membrane cost

The unit prices of various raw materials are as follows: Quartz- Rs. 10/kg; $CaCO_3$- Rs. 240/kg; Fly ash- Rs. 28/kg and polyvinyl alcohol (PVA) - Rs. 720/kg.

Inorganic precursor formulation for membrane (M1-M3) on weight basis:

Raw materials	Membrane M1 (Wt. %)	Membrane M2 (Wt. %)	Membrane M3 (Wt. %)
Fly ash	80	80	70
Quartz	20	10	20
CaCO3	-	10	10
PVA	0.8	0.8	0.8
Cost of one support (22 g for support)	$\frac{(80\times22\times28+20\times22\times10+0.8\times22\times720)}{100\times1000}$ = Rs. 0.663	$\frac{(80\times22\times28+10\times22\times10+10\times22\times240+0.8\times22\times720)}{100\times1000}$ = Rs. 1.169	$\frac{(70\times22\times28+20\times22\times10+10\times22\times240+0.8\times22\times720)}{100\times1000}$ = Rs. 1.130
The currency conversion factor used in all calculations is 1 Rs = 0.015 $			
The area of the membrane supports (55 mm diameter and 5 mm thickness) (M1-M3) = 23.736 cm^2			
Membrane support disc cost (Rs./cm^2)	**0.0279**	**0.0492**	**0.0476**
(A) Membrane support disc cost ($/$m^2$)	**4.1913**	**7.3876**	**7.1375**
The laboratory ball mill enables for the mixing of raw materials of 20 membrane supports in one run (0.33 h).			

The laboratory hydraulic press and circular shaped mould are used for pressing of 20 membrane supports in 1 h operation

The hot air oven is used for initial drying at 100 and 200°C of 20 membrane supports in one run (48 h).

The laboratory grade muffle furnace enables the fabrication of 20 membrane supports in one sintering run (17 h).

Silicon Carbide (SiC) abrasive papers 5 used for polishing of 20 membrane supports with time required of (5 h- 2.5 h sonication time) 2.5 h.

Sonication bath used for cleaning of 20 membrane supports with operation time of 2.5 h.

Manpower requirement = 500 Rs/Day; here working hours 8 h per day
Total manpower requirement is for 10 h [(10×1/8 day) = 1.25 days] to fabricate 20 membrane supports

(B) Manpower cost= $\frac{500(Rs/day)\times 1.25 days}{20\times 23.746 cm^2}$ = **1.31601 Rs/cm^2 = 197.4017 \$/m^2**

Electricity tariff charge = 6.45 Rs/kW. h (1 hp = 746 W = 0.746 kW; 1 W = 1 J/s)
Electricity consumed to fabricate 20 membrane supports

(a) Ball mill = 5 hp = 3.73 kW; [(0.33 h×3.73 kW×6.45 (Rs/kW. h))/(20×23.746 cm^2)] = 0.01672 Rs/cm^2

(Time required for mixing of raw materials for 20 supports = 0.33 h)

(b) Hydraulic press = 2 hp = 1.492 kW; [(1 h×1.492 kW×6.45 (Rs/kW. h))/(20×23.746 cm^2)] = 0.02026 Rs/cm^2

(Time required to press 20 supports = 1 h)

(c) Hot air oven = 2.5 kW; [(48 h×2.5 kW×6.45 (Rs/kW. h)/(20×23.746 cm^2)] = 0.08149 Rs/cm^2

(Time consumed for drying of 20 supports at 100 and 200°C = 2 days = 48 h)

(d) Muffle furnace = 4 kW; [(17 h×4 kW×6.45 (Rs/kW. h)/(20×23.746 cm^2)] = 0.92352 Rs/cm^2

(Sintering time required to fabricate 20 membrane supports = 17 h)

(e) Sonication bath = 85 W= 0.085 kW; [(2.5 h×0.085 kW×6.45 (Rs/kW. h)/(20×23.746 cm^2)] = 0.00289 Rs/cm^2

(Sonication time to clean 20 membrane supports = 2.5 h)

(C) Total electricity cost (a+b+c+d+e) = 0.01672 + 0.02026 + 0.08149 + 0.92352 + 0.00289
= **1.04488 Rs/cm^2 = 156.7317 \$/m^2**

Equipment cost (straight line depreciation method applied for all equipment's with assumed 10 years of life time for each equipment)

(a) Ball mill cost = [(0.33 h×0.64103 Rs/h)/(20×23.746 cm^2)] = 0.0004 Rs/cm^2

(b) Circular shaped mould cost = [(1 h×0.11218 Rs/h)/(20×23.746 cm^2)] = 0.0002 Rs/cm^2

(c) Hydraulic press cost = [(1 h×1.60256 Rs/h)/(20×23.746 cm^2)] = 0.0034 Rs/cm^2

(d) Hot air oven cost = [(48 h×0.64103 Rs/h)/(20×23.746 cm^2)] = 0.0648 Rs/cm^2

(e) Muffle furnace cost (Programmable) = [(30 h×4.80769 Rs/h)/(20×23.746 cm^2)] = 0.3037 Rs/cm^2

(f) Ultrasonic bath cost = [(2.5 h×0.40064 Rs/h)/(20×23.746 cm^2)] = 0.0021 Rs/cm^2

(D) Total equipment consumed cost (a+b+c+d+e+f) = 0.0004+0.0002+0.0034+0.0648+0.3037+0.0021
= **0.3746 Rs/cm^2 = 56.1900 $/$m^2$**

Miscellaneous cost

(a) 5 SiC abrasive papers required for polishing of 20 membrane supports = 5×8 = Rs 40;
[40 Rs/(20×23.746 cm^2)] = 0.0842 Rs/cm^2

(b) 3 tissue rolls required for cleaning of ball mill and mould for making of 20 membrane supports= 3×25 = Rs 75;
[75 Rs/(20×23.746 cm^2)] = 0.1579 Rs/cm^2

(c) 100 ml acetone required for cleaning mould during making of 20 membrane supports =
[(813 Rs ×100 ml)/(2500 ml ×20×23.746 cm^2)] = 0.0685 Rs/cm^2

(E) Overall miscellaneous cost = (a)+(b)+(c) = 0.0842+0.1579+0.0685= **0.3106 Rs/cm^2 = 46.5931 $/$m^2$**

(F) Total cost required for Manpower (B) + Electricity (C) + Equipment (D) + Miscellaneous (E) =
= 1.13601 Rs/cm^2 + 1.04488 Rs/cm^2 + 0.37465 Rs/cm^2 + 0.31062 Rs/cm^2 = **2.80213 Rs/cm^2**
= 197.4017 $/$m^2$ + 156.7317 $/$m^2$ + 56.1900 $/$m^2$ + 46.5931 $/$m^2$ = **456.9165 $/$m^2$**

	Membrane M1	**Membrane M2**	**Membrane M3**
The overall fabrication cost of membrane support (Raw materials cost + Manpower cost + Electricity cost + Equipment cost + Miscellaneous cost) (Rs/cm^2) **[(A)+(B)+(C)+(D)+(E)]**	2.83003 **(3 Rs/cm^2)**	2.85133 **(3 Rs/cm^2)**	2.84973 **(3 Rs/cm^2)**
The overall fabrication cost of membrane support (Raw materials cost + Manpower cost + Electricity cost + Equipment cost + Miscellaneous cost) ($/$m^2$) **[(A)+(B)+(C)+(D)+(E)]**	461.1078 **(462 $/$m^2$)**	464.3041 **(465 $/$m^2$)**	464.054 **(465 $/$m^2$)**

(2) Equipment cost

Equipment	Cost (Rs)	Year of purchase	Life time of equipment (years)	Cost of equipment for 1 h use (Rs/h)	Time for equipment usage (h) to make 20 membranes with 55 mm diameter and 5 mm thickness	Cost of equipment for making of membrane with unit area (cm^2) (Rs/cm^2)
Ball mill	40000	2010	10	$\frac{(40000Rs)}{(10\times52\times6\times20h)}$ = 0.64103	0.33	$\frac{0.33h\times0.64103Rs/h}{20\times23.746cm^2}$=0.0004
Circular shaped mould	7000	2011	10	$\frac{(7000Rs)}{(10\times52\times6\times20h)}$ = 0.11218	1	$\frac{1h\times0.11218Rs/h}{20\times23.746cm^2}$=0.0002
Hydraulic press	100000	2010	10	$\frac{(100000Rs)}{(10\times52\times6\times20h)}$ = 1.60256	1	$\frac{1h\times1.60256Rs/h}{20\times23.746cm^2}$=0.0034
Hot air oven	40000	2011	10	$\frac{(40000Rs)}{(10\times52\times6\times20h)}$ = 0.64103	48	$\frac{48h\times0.64103Rs/h}{20\times23.746cm^2}$=0.0648
Muffle furnace	300000	2011	10	$\frac{(300000Rs)}{(10\times52\times6\times20h)}$ = 4.80769	30	$\frac{30h\times4.80769Rs/h}{20\times23.746cm^2}$=0.3037
Sonication bath	25000	2011	10	$\frac{(25000Rs)}{(10\times52\times6\times20h)}$ = 0.40064	2.5	$\frac{2.5h\times0.40064Rs/h}{20\times23.746cm^2}$=0.0021

(3) Separation cost

Oil-in-water emulsions treatment cost	Membrane M1	Membrane M2	Membrane M3
Permeate flux through unit (m^2) area of membrane at applied pressure of 69 kPa and feed concentration of 200 mg/L	4.15×10^{-5} (m^3/m^2 s)	3.37×10^{-5} (m^3/m^2 s)	4.13×10^{-5} (m^3/m^2 s)
Amount of oil-in-water emulsions processed per year	310752 (L/Year)	252345.6 (L/Year)	309254.4 (L/Year)
Total direct (fixed) cost [Empty N_2 cylinder cost + dead end flow filtration set up cost)	52 ($/Year)	52 ($/Year)	52 ($/Year)
Operating cost (N_2 gas consumable cost per year for treatment of oil-in-water emulsion by each membrane)	10 ($/Year)	10 ($/Year)	10 ($/Year)
Membrane cost	462 ($/$m^2$)	465 ($/$m^2$)	465 ($/$m^2$)
Depreciation	66 ($/Year)	67 ($/Year)	67 ($/Year)
Membrane cleaning and maintenance cost (@ 3% of total cost of the membrane system)	1.56 ($/Year)	1.56 ($/Year)	1.56 ($/Year)
Labor cost (@ 2% of total cost of the membrane system)	1.04 ($/Year)	1.04 ($/Year)	1.04 ($/Year)
The overall cost for the treatment of oil-in-water emulsions ($/Year)	**525 ($/Year)**	**525 ($/year)**	**525 ($/Year)**